The mechanisms of larval calcification in the mussel, *Mytilus edulis*

Dissertation

zur Erlangung des akademischen Grades eines Doktors der Naturwissenschaften

- Dr. rer. nat. -

an der Mathematisch-Naturwissenschaftlichen Fakultät der Christian-Albrechts-Universität zu Kiel

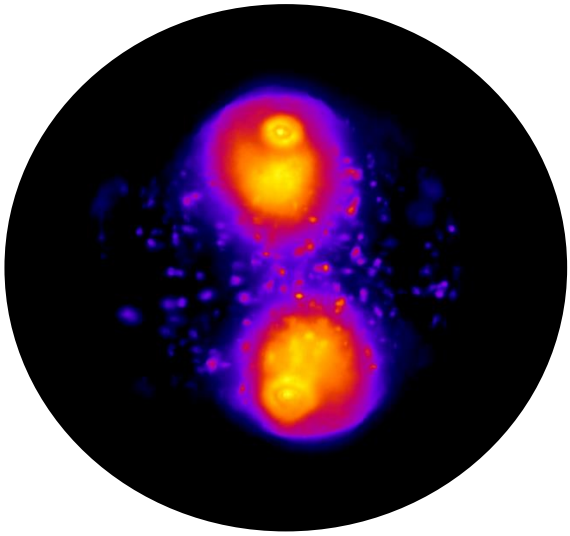

vorgelegt von

Kirti Ramesh

Kiel, December 2017

GEOMAR
Helmholtz Centre for Ocean Research Kiel

Christian-Albrechts-Universität zu Kiel

The cover photo is taken using correlative fluorescence-Raman microscopy and displays a *Mytilus edulis* larva that has begun the process of shell deposition, during the trochophore stage. The calcein labelled larval shell is visible as two fluorescent valves.

1. Gutachter / Referee: PD. Dr. Frank Melzner

2. Gutachter / Referee: Prof. Dr. Thorsten Reusch

Tag der mündlichen Prüfung /Date of Disputation: Kiel, 25.01.2018

Zum Druck genehmigt /Approved for Print: Kiel, 25.01.2018

Contents

Summary

The mollusc shell is a composite biomineral consisting of calcium carbonate and an associated organic matrix. Biomineralisation in molluscs begins during early ontogenetic development, where larval calcification is characterized by rapid rates of mineral deposition. Despite these rapid rates of early calcification, no information exists on the mechanistic basis of larval shell formation. In this thesis, I use polarized light microscopy, *in vivo* confocal Raman microscopy as well as Fourier transform infrared spectroscopy to investigate the composition of the first larval shell (Prodissoconch I, PD I) in *Mytilus edulis* larvae. No evidence for amorphous calcium carbonate (ACC) precursor phases is detected from the onset of shell formation to the completion of the PD I shell. Subsequent analyses of larval shell composition in three other bivalve species, *Mercenaria mercenaria*, *Crassostrea gigas* and *Crassostrea virginica* reveals the absence of ACC precursor phases in all three species. These results suggest that the current perception that ACC is a precursor phase to aragonite during bivalve larval calcification requires critical reconsideration.

Anthropogenic rise in seawater acidification resulting from increases in atmospheric CO_2 is associated with reduced carbonate concentrations. This process of seawater acidification has negative impacts on bivalve growth, calcification and survival during ontogeny consequently creating bottlenecks during larval development. Ion-selective microelectrode measurements reveal alkaline conditions with respect to ambient seawater pH by 0.18 pH units and higher carbonate (14 µmol kg^{-1}) and calcium concentrations (by 0.1 mM kg^{-1}) in the space beneath the growing shell. This promotes the rapid synthesis of shell carbonates, as the saturation state of aragonite (Ω_{arag}) is elevated. Microelectrode measurements in the calcification space of larvae exposed to acidified seawater reveal a significant drop in pH, carbonate and Ω_{arag} that can partially explain observations of decreased shell growth. The ability to elevate pH at the site of calcification in *M. edulis* larvae above that of seawater is exhausted between 1500–2000 µatm. While Ω_{arag} reaches undersaturation at 999.5 µatm, shell dissolution is only observed at extreme pCO_2 (2000 and 2500 µatm), indicating that *M. edulis* larvae may be able to modify the composition of their shell organic matrix to counteract dissolution. These results illustrate the limited physiological capacity of *M. edulis* larvae to counter changes in seawater chemistry.

The Baltic Sea is characterized by a decreasing salinity gradient from the Kattegat transition zone to the eastern basins. This reduction in salinity from west to east is accompanied by reduced seawater calcium ion concentrations. In order to investigate the interplay between *M. edulis* larval calcification and seawater calcium, microsensor measurements in the

calcification space of *M. edulis* larvae reared at a range of calcium concentrations are performed. These measurements reveal that calcium dynamics in the calcification space are strongly linked to seawater calcium concentrations. Further, at particularly low concentrations of seawater calcium, larvae have a very limited capacity to enrich calcium in the calcification space (by 0.03-0.06 mM) to delay mineral dissolution. PD I larval calcification is highly dependent on seawater calcium availability. *M. edulis* larvae exhibit delays in larval development and incomplete PD I formation at low calcium concentrations (<2 mM). Therefore, projected climate change induced patterns of desalination in the Baltic Sea may lead to a westward shift in *M. edulis* populations due to impaired PD I calcification performance.

Finally, in this thesis, I aimed to identify putative membrane bound ion transport proteins that support the rapid rates of larval calcification. I utilized a substrate limited approach (C_T reductions by ca. 51%) to investigate transcriptomic responses of proteins taking part in the translocation of calcification substrates, calcium and bicarbonate. Drastic reductions in C_T induced differential expression of only 53 out of 29,177 TRINITY genes. Among this small subset of genes, the differential expression of one anion transport protein (SLC26 family) and several proteins with previously demonstrated association to mammalian calcification processes is observed. The SLC26 candidate (upregulated 2.3-2.9 fold during shell formation) is similar to mammalian SLC26 isoforms that transport chloride, sulphate and bicarbonate. Further, developmental expression profiles for several ion transport proteins are examined and correlated with larval calcification. In particular, the elevated expression of proteins involved in bicarbonate transport (anion exchangers, sodium bicarbonate transporters, SLC4 and SLC26 families) and calcium transport (sarco/endoplasmic reticulum calcium ATPases, sodium/calcium exchangers, calcium channels) suggests a model for cellular pathways involved in ion transport during *M. edulis* larval calcification. Further characterization of ion transport – candidate genes identified in this study using heterologous expression and electrophysiological techniques, as well as knock - down techniques (RNAi) is necessary to understand precise substrate transport mechanisms.

In conclusion, *in vivo* techniques provide no evidence for ACC precursors in bivalve larvae and *M. edulis* larvae are observed to secrete crystalline shells at the trochophore stage. Further, *M. edulis* larvae express a suite of membrane-bound ion transport proteins for acid-base regulation and calcification relevant substrate transport during larval development. The activity of these ion transport proteins also likely provides *M. edulis* larvae with the capacity to modify the carbonate chemistry at the site of mineral deposition, which consequently

promotes calcification by the elevation of Ω_{arag}**.** The physiological capacity to modify the abiotic conditions of the calcification space defines organismal vulnerability to unfavourable conditions such as ocean acidification and desalination.

Evidence for adaptation potential in *M. edulis* is observed, where populations originating from habitats experiencing natural fluctuations in pCO_2 exhibit differential sensitivity to simulated ocean acidification compared to populations from less variable environments (Thomsen et al 2017a). However, coastal habitats that experience upwelling and consequent fluctuations in carbonate chemistry are projected to experience the most dramatic increases in seawater pCO_2 (Melzner et al 2013). Consequently, further experiments should aim to investigate potential rates of adaptation in the early larval calcification performance and the plasticity of larval shell stability.

Zusammenfassung

Die Schale von Mollusken ist ein zusammengesetztes Biomineral, bestehend aus dem Mineral Calciumcarbonat und einer damit assoziierten organischen Matrix. Die Biomineralisation von Mollusken beginnt während der frühen ontogenetischen Entwicklung, wo die larvale Kalzifizierung durch hohe Ablagerungsraten von Mineralien gekennzeichnet ist. Trotz dieser hohen Kalzifizierungsraten in frühen Stadien gibt es keine Angaben über die mechanistische Grundlage larvaler Schalenbildung. In der vorliegenden Arbeit verwende ich polarisierte Lichtmikroskopie, *in vivo* konfokale Raman-Mikroskopie sowie Fourier-Transformations-Infrarotspektroskopie, um die Zusammensetzung von frühen larvalen Schalen (Prodissoconch I, PD I) von *Mytilus edulis* Larven zu erforschen. Es besteht kein Nachweis für amorphe Calciumcarbonat (ACC)-Vorläuferphasen vom Beginn der Schalenbildung bis zur Vollendung der PD I Schale. Folgende Analysen von larvaler Schalenzusammensetzung in drei anderen Muschelarten, *Mercenaria mercenaria*, *Crassostrea gigas* und *Crassostrea virginica*, zeigen das Fehlen von ACC-Vorläuferphasen in allen drei Arten. Diese Ergebnisse deuten darauf hin, dass die derzeitige Auffassung, ACC sei eine Vorläuferphase von Aragonit während der larvalen Muschelkalzifizierung, einer kritischen Nachprüfung bedarf.

Der anthropogene Anstieg der Meerwasserversauerung, aufgrund von zunehmendem CO_2 in der Atmosphäre, geht einher mit verminderten Carbonatkonzentrationen. Dieser Prozess der Meerwasserversauerung hat einen negativen Einfluss auf das Wachstum, die Kalzifizierung und das Überleben von Muscheln während der Ontogenese, was zu Engpässen während der Larvenentwicklung führt. Ionenselektive Mikroelektrodenmessungen zeigen, dass in Bezug zu Meerwasser in dem Bereich unter der wachsenden Schale alkalische Bedingungen mit einem um 0,18 Einheiten erhöhten pH-Wert sowie höhere Carbonat- (14 µmol kg^{-1}) und Calciumkonzentrationen (um 0,1 mM kg^{-1}) herrschen. Dies fördert eine schnelle Synthese von Schalencarbonaten, da der Sättigungsgrad von Aragonit (Ω_{arag}) erhöht ist. Mikroelektrodenmessungen im Kalzifizierungsbereich von Larven, die Meerwasserversauerung ausgesetzt sind, zeigen eine signifikante Verminderung des pH-Wertes, des Carbonats und Ω_{arag}, was zum Teil die Beobachtungen von reduziertem Schalenwachstum erklärt. Die Fähigkeit, den pH-Wert an der Kalzifizierungsstelle in *M. edulis* Larven über den des Meerwassers zu erhöhen, ist zwischen 1500-2000 µatm erschöpft. Während Ω_{arag} bei 999,5 µatm eine Untersättigung erreicht, wird eine Auflösung der Schale erst bei extremen pCO_2-Werten (2000 und 2500 µatm) beobachtet, was darauf hinweist, dass *M. edulis* Larven möglicherweise in der Lage sind, die Zusammensetzung der organischen

Matrix ihrer Schale zu verändern, um einer Auflösung entgegen zu wirken. Diese Ergebnisse zeigen die eingeschränkte physiologische Kapazität von *M. edulis* Larven, Veränderungen der Meerwasserchemie entgegen zu wirken. Die Ostsee ist gekennzeichnet durch einen abnehmenden Salzgehaltsgradienten von der Kattegat-Übergangszone bis zu den östlichen Becken. Diese Verminderung des Salzgehaltes von Westen nach Osten wird begleitet von Verringerungen von Calcium im Meerwasser. Um die Zusammenwirkung von Kalzifizierung in *M. edulis* Larven und Calciumgehalt im Meerwasser zu untersuchen, wurden Mikrosensormessungen im larvalen Kalzifizierungsbereich von *M. edulis* Larven in verschiedenen Calciumkonzentrationen durchgeführt. Diese Messungen zeigen, dass Calcium-Dynamiken im Kalzifizierungsbereich stark mit Meerwasser-Calciumkonzentrationen gekoppelt sind. Des Weiteren haben Larven bei besonders niedrigen Konzentrationen von Calcium im Meerwasser eine sehr begrenzte Kapazität, Calcium im Kalzifizierungsbereich anzureichern, um eine Auflösung der Mineralien hinauszuzögern. Larvale PD I-Kalzifizierung ist stark von der Verfügbarkeit von Calcium im Meerwasser abhängig, wobei *M. edulis* Larven Verzögerungen in der Larvenentwicklung und unvollständiges PD I-Wachstum bei niedrigen Calciumkonzentrationen (<2 mM) aufweisen. Daher könnte eine vom Klimawandel herbeigeführte Entsalzung in der Ostsee zu einer Verlagerung von *M. edulis* Beständen in Richtung Westen führen, bedingt durch eine beeinträchtigte PD I-Kalzifizierungsleistung.

In dieser Arbeit wurde ein substratlimitierten Ansatz (C_T-Reduzierungen von ca. 51%) zur Untersuchung von transkriptomischen Reaktionen in *M. edulis* Larven verwendet, um vermeintliche membrangebundene Ionentransportproteine zu identifizieren, die die hohen larvalen Kalzifizierungsraten fördern, indem sie bei der Translokation von Kalzifizierungssubstraten mitwirken. Drastische Verminderungen von C_T riefen eine differentielle Expression von nur 53 von insgesamt 29 177 Genen hervor. Aus dieser kleinen Untergruppe von Genen sind ein Anionentransportprotein (SLC26 Familie der Anionentransporter) und mehrere Proteine mit bereits nachgewiesener Verbindung zu Kalzifizierungsprozessen bei Säugetieren differentiell exprimiert. Der SLC26-Kandidat (2,3 – 2,9)-fach hochreguliert während der Schalenbildung) ist ähnlich den SLC26 Isoformen von Säugetieren, welche Chlorid, Sulfat und Bicarbonat transportieren. Weiterhin wurden die Expressionsprofile während der Entwicklung für mehrere Ionentransportproteine untersucht und mit der Kalzifizierung von Larven korreliert. Insbesondere die erhöhte Expression von Proteinen, die im Bicarbonat-Transport (Anionenaustauscher, Natriumbicarbonat-Transporter, SLC4 und SLC26 Familien) und im Calcium-Transport (sarko/endoplasmatisches Retikulum-Calcium-ATPasen, Natrium-/Calcium-Austauscher, Calciumkanäle) involviert sind, lässt auf

zelluläre Signalwege während des Ionentransports bei der Kalzifizierung von *M. edulis* Larven schließen. Eine weitere Charakterisierung von Ionentransport-Kandidatengenen, die in dieser Studie identifiziert wurden, unter Verwendung von heterologer Expression und elektrophysiologischer sowie Knock-down-Techniken (RNAi), ist notwendig, um die genauen Substrattransportmechanismen zu verstehen. Zusammenfassend liefern *in vivo* Techniken keine Hinweise auf ACC-Vorläuferphasen in Muschellarven. Darüber hinaus bilden *M. edulis* Trochophoralarven kristalline Schalen ab dem Beginn der Kalzifizierung. Weiterhin exprimieren *M. edulis* Larven eine Gruppe von membrangebundenen Ionentransportproteinen zur Säure-Base-Regulierung und zum kalzifizierungsrelevanten Substrattransport während der Larvenentwicklung. Die Aktivität dieser Ionentransportproteine ermöglicht es *M. edulis* wahrscheinlich auch die Carbonatchemie an Stellen der Mineralablagerung zu verändern, welche durch Erhöhung des Ω_{arag} die Kalzifizierung fördert. Die physiologische Kapazität, die abiotischen Bedingungen im Kalzifizierungsbereich zu verändern, bestimmt die Anfälligkeit von Organismen gegenüber ungünstigen Bedingungen, wie zum Beispiel Ozeanversauerung und eine niedrige Calciumverfügbarkeit im Meerwasser. Hinweise auf ein Anpassungspotential von *M. edulis* wurden festgestellt, wobei Populationen aus Gebieten mit natürlichen pCO_2-Schwankungen anders auf simulierte Ozeanversauerung reagieren als Populationen aus weniger variablen Umgebungen (Thomsen et al 2017a). Küstengebiete, die von Tiefenwasserauftrieb und daraus folgenden pCO_2-Schwankungen betroffen sind, werden jedoch in Zukunft den drastischsten Anstieg von pCO_2 im Meerwasser erfahren (Melzner et al 2013). Daher sollten sich zukünftige Experimente mit der Erforschung von möglichen Anpassungsraten der Kalzifizierungsleistung im frühen Larvenstadium und der Plastizität der Schalenstabilität von Larven beschäftigen.

List of Abbreviations

ACC	Amorphous calcium carbonate
A_T	Total alkalinity
Ca^{2+}	Calcium
$[Ca^{2+}]$	Concentration of calcium
Ca^{2+} ATPase	Calcium ATPases
$CaCO_3$	Calcium carbonate
Cl^-	Chloride
CO_2	Carbon dioxide
$[CO_3^{2-}]$	Concentration of carbonate
CRM	Confocal Raman microscopy
CS	Calcification space
C_T	Total dissolved inorganic carbon
FIB-TEM	Focused Ion Beam Transmission Electron Microscopy
FSW	Filtered seawater
FTIR	Fourier transform infrared
H^+	Proton
HCO_3^-	Bicarbonate
$[HCO_3^-]$	Concentration of bicarbonate
HKA	Proton/potassium ATPase
hpf	Hours post fertilisation
K^+	Potassium
K_{sp}	thermodynamic solubility product
Na^+	Sodium
NBC	Sodium bicarbonate cotransporter
NCX	Sodium calcium exchanger
OA	Ocean acidification
pCO_2	Partial pressure of carbon dioxide
PD I	Prodissoconch I
PD II	Prodissoconch II
RNAi	RNA interfence
SEM	Scanning electron microscopy
SERCA	Sarco/endoplasmic reticulum calcium ATPase
SLC	Solute carrier family
XRD	X-ray diffraction
Ω	Saturation state
Ω_{arag}	Saturation state of aragonite

1. Introduction

1.1 Formation of the larval bivalve shell

The phylum Mollusca is a plastic and diverse metazoan group with first appearances recognized in the fossil record dating back ca. 500 million years to the early Cambrian period (Parkhev 2008). In the periods following their appearance, there was a rapid diversification into the eight major molluscan classes still present today (Erwin 1994; Wanninger et al 2008, Haszprunar et al 2008, Kocot et al 2011). Their evolutionary success is thought to be partly attributed to the presence of an external shell made of calcium carbonate ($CaCO_3$), which provides protection and structural support for their soft tissues (Marin and Luquet 2004). The structural diversity of adult mollusc shells is vast and research has focused on the biological control underlying this phenotypic diversity (Weiner and Addadi 2011, Wolf et al 2012). In addition, an understanding of biomineralisation processes is necessary to identify the vulnerability of calcifying organisms to abiotic stressors (Thomsen et al 2015, Mette et al 2016, Marali et al 2017). Despite the diversity of adult mollusc shell structures and $CaCO_3$ polymorph composition (aragonite, calcite, vaterite, etc. see Nehrke et al 2012), formation of the first mineralized structures during larval development is morphologically similar between species, where the epithelial cells involved in shell secretion exhibit similar enzymatic histochemistry within the region of the shell gland and shell field for enzymes such as oxidases, peroxidases and phosphatases (Kniprath 1981). In addition, the cellular differentiation processes of shell forming cells are conserved across Conchiferan molluscan classes, where the shell-forming epithelial cells exhibit homologous lineages (Hohagen and Jackson 2013). Conchiferan molluscs such as bivalves make use of a homologous organ, termed the shell field, during their shell-less, non-feeding trochophore larval stages to biomineralise the first mineralised structure (Saranchova and Flyachinskaya 2001, Eyster 1983, Hohagen 2013). In bivalve larvae, ectodermal cells in the dorsal region thicken and invaginate to form the shell gland (Kniprath 1981, Fig. 1.1). Initial shell mineralisation in bivalve larvae takes place during the trochophore larval stage, within the shell field region. An ensuing evagination of the shell gland and flattening of ectodermal cells gives rise to the so-called shell field (Kniprath 1981, Fig. 1.1)(Eyster 1983). The shell field evaginates during trochophore stages and the surrounding epithelial cells secrete an initial organic layer which is composed of a suite of biomineralising proteins and polysaccharides (Weiss and Schönitzer 2006). This organic layer is termed the periostracum and is thought to protect the first shell structures from dissolution during adverse environmental conditions such as lowered aragonite saturation state (Kniprath 1981, Eyster 1983, Waldbusser et al 2013). This

organic layer forms the template for calcification. Continual deposition of calcium carbonate onto the organic layer as it spans over the surface of the larval body rigidifies and laterally compresses the larva (Aranda-Burgos et al 2014). The first larval shell, prodissoconch I (PD I, Fig. 1.2), marks the D-veliger larval stage and is composed solely of aragonite (Medakovic et al 1997). The relative rates of calcification in bivalve larvae are distinctly elevated in comparison to adults, where bivalve larvae secrete an aragonitic shell almost equivalent to their mass in the span of two days (Waldbusser et al 2013). The formation of PD I is followed by the secretion of prodissoconch II (PD II, veliger stage), which is characterized by the presence of growth lines on the shell. The shell forming epithelial cells within the shell field ultimately differentiate into the shell-forming organ in juveniles and adults known as the mantle. Following metamorphosis from the (pedi)veliger stage to juveniles, where the larva reabsorbs its velum and develops a muscular foot, the mantle secretes new shell layers (dissoconch) at the edge of the prodissoconchs that formed previously (Kniprath 1980, Hohagen and Jackson 2013).

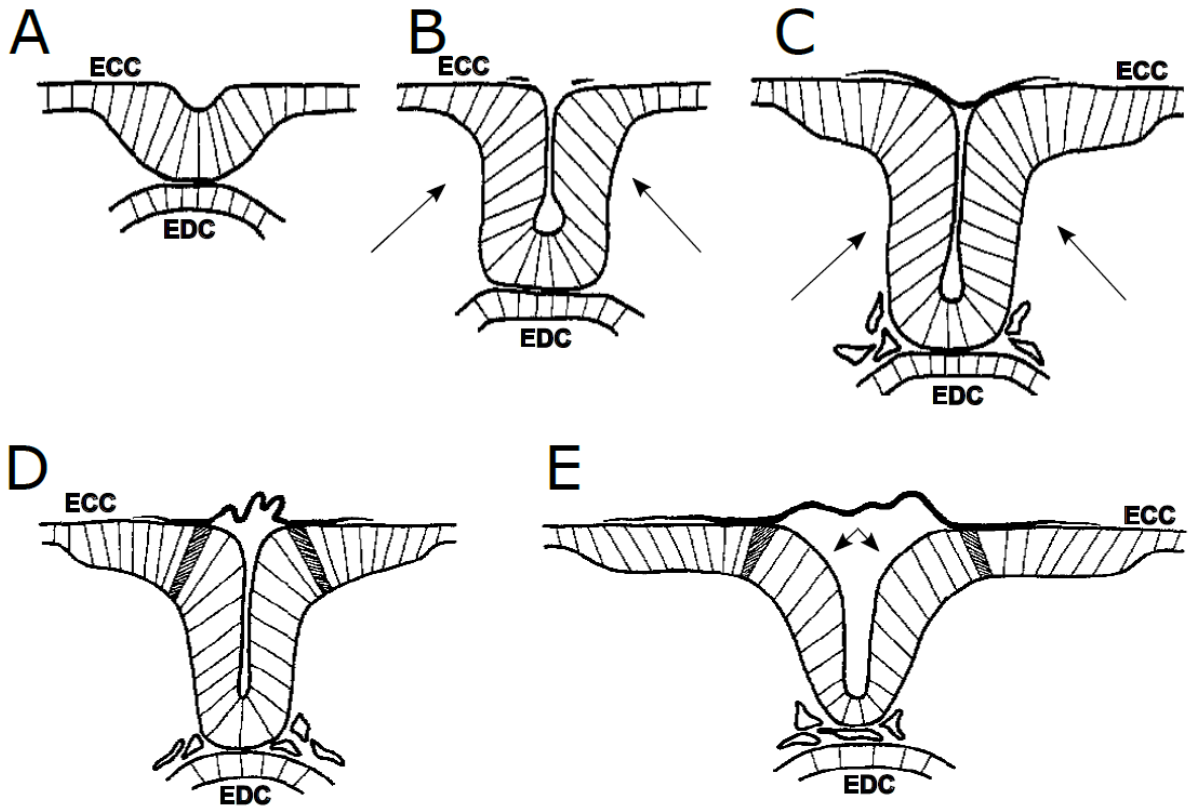

Figure 1.1 The development of the shell field in the gastropod *Lymnaea stagnalis* (A-C) The invagination of the shell gland. The elongation of the ectodermal cells (ECC) is initiated by the contact of these cells to underlying endodermal cells (EDC). Thus begins the initial specification of the molluscan shell field (Hohagen 2013). The arrows point towards the ectodermal cells that are undergoing invagination. (D-E) Subsequent evagination of the shell gland to form the shell field and arrows in (E) point towards the evaginated cells. Adapted from Kniprath (1977).

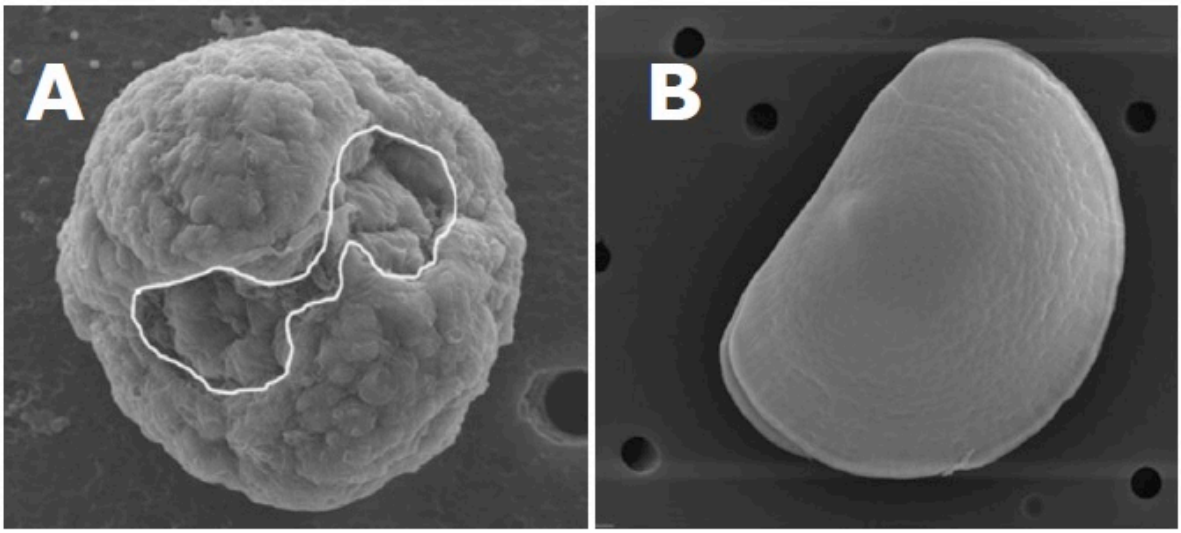

Figure 1.2 Scanning electron micrographs of *Mytilus galloprovincialis* larval shell formation (A)Trochophore larvae with superimposed margins of the shell field and (B) the prodissoconch I (PD I) larval shell marks the D-veliger stage. Adapted from Balbi et al (2016).

1.2 Amorphous precursors for shell formation

The formation of biomineralized structures was initially hypothesized to occur via the crystallization of super saturated solutions based on the observation that shells form under ambient temperature and pressure (Marin et al 2012). However, this view has been relinquished based on observations that the calcification space (extrapallial space) in molluscs in fact is under saturated with respect to calcium carbonate (Misogaines and Chasteen 1979, Heinemann et al 2012). In addition, models suggest that the necessary volumes of such super saturated solutions would be too large to facilitate biomineralization in many taxa (Addadi et al 2006). Consequently, the current notion regarding mineral precipitation is based on the high degree of biological control underlying biomineralization. (Addadi et al 2003, Marin et al 2012). Novel descriptions of biomineralisation suggest that it occurs via colloidal precursors that go to form nanogranular calcium carbonate structures (Wolf et al 2016). The hypothesis of biologically controlled mineralization derives from observations of selective crystal nucleation in the presence of organic molecules and the accumulation of amorphous precursors in a wide range of taxa (Marie et al 2012, Weiss et al 2002, Vidavsky et al 2014, 2015, Von Euw et al 2017). Transient amorphous precursors such as amorphous calcium carbonate (ACC) have no defined growth directions and can be shaped into various forms which may serve an important advantage to calcifying organisms that form intricate structures (Bentov et al 2016). In addition, amorphous phases are less brittle due to a lack of cleavage planes and have the potential to incorporate larger amounts

of impurities than crystalline polymorphs (Aizenberg et al 2002, Bentov and Erez 2006) and therefore offer several advantages to calcifying organisms.

The first observations for amorphous calcium carbonate (ACC) as a precursor phase to crystalline polymorphs during larval calcification was reported in sea urchins, where ACC transformed into a magnesium-bearing calcite spicule (Beniash et al 1997, Politi et al 2008). Subsequently, reports of ACC as a precursor phase during calcification have become widespread across a range of taxa (Weiss et al 2002, Raz et al 2002, Mahamid et al 2008, Von Euw et al 2017). Calcifying larvae have become model systems for understanding biomineralisation processes and the role of organics/magnesium in stabilizing biogenic ACC (Weiss et al 2002, Raz et al 2003, Vidavsky et al 2014, 2015). In addition, the relatively instable nature of ACC precursor phases have been used to infer vulnerability of larval calcification processes in many taxa, since ACC is ca. 30 fold more unstable than its crystalline counterparts (Kurihara et al 2008). However, the role of ACC in larval calcification, particularly whether it constitutes a bulk of larval shell carbonates remains an open question.

Mineral composition of bivalve larval shells

Early studies using bulk X-ray diffraction (XRD) on the larval shells of the bivalve species the European oyster (*Ostrea edulis*), demonstrated they were composed of aragonite (Waller 1981, Medakovic et al 1997). A comparative analysis between adult shells and whole larvae of the oyster, *Ostrea edulis* observed relatively broad peaks for aragonite in larval XRD spectra (Medakovic et al 1997). The authors attributed broadening of XRD aragonite peaks in larval samples to the presence of the somatic tissue and periostracum which they termed amorphous material (Medakovic et al 1997). However, this description of amorphous material has been misinterpreted for presence of the inorganic calcium carbonate precursor, ACC, in subsequent reports. More recently, XRD analyses have produced conflicting results, suggesting the presence of ACC in larval oysters (Miyazaki et al 2010). For example, a lack of crystal derived peaks in XRD analyses coinciding with increases in calcium (EDS analyses) have led to descriptions of the presence of ACC in veliger larvae of *Pinctada fucata* (Miyazaki et al 2010).

The key paper describing ACC as a precursor phase for aragonite during larval calcification was proposed by Weiss et al (2002) based on analysis of veliger larval shells using Raman and Fourier transform infrared (FTIR) spectroscopy in the bivalves, *Mercenaria mercenaria* and *Crassostrea gigas* and suggested the presence of ACC in both species. In contrast, recent evidence using Focused Ion Beam Transmission Electron Microscopy (FIB-TEM) techniques demonstrate the presence of crystalline aragonite in the veliger larvae of the

oysters *Crassostrea nippona* and *Pinctada fucata*, with no evidence for an ACC phase (Kudo et al 2010, Yokoo et al 2011). Table 1.1 summarizes the main findings of studies investigating the composition of mollusc larval shells published to date.

Table 1.1 Techniques used to study mineral composition and main findings of studies investigating calcification in larval molluscs. Note the lack of species specific patterns in reported observations of ACC.

Publication	Species	Class	Technique	Shell Composition
Stenzel (1964)	*Crassostrea virginica*	Bivalvia	XRD	Aragonite
LaBarbera (1974)	*Tridacna squamosa*	Bivalvia	XRD	Aragonite
Carriker and Palmer (1979)	*Crassostrea virginica*	Bivalvia	XRD	Aragonite
Iwata (1980)	*Haliotis discus hannai*	Gastropoda	XRD, Electron diffraction	Aragonite
Waller (1981)	*Ostrea edulis*	Bivalvia		Aragonite
Eyster (1986)	*Crepidula fornicate* and *Aeolidia papillosa*	Gastropoda	XRD	Aragonite
Castilho (1989)	*Anodonta cygnea*	Bivalvia	XRD	Aragonite
Medakovic et al (1989)	*Ostrea edulis*	Bivalvia	XRD	Aragonite
Lee (1990)	*Crassostrea virginica*	Bivalvia	Electron diffraction	Aragonite
Togo et al (1991)	*Neptunea arthritica*	Gastropoda	XRD	Aragonite
Medakovic et al (1997)	*Ostrea edulis*	Bivalvia	XRD	Aragonite
Medakovic (2000)	*Mytilus edulis*	Bivalvia	XRD	Aragonite
Hasse et al (2000)	*Biomphalaria glabrata*	Gastropoda	XRD and X-ray absorption spectroscopy	ACC
Mao Che et al (2001)	*Pinctada margaritifera*	Bivalvia	XRD	Aragonite

Weiss et al (2002)	*Mercenaria mercenaria* and *Crassostrea gigas*	Bivalvia	Raman and FTIR spectroscopy	ACC
Marxen (2003)	*Biomphalaria glabrata*	Gastropoda	XRD and X-ray absorption spectroscopy	ACC
Lee (2006)	*Crassostrea gigas*	Bivalvia	XRD and FTIR spectroscopy	Aragonite
Marxen (2008)	*Biomphalaria glabrata*	Gastropoda	Synchrotron radiation microcomputer tomography	Aragonite
Jardillier et al (2008)	*Haliotis tuberculata*	Gastropoda	Raman and Infrared spectroscopy	Aragonite
Auzoux-Bordenave et al (2010)	*Haliotis tuberculata*	Gastropoda	Energy dispersive X-ray spectrometry and infrared spectroscopy	ACC
Kudo et al (2010)	*Crassostera nippona*	Bivalvia	FIB-TEM	Aragonite
Miyazaki et al (2010)	*Crassostrea gigas* and *Pinctada fucata*	Bivalvia	XRD and energy dispersive X-ray spectrometry	ACC
Yokoo et al (2011)	*Pinctada fucata*	Bivalvia	FIB-TEM	Aragonite
Thompson et al (2014)	*Argopecten*	Bivalvia	Raman	Aragonite

	irradians, *Mercenaria mercenaria*, *Crassostrea virginica*, *Mulinia lateralis*, *Tagelus plebeius*, *Ischadium recurvum* and *Rangia cuneata*	spectroscopy

Parallel to direct investigations of mineral composition in larval mollusc shells, studies have also proposed the presence of ACC based on structural observation derived from scanning electron microscopy (SEM, Weiss et al 2002). Structural analysis of bivalve larval shells using SEM, reveals the presence of three distinct layers in the larval shell: an outer prismatic layer, a granular-homogenous layer and an inner prismatic layer (Fig 1.3, Waller 1981, Weiss et al 2002). Etching of the larval shells of *M. mercenaria* using deionized water, revealed substantial dissolution of the mineral within the granular-homogenous layer. Etching experiments are based on the relative stability of crystalline calcium carbonate polymorphs in water. In comparison, ACC phases exhibit significant dissolution of mineral surface exposed to water. In addition, dissolution was also detectable in the prismatic layer, which led authors to suggest both layers contain significant amounts of ACC (Weiss et al 2002). In contrast, Kudo et al (2010) demonstrated the granular-homogenous layer to be composed of only crystalline aragonite in veliger shells of *C. nippona*. Therefore, inconsistencies remain regarding the occurrence and the functional role of calcium carbonate polymorphs in bivalve development, with direct *in vivo* investigations of larval calcification lacking.

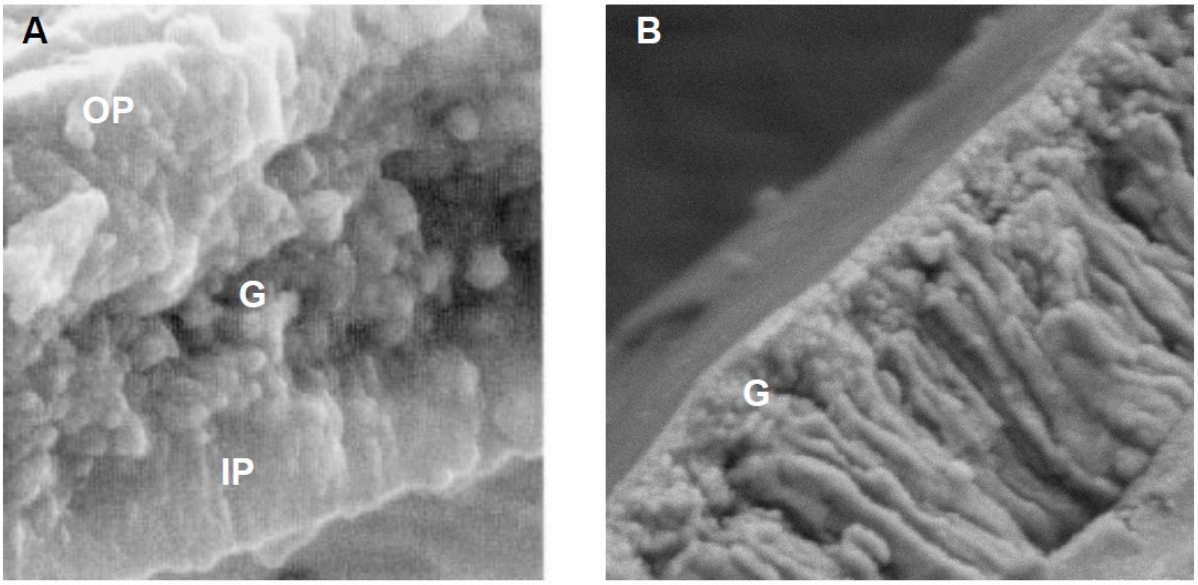

Figure 1.3 Scanning electron micrographs demonstrate that the larval bivalve shell consists of distinct layers (A) PD I larval shell of *Mercenaria mercenaria* exhibiting three layers, Adapted from Weiss et al (2002) and (B) PD I larval shell of *Mytilus edulis* exhibiting a distinct granular-homogenous layer (Ramesh and Melzner, unpublished). Abbreviations: outer prismatic (OP), Granular-homogenous (G) and inner prismatic (IP).

1.3 Mechanisms of ion transport for mollusc shell formation

1.3.1 Transcellular and paracellular pathways

Ion transport and homeostasis are essential physiological processes underlying calcification. In molluscs, the process of shell biomineralisation requires the uptake, storage and transport of many ions, particularly calcium (Ca^{2+}) and bicarbonate (HCO_3^-). These ions may be transported to the site of calcification across cell membranes, via active ion transport proteins and secondary acid-base/ion regulatory membrane bound proteins (transcellular pathway). Evidence in support of an active, energy consuming, transcellular pathway during calcification in molluscs is derived from pharmacological data demonstrating the inhibition of membrane-bound acid-base regulatory proteins coupled to reductions in calcification (Ebanks et al 2010a, 2010b) and trace element/calcium ratios (Carre et al 2006). In addition, molecular cloning, localization and expression of calcium ATPases (Ca^{2+} ATPase) in the calcifying mantle tissue of oysters provides circumstantial evidence for calcium transport through a transcellular pathway during calcification (Fan et al 2007, Wang et al 2008). However, the calcium transport proteins that have been characterized in adult molluscs lack functional evidence for their role in calcification. For instance, the putative role of these transport proteins in calcification is based on cloning and localized expression patterns of Ca^{2+} ATPase isoforms (Fan et al 2007). In addition, the function and activity of these proteins has not been investigated in mollusc larvae. The cellular pathways elicited for the transport and

accumulation of Ca^{2+} and HCO_3^- are fundamentally conserved in eukaryotes and all typical ion transport proteins are present in molluscs (Zhang et al 2012). Therefore, the mechanisms to transport ions and generate cellular electrochemical gradients are likely conserved in molluscs. In addition to acquisition of the substrates for calcification (Ca^{2+} and HCO_3^-), calcifying organisms also need to remove equivalent amounts of proton (H^+) end products from the site of calcification (Thomsen et al 2015). To enable the translocation of protons, organisms may employ active transport proteins (V-type H^+-ATPase, H^+/K^+-ATPase) or secondary active transport proteins (Na^+/H^+ exchangers, voltage gated H^+ channels). The activity of such H^+ translocation pathways is supported by evidence of expression (Barron et al., 2012; Li et al., 2016; Mann and Jackson, 2014) and activity (Kaloyianni et al 2005) in several mollusc species. In mollusc larvae, it is unclear which proton extrusion pathways play a role in regulating pH at the site of calcification. Evidence based on empirical studies on human erythrocytes for calcium-proton exchange via a Ca^{2+} ATPase has been proposed as a pathway in marine calcifiers but requires critical review (Niggli et al 1982, Kingsley and Watabe 1987, McConnaughey and Falk 1991, McConnaughey and Gillikin 2008).

Organisms may also employ the paracellular pathway where ionic substrates for calcification (Ca^{2+}, HCO_3^-) are acquired by diffusion and convection of Ca^{2+} and HCO_3^- across epithelia from seawater to the calcification space. For the freshwater mollusc, *Anodonta cygnea*, it has been demonstrated that the paracellular pathway in calcifying mantle epithelia accounts for ca. 50% of calcium transport (Bleher and Machado 2004). In other calcifying phyla, experiments with membrane impermeable dyes such as calcein suggest a paracellular route by which these molecules are incorporated into calcified coral skeletons (Erez and Braun, 2007, Tambutté et al 2011, 2012, Gagnon et al 2012). Finally, it is also possible that calcification substrates are accumulated intracellularly within vesicles, which are then deposited into the growing shell via exocytosis. Such a mechanism of intracellular calcification has been demonstrated in sea urchin larvae (Vidavsky et al 2014, 2015, 2016), where numerous large vesicles >1 µm accumulate ACC for subsequent deposition into the larval skeleton, where it then transforms to calcite. In mollusc larvae, no such investigations of intracellular calcification have been attempted. However, evidence for ACC precursors during larval shell formation (Weiss et al 2002) lends support to the intracellular calcification pathway in molluscs. In addition, presence of crystalline calcite in oyster hemocytes and subsequent deposition onto the shell has been observed during induced shell repair (Mount et al 2004, Johnstone et al 2015).

At present it remains largely unknown in molluscs to which extent these different pathways (transcellular, paracellular, vesicular) contribute to calcification. In particular, the mechanisms underlying substrate transport during early ontogenetic stages of molluscs remain an enigma, despite their rapid calcification rates.

1.4 Larval calcification in molluscs is vulnerable to environmental stress

Decreases in seawater pH driven by increases in anthropogenic CO_2, termed as ocean acidification (OA) is also coupled to a reduction in the availability of carbonate ions (CO_3^{2-}) as illustrated in the Bjerrum plot (Fig 1.4). Diffusion of CO_2 in seawater results in formation of carbonic acid, which is followed by a dissociation of bicarbonate (HCO_3^-), CO_3^{2-} and excess protons. However, the equilibrium of dissolved inorganic carbon (the sum of the concentrations of three coexisting species: HCO_3^-, CO_3^{2-}, and uncharged dissolved CO_2) is pH dependent.

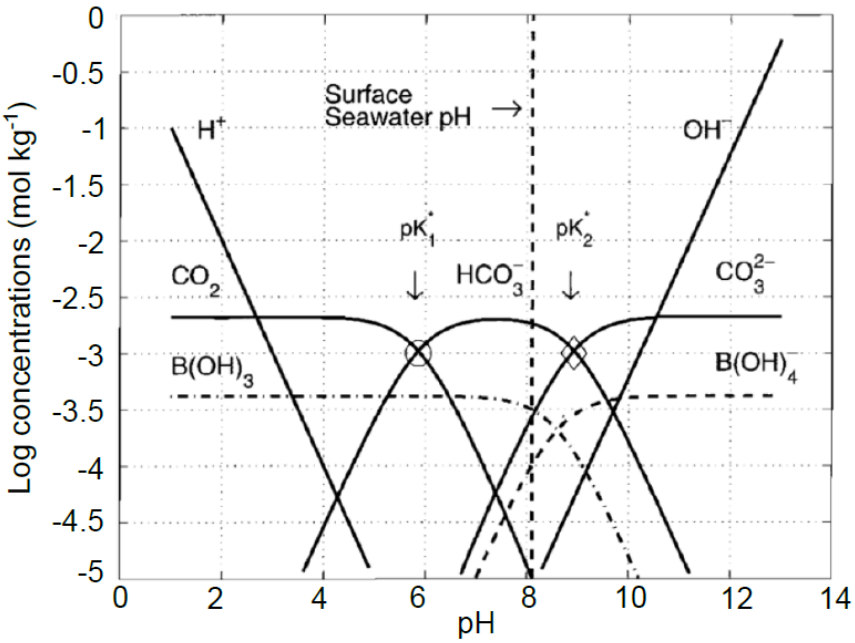

Figure 1.4 pH dependency of the three carbonate system species: CO2, HCO3- and CO32-.The dashed line illustrates the mean ocean surface pH (Taken from Zeebe and Wolf-Gladrow 2001).

As a result of the shift towards decreased [CO_3^{2-}] by increased [CO_2], the saturation state (Ω) of the different polymorphs of calcium carbonate ($CaCO_3$) will also decrease in line with equation (1):

$$\Omega = \frac{[Ca^{2+}] \times [CO_3^{2-}]}{K_{sp}} \qquad (1)$$

where 'K_{sp}' is the thermodynamic solubility product specific for the calcium carbonate polymorph formed. The rates of inorganic $CaCO_3$ precipitation (r) are related to Ω by equation (2):

$$r = k(\Omega - 1) \quad (2)$$

where 'k' is the calcification constant (Morse et al 2007). Therefore, for a given system where 'k' is constant, calcification rates equal zero when Ω = 1. Consequently, larval calcification in molluscs is intrinsically linked to modifications of seawater carbonate chemistry. Direct and indirect effects of increased anthropogenic CO_2 have been widely investigated and early ontogenetic stages have been identified to be particularly sensitive to predicted changes in ocean chemistry resulting from increased atmospheric CO_2 concentrations (Sabine et al 2010, Barton et al 2012, Waldbusser et al 2013, 2015). Early ontogenetic stages of bivalve molluscs have been observed to exhibit reductions in growth and calcification rates, increased shell malformations, shell dissolution and reduced survival as a result of elevated atmospheric CO_2 (Gazeau et al 2010, 2013, Barton et al 2012, Ventura et al 2016, Frieder et al 2017). Although, in several bivalve species, survival has been shown to be unaffected by increased atmospheric CO_2, despite reduced growth and calcification (Miller et al 2009, Gaylord et al 2011, Bechmann et al 2011). In addition, empirical studies have demonstrated that bivalve larvae continue to secrete aragonitic shells even when surrounding seawater is undersaturated with respect to Ω_{arag} (Waldbusser et al 2013, 2015), despite its relative solubility in comparison to other crystalline polymorphs such as calcite (Raz et al 2002). Therefore, it has been suggested that bivalve larvae must modulate the carbonate chemistry at the site of calcification to maintain mineral deposition (Waldbusser et al 2015). Evidence for active regulation of carbonate chemistry at the site of calcification has been demonstrated for several marine organisms (de Nooijer et al 2009, Cai et al 2016, Cornwall et al 2017, Comeau et al 2017). However, no direct measurements of the abiotic conditions at the site of calcification in larval molluscs have been conducted to date.

The expected processes of seawater acidification are particularly pertinent to coastal zones, where carbonate chemistry of seawater is subjected to seasonal upwelling events and hypoxia (Melzner et al 2013, Thomsen et al 2013, 2017a, b). Such seasonal changes in carbonate chemistry may act as a synergistic or additive stress to organisms encountering OA (Melzner et al 2013). Although upwelling events have been observed to result in mass

mortality of calcifying bivalve larvae (Barton et al 2012), more recently the role of such seasonal cycles is examined in defining organismal adaptation potential to OA (Thomsen et al 2017a). The Baltic Sea is among the coastal ecosystems that experiences seasonal upwelling events that are characterized by drastic increases in seawater pCO_2 (Sarderne et al 2013, Thomsen et al 2017a). In addition to OA, reductions in [Ca^{2+}] (for example as a result of low salinity) can also negatively affect larval calcification by decreasing Ω according to equations (1) and (2). For example, in the freshwater gastropod, *Lymnaea stagnalis*, larvae exposed to reduced availability of [Ca^{2+}] exhibited reduced growth rates (Ebanks et al 2010b). However, the relationship between [Ca^{2+}] availability and marine mollusc calcification remains poorly understood. Projected changes in precipitation patterns as a result of climate change will induce a reduction in salinity and consequently, [Ca^{2+}] for the Baltic Sea (Gripenberg 1937, Ohlson and Anderson 1990, Kremling and Wilhelm 1997). For the Baltic Sea catchment area, a projected decrease in salinity between 29 and 45 % is expected (Meier et al 2006). Previous research has demonstrated that growth rates in juvenile *M. edulis* and larval shell lengths are reduced at low salinities (Innes and Haley, 1977, Almada-Villela 1984, Sanders et al 2018). However, these studies did not examine the influence of [Ca^{2+}] on *M. edulis* calcification and physiology at reduced salinities. Finally, in addition to expected salinity driven decreases in [Ca^{2+}], calcification in the Baltic blue mussel, *M. edulis* x *trossulus* will also be affected by salinity driven changes in total inorganic carbon (C_T). C_T is predominantly controlled by the total alkalinity (A_T) of a system and with regard to the Baltic Sea, A_T has been demonstrated to correlate with salinity for different basins, with the exception of the Gulf of Riga (Beldowski et al 2010). This emphasizes the need to investigate the relationship between larval calcification and [Ca^{2+}], particularly in the context of predicted climate change (low salinity, low [Ca^{2+}], high pCO_2, low pH, low C_T).

1.5 Bivalves as a model for the study of shell development processes

Bivalves such as *Mytilus edulis* are important reef-forming foundation species that provide vital ecosystem services including shoreline protection, aquaculture and water filtration (Ekstrom et al 2015). Within certain regions of the Baltic Sea, the blue mussel, *M. edulis* x *trossulus* complex has been observed to contributte up to 80% of the total animal biomass in hard bottomed ecosystems and is responsible for increased biodiversity of benthic invertebrates compared to habitats where mussels are absent (Jansson and Kautsky 1977, Kautsky 1982, Norling and Kautsky 2008). Bivalves such as *M. edulis* are important reef-

forming, ecosystem engineers that impact the diversity and productivity of their surrounding habitats. For these reasons, species such as *M. edulis* have been employed to study several developmental processes including shell formation (Kniprath 1980, Medakovic 2000, Marie et al 2011). Recent genomic and proteomic advances have presented avenues for novel research to clarify unknown aspects of bivalve shell formation (Jackson et al 2010, Zhang et al 2012, Hüning et al 2013, 2016). Organic components present in mollusc shells and the genes involved in adult molluscan biomineralisation are beginning to be identified (Jackson et al. 2006, 2010, Wang et al. 2011, Arivalagan et al 2016, Feng et al 2017). However, understanding of how these genes are regulated during larval calcification is elusive. More recently, studies have focused on the effects of anthropogenic increases in atmospheric CO_2 on aspects of bivalve larval calcification including calcification rates, shell length and structure (Gazeau et al 2013, Ventura et al 2016, Fitzer et al 2016). Due to the increased research on the effects of climate change and carbonate chemistry on bivalve larval calcification, focus is required to understand basic calcification processes to accurately identify relationship between environmental conditions and vulnerability of these processes. However, to date there is no information available regarding the abiotic conditions facilitating rapid PD I shell formation and ion transport pathways involved in calcification in larval bivalves. This thesis characterizes the formation of the first shell in *M. edulis* and sheds light on the framework for bivalve larval calcification.

1.6 Research Questions

Does ACC form a bulk of shell carbonates during larval development?

Analysis of PD I larval shells using Raman and infrared spectroscopy in the bivalves, *Mercenaria mercenaria* and *Crassostrea gigas* suggested the presence of an ACC precursor phase, in both species during shell formation which subsequently transforms to aragonite (Weiss et al 2002). However, more recently, studies have found no evidence for ACC in PD I larval shells of oysters using Focused Ion Beam Transmission Electron Microscopy (FIB-TEM) techniques (Kudo et al 2010, Yokoo et al 2011). Rather, these authors exclusively observed the presence of crystalline aragonite in the veliger larvae of the oysters *Crassostrea nippona* and *Pinctada fucata*, with no evidence for the intermittent presence of an ACC phase (Kudo et al 2010, Yokoo et al 2011). The conflicting results mentioned above illustrate the need for studying more species using a variety of methodological approaches. In addition to analyses of the PD I larval shell, investigations of ACC as a precursor prior to the deposition of the first mineralized structures (during trochophore stages) is crucial to understanding the role of ACC throughout larval shell formation. Within this thesis, I address whether ACC is a precursor phase involved in blue mussel (*Mytilus edulis*) shell formation using *in vivo* confocal Raman microscopy (CRM) for the first time.

Which cellular pathways for ion transport are implicit in *M. edulis* larval calcification?

Bivalve larvae exhibit immense calcification rates where they can precipitate a shell mass that is almost equivalent to their own body mass within two days (Waldbusser et al 2013). However, the cellular mechanisms underlying transport of calcification substrates (Ca^{2+}, HCO_3^-) to the site of calcification remain largely unexplored in these ontogenetic stages. In sea urchin larvae, calcification has been observed to occur through the accumulation of ACC within vesicles that are subsequently deposited into the larval skeleton (Vidavsky et al 2014). Evidence for ACC precursors during larval shell formation in bivalves (Weiss et al 2002) supports the hypothesis of vesicular transport of calcification substrates. In order to determine the pathways enabling transport of calcification substrates (Ca^{2+} and CO_3^{2-}), I subject larvae to calcein pulse-chase experiments to follow the accumulation and deposition of calcium. In addition, I subject larvae to conditions of substrate limitation (low C_T) that has been previously demonstrated to negatively impact larval calcification (Thomsen et al 2015). Subsequently, I examine larvae for their transcriptomic responses to substrate limitation to identify candidate ion transport pathways of Ca^{2+} and HCO_3^-. Finally, I investigate the developmental expression

patterns of key ion transport proteins to shed light on the role of these transporters during larval calcification.

What are the abiotic conditions of extracellular space at the mineral interface in rapidly calcifying *M. edulis* larvae?

Critical to the biomineralisation process is the ability of organisms to regulate pH at the site of calcification. For example, foraminifera have been observed to show alkaline conditions by over 0.5 pH units (Erez 2003) and corals by over 1 pH unit (Al-Horani et al 2003). However, it is unclear to what extent bivalve larvae can control the carbonate chemistry of the extracellular space underneath the shell. Recent studies have demonstrated that bivalve larvae are able to develop shells even when the surrounding seawater is undersaturated with respect to Ω_{arag} (Gazeau et al 2010, Waldbusser et al 2015). Therefore, it has been suggested that larvae are capable of elevating Ω_{arag} at the site of calcification via active ion transport mechanisms (Waldbusser et al 2015). Using glass, ion-selective microelectrodes, I examined pH, $[CO_3^{2-}]$ and $[Ca^{2+}]$ in the calcifying, D-veligers to calculate the carbonate chemistry at the mineral interface of *M. edulis* larvae in order to understand the biological control larval *M. edulis* exhibit on their calcifying space.

How are the abiotic conditions of the extracellular space at the mineral interface affected by changes in seawater pCO_2 and $[Ca^{2+}]$?

It has been demonstrated that *M. edulis* larvae successfully develop and settle in spite of fluctuating pCO_2 between ca. 260 and 2800 µatm and the elevated mortality at 2400 µatm (Thomsen et al 2017). In addition to conditions of low pH driven by anthropogenic increases in CO_2 and upwelling events, estuarine mussel populations are likely to face conditions of reduced salinity and $[Ca^{2+}]$ also resulting in lowered Ω_{arag} (Meier et al. 2006; Gräwe et al. 2013). This ability to calcify under conditions of low Ω_{arag} may result from the ability to protect calcified shells by modulating the organic cover (periostracum) and composition of the organic matrix. Alternatively, larvae may be able to protect their shells from dissolution by modulating the carbonate chemistry of the extracellular space below their shells. In order to obtain a mechanistic understanding of the processes leading to physiological vulnerability to OA, I performed experiments to measure the abiotic conditions at the mineral interface in larvae exposed to range of seawater pCO_2.

2. Results

List of manuscripts and declaration of my contribution to the following manuscripts:

Manuscript 1

Kirti Ramesh, Frank Melzner, Andrew W. Griffith, Christopher J. Gobler, Caroline Rouger, Deniz Tasdemir & Gernot Nehrke (*in review*) *In vivo* characterisation of bivalve larval shells: a confocal Raman microscopy study. Journal of the Royal Society Interface.

I designed the study together with my thesis advisor, Frank Melzner and maintained larval cultures of *Mytilus edulis*. Together with the last author, I collected and analysed the data. I wrote the manuscript together with Gernot Nehrke, with support from Frank Melzner. All coauthors contributed to manuscript revisions.

Manuscript 2

Kirti Ramesh, Marian Y. Hu, Jörn Thomsen, Markus Bleich & Frank Melzner (2017) Mussel larvae modify calcifying fluid carbonate chemistry to promote calcification. Nature Communications 8: 1709. doi:10.1038/s41467-017-01806-8

I designed and performed the experiment together with my thesis advisor, Frank Melzner. I wrote the manuscript together with Frank Melzner. All coauthors contributed to manuscript revisions.

Manuscript 3

Jörn Thomsen, **Kirti Ramesh**, Trystan Sanders, Markus Bleich & Frank Melzner (*in review*) Calcification in a marginal sea – influence of seawater [Ca^{2+}] and carbonate chemistry on bivalve shell formation. Biogeosciences.

The first author, Jörn Thomsen designed the study and carried out calcium limitation experiments. I performed the microelectrode measurements to characterise [Ca^{2+}] dynamics in the calcification space of larvae. Jörn Thomsen wrote the manuscript and all coauthors contributed to manuscript preparations and revisions.

Manuscript 4

Kirti Ramesh, Tejaswi Yarra, Melody S. Clark, Uwe John & Frank Melzner (to be submitted to BMC Genomcs) Identification of ion transporters during calcification in the larval mussel, *Mytilus edulis*.

I designed the study together with my thesis advisor, Frank Melzner. I performed the experiment, library preparations for Illumina sequencing, analyzed the data and wrote the manuscript together with Tejaswi Yarra, with support from Frank Melzner..

In vivo characterisation of bivalve larval shells: a confocal Raman microscopy study

Kirti Ramesh[1], Frank Melzner[1], Andrew W. Griffith[2], Christopher J. Gobler[2], Caroline Rouger[1], Deniz Tasdemir[1], Gernot Nehrke[3]

[1]Marine Ecology, GEOMAR Helmholtz Centre for Ocean Research Kiel, Germany
[2]School of Marine and Atmospheric Sciences, Stony Brook University, Stony Brook, New York, USA
[3]Alfred Wegener Institute for Polar and Marine Research, Am Handelshafen 12, Bremerhaven, Germany

*Corresponding author (kramesh@geomar.de)

Abstract

In vivo confocal Raman microscopy (CRM), polarized light microscopy and Fourier transform infrared spectroscopy (FTIR) were used to determine if a significant amount of amorphous calcium carbonate (ACC) exists within larval shells of Baltic mytilid mussels and whether the amount of ACC varies during larval development. No evidence for ACC was found from the onset of shell deposition at 21 hours post fertilization (hpf) until 48 hpf. Larval *Mytilus* shells were crystalline from 21 hpf onwards and exhibited CRM and FTIR peaks characteristic of aragonite. Prior to shell deposition at 21 hpf, no evidence for carbonates was observed through *in vivo* CRM. We further analysed the composition of larval shells in three other species, *Mercenaria mercenaria*, *Crassostrea gigas* and *Crassostrea virginica* and observed no evidence for ACC, which is in contrast to previous work on the same species. Our findings indicate that larval bivalve shells are composed of crystalline aragonite and we demonstrate that conflicting results related to sub-optimal measurements and misinterpretation of CRM spectra. Our results demonstrate that the common perception that ACC generally occurs as a stable and abundant precursor during larval bivalve calcification needs to be critically reviewed.

Keywords: Aragonite, Larval Shell, Mussel

In vivo characterisation of bivalve larval shells: a confocal Raman microscopy study

Kirti Ramesh[1], Frank Melzner[1], Andrew W. Griffith[2], Christopher J. Gobler[2], Caroline Rouger[1], Deniz Tasdemir[1], Gernot Nehrke[3]

[1]Marine Ecology, GEOMAR Helmholtz Centre for Ocean Research Kiel, Germany
[2]School of Marine and Atmospheric Sciences, Stony Brook University, Stony Brook, New York, USA
[3]Alfred Wegener Institute for Polar and Marine Research, Am Handelshafen 12, Bremerhaven, Germany

Abstract

In vivo confocal Raman microscopy (CRM), polarized light microscopy and Fourier transform infrared spectroscopy (FTIR) were used to determine if a significant amount of amorphous calcium carbonate (ACC) exists within larval shells of Baltic mytilid mussels and whether the amount of ACC varies during larval development. No evidence for ACC was found from the onset of shell deposition at 21 hours post fertilization (hpf) until 48 hpf. Larval *Mytilus* shells were crystalline from 21 hpf onwards and exhibited CRM and FTIR peaks characteristic of aragonite. Prior to shell deposition at 21 hpf, no evidence for carbonates was observed through *in vivo* CRM. We further analysed the composition of larval shells in three other species, *Mercenaria mercenaria*, *Crassostrea gigas* and *Crassostrea virginica* and observed no evidence for ACC, which is in contrast to previous work on the same species. Our findings indicate that larval bivalve shells are composed of crystalline aragonite and we demonstrate that conflicting results are related to sub-optimal measurements and misinterpretation of CRM spectra. Our results demonstrate that the common perception that ACC generally occurs as a stable and abundant precursor during larval bivalve calcification needs to be critically reviewed.

Introduction

Molluscan larvae, whose calcium carbonate shells provide structural support and protection, exhibit much higher relative calcification rates than adult forms [1]. This high energetic investment renders them vulnerable to environmental disturbances such as ocean acidification [2, 3, 4]. The biological control and structural diversity of shell formation in molluscs has received much attention since a better understanding of biomineralisation processes is crucial to understand vulnerability to abiotic stressors [1, 5, 6, 7, 8]. Despite the high diversity in shell structure and polymorph composition found in adult mollusc shells, calcification during larval development is morphologically similar between species. Cell lineages involved in shell formation are homologous and exhibit a similar enzymatic histochemistry [9]. Further, preceding shell formation, the cellular differentiation processes of shell forming cells are conserved across molluscan classes [10]. In bivalves, ectodermal cells in the dorsal region thicken and invaginate to form the shell gland [9]. A subsequent evagination of the shell gland

and flattening of ectodermal cells gives rise to the so-called shell field [9]. Shell mineralization in bivalve molluscan larvae takes place during the trochophore larval stage, within the shell field region [11]. The shell field evaginates during the trochophore stage and the surrounding epithelia secrete an early organic layer which is assumed to protect the first shell structures from dissolution during adverse environmental conditions such as lowered saturation state for aragonite [3, 11]. This early organic layer is continually mineralized as it spans over the surface of the larval body, with a small fraction that remains unmineralized at the growing edge of the shell [12]. Shell calcification laterally compresses the larva and the epithelial cells within the shell field are presumably responsible for the secretion of the first larval shell, prodissoconch I (PD I, D-veliger stage) [13]. At this early stage, the shell is composed solely of aragonite [14, 15, 16, 17]. The formation of PD I is followed by the secretion of prodissoconch II (PD II, veliger stage), which is characterized by the presence of growth lines. The shell forming epithelial cells within the shell field ultimately differentiate into the shell-forming organ in juveniles and adults, the mantle. Following metamorphosis from the (pedi)veliger stage to juveniles, the mantle secretes new shell layers (dissoconch) at the edge of prodissoconch II that formed previously [10, 18].

Adult and juvenile mytilid shells consist of two distinct layers that are composed of different calcium carbonate polymorphs: aragonitic tablets (inner nacreous layer) and calcitic prisms (outer layer) [19]. However, within the first two days of development, larval bivalves rapidly secrete wholly aragonitic shells, the mass of which corresponds to ca. 90% of their somatic body mass [3]. This shell deposition process must involve a rapid accumulation and transport of calcium and carbonate ions to the shell field region. Organisms may utilize transepithelial transport (cellular and paracellular pathways) to enable accumulation of calcium and carbonate ions directly at the site of calcification. Alternatively, amorphous calcium carbonate (ACC) precursor phases could be accumulated intracellularly to be exocytosed onto the growing shell [20]. Such a mechanism has been demonstrated in larval echinoderms, where intracellular vesicles containing calcium carbonate are widely distributed across the larva and are subsequently deposited onto the larval spicules [21]. Such detailed understanding is lacking in mollusc larval stages. Analysis of larval bivalve shells (*Mercenaria mercenaria*, *Crassostrea gigas*) using Raman and infrared spectroscopy has also suggested the presence of an ACC precursor phase [22]. However, more recently, studies have found no evidence for ACC in larval shells of oysters using Focused Ion Beam Transmission Electron Microscopy (FIB-TEM) techniques [23, 24]. Rather, these authors exclusively observed the presence of crystalline aragonite in the veliger larvae of the oysters *Crassostrea nippona* and *Pinctada fucata*, with no evidence for the intermittent presence of an ACC phase [23, 24]. ACC is a highly unstable polymorph of calcium carbonate and its solubility is almost 30 times higher than that of aragonite [2, 25]. Therefore, an understanding of its role in

biomineralisation is crucial for predicting the vulnerability of early calcification processes to environmental disturbances, in particular of the oceanic carbonate system [1, 3].

The conflicting results mentioned above illustrate the need for studying more molluscan species using a variety of methodological approaches. Here, we address the question whether ACC is a precursor phase involved in mytilid mussel shell formation using *in vivo* confocal Raman microscopy (CRM) for the first time. CRM offers a high spatial (1 μm) and temporal resolution to follow the initial appearance of crystalline structures and to determine their phase composition from the earliest calcifying stages (trochophore stages) to D-veligers and freshly settled juveniles. In addition, we present results from Fourier Transform Infrared (FTIR) spectroscopy on *Mytilus* D-veliger shells and CRM analyses on larval shells from three additional bivalve species, *Mercenaria mercenaria*, *Crassostrea gigas* and *Crassostrea virginica* to investigate the role of ACC in bivalve larval shell formation.

Materials & Methods

Animal Collection & Larval Culture

Adult and juvenile mussels *Mytilus* were collected in Kiel Fjord (54°19.8'N; 10°9.0'E) in June 2015 and 2016. Kiel mytilids are *Mytilus edulis* x *trossulus* hybrids with a high *Mytilus edulis* fraction. We will refer to them as Baltic *Mytilus edulis*-like according to Stuckas et al. [26]. Adult animals were spawned as described previously, at pH_{NBS} 8.1 and a salinity of 16 psu [12]. Larvae were maintained at GEOMAR at 17°C until 48 hours post fertilization (hpf). Larvae from five separate fertilizations were analyzed for the presence of ACC, aragonite and calcite. Adult Pacific oysters, *Crassostrea gigas* were collected from Sylt, Germany and spawned as described previously [27] at pH_{NBS} 8.20 and a salinity of 34 psu. Larval cultures were maintained at GEOMAR at 22°C until 24 hpf, when D-veliger stages were reached. Adult hard clams, *Mercenaria mercenaria* were obtained from Ocean Rich distributors (Brookhaven, NY,USA) and adult Eastern oysters, *Crassostrea virginica* were obtained from the Shinnecock Bay Restoration Program (NY, USA; 40°51' 50.4''N; 72° 29' 27.6''W). Adult *M. mercenaria* and *C. virginica* were spawned as described previously at pH_{NBS} 8.12 and a salinity of 30 psu [28]. Larval cultures were maintained at 24°C until 12 days post fertilization (dpf, *M. mercenaria*) and 10 dpf (*C. virginica*) at Stony Brook University's Southampton Marine Sciences Center (Southampton, NY,USA). Baltic *Mytilus edulis*-like larvae were analyzed alive and frozen, whereas larvae of *M. mercenaria*, *C. gigas* and *C. virginica* were analyzsed frozen. Samples of *M. mercenaria* and *C. virginica* were transferred to GEOMAR, Kiel from the USA on dry ice.

Confocal Raman Microscopy

To investigate the calcium carbonate polymorphs present during shell formation of Baltic *M. edulis*-like, we used a WITec alpha 300R (WITec GmbH, Germany) confocal Raman microscope (CRM) equipped with a 488 nm laser diode housed at the Alfred Wegener Institute in Bremerhaven. An ACC standard was prepared at 1°C according to the method described in Rodriguez-Blanco et al. [29]. Briefly, equal volumes of cooled (1°C) 10 mM $CaCl_2$ and Na_2CO_3 solutions were combined and the resulting suspension was vacuum filtered (0.2µm). Stable ACC was recovered by washing the filtered solids with isopropanol and drying them in air. Reference spectra of calcite (Iceland spar) and aragonite (single crystal, Spain) were obtained using in-house standards also reported in a previous publication [30]. An ACC-aragonite mixture was prepared by mixing equal masses of powdered ACC and aragonite standards using a pestle and mortar. The resulting mixture was placed between a glass slide and coverslip and mapped using CRM to demonstrate the ability of the technique to discriminate between multiple calcium carbonate polymorphs in a sample. Initial analyses were performed on frozen, 48 hpf D-veliger Baltic *M. edulis*-like larvae that were stored and prepared as described by Weiss et al. [22]. In brief, 48 hpf larvae were shock-frozen in liquid nitrogen and stored at -20°C till further use. Samples were thawed at room temperature and analysed wet on calcium fluoride discs (Korth Kristalle GmbH, Germany). *In vivo* Raman measurements were performed on Baltic *M. edulis*-like larvae between 20-48 hpf. The same samples investigated by means of CRM *in vivo* measurements were characterized using a Zeiss Axio Scope.A1 polarized light microscope, located beside the CRM instrument. *In vivo* measurements on individual larvae at the CRM were performed for up to 1 hour and vitality of larvae was ensured by visual observation of ciliary movement. Larvae were concentrated in filtered seawater (0.2 µm) using a 20 µm sieve. The drop containing the larvae (ca. 30 µL) was sandwiched between a glass slide and a glass coverslip, using cotton fibres as a spacer to prevent damages and confine the larvae in a hydrated environment. CRM measurements on Baltic *M. edulis*-like shells exhibited the presence of the typical Raman peaks associated with polyenes [22]. The polyene related Raman peak in Baltic *M. edulis*-like (at 1098 rel.cm^{-1}) occurs very close to the position of the strongest carbonate peak for calcite and aragonite (1086 rel.cm^{-1}) (e.g. [31, 32]). High spectral resolution grids (grating with 1800 g/mm and 2400g/mm, BLZ 500 nm) were used to allow resolve these peaks. Resin-embedded (Araldite 2020, Huntsman International LLC., USA), polished cross-sections of freshly settled juveniles from Kiel Fjord were used to study the transition zone of the larval shell to the dissonconch. Briefly, cross sections of juvenile Baltic *M. edulis*-like resin embedded shells were ground on a LOGITECH PM2A Precision Lapping/Polishing Machine using waterproof silicon carbide paper in the qualities of P1200, P2400, P4000 (Struers, Denmark). This grinding step was followed by a polishing step using a Struers diamond suspension of 3µm and subsequent rinsing of the sample using de-ionised water. A detailed description of the method used to map and identify the

calcium carbonate polymorph distribution by CRM was described elsewhere [33, 34]. Raman spectra for frozen D-veliger larvae of the three additional species were collected on wet samples using a water immersion objective (Nikon, NIR APO 60x, WI NA 1.0). The *in vivo* CRM measurements (larval samples) were performed using a 20x objective (Zeiss, LD Plan NeoFluar NA 0.4). Juveniles were measured using a Zeiss LD Plan NeoFluar 20x objective having a numerical aperture of 0.4. For each sample, 5–10 spectra were acquired along a transect across the longitudinal section of the shell. Spectral analysis and image processing were performed using WITec Project software v. 2.04 (WITec GmbH, Germany). Spectra were plotted using R (Version 3.3.2, R Development Core Team, R: http://www.R-project.org/. 2011) and packages ggpmisc, ggplot2 and ggspectra.

Fourier Transform Infrared Spectroscopy (FTIR)

Reference spectra were measured for powdered aragonite and ACC standards that were prepared or acquired as described above. Infrared absorption spectra for larval shells were obtained according to Weiss et al. [22]. Briefly, ca. 100,000 Baltic *M. edulis*-like larvae were harvested at 48hpf and shock frozen in liquid nitrogen. Samples were stored at -20°C for subsequent analyses and thawed at room temperature prior to use. Larval shells were treated with 2.5% sodium hypochlorite for seven minutes followed by three rinses in de-ionized water to remove organic tissue [35]. Larval shells were subsequently air dried and ground to a fine powder using a plastic pestle suitable for Eppendorf tubes. FTIR spectra were collected using a Spectrum Two FT-IR spectrometer (Perkin Elmer), equipped with a UATR (single reflection diamond) on dried larval shell powder. Spectra were obtained in the range of 450-4000 cm^{-1} and Spectrum 10 software was used to perform background subtractions.

Replication

In vivo CRM spectra were collected from four Baltic *M. edulis*-like larvae at both 20 hpf and 21 hpf, for least three positions on the shell of each larvae. Additionally, 3 and 5 Baltic *M. edulis*-like larvae were measured using CRM at 25 hpf and 28 hpf, respectively. For analyses on frozen D-veligers, spectra were collected from 15, 5, 4 and 5 larvae of Baltic *M. edulis*-like, *M. mercenaria*, *C. virginica* and *C. gigas,* respectively, with spectra taken from 4-8 positions of the shell, per larva. CRM spectra were collected from 3 juvenile animals at 4-10 positions along the shell.

Results

The initial larval shell formation was detected at 21 hpf by using the birefringence of aragonite observed between crossed polarizers (Fig. 1A, [12]). The birefringence increased gradually and was observed for both shell valves (arrows in Fig. 1B). The mineralized shell entirely covered the embryo surface after 48 hpf. No birefringence was observed before 21 hpf, indicating the absence of a shell.

However, larvae exhibited an evagination of the shell field, which has been previously been determined to be related to the presence of an early organic layer between 18-20 hpf [12]. Spectral analysis of the region of the shell field prior to calcification at 18 hpf, using multiple point measurements, revealed characteristic spectra for organic pigments at 1157 and 1524 rel. cm^{-1}(Fig. 1D). Spectra of organic shell polyenes following calcification in Baltic *M. edulis*-like larval shells showed peaks at 1098 and 1479 rel. cm^{-1} (Supplementary Fig S1).

We next analyzed the larval shells at their earliest presence and followed their growth. In order to identify the occurrence ACC, we measured an ACC standard (showing a characteristic Raman peak at 1079 rel. cm^{-1}, Fig. 1F1, 1F2, Table 1) and aragonite and calcite standards showing characteristic peaks for aragonite at 155.3, 208.9 rel. cm^{-1} and 1086 rel. cm^{-1} with double peaks at 702.6 and 704.8 rel. cm^{-1} (Fig. 1G1, 1G2, Table 1) and characteristic peaks for calcite at 156, 283.1 and 1087 rel. cm^{-1} (Table 1). The standards were measured under the same conditions (laser intensity, pinhole) as the samples to guarantee comparability. Note the difference of seven to eight wave numbers between the spectra of ACC and crystalline phases for the carbonate stretching mode (1079 (ACC) versus 1086 (aragonite), Fig. 1F2, 1G2). This difference in stretching mode is due to the fact that each calcium carbonate polymorph has a unique set of Raman bands, related to their unique structure. The bond length, bond strength and thus the structural neighborhood around the CO_3^{2-} groups differs, resulting in different positions of the Raman peaks [33, 36]. A Raman spectrum obtained from a sample in which two phases are present will result in a spectrum that exhibits the peaks of both phases, but peaks will not merge into one peak with an intermediate peak position. We prepared and mapped an ACC- aragonite mixture to highlight the suitability of the CRM techniques to detect multiple phases present in a sample, on a nanometer scale using appropriate grids (2400 g/mm, BLZ 500 nm). Fig. 2 demonstrates the suitability of CRM techniques to accurately distinguish peak positions of the v_1 carbonate stretching mode in the ACC-aragonite mixture mapped, where the presence of ACC can be inferred from the asymmetric shape of the v_1 peak due to the addition of the characteristic v_1 band of ACC at 1079 rel.cm^{-1} (Fig. 2 B-C). Similar asymmetric v_1 peaks were found by Jacob et al. [37] when studying ACC – crystalline carbonate mixtures present in the sternum of the isopod, *Porcellio scaber*.

In vivo CRM spectral analyses of Baltic *M. edulis*-like trochophore larval shells at 21 hpf reveal peaks at 703.1-703.8 and 1086 rel. cm^{-1}, indicating the presence of aragonite as the major fraction of shell carbonate at the onset of shell formation. The larval shell at the PDI stage (48 hpf, 106 $\pm$ 2.3 µm length, Fig. 3A) shows characteristic aragonite peaks at 155, 207, 704 and 1087 rel. cm^{-1} (Fig. 3D). Fig. 1E shows the Raman spectral map for the carbonate stretching mode (1084.5-1086.5 rel. cm^{-1}) for the boxed region of a trochophore larva at 21 hpf in Fig. 1C. In addition, CRM spectra revealed strong

peaks at 1098 rel. cm^{-1} which is a reported polyene pigment peak specific to *Mytilus edulis* shells [31, 32]. All specimens examined exclusively contained aragonite in their larval shell. There was no evidence for the presence of ACC in the spectral analyses of Baltic *M. edulis*-like larval shells from the onset of calcification at 21 to 48 hpf. In order to test whether ACC precursors form the bulk of PD I larval shell carbonates in other bivalve species, we investigated Raman spectra of three additional larval bivalve species, *Mercenaria mercenaria*, *Crassostrea gigas* and *Crassostrea virginica*. The spectra from all three species exclusively revealed peaks at 155, 208, 703 and 1086 rel.cm^{-1} indicative of crystalline aragonite in the PD I shell (Fig. 4A-G).

A 2D Raman map was obtained for the cross section of the juvenile Baltic *M. edulis*-like shell to map the distribution of calcium carbonate polymorphs (Fig. 5A). The larval prodissoconchs clearly show the characteristic Raman peaks of aragonite at 155, 207 and 1087 rel. cm^{-1} (Fig. 5E, red). For the transition from aragonite to calcite, we recorded peaks specific to aragonite and calcite, indicating that the two polymorphs exist as distinct phases in the shell with no signs for ACC phases at the layer boundaries (Fig. 5). The transformation to a calcitic shell marks the starts of the dissoconch with characteristics calcitic peaks at 156, 282 and 1087 rel. cm^{-1} (Fig. 5F, blue).

Additional measurements using FTIR

The aragonite standard exhibited characteristic peaks of crystalline calcium carbonate polymorphs with distinct bands at 713 cm^{-1} (v_4), 860 cm^{-1} (v_2), a small band at 1086 cm^{-1} (v_1) and a large vibration between 1440–1500 cm^{-1} (v_3) (Fig. 6). FTIR spectra of the ACC standard are characterized by the lack of the vibration at v_4 region (713 cm^{-1}, Fig. 6) which is attributed to the OCO bending [38], consistent with previous research [39, 40]. Bulk measurements of Baltic *M. edulis*-like larval shell samples revealed peaks at 713 cm^{-1} and 860 cm^{-1} indicative of crystalline aragonite (Fig. 6).

Discussion

Polymorph composition of the shell

In this study, we aimed to clarify whether amorphous calcium carbonate (ACC) plays a major role in larval shell formation in Baltic blue mussels (*M. edulis*-like). At the onset of calcification during the trochophore stage (21 hpf), we observed characteristic spectra for aragonite using *in vivo* CRM analyses (Fig. 1). To our knowledge, this is the first *in vivo* phase identification in a mollusc species, and during early shell deposition (trochophore stage). This developmental point was chosen for analyses since previous work has demonstrated that mussel larvae do not accumulate calcium carbonate prior to this developmental time point [12]. Our data do not provide evidence for the presence of amorphous precursors during larval calcification in Baltic *M. edulis*-like, although we analyzed the larval shell at the earliest time point possible (trochophore stage). In addition, cross-

sections of juvenile Baltic *M. edulis*-like shells reveal a distinctive separation between aragonitic and calcitic areas. Raman scans of juvenile shells with a sub-micron scale spatial resolution provide no evidence for ACC in the region close to the outer organic layer (periostracum) as observed previously for two freshwater adult bivalve species, *Hyriopsis cumingii* and *Diplodon chilensis* using Raman spectroscopy and FIB-TEM, high resolution TEM and electron energy-loss spectroscopy methods [37]. The FTIR spectra collected from larval shells also exhibited only characteristic bands of aragonite with v_4 and v_2 bands at 713 cm^{-1} and 860 cm^{-1}, respectively (Fig. 6). As we could demonstrate that we are able to detect small quantities of ACC in ACC – aragonite mixtures (Fig 2), we are confident that we would have detected ACC if it had been present. Other investigators have determined ACC in biological samples using CRM, including marine taxa, which further lends support to our methods [25, 41, 42, 43].

Our findings suggest that the rapid calcification of PD I in Baltic *M. edulis*-like larvae may arise from the direct deposition of aragonite. Absence of ACC phases and direct deposition of crystalline phases has also been proposed for initial shell formation in bivalve larvae [23, 24], nacre formation in adult molluscs [44] and the polychaete larval tubeworms, *Hydroides elegans* [45]. The rapid precipitation of a crystalline shell supports the necessity for a rigid external skeleton during larval development in bivalves. Rapid PD I shell formation enables muscle attachment and lateral compression of the larval body for swimming and feeding [45]. Our results indicate that the observed sensitivity of larval bivalves to ocean acidification stress [1, 2, 3, 4] is not related to the presence of high amounts of ACC, which is more soluble than aragonite. Rather, the high sensitivity of larval bivalves to acidification may be associated with the reduced ability of these organisms to modulate the carbonate chemistry of their calcification space [12], limited maternally derived energy reserves [3] and the very high rates of shell deposition during that life stage [3, 46].

Our results conflict with those of Weiss et al. [22], as we could not detect ACC in veliger shells. We attribute these differences to a number of factors. First, it has to be pointed out that in the study of Weiss et al. [22], the identification of ACC in *Mercenaria mercenaria* larval shells was based on the presence of the Raman peak at 1087 rel. cm^{-1}, which is an incorrect assignment. 1087 rel. cm^{-1} is the typical peak position for calcite and aragonite, whereas the ACC peak is characteristically about 8 rel. cm^{-1} lower (1079 rel. cm^{-1}) [25, 29]. Second, weak peaks or absence of peaks at 156 and 205 rel. cm^{-1} (lattice modes) and analyses of peak intensity ratios of the lattice mode (205 rel. cm^{-1}) and v_1 peak (1086 rel. cm^{-1}) have been attributed to the presence of ACC phases in veliger larval mollusc shells [22]. However, weak peaks at 156 and 205 rel. cm^{-1} can be related to high background to signal ratio. Additionally, peak intensities at 156 and 205 rel. cm^{-1} are influenced by the orientation of crystallites as described by Nehrke & Nouet [47]. This is illustrated by Fig. 4A, B, D, where we analyzed the same

M. mercenaria larval shell with different lenses: the switch from a 20x to a 60x water immersion objective with a high numerical aperture reduces the background to signal ratios of Raman spectra. An important consideration during CRM analyses is the focal plane spectra are collected from due to the similarities in spectra between ACC and water (broad peak between wavenumbers 100-300 rel.cm^{-1}). However, the spectra for water are not accompanied by a v_1 peak for carbonate, as observed for ACC (Fig. 4C). We re-analysed both species studied by Weiss et al. ([22], *M. mercenaria*, *C. gigas*) and could not confirm the presence of ACC in their shells using our improved technical setup. Instead, we exclusively were able to detect aragonite as the major carbonate phase in D-veliger shells. By using a 488 nm laser to reduce intrinsic fluorescence we could acquire Raman spectra in both, *M. mercenaria* and *C. gigas* shells (Fig. 4F-G). For *C. gigas* shells, Weiss et al. [22] suggested that the peak height ratio of FTIR peaks at 856 cm^{-1}/713 cm^{-1} points towards the presence of ACC in larval shells. However, such ratios have been empirically demonstrated to be influenced by particle size [48] similar to particle sizes previously reported for ACC in larval shells [22] thus are not diagnostic for ACC. In addition, the presence of a peak at 713 cm^{-1} in FTIR spectra is characteristic of crystalline calcium carbonate polymorphs [41] and the assignment of amorphous phases using FTIR in other marine taxa is based solely on the lack of a peak at 713 cm^{-1} [39, 49]. Controlled ACC crystallization experiments by addition of water clearly demonstrate the appearance of a v_4 peak at 712 cm^{-1} in FTIR spectra [50]. Recently, it has been suggested that molluscan larvae may utilize seed crystals to initiate shell formation based on empirical data from a FIB-TEM study on the D-veliger larvae of *Pinctada fucata* [24]. FIB-TEM techniques have been demonstrated to suitably identify the presence of ACC in biological [51, 52] and synthetic samples [53], avoiding laser-induced transformation of ACC or cryogenic sample preparation. This novel model for larval shell formation suggests the direct precipitation of seed crystals onto the organic matrix, which subsequently induces the inorganic precipitation of carbonate mineral. Based on these observations and our findings, we suggest that the direct deposition of aragonite may be an alternative mechanism for initial shell formation in bivalve larvae. Alternatively, formation of ACC precursors that transform rapidly into a crystalline phase during larval calcification cannot be excluded, as we would have not been able to detect such a phenomenon with our methods. For example, DeVol et al. [54] observed ACC to be localized to small regions of the surface of nacre tablets in the abalone, *Haliotis rufescens* using nm resolution methods, photoemission electron spectromicroscopy (PEEM) and X-ray absorption near-edge structure (XANES) spectroscopy. In summary, evidence from the present study suggests that the major stable mineral phase during biomineralization in Baltic *M. edulis*-like larvae and juveniles, as well as other bivalve larvae, is crystalline calcium carbonate and not ACC.

Pigments in the shell

We show that prior to mineral deposition at 21 hpf, CRM analyses of larvae between 18-21 hpf reveals characteristic spectra for organic pigments in the region of the shell field (Fig. 1D). These peaks are located at 1158 and 1524 rel. cm^{-1}, which are characteristic peaks for carotenoid pigments attributed to the carbon-carbon double bond stretching mode and the carbon-carbon in-plane single bond stretching mode respectively (Fig. 1D, [55, 56]). The presence of carotenoids in molluscs is widely reported for soft tissues, shells and pearls with putative roles of these molecules in mollusc defence and crystallography [31, 57, 58]. The spectral position of Raman peaks for organic pigments such as carotenoids and polyenes relates to the structure and composition of these molecules, defined by the carbon-carbon bonds [31]. A comparison of our data with previous data for carotenoid pigments and polyenes in *M. edulis* and other species is given in Fig. 7A [31, 32, 55]. Note the distinctly different grouping of polyenes (shifted to smaller wavenumbers) in comparison to carotenoid pigments, where the peaks recorded in the present study prior to calcification fall in line with characteristic organic peaks for β-carotene in Fig 7A. In calcifying 21 hpf larvae, spectra for carotenoid pigments are recorded on the surface of the larval body whereas characteristic organic peaks for *M. edulis* polyene pigments around 1098 rel. cm^{-1} as reported by Hedegaard et al. [31] are only observed when calcium carbonate is incorporated (Fig.7-C), suggesting that these carotenoid pigments undergo structural changes when they are incorporated into the mineral phase. Despite the established association of polyene pigments in molluscan shells, there is no information on the mechanisms of shell pigment formation for any mollusc species. In corals, the structural transformation of polyenes within mineralized structures has been demonstrated by Maia et al. [59], where demineralization resulted in shifts of the polyene peaks, related to changes in the composition of double and single carbon bonds of pigments. Gene expression analyses for one shell protein (ependymin-related protein) revealed a strong correlation to shell pigmentation in the tropical abalone, *Haliotis asinina* [60]. These authors suggest that changes in the composition of polyenes during calcification may be linked to the formation of organic complexes with shell matrix proteins [60]. Formation of such organic complexes between calcium carbonate and carotenoids has been reported for the hydrocoral *Errina antarctica* [61]. To our knowledge, this is the first report of structural transformation (C=C and C-C bonds) from carotenoid pigments to the species-specific pigment polyenes in the shell of the Baltic *M. edulis*-like larvae. The conversion of carotenoids to species-specific shell polyenes may be a conserved mechanism and further analysis of pigments during the course of calcification in other mollusc species is needed to investigate this possibility.

Conclusions

(1) Initial crystal formation occurs during the swimming, trochophore stage observed using techniques suitable for the detection of ACC in biological samples.
(2) From the onset of calcification to the formation of the juvenile shell, there is no evidence for ACC precursors in Baltic *M. edulis*-like larvae using *in vivo* confocal Raman and FTIR spectroscopy.
(3) CRM analyses of veliger larval shells from three other bivalve species (*M. mercenaria*, *C. gigas*, *C. virginica*) exhibit characteristic spectra for aragonite challenging the current view of bivalve larval shell formation.
(4) During larval shell formation, polyenes are deposited within the shell that may derive form the structural transformation of carotenoid pigments, which are present within the shell field area prior to the formation of the mineral phase.

Author Contributions

KR and FM designed the study and maintained larval cultures. AG and CG cultured and provided samples of *Mercenaria mercenaria* and *Crassostrea virginica*. KR, GN and FM collected data. KR and GN analysed the data. KR, FM and GN wrote the manuscript. CR and DT supported FTIR measurements. All authors commented on the manuscript and gave their final approval for publication.

Conflicts of Interest

The authors declare no competing interests.

Acknowledgments

The authors thank Ms. Cornelia Ulrich for technical support during FTIR measurements.

Funding

This study is funded by the European Union's Seventh Framework Programme [FP7] ITN project 'CACHE' under REA grant agreement #[605051]13.

References

1. Thomsen J, Haynert K, Wegner KM, Melzner F. 2015 Impact of seawater carbonate chemistry on the calcification of marine bivalves. *Biogeosciences* **12**, 4209-4220.
2. Kurihara H. 2008 Effects of CO_2-driven ocean acidification on the early developmental stages of invertebrates. *Mar. Ecol. Prog. Ser.* **373**, 275–284.
3. Waldbusser G, Brunner EL, Haley B., Hales B, Langdon CJ, Prahl FG. 2013 A developmental and energetic basis linking larval oyster shell formation to acidification sensitivity. *Geophys. Res. Lett.* **40**, 2171-2176.
4. Gazeau F, Parker LM, Comeau S, Gattuso JP, O'Connor WA, Martin S, Portner HO, Ross PM. 2013 Impacts of ocean acidification on marine shelled molluscs. *Mar. Biol.* **160**, 2207-2245.

5. Mette MJ, Wanamaker AD, Carroll ML, Ambrose WG, Retelle MJ. 2016 Linking large-scale climate variability with *Arctica islandica* shell growth and geochemistry in northern Norway. *Limnol Oceanogr* **61**, 748-764.
6. Waldbusser GG, Hales B, Langdon CJ, Haley BA, Schrader P, Brunner EL, Gray MW, Miller CA, Giminez I. 2015 Saturation-state sensitivity of marine bivalve larvae to ocean acidification. *Nat. Clim. Change.* **5**, 273–280.
7. Waldbusser GG, Hales B, Langdon CJ, Haley BA, Schrader P, Brunner EL, Gray MW, Miller CA, Giminez I, Hutchinson G. 2015 Ocean Acidification Has Multiple Modes of Action on Bivalve Larvae. Plosone. doi: 10.1371/journal.pone.0128376.
8. Marali S, Schone BR, Mertz-Kraus R, Griffin SM, Wanamaker AD, Matras U, Butler PG. 2017 Ba/Ca ratios in shells of *Arctica islandica* - Potential environmental proxy and crossdating tool. *Palaeogeogr. Palaeoclimatol. Palaeoecol.* **465**, 347-361.
9. Kniprath E. 1981 Ontogeny of the molluscan shell field: A review. *Zool. Scri.* **10**, 61-79.
10. Hohagen J, Jackson DJ. 2013 An ancient process in a modern mollusc: early development of the shell in *Lymnaea stagnalis*. *BMC Dev. Biol.* **13**, 27 doi:10.1186/1471-213X-13-27.
11. Eyster LS. 1983 Ultrastructureof early embryonic shell formation in the opisthobranch gastropod *Aeolidia papillosa*. *Biol. Bull.* **165**, 394-408
12. Ramesh K, Hu MY, Thomsen J, Bleich M, Melzner F. 2017 Mussel larvae modify calcifying fluid carbonate chemistry to promote calcification. *Nat. Comm.* (in review).
13. Aranda-Burgos JA, Da Costa F, Novoa S, Ojea J, Martinez-Patino D. 2014 Embryonic and larval development of *Ruditapes Decussatus* (Bivalvia: Veneridae): A study of the shell differentiation process. *J. Molluscan Stud.* **80**, 8-16.
14. Iwata K. 1980 Mineralization and architecture of the larval shell of *Haliotis discus* hannai Ino, (Archaeogastropoda). *J. Fac. of Sci.* Hokkaido University **19**, 305-320.
15. Castilho F, Machado J, Reis ML, Sá C. 1989 Ultrastructural study of the embryonic and larval shell of *Anodonta cygnea*. *Can. J. Zool.* **67**, 1659-1664.
16. Medakovic D, Popovic S, Grzeta B, Plazonic M, Hrs-Brenko M. 1997 X-ray diffraction study of calcification processes in embryos and larvae of the brooding oyster *Ostrea edulis*. *Mar. Biol.* **129**, 615-623.
17. Thompson CM, North EW, White SN, Gallager SM. 2014 An analysis of bivalve larval shell pigments using micro-Raman spectroscopy. *J. Raman Spectrosc.* **45**, 349-358.
18. Kniprath E. 1980 Larval development of the shell and the shell gland in *Mytilus* (Bivalvia). *Roux. Arch. Dev. Biol.* **188**, 201–204.
19. Griesshaber E, Wolfgang W, Ubhi HS, Huber J, Nindiyasari F, Maier BJ, Ziegler A. 2013 Homoepitaxial meso- and microscale crystal co-orientation and organic matrix network structure in *Mytilus edulis* nacre and calcite. *Acta Biomater.* **9**, 9492-9502.
20. Weiner S, Addadi L. 2011 Crystallization pathways in biomineralisation. *Annu. Rev. Mater. Res.* **41**, 21-40.
21. Vidavsky N, Addadi S, Mahamid J, Shimoni E, Ben-Ezra D, Shpigel M, Weiner S, Addadi L. 2014 Initial stages of calcium uptake and mineral deposition in sea urchin embryos. *Proc. Nat. Acad. Sci. USA* **111**, 39-44.
22. Weiss I, Tuross N, Addadi L, Weiner S. 2002 Mollusc larval shell formation: amorphous calcium carbonate is a precursor phase for aragonite. *J. Exp. Zool.* **293**, 478-491.
23. Kudo M, Kameda J, Saruwatari K, Ozaki N, Okano K, Nagasawa H, Kogure T. 2010 Microtexture of larval shell of oyster, *Crassostrea nippona*: a FIB-TEM study. *J. Struct. Biol.* **169**, 1-5.
24. Yokoo N, Suzuki M, Saruwatari K, Aoki H, Watanabe K, Nagasawa H, Kogure T. 2011 Microstructures of the larval shell of a pearl oyster, *Pinctada fucata*, investigated by FIB-TEM technique. *Am. Mineral.* **96**, 1020-1027.

25. Raz S, Testeniere O, Hecker A, Weiner S, Luquet G. 2002 Stable amorphous calcium carbonate is the main component of the calcium storage structures of the crustacean *Orchestia cavimana*. *Biol. Bull.* **203**, 269-274.
26. Stuckas H, Knöbel L, Schade H, Breusing C, Hinrichsen HH, Bartel M, Langguth K, Melzner F. 2017 Combining hydrodynamic modelling with genetics: Can passive larval drift shape the genetic structure of Baltic *Mytilus* populations? *Mol. Ecol.* **26**, 2765-2782.
27. Barton A, Hales B, Waldbusser GE, Langdon C, Feely RA. 2012 The Pacific oyster, *Crassostrea gigas*, shows negative correlation to naturally elevated carbon dioxide levels: Implications for near-term ocean acidification effects. *Limnol. Oceanogr.* **57**, 698-710.
28. Talmage S, Gobler C. 2009 The effects of elevated carbon dioxide concentrations on the metamorphosis, size and survival or larval hard clams (*Mercenaria mercenaria*), bay scallops (*Argopecten irradians*), and Eastern oysters (*Crassostrea virginica*). *Limnol. Oceanogr*. **54**, 2072-2080.
29. Rodriguez-Blanco JD, Shaw S, Benning LG. 2008 How to make 'stable' ACC: protocol and preliminary structural characterization, *Mineral. Mag.* **72**, 283-286.
30. Kranz SA, Wolf-Gladrow D, Nehrke G, Langer G, Rost B. 2010 Calcium carbonate precipitation induced by the growth of the marine cyanobacterium *Trichodesmium*. *Limnol. Oceanogr.* **55**, 2563–2569.
31. Hedegaard C, Bardeau JF, Chateigner D. 2006 Molluscan shell pigments: an in situ resonance Raman study. *J. Molluscan Stud.* **72**, 157–162.
32. Stemmer K, Nehrke G, 2014 The distribution of polyenes in the shell of *Arctica islandica* from North Atlantic localities: a confocal Raman microscopy study. *J. Molluscan Stud.* **80**, 365–370.
33. Nehrke G, Poigner H, Wilhems-Dick D, Brey T, Abele D. 2012 Coexistence of three calcium carbonate polymorphs in the shell of the Antarctic clam *Laternula elliptica*. *Geochem. Geophys. Geosyst.* **13**, 1–8.
34. Wall M, Nehrke G. 2012 Reconstructing skeletal fiber arrangement and growth mode in the coral *Porites lutea* (Cnidaria, Scleractinia): a confocal Raman microscopy study. *Biogeosciences* **9**, 4885–4895.
35. Schonitzer V, Weiss IM. 2007 The structure of mollusc larval shells formed in the presence of the chitin synthase inhibitor Nikkomycin Z. *BMC Struct. Biol.* **7**, 71.
36. Urmos J, Sharma SK, Mackenzie FT. 1991 Characterization of some biogenic carbonates with Raman spectroscopy. *Amer Mineral.* **76**, 641–646.
37. Jacob DE, Wirth R, Soldati AL, Wehrmeister U, Schreiber A. 2011 Amorphous calcium carbonate in the shells of adult Unionoida. *J. Struct. Biol.* **173**, 241-249.
38. Anderson FA, Brecevic L. 1991 Infrared spectra of amorphous and crystalline calcium carbonate. *Acta Chem. Scand*. **45**, 1018-1024.
39. Aizenberg J, Lambert G, Weiner S, Addadi L. 2002 Factors involved in the formation of amorphous and crystalline calcium carbonate: A study of an ascidian skeleton. *J. Am. Chem. Soc.* **124**, 32-39.
40. Hodson ME, Benning LG, Demarchi B, Penkman KEH, Rodriguez-Blanco JD, Schofield PF, Versteegh EAA 2015 Biomineralisation by earthworms - an investigation into the stability and distribution of amorphous calcium carbonate. *Geochem. Trans.* **16**, 4.
41. Hild S, Marti O, Ziegler A. 2008 Spatial distribution of calcite and amorphous calcium carbonate in the cuticle of the terrestrial crustaceans *Porcellio scaber* and *Armadillidium vulgare*. *J. Struct. Biol.* **163**, 100-108.
42. Weiner S, Levi-Kalisman Y, Raz S, Addadi L. 2003 Biologically formed amorphous calcium carbonate. *Connect Tissue Res.* **44**, 214-218.
43. Wehrmeister U, Jacob DE, Soldati AL, Loges N, Häger T, Hofmeister W. 2010 Amorphous, nanocrystalline and crystalline calcium carbonates in biological materials. *J. Raman Spectrosc*. **42**, 926-935.

44. Saruwatari K, Matsui T, Mukai H, Nagasawa H, Kogure T. 2009 Nucleation and growth of aragonite crystals at the growth front of nacres in pearl oyster, *Pinctada fucata*. *Biomaterials* **30**, 3028–3034.
45. Chan VBS, Toyofuku T, Wetzel G, Saraf L, Thiyagarajan V, Mount AS. 2015 Direct Deposition of crystalline aragonite in the controlled biomineralization of the calcareous tubeworm. *Front. Mar. Sci.* **2**, doi: 10.3389/fmars.2015.00097.
46. Galtsoff PS. 1964 The American oyster, *Crassostrea virginica* Gmelin. Chapter 16: Larval development and metamorphosis. Fishery Bulletin, North East Fishery Science Centre.
47. Nehrke G, Nouet J. 2011 Confocal Raman microscope mapping as a tool to describe different mineral and organic phases at high spatial resolution within marine biogenic carbonates: case study on *Nerita undata* (Gastropoda, Neritopsina). *Biogeosciences* **8**, 3761-3769.
48. Kristova P, Hopkinson LJ, Rutt KJ. 2015 The Effect of the Particle Size on the Fundamental Vibrations of the [CO_3^{2-}] Anion in Calcite. *J. Phys. Chem. A* **119**, 4891-4897.
49. Salter MA, Harborne AR, Perry CT, Wilson RW 2017 Phase heterogeneity in carbonate production by marine fish influences their roles in sediment generation and the inorganic carbon cycle. *Sci. Rep.* **7**. doi: 10.1038/s41598-017-00787-4.
50. Khouzani MF, Chevrier DM, Guettlein P, Hauser K, Zhang P, Hedin N, Gebauer D. 2015 Disordered amorphous calcium carbonate from direct precipitation. *Cryst. Eng. Comm.* **17**, 4842-4849.
51. Hikida T, Nagasawa H, Kogure T. 2003 Characterization of amorphous calcium carbonate in the gastrolith of cray fish, *Procambarus clarkia*. In I. Kobayashi and H. Ozawa, Eds., Biomineralization (BIOM2001), 81–84. Tokai University Press, Kanagawa, Japan.
52. Yokoo N. 2012 Investigation of amorphous calcium carbonate (ACC) in biomineralisation. Department of Earth and Planetary Science. The University of Tokyo Graduate School of Science.
53. Suzuki M, Nagasawa H, Kogure T. 2006 Synthesis and structure of hollow calcite particles. *Cryst. Growth Des.* **6**, 2004–2006.
54. DeVol RT, Sun CY, Marcus MA, Coppersmith SN, Myneni SCB, Gilbert PUPA. 2015 Nanoscale transforming mineral phases in fresh nacre. *J. Amer. Chem.l Soc.* **137**, 13325-13333.
55. Tschirner N, Schenderlein M, Brose K, Schlodder E, Mroginski MA, Hildebrandt P, Thomse, C. 2008 Raman excitation profiles of beta-carotene - novel insights into the nature of the v1-band. *Phys. Status Solidi B.* **245**, 2225-2228.
56. Baranska M, Romana M, Dobrowolski J, Schulz H, Baranski R. 2013 Recent advances in Raman analysis of plants: Alkaloids, carotenoids, and polyacetylenes. *Curr. Anal. Chem.* **9**, 108-127.
57. Matsuno T, Hirao S. 1989 Marine carotenoids. In R. G. Ackman (Ed.). Marinebiogenic lipids, fats, and oils (**1**, 251–388). Boca Raton, FL: CRC Press.
58. Vershinin A. 1996 Carotenoids in mollusca: Approaching the functions. *Comp. Biochem. Physiol. B. Biochem. Mol. Biol.* **133**, 63-71.
59. Maia LF, de Oliveira VE, Oliveira MER, Reis FD, Fleury BG, Edwards HGM, de Oliveira LFC. 2013 Colour diversification in octocorals based on conjugated polyenes: A Raman spectroscopic view. *J. Raman Spectrosc*. **44**, 560-566.
60. Jackson DJ, Wörheide G, Degnan BM. 2007 Dynamic expression of ancient and novel molluscan shell genes during ecological transitions. *BMC Evol. Biol.* **7**, 160.
61. Czeczuga B. 1985 Carotenoid-Calcium Carbonate Complex from the Hydrocoral *Errina antarctica*. Biochem. Syst. Ecol. **13**, 455-457.

Fig. 1 Trochophore shell deposition in Baltic *Mytilus edulis*-like (**A-B**) Birefringent shells are denoted by arrows in trochophore larvae (21 hpf). (**C**) Transmission image of a calcifying trochophore larva at 21 hpf. The boxed region was subjected to a Raman scan. (**D**) Raman spectra of the organic shell cover in prior to shell deposition at 20 hpf. (**E**) (**F**) Raman scan for the boxed region in (C) was integrated for CO_3^{2-}-stretching (1082.5–1087.5 rel. cm^{-1}). (**F1**) Raman spectrum of an ACC standard. (**G1**) Raman spectrum of an aragonite standard. (**H1**) Raman spectrum of an *in vivo* trochophore larval shell. (**F2**) The CO_3^{2-}-stretching mode of ACC in (F1). (**G2**) The CO_3^{2-}-stretching mode of aragonite in (G1). (**H2**) The CO_3^{2-}-stretching mode of an *in vivo* trochophore shell in (H1) to illustrate the presence of aragonite-specific CO_3^{2-}-stretching in the shell.

Fig. 2 CRM analyses of an ACC-aragonite mixture (**A**) Raman scan of ACC-aragonite mixture that was integrated for CO_3^{2-}-stretching mode of both polymorphs (red, aragonite, 1080.4–1090.4 rel. cm^{-1})(blue, ACC, 1070.6-1075.6). (**B-C**) Raman spectra of ACC and aragonite in the mixture to illustrate the sensitivity of CRM techniques to detect the presence of multiple polymorphs on a nanometer scale. (**D**) The CO_3^{2-}-stretching mode of ACC. (**E-F**) Raman spectra of the CO_3^{2-}-stretching mode presented in (B) and (C) respectively.

Fig. 3 Prodissoconch I shell deposition in Baltic *Mytilus edulis*-like (**A**) Transmission image of a D-veliger larva at 48 hpf, for which multiple point Raman spectra were acquired. (**B**) Raman spectrum of an ACC standard. (**C**) Raman spectrum of an aragonite standard. (**D**) Raman spectrum of the D-veliger larval shell in (A) at point 'D'.

Fig. 4 Raman spectra acquired from the veliger larval shells of three different larval species (**A**) Raman spectrum of a *Mercenaria mercenaria* larval shell acquired using a 20x objective and a grid 600 g/mm, BLZ 500 nm (**B**) Raman spectrum of a *Mercenaria mercenaria* larval shell acquired using a 20x objective and a grid 1800 g/mm, BLZ 500 nm (**C**) Raman spectra of seawater acquired using the 60x water immersion objective to illustrate the similarity of water and ACC peaks between 75-225 rel.cm^{-1}. (**D**) Raman spectra at the surface of a *Mercenaria mercenaria* larval shell acquired using the 60x water immersion objective (**E**) Raman spectra at the focal plane of the *Mercenaria mercenaria* larval shell acquired using the 60x water immersion objective. (**F**) Raman spectra of a *Crassosterea virginica* larval shell. (**G**) Raman spectra of a *Crassosterea gigas* larval shell.

Fig. 5 Juvenile shell deposition in Baltic *Mytilus edulis*-like (**A**) Transmission image of a resin-embedded juvenile shell. The boxed region was subjected to a Raman scan. (**B**) Raman scan for the boxed region in (A) was integrated for CO_3^{2-}-stretching mode (1081.3-1091.3 rel. cm^{-1}, in red) and calcite lattice mode (268.4–298.4 rel. cm^{-1}, in blue). (**C**) Raman spectrum of an aragonite standard. (**D**)

Raman spectrum of a calcite standard. (**E**) Raman spectrum of the juvenile shell in (A) at point 7. (**F**) Raman spectrum of the juvenile shell in (A) at point 8.

Fig. 6 FTIR spectra of Baltic *M. edulis*-like larval shells (**A**) FTIR spectrum of an ACC standard. (**B**) FTIR spectrum of an aragonite standard. **(C**) FTIR spectrum of D-veliger Baltic *M. edulis*-like shells. (**D**) FTIR spectrum of aragonite from an adult Baltic *M. edulis*-like shell.

Fig. 7 Presence of pigment polyenes in larval shells of Baltic *Mytilus edulis*-like (**A**) Plot of the relative wave numbers for pigment polyenes measured in the shells several mollusc species. Data presented from Hedegaard et al. [31], Stemmer & Nehrke [32] and Tschirner et al. [55]. (**B**) Raman scan for the boxed region in Fig. 1E was integrated for CO_3^{2-}-stretching mode and Baltic *M. edulis*-like shell polyene (1076-1146 rel. cm^{-1}, in red) and carotenoids (1150.5–1170.5 rel. cm^{-1}, in blue). (**C**) Raman spectra for carotenoids around the growing edge of the shell (blue) and the larval shell and associated polyenes (red).

Table 2. Characteristic Raman shifts of calcium carbonate polymorphs and polyene pigments.

Sample	Characteristic wavenumber (cm^{-1})	Reference
ACC CO_3 stretching	1079	Raz et al. [253]
Aragonite CO_3 stretching	1085-1087	Urmos et al. [35]
Calcite CO_3 stretching	1086-1087	Urmos et al. [35]
ACC lattice vibrations	150-250	Raz et al. [25]
Aragonite lattice vibrations	155, 206 and double peaks at 704	Nehrke et al. [33]
Calcite lattice vibrations	156, 282 and 711	Nehrke et al. [33]
Mytilus edulis polyenes	1098 and 1484	Hedegaard et al. [31]

Figure 1

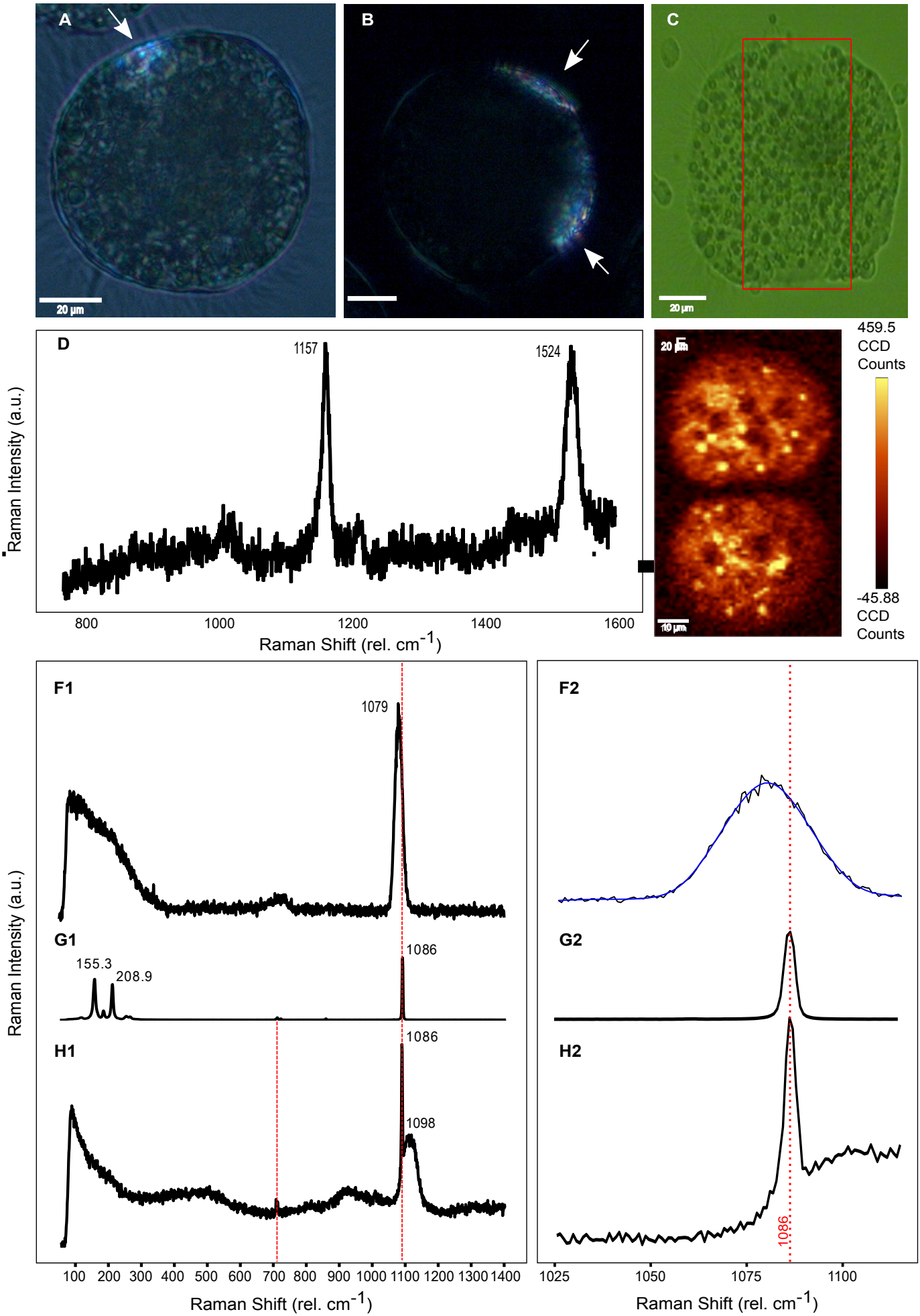
A
B
C
20 µm
20 µm
D
1157
1524
Raman Intensity (a.u.)
800
1000
1200
1400
1600
Raman Shift (rel. cm-1)
20 µm
10 µm
459.5
CCD
Counts
-45.88
CCD
Counts
F1
1079
G1
155.3
208.9
1086
H1
1086
1098
F2
G2
H2
1086
Raman Intensity (a.u.)
100 200 300 400 500 600 700 800 900 1000 1100 1200 1300 1400
Raman Shift (rel. cm-1)
1025
1050
1075
1100
Raman Shift (rel. cm-1)

Figure 2

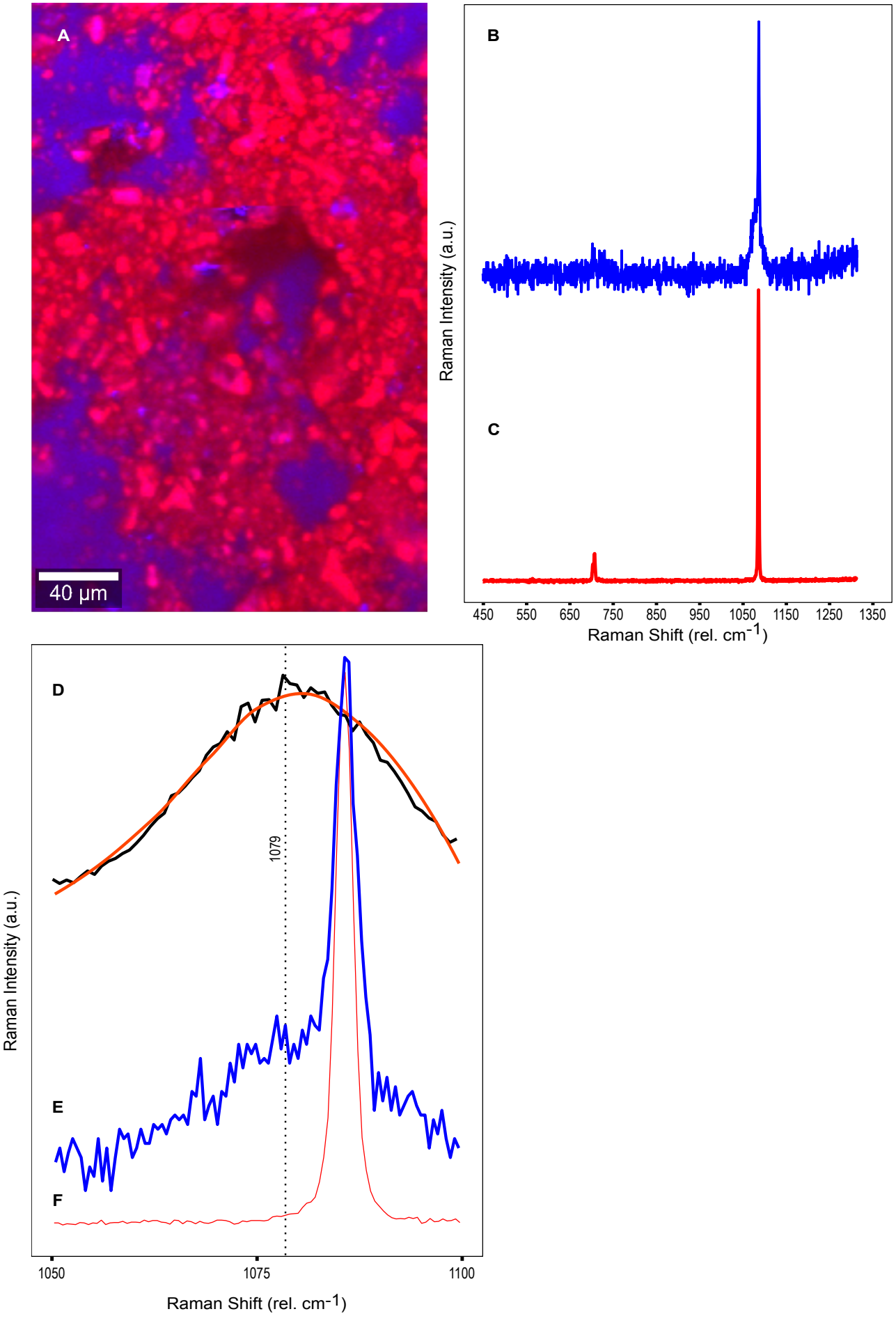
A
40 µm
B
C
Raman Intensity (a.u.)
450
550
650
750
850
950
1050
1150
1250
1350
Raman Shift (rel. cm^{-1})
D
1079
E
F
Raman Intensity (a.u.)
1050
1075
1100
Raman Shift (rel. cm^{-1})

Figure 3

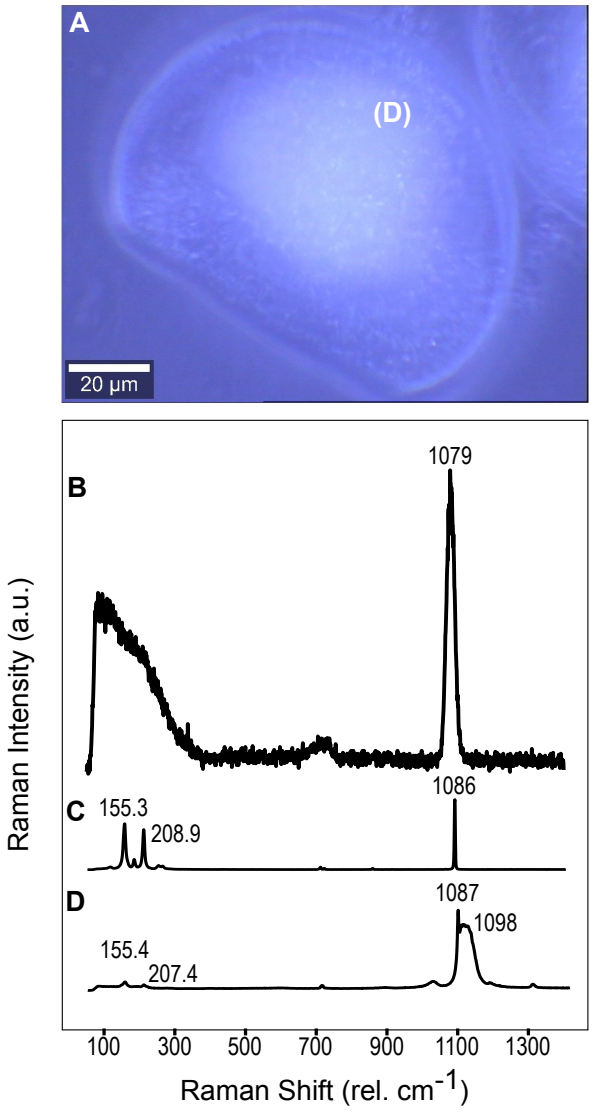
A
(D)
20 µm
B
1079
C
155.3
208.9
1086
D
155.4
207.4
1087
1098
Raman Intensity (a.u.)
100
300
500
700
900
1100
1300
Raman Shift (rel. cm-1)

Figure 4

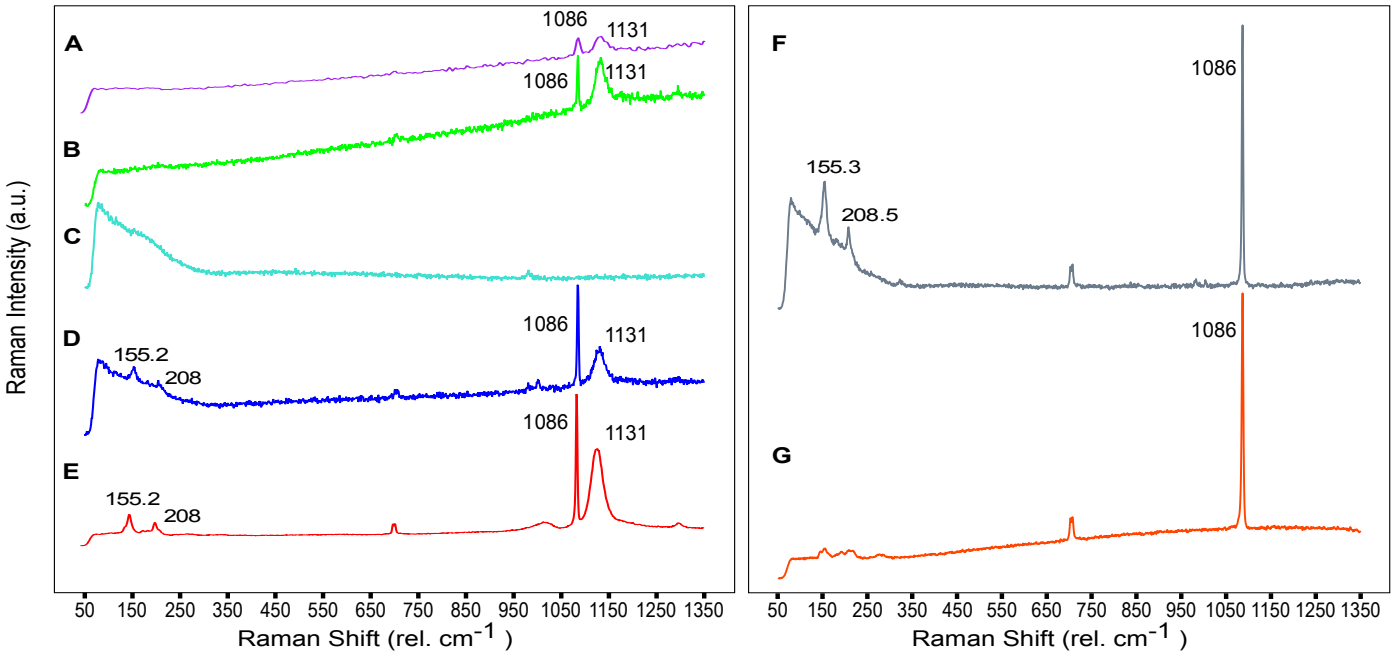
A
B
C
D
E
F
G
1086
1131
155.2
208
155.3
208.5
Raman Intensity (a.u.)
50 150 250 350 450 550 650 750 850 950 1050 1150 1250 1350
Raman Shift (rel. cm-1)

Figure 5

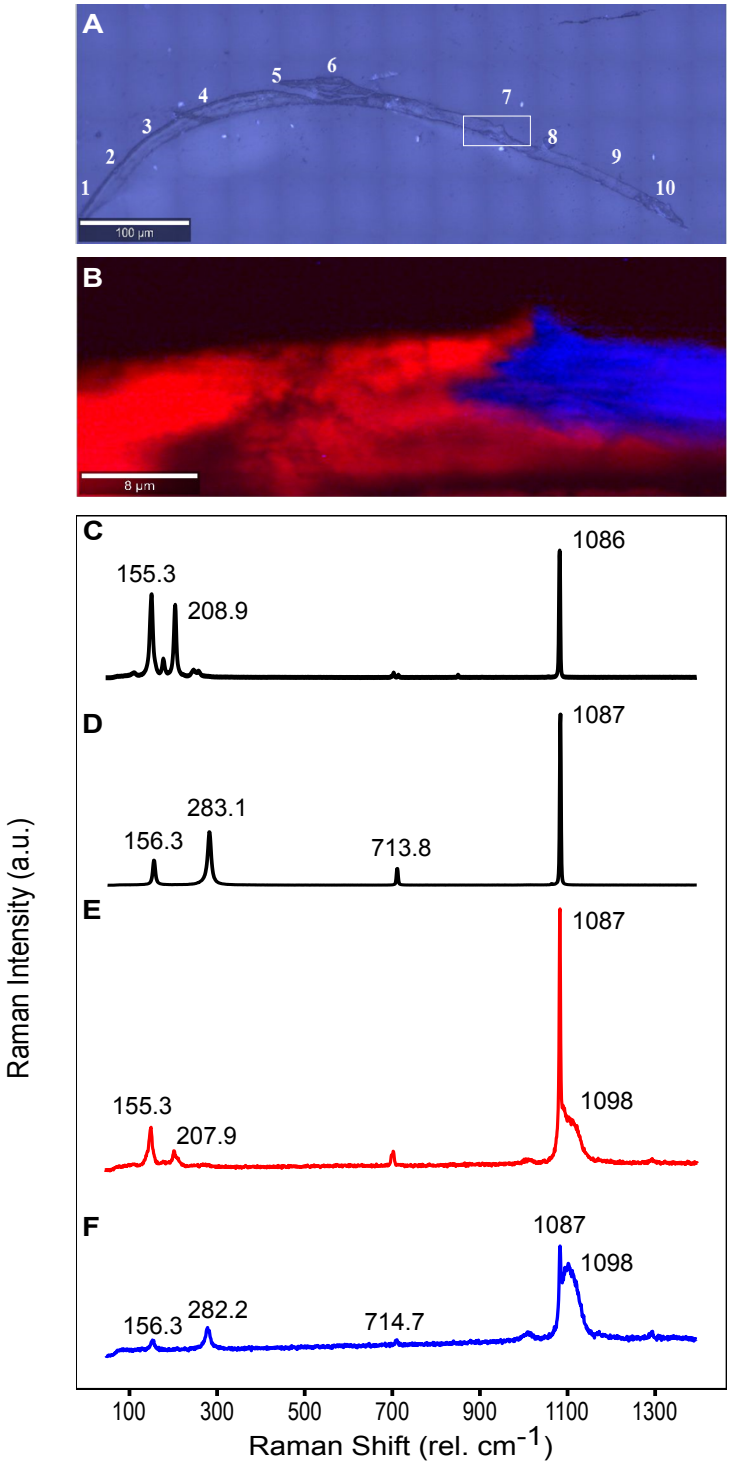
A
1
2
3
4
5
6
7
8
9
10
100 µm
B
8 µm
C
155.3
208.9
1086
D
156.3
283.1
713.8
1087
E
155.3
207.9
1098
1087
F
156.3
282.2
714.7
1087
1098
Raman Intensity (a.u.)
100
300
500
700
900
1100
1300
Raman Shift (rel. cm-1)

Figure 6

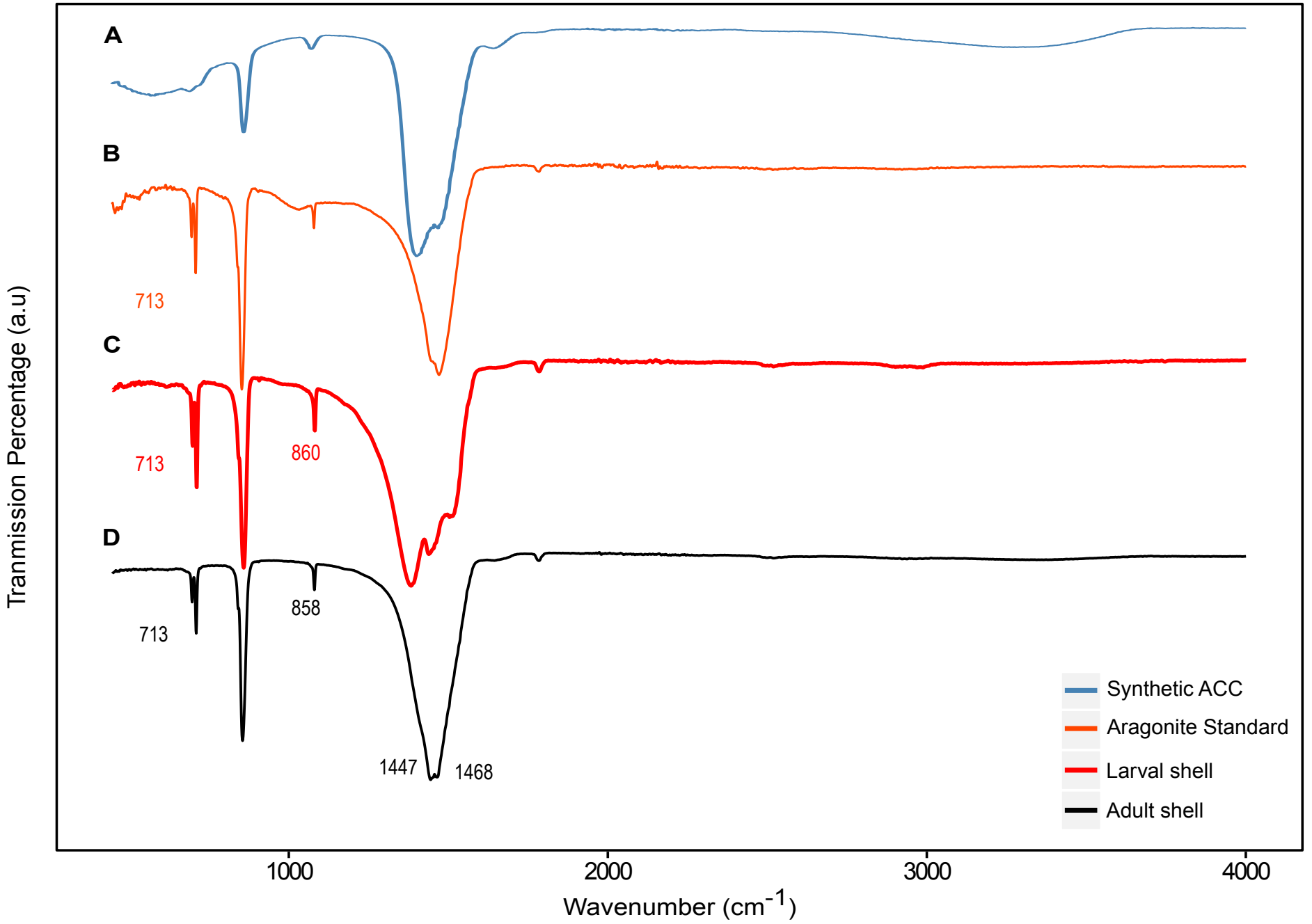
A
B
C
D
713
713
860
713
858
1447
1468
Tranmission Percentage (a.u)
1000
2000
3000
4000
Wavenumber (cm^{-1})
Synthetic ACC
Aragonite Standard
Larval shell
Adult shell

Figure 7

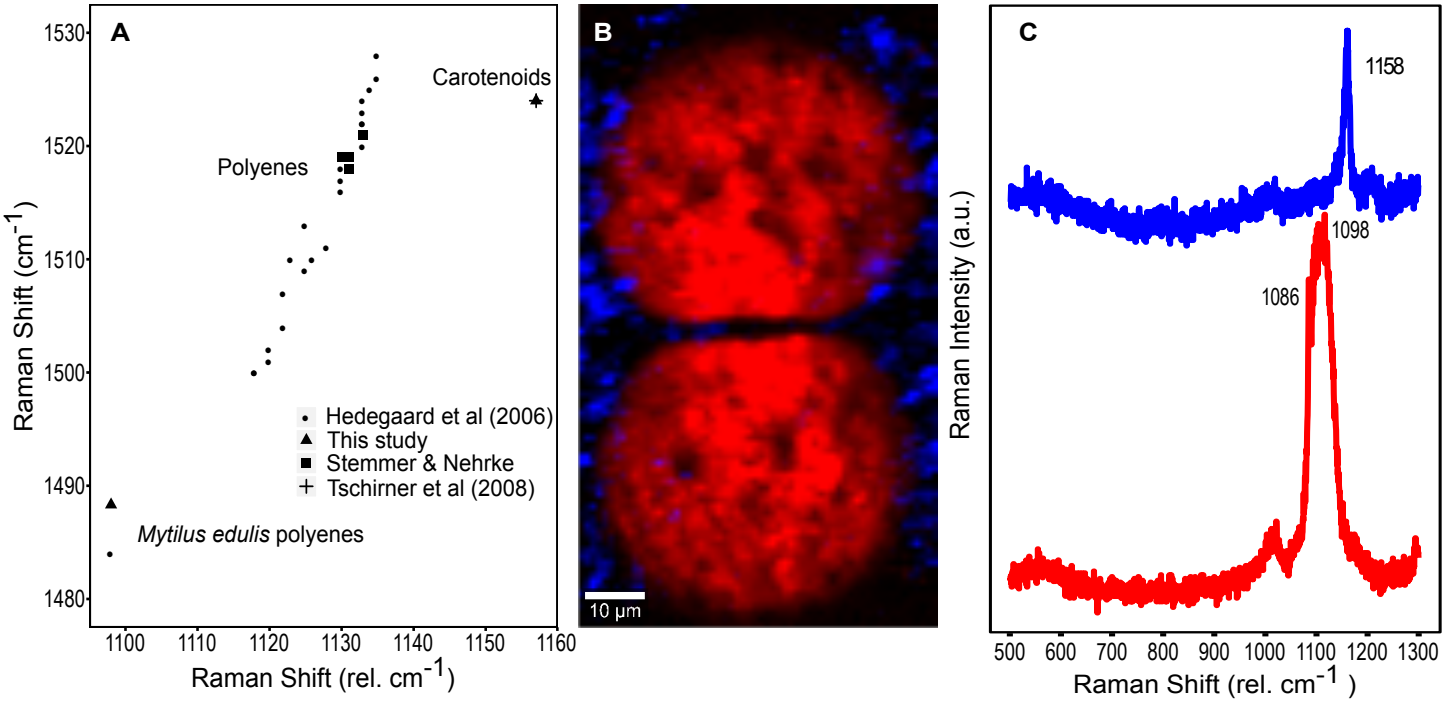
A
Carotenoids
Polyenes
Hedegaard et al (2006)
This study
Stemmer & Nehrke
Tschirner et al (2008)
Mytilus edulis polyenes
Raman Shift (cm-1)
Raman Shift (rel. cm-1)
B
10 µm
C
1158
1098
1086
Raman Intensity (a.u.)
Raman Shift (rel. cm-1)

nature COMMUNICATIONS

49

ARTICLE

DOI: 10.1038/s41467-017-01806-8 OPEN

Mussel larvae modify calcifying fluid carbonate chemistry to promote calcification

Kirti Ramesh[1], Marian Y. Hu[2], Jörn Thomsen[1], Markus Bleich[2] & Frank Melzner[1]

Understanding mollusk calcification sensitivity to ocean acidification (OA) requires a better knowledge of calcification mechanisms. Especially in rapidly calcifying larval stages, mechanisms of shell formation are largely unexplored—yet these are the most vulnerable life stages. Here we find rapid generation of crystalline shell material in mussel larvae. We find no evidence for intracellular $CaCO_3$ formation, indicating that mineral formation could be constrained to the calcifying space beneath the shell. Using microelectrodes we show that larvae can increase pH and $[CO_3^{2-}]$ beneath the growing shell, leading to a ~1.5-fold elevation in calcium carbonate saturation state (Ω_{arag}). Larvae exposed to OA exhibit a drop in pH, $[CO_3^{2-}]$ and Ω_{arag} at the site of calcification, which correlates with decreased shell growth, and, eventually, shell dissolution. Our findings help explain why bivalve larvae can form shells under moderate acidification scenarios and provide a direct link between ocean carbonate chemistry and larval calcification rate.

[1] GEOMAR Helmholtz Centre for Ocean Research Kiel, 24148 Kiel, Germany. [2] Institute of Physiology, Christian-Albrechts-University Kiel, 24098 Kiel, Germany. Correspondence and requests for materials should be addressed to K.R. (email: kramesh@geomar.de) or to F.M. (email: fmelzner@geomar.de)

Understanding the impacts of ocean acidification (OA) on reef forming bivalves (oysters, mussels) is an important challenge, as these foundation species provide several essential ecosystem services[1]. Adult life stages of several bivalve species have been shown to be relatively vulnerable to OA[2–4]. However, bivalve larvae are particularly sensitive and respond negatively through impaired growth and calcification[5], increased shell malformation[6] and dissolution[7], as well as increased mortality[3]. Calcification performance of larval stages might be the main bottleneck determining vulnerability of bivalves to ongoing OA. However, despite existing information on the impacts of OA on bivalves, the physiological mechanisms driving their sensitivity to OA remain unknown.

In marine systems, calcification is highly dependent on external seawater carbonate chemistry[8, 9]. Many marine species are primarily impacted by OA induced changes in body fluid pCO_2 and associated secondary acid–base regulatory processes that can impair fitness relevant traits, including development and calcification[10, 11]. However, shell formation rate of early bivalve larvae with very high relative calcification rates correlates best with the seawater saturation state of aragonite (Ω_{arag})[9] or equivalently, the ratio of bicarbonate to protons ($[HCO_3^-]/[H^+]$)[8]. This is due to

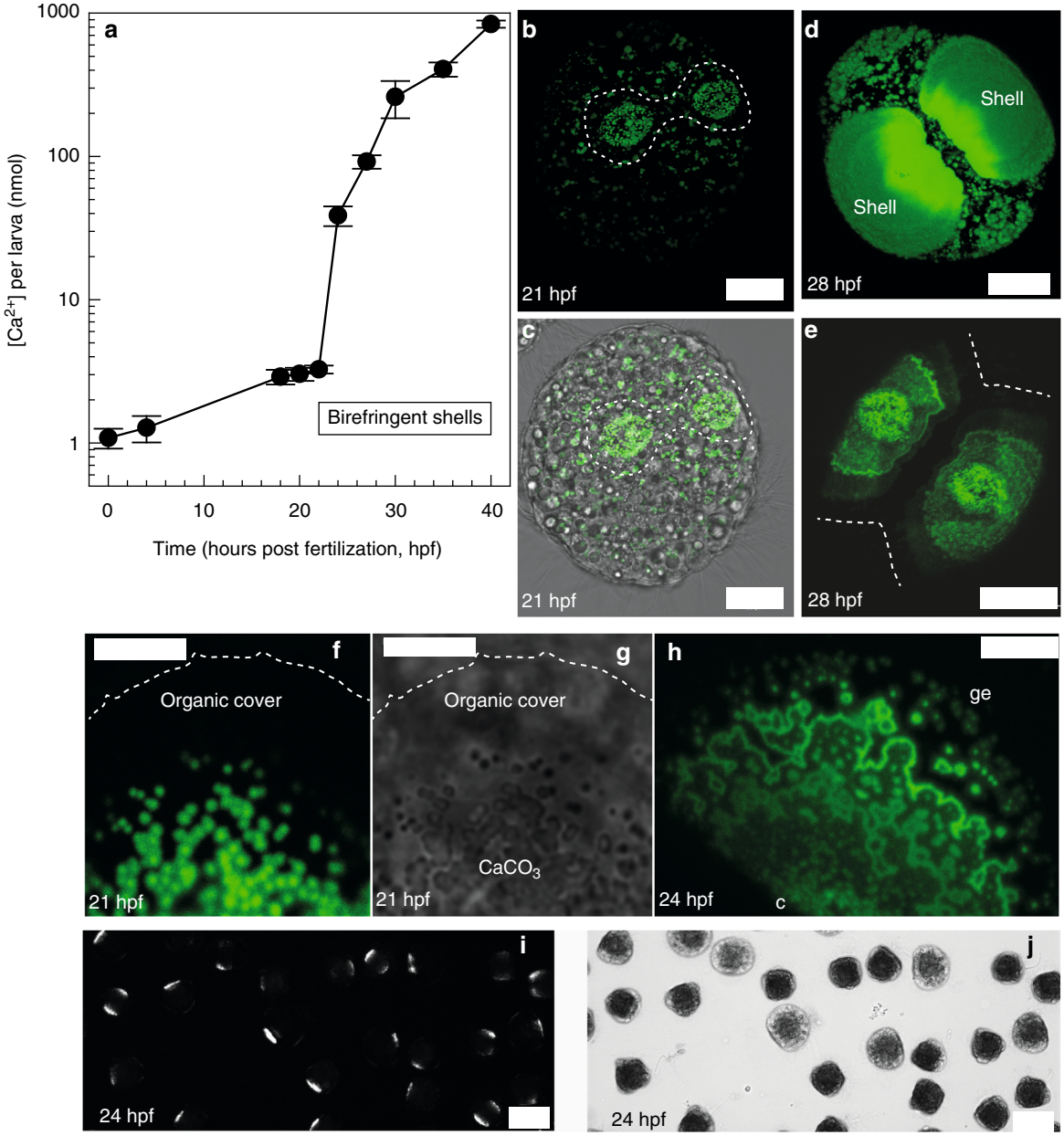

Fig. 1 Calcium accumulation and in vivo larval shell formation from Exp 1 and 2. **a** larval calcium accumulation during the first 48 hpf, $N = 4$ fertilizations, means and s.d. Shells are birefringent from 21 hpf onwards. **b** Confocal projection of early stage of shell formation in 21 hpf trochophore larva, calcein positive particles are deposited onto tissue facing side of organic shell cover and numerous calcein positive intracellular vesicles are visible underneath. Shell organic cover boundaries indicated by dashed line. **c** Same larva, merged transmission and calcein fluorescence images. **d** confocal projection of 28 hpf larva viewed from the hinge, which is not calcified yet. Shell fluorescence overexposed to visualize intracellular calcein positive vesicles. **e** Same larva imaged at lower intensity to illustrate shell details, calcein positive particles visible in the centre of each valve, dotted line indicates boundaries of the organic shell cover. **f** Close-up of calcein positive deposits attached to the organic shell cover in 21 hpf larva, organic cover boundary indicated by dotted line. **g** Same larva, transmission image. **h** Confocal projection of shell material secreted by 24 hpf larva, note deposits at the centre of the valve (c) and at the growing edge (ge). **i** Larvae in vivo under crossed polarized light, see also Supplementary Movie 1 for swimming and rotating larvae. **j** Same larvae, transmitted light. Scale bars: 20 µm **b**–**e**, 5 µm **f**–**h**, 75 µm **i**, **j**

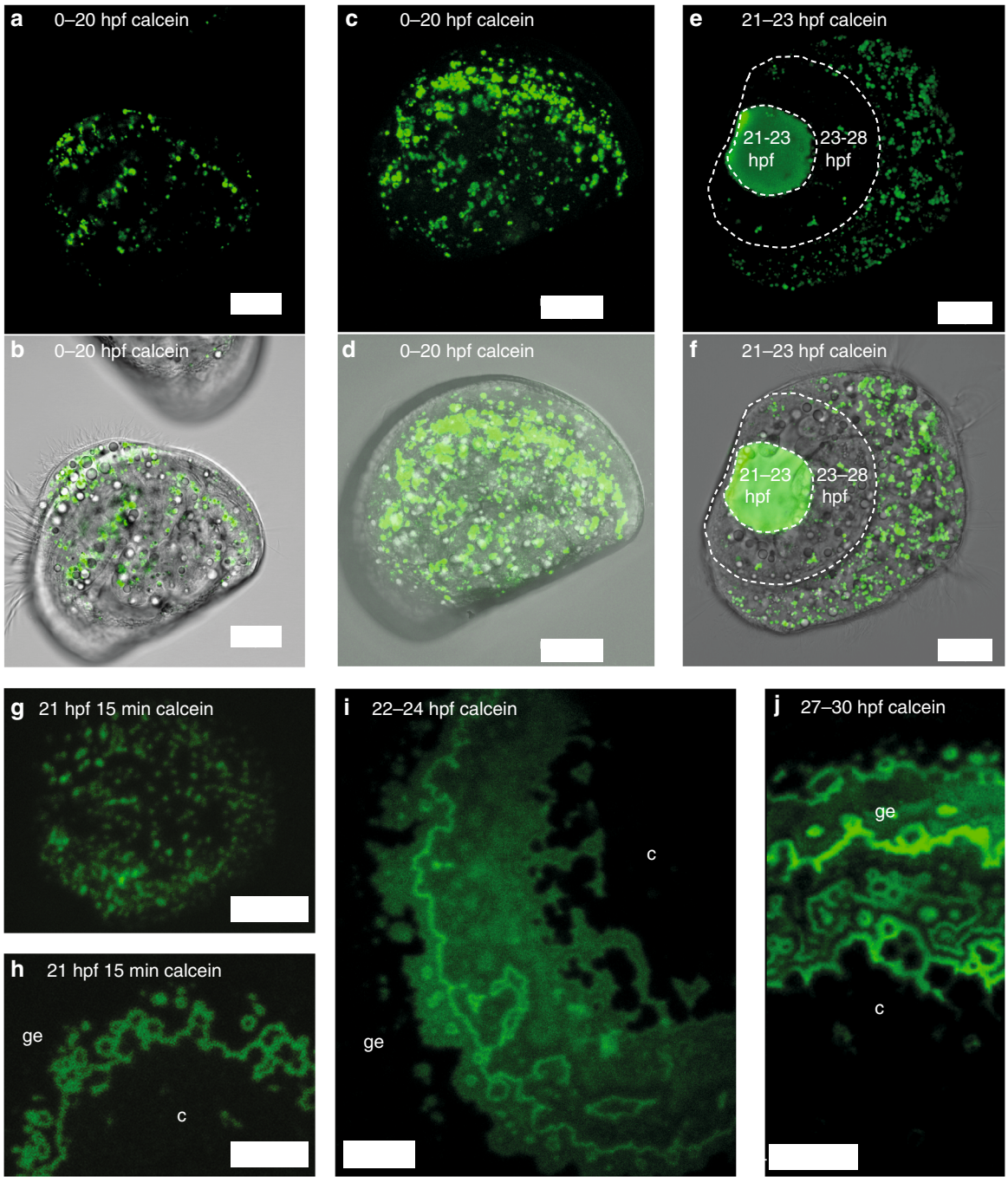

Fig. 2 Calcein pulse-chase experiments and in vivo confocal microscopy from Exp 2. **a**, **b** Calcein fluorescence image and merged fluorescence and transmission images of larva cultured in calcein between 0–20 hpf, followed by development in filtered seawater (FSW) until 48 hpf, 1 µm thick section through body and shell to illustrate lack of calcein fluorescence in the shell. **c**, **d** Same animal, confocal projection through one entire shell valve and body to illustrate numerous calcein positive intracellular vesicles yet no fluorescence in the shell. **e**, **f** Confocal projection of calcein fluorescence of larva cultured in calcein FSW between 21–23 hpf. Shell material formed between 21–23 hpf is calcein labeled, shell material formed between 23–28 hpf is not. Calcein label of vesicles present at 28 hpf has apparently not been transferred into the shell. **g**, **h** 21 hpf animals stained with calcein for 15 min, then washed and cultured in FSW, calcein positive particles on periostracum **g**, shell growth bands in a slightly more advanced larva from the same fertilization **h**. **i** Confocal projection of shell calcein fluorescence of larva cultured in seawater with calcein pulse between 22–24 hpf. **j** Confocal projection of shell calcein fluorescence of larva cultured in seawater with calcein pulse between 27–30 hpf. c = centre of shell valve, ge = growing edge of shell valve. Scale bars: 20 µm **a**–**f**, 5 µm **h**, **i**, 10 µm **j**

the need to accumulate high amounts of calcification substrates (HCO_3^-, Ca^{2+}) and to excrete equivalent amounts of end products (H^+). Early larval stages (trochophore larvae) form a shell field during the first day of life, which then grows over the larval body within the next day until the first larval shell, the so-called prodissoconch I (PD I) is completed (veliger stage). During this brief time interval, bivalve larvae can precipitate a shell mass that is almost equivalent to their own body mass[12].

It is unknown at present whether the substrates for calcification (HCO_3^-, Ca^{2+}) are directly transferred via transcellular or paracellular routes to the calcification space (CS), the extracellular space directly underneath the growing shell. Alternatively, it is

also possible that calcification substrates in larvae are accumulated intracellularly in vesicles, which are then deposited into the growing shell via exocytosis. Presence of intracellular crystalline calcite and deposition onto the shell has been observed in oyster hemocytes during shell repair[13, 14]. Intracellular formation of amorphous calcium carbonate (ACC) precursors could be demonstrated in sea urchin larvae[15], where numerous large vesicles >1 µm accumulate calcium carbonate for subsequent deposition into the larval skeleton, where it then transforms to calcite[16]. In bivalve larvae, no such observations of intracellular ACC formation have been attempted. However, there is circumstantial evidence for a minor ACC fraction in larval bivalve shells that might be a precursor to aragonite, the major $CaCO_3$ polymorph of the shell[17]. This would support the intracellular ACC formation hypothesis. Intracellular ACC formation could be beneficial during OA stress, as intracellular pH typically is much more tightly regulated than extracellular pH, thereby providing stable conditions for vesicular carbonate precipitation[18].

It is also unclear, to what extent bivalve larvae can control the carbonate chemistry of the extracellular CS underneath the shell. OA induced changes in carbonate chemistry at the CS could lead to internal shell dissolution and reduced rates of shell deposition. The chemical composition of this space should govern precipitation and dissolution rates (r) for inorganic carbonates according to:

$$\mathbf{r} = k\left(\Omega_{\mathrm{arag}} - 1\right) \quad (1)$$

where 'k' is the rate constant[9, 19]. For a given system with $k =$ constant, Ω_{arag} determines calcification rates and $r = 0$ when $\Omega_{\mathrm{arag}} = 1$. However, dissolution of biogenic aragonite in bivalve shells has been empirically observed to occur at $\Omega_{\mathrm{arag}} > 1$[20], likely due to the higher solubility of biogenic carbonates. On the other hand, bivalve larvae have been observed to develop shells even when the surrounding seawater is undersaturated with respect to Ω_{arag}[6, 9]. Therefore, it has been suggested that larvae are capable of elevating Ω_{arag} at the site of calcification via active ion transport mechanisms[9]. Alternatively, modulation of the fraction and type of organic shell matrix molecules might enable continued calcification when $\Omega_{\mathrm{arag}} < 1$[9]. In order to obtain a mechanistic understanding of the processes leading to tolerance vs. vulnerability to OA, it is paramount to obtain direct estimates of the carbonate chemistry at the tissue–shell interface in these minute, 80–100 µm sized larvae.

Owing to the lack of understanding of the processes leading to first larval shell formation, here we investigate the initial dynamics of calcium uptake and deposition using in vivo confocal and polarized microscopy in mussel (*Mytilus edulis*) larvae. We use calcein labeling to test whether calcium carbonate is accumulated intracellularly in vesicles and later deposited into the shell and how rapidly calcium is accumulated within the first larval shell. Further, we investigate the chemical composition of the extracellular CS using ion-selective microelectrodes for pH, CO_3^{2-} and Ca^{2+}. Finally, we subject larvae to OA conditions and investigate how changes in seawater carbonate chemistry impact carbonate chemistry at the CS and correlate with shell growth and dissolution. We find no evidence for intracellular calcification via large intracellular vesicles (>1 µm), but demonstrate very rapid appearance of calcein label in the shell. Larvae are able to manipulate carbonate chemistry at the CS to enhance rates of calcium carbonate precipitation, but cannot maintain favorable conditions when they are exposed to OA. Decreases in pH, $[CO_3^{2-}]$ and Ω_{arag} at the site of calcification under OA conditions lead to reduced shell length growth and, ultimately, shell dissolution.

Results

No evidence for intracellular larval calcification. To understand how the larval PD I shell is formed during the first 2 days of life and whether intracellular accumulation of calcium carbonate in large vesicles plays a role in shell formation, we conducted several time series experiments at 17 °C. Calcium accumulation of whole larvae was measured at ten developmental time points using flame photometry (Fig. 1a). During the first 22 hours post fertilization (hpf, trochophore stage), we detected a moderate, ca. 3-fold increase in larval calcium content. In contrast, an exponential, 250-fold increase in $[Ca^{2+}]$ was observed between 22–40 hpf. This increase correlated with the first appearance of calcein labeled particles attached to the organic cover (the periostracum) of each valve of the growing shell field at 21 hpf (Fig. 1b, c) and progressive expansion of the shell valves, as indicated by extensive calcein labeling of newly formed shell material (Figs. 1 and 2). Once calcein positive structures were deposited on the organic shell cover (Fig. 1f, g), subsequent calcein label appeared in meandering bands that interconnected the initially deposited particles and extended the shell valves across the larval body (Figs. 1h and 2h–j). Using crossed polarized microscopy we could demonstrate that the growing shell is birefringent from 22 hpf onwards (Fig. 1i, j, Supplementary Movie 1), indicating the presence of a high fraction of crystalline aragonite. Presence of aragonite in larval *M. edulis* shells from 22 hpf (at 18 °C) onwards has previously been observed using XRD[21] and early veliger shells of other bivalve species also consist of aragonite[22, 23]. Video recordings of swimming and rotating larvae under crossed polarized light indicate that the entire shell is birefringent (Supplementary Movie 1). These findings indicate that if ACC is deposited onto the growing shell, the majority must rapidly (within minutes to hours) transform into crystalline aragonite.

When culturing larvae in calcein containing filtered seawater (FSW), numerous large (0.5–3 µm diameter) calcein positive vesicles were observed in all cells (Fig. 1b, c). In order to determine, whether these vesicles contribute calcium carbonate to the shell, we conducted a series of calcein pulse-chase experiments. When staining larvae with calcein during 0–20 hpf and growing them afterwards in calcein-free seawater until 48 hpf (Fig. 2a–d), none of the vesicular calcein label appeared in the shell, indicating that larvae do not accumulate a significant intracellular calcium reservoir prior to shell formation. This is in accordance with our larval calcium content measurements (Fig. 1a). When larvae were labeled for 15–180 min with calcein during the initial shell formation phase (21–30 hpf) and then cultured in non-labeled FSW for several more hours (Fig. 2b), the label rapidly (within <15 min, Fig. 2g, h) appeared in the shell and in many intracellular vesicles. However, none of this intracellular label was found in shell material formed after the calcein labeled FSW had been removed (Fig. 2e, f). This also suggests that, unlike in echinoderm larvae[15], large intracellular calcein positive vesicles do not serve as a calcium reservoir for shell formation. The most parsimonious explanation for our findings is that rapid transepithelial transport of substrates (Ca^{2+}, HCO_3^-) to the CS enables extracellular shell formation. Transport of calcification substrates through transepithelial pathways (transcellular and paracellular) has been observed in several biological systems[24–26]. The rapid appearance of calcein label in the growing shell (<15 min, Fig. 2g, h) suggests that mussel larvae epithelia are relatively "leaky", allowing the relatively large calcein molecule (0.6 kDa) to pass via paracellular pathways to the CS. Similarly, calcification substrates (Ca^{2+}, HCO_3^-/CO_3^{2-}) could take a similar route from seawater to the CS. This would make the calcification process vulnerable to fluctuations in extracellular carbonate chemistry at the CS.

Carbonate chemistry at the CS is influenced by OA. In order to characterize the carbonate chemistry at the CS, microelectrode measurements were performed in the extracellular space below

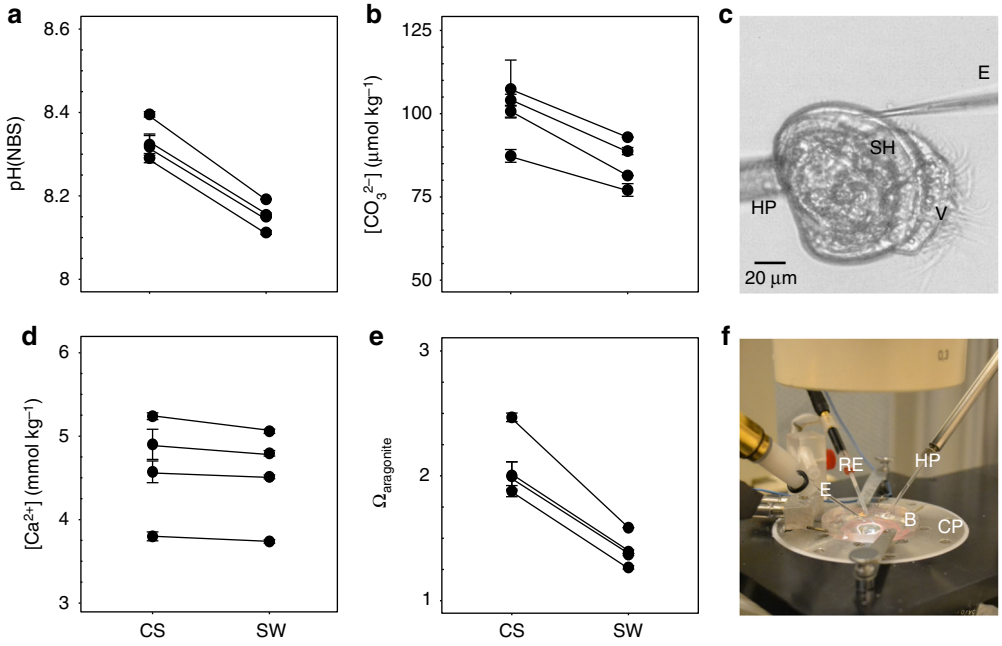

Fig. 3 Carbonate chemistry parameters in the calcification space of PD I larvae from Exp 3. **a** pH_{NBS}. **b** $[CO_3^{2-}]$. **c** Image of larva attached to a holding pipette (HP) with the tip of the measuring electrode (E) visible at the site of calcification (CS), below the shell (SH), V = velum. **d** $[Ca^{2+}]$. **e** Ω_{arag}. **f** Setup for microelectrode measurements showing inverted microscope, the electrode, holding pipette, water bath (B), reference electrode (RE) and cooling plate (CP). Plotted data are the mean ± s.d. from $N = 4$ fertilizations and 5 larvae for each treatment and fertilization

the growing shell edge in PD I veliger larvae (Fig. 3a–f). Our measurements demonstrate that early veliger larvae have active control over the carbonate chemistry of the fluid adjacent to the growing shell, which is in contrast to the situation in adult mussels, where extrapallial fluid pH and Ω_{arag} are lower than the respective seawater values[27]. Under control conditions, pH at the site of calcification (pH_{CS}) was found to be elevated by ca. 0.2 pH units with respect to the surrounding seawater pH (pH_{SW}, $v = 325$, $p < 0.01$, Fig. 3a), $[CO_3^{2-}]$ by 14 µmol kg^{-1} ($t = -9.8338$, $p < 0.01$, Fig. 3b) and $[Ca^{2+}]$ by ca. 0.1 mmol kg^{-1} ($v = 185$, $p < 0.05$, Fig. 3d). These conditions favor calcification and prevent dissolution, as they lead to a significant increase in Ω_{arag} at the tissue–shell interface: Ω_{arag} is increased from seawater values of ca. 1.4 to 2.2 at the site of calcification ($v = 325$, $p < 0.01$, Fig. 3e). Using Eq. (1), this increase in Ω_{arag} would enhance calcification rates by a factor of ca. 2.7. The mechanisms underlying this pH regulatory effort are yet unexplored in bivalves. Rapid aragonite deposition in mussel larvae has been correlated with increased activity of carbonic anhydrase, but it is unclear if it plays a role in CS carbonate chemistry regulation[21]. However, based on larval oyster gene expression data, all typical pH regulatory proteins that are commonly utilized to control extracellular and intracellular pH in marine metazoans are expressed in bivalve larvae[28].

When larvae were reared under simulated OA conditions, pH_{CS} and pH_{SW} declined linearly with increasing pCO_2 (Fig. 4a). The offset between pH_{CS} and pH_{SW} could be maintained up to pCO_2 values of about 1,500–2,000 µatm. In fact, $\Delta[H^+]$ between SW and CS remained constant between 500 and 1,500 µatm, indicating that acidification cannot be compensated by increased rates of proton removal from the CS. While $[Ca^{2+}]_{CS}$ remained constant over the entire range of pCO_2 levels tested, $[CO_3^{2-}]_{CS}$ strongly declined with $[CO_3^{2-}]_{SW}$, from ca. 100 to 39 µmol kg^{-1} (Fig. 4d). The sigmoidal collapse of $[H^+]$ gradients indicates the sensitivity threshold of the extracellular pH_{CS} regulation machinery (Fig. 4c). Together, these changes led to a strong exponential decline in Ω_{arag} at the CS, albeit with a significant positive offset between SW and CS: undersaturation ($\Omega_{arag} < 1$) at the CS occurred at a seawater pCO_2 ca. 999.5 µatm while undersaturation in SW was already reached at ca. 723.6 µatm (Fig. 4f). This finding illustrates the ability of mussel larvae to offset impacts of OA at the mineral interface to some degree, but also demonstrates the limited capacity of the regulatory system. Changes in carbonate chemistry at the CS likely impact both, catalytic function of extracellular pH sensitive enzymes involved in shell matrix processing, as well as rates of carbonate precipitation and dissolution[12, 29].

Low Ω_{arag} at the CS leads to reduced growth and dissolution. In accordance with the CO_2 induced progressive decrease in Ω_{arag} at the tissue–mineral interface, calcification rates (i.e. shell length at the PD I veliger stage) decreased in a linear fashion (Fig. 5a), a finding that is in accordance with several other studies on mussel and oyster larvae[3, 6–8]. However, mussel larvae were able to form fully developed PD I veliger shells in all treatments, even at seawater pCO_2 values that resulted in Ω_{arag} undersaturation at the CS. While a range of studies has demonstrated that mortality and rates of shell deformation are increased at very high seawater pCO_2 (>2,000 µatm), some larvae are clearly able to overcome the adverse carbonate chemistry conditions—potentially via modulation of organic matrix components that stabilize precipitated carbonate material or via production of chemically more resistant nanogranular building blocks[30]. In addition, it has been empirically demonstrated that bivalves continually experience dissolution of the internal surface of their shell, even under conditions where $\Omega_{arag} > 1$[20], which is due to the inherently higher solubility of biogenic carbonates. Therefore, elevation of Ω_{arag} at the CS in mussel larvae may be crucial to help offset shell dissolution. In order to investigate, whether $\Omega_{arag} < 1$ at the CS leads to shell dissolution, as recently shown for oyster larval stages[7], we conducted another calcein labeling experiment: larvae were reared for 21 h under control conditions, labeled with calcein for 3 h and then exposed to acidified conditions for 3 days (Fig. 5c) to determine, whether labeled shell material would dissolve once deposited. Shell fluorescence intensity of the labeled shell parts followed a sigmoidal pattern (Fig. 5b), with significant decreases

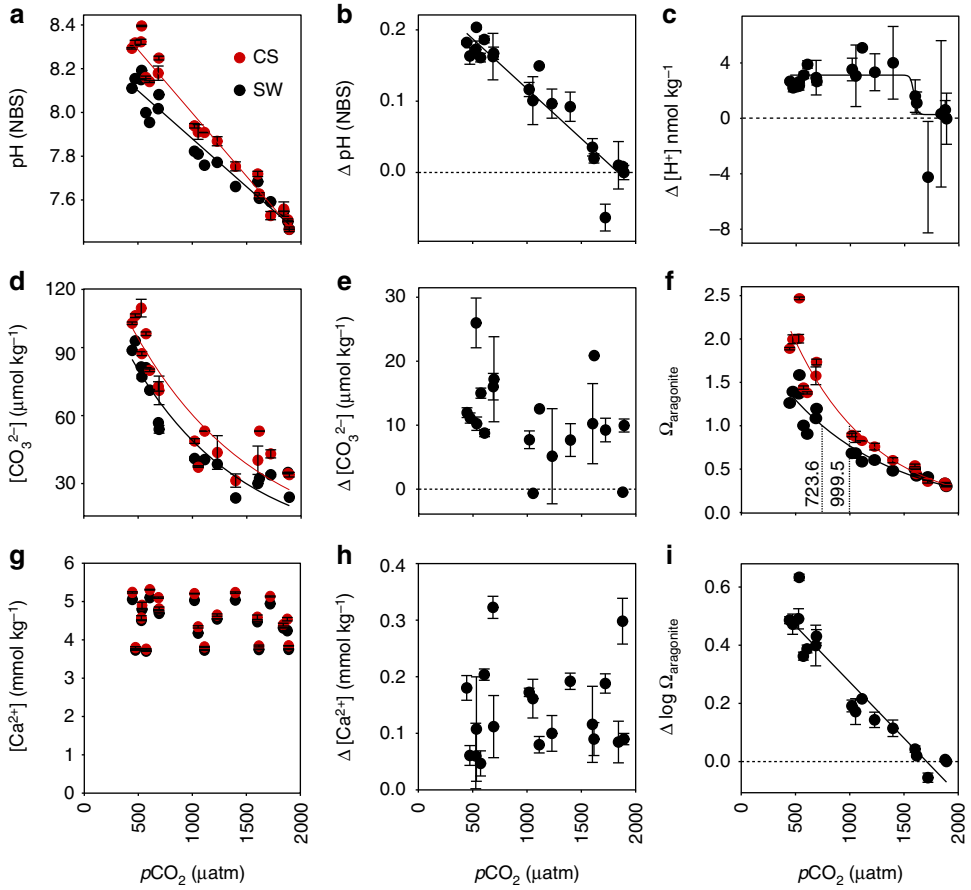

Fig. 4 Impact of OA, in black on carbonate chemistry parameters at the site of calcification in red from Exp 3. **a** pH_{NBS} **b** ΔpH_{NBS} (CS-SW) **c** Δ $[H^+]$ **d** $[CO_3^{2-}]$ **e** Δ $[CO_3^{2-}]$ (CS-SW) **f** Ω_{arag} **g** $[Ca^{2+}]$ **h** Δ$[Ca^{2+}]$ **i** Δ log Ω_{arag}. Plotted data are the mean + s.d. from $N = 4$ fertilizations and 5 larvae for each treatment and fertilization.

in fluorescence (by ca. 20%) likely related to decreases in shell thickness[31] only detectable at very high levels of OA (2000 and 2500 µatm). This finding is in contrast to strong dissolution effects observed in larval oysters at lower pCO_2, but indicates the high degree of biological control over mineral integrity in mussels even under strongly acidified conditions[7].

Ion and acid–base regulation are metabolically costly, as is the production of organic matrix components for shell formation[32, 33]. It is unclear what the costs for maintenance of the observed gradient in Ω_{arag} are, but the inability of mussels to increase the proton gradient between SW and CS with increasing levels of OA indicates a fixed ion regulatory capacity at the tissue-mineral interface. Our results suggest that observed reductions in calcification with OA could be primarily attributed to decreased rates of $CaCO_3$ precipitation at decreasing Ω_{arag} at the CS. In summary, we provide novel evidence of how ocean acidification influences Ω_{arag} at the larval tissue-shell interface. Significant, but ultimately limited ion regulatory capacity to overcome acid–base challenges at the CS contributes to vulnerability of mussel larvae to ocean acidification. Although mussel larvae have been shown to successfully complete larval development in coastal habitats that are already CO_2 enriched today[34], future changes in coastal ocean carbonate chemistry may rapidly deplete this limited degree of ion regulatory control[10].

Methods

Animal collection and larval culture. Adult *Mytilus edulis* were collected in April–June 2015 and 2016 from Kiel Fjord, outside GEOMAR. Spawning was induced by rapidly increasing water temperatures to 18–24 °C and gametes were collected in filtered seawater (FSW, 0.2 µm). A total of >50 separate fertilizations were obtained during this period to conduct four experiments (Exp 1–4). 30 min following fertilization, embryos were checked for presence of polar bodies and embryo cleavage and placed in 2–10 L glass bottles filled with FSW at a density of 100 embryos per mL (Exp 1) or 10 embryos per mL (Exp 2–4) at a temperature of 17 °C. Culture bottles were gently and continuously aerated using pressurized air supplied through plastic tubing, connected to 10 mL plastic Pasteur pipettes. Following PD I veliger development, FSW was daily supplemented with *Rhodomonas salina* to reach a final concentration of 10,000 cells ml^{-1}. For the OA experiments (Exp 3, 4), FSW was continuously aerated with CO_2-enriched air (400, 800, 1,250, 1,600, or 2,000 µatm). Cultures were maintained at a natural salinity of 14–15‰.

Carbonate chemistry measurements and calculations. Carbonate chemistry samples were collected from the culture bottles just before adding embryos to the bottles. Samples were collected in 52 ml Duran Schott glass bottles with glass stoppers and preserved by the addition of 10 µl of saturated $HgCl_2$ solution. Dissolved inorganic carbon (C_T) was analyzed using an AIRICA C_T analyzer (Marianda, Germany). Seawater carbonate system speciation (pCO_2, total alkalinity, $[HCO_3^-]$, $[CO_3^{2-}]$) was calculated from C_T and pH_{NBS} using CO2SYS[35] with dissociation constants for $KHSO_4$[36]and the carbonate system (K1 and K2)[37, 38]. Certified seawater reference materials (batch 142; Scripps Institution of Oceanography, University of California, San Diego, CA, USA) were used to ensure accuracy of C_T measurements. Saturation state of aragonite was calculated using $[Ca^{2+}]$ and $[CO_3^{2-}]$ from microelectrode measurements and the apparent solubility product for aragonite calculated for the respective salinity and temperature conditions according to Mucci[39].

Calcium accumulation. Exp 1: To investigate calcium accumulation, larvae between 4 and 40 hpf from $N = 5$ replicate families were collected on a 20 µm mesh and transferred to a 2 ml Eppendorf tube using a plastic Pasteur pipette. For each development stage, 90,000–300,000 individuals were collected. Samples were centrifuged and the supernatant was discarded. The samples were then vortexed in 500 µl distilled water and centrifuged for 10 min at 21,800 r.p.m. The supernatant was discarded and the larval pellet was dissolved in 500 µl 10 M HCl. Samples were

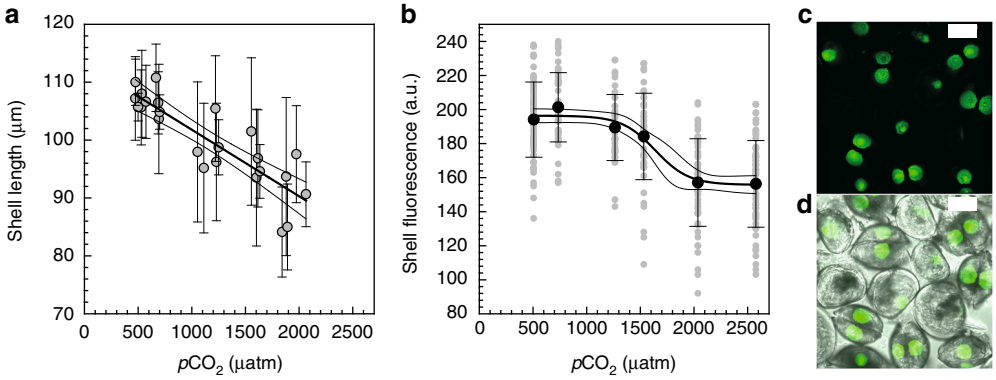

Fig. 5 Impact of CO_2-driven seawater acidification on calcification in PD I larvae from Exp 3 and 4. **a** Shell length at PD I, veliger larval stage. Data are means ± s.d. from $N = 5$ fertilizations and 10–25 animals per treatment and fertilization. Linear regression: shell length (µm) = 113.3–0.0115 pCO_2 (µatm), $R^2 = 0.74$, $F_{(1,22)} = 63$, $p < 0.001$. **b** Calcein fluorescence intensity of larval shell portions formed during 21–24 hpf imaged following 3 day exposure to OA. Data are the mean ± s.d. from one experiment. Sigmoidal regression: fluorescence intensity (a.u.) = 155.8 + 40.6/(1 + exp (−(pCO_2 − 1639)/−156.1)), $R^2 =$ 0.36, $F_{(3,338)} = 64$, $p < 0.001$. **c** Calcein fluorescence confocal projections of larvae used to measure shell dissolution. **d** Merged fluorescence and transmission images. Scale bars: 75 µm

analyzed using a flame photometer (EFOX 5053, Eppendorf) that was calibrated using urine standards (Biorapid). Calcium concentrations were normalized per larvae following a background subtraction for the HCl larvae were dissolved in. Larvae from each developmental stage were sampled and fixed in 4% PFA buffered to pH 8.1. Larval samples were subsequently analyzed to assess mineralization using an inverted microscope (Leica DMi8) equipped with crossed polarized light filters.

Calcein pulse-chase. Exp 2: Larval cultures were stained using 50 mg l^{-1} calcein label at pH 8.2 in FSW for various time periods, ranging from continuous culture (4–48 hpf) in calcein labeled FSW (>$N = 30$ separate experimental fertilizations) to 15–180 min calcein labeling intervals during key phases of the shell formation process ($N = 3$ separate experiments per time interval). Following labeling, animals were concentrated while constantly submerged in FSW using 20 µm nylon mesh sieves and gently washed using FSW until no traces of calcein were visible. Subsequently, animals were either directly imaged or cultured in unlabeled FSW and sampled a few hours later. For confocal microscopy, larvae were placed on microscopy slides suspended in FSW and covered with glass coverslips supported by ca.30-µm-thick fibers as spacers. Larvae were then imaged in vivo with a Zeiss LSM510 using a Plan Neofluar 40×/1.3 oil objective and a 505–530 nm band-pass filter at an excitation wavelength of 488 nm. Images (10–30 µm thick z-stacks of 1 µm optical sections) were collected within 20–30 min at 20 °C and processed to create 3D projections using Zeiss LSM510 software. Typically, larvae remained viable for >60 min under these conditions.

Calcifying space carbonate chemistry. Exp 3: Using ion-selective electrodes, H^+, CO_3^{2-} and Ca^{2+} concentration were measured below the surface of the shell in 48 h veliger larvae (5 animals from each treatment for each of $N = 4$ separate fertilizations, Supplementary Table 1). Microelectrode construction and measurements were performed as described previously[18, 40, 41]. Briefly, borosilicate glass capillary tubes (GB150F-8P, Science Products) were pulled using a DMZ-Universal puller (Zeitz Instruments) to a diameter of 1–3 µm and silanized with dimethyl chlorosilane (Sigma-Aldrich) at 200 °C for 4 h. The pH selective microelectrodes were back filled with a KCL based electrolyte (300 mM KCl, 50 mM $NaPO_4$, pH 7) and front loaded with a H^+ ionophore (H^+ ionophore III, Sigma Aldrich). The calcium selective microelectrodes were back filled with a KCl based electrolyte (200 mM KCl, 2 mM $CaCl_2.2H_2O$) and front loaded with a Ca^{2+} ionophore (Ca^{2+} ionophore II, Sigma Aldrich). The carbonate selective microelectrodes back filled with a $CaCO_3$ based electrolyte (19.1 g l^{-1} $Na_2B_4O_7$*$10H_2O$ adjusted with 100 mM HCl to pH 9.0, amended with 0.2 mM $CaCO_3$ after which the pH was again brought to 9.0) and front loaded with a CO_3^{2-} ionophore (N,N,-dioctyl-3α,12α-bis(4-trifluoroacetylbenzoxy)-5β-cholan-24-amide, TFAP-CA, Sigma Aldrich). To measure pH, carbonate and calcium gradients, the larvae were transported to the microscope set up in Duran Schott glass bottles (500 ml). Measurements were performed within 2 h of transporting larvae and no changes in carbonate chemistry in the bottles were observed. For each pCO_2 treatment, measurements from 5 larvae per fertilization were obtained within 30 min. Larvae were concentrated submerged in respective FSW media using a 50 µm mesh and placed into a perfusion chamber mounted on an inverted microscope (Axiovert 135; Zeiss) at a density of 100 ml^{-1}. The microscope was equipped with a temperature controlled stage, connected to a water cooling system to maintain water bath temperatures at constant 17 °C±0.1 °C. Larvae were held in position using a holding pipette with a tip diameter of ca. 25 µm, to which a slight vacuum was applied (Fig. 3c). The ion-selective probe was mounted on a remote-controlled micro-manipulator and was introduced beneath the shell from the side of the growing edge (Fig. 3f) and typically the larvae reacted by closing their valves. However, when open, the microelectrode was inserted 3–4 µm from the shell edge until the glass tip of the microelectrode reached the inorganic (hard) inner surface of the shell. The microelectrode was held in position in this space near the inner shell surface, between the shell and tissue. Measurements were conducted using a high impedance amplifier (World Precision Instruments, FD223). Stable mV readings were obtained within 5–10 s. The Nernstian property of each microelectrode (ca. 52–54 mV for pH electrodes and ca. 24–27 mV for $[CO_3^{2-}]$ and $[Ca^{2+}]$ electrodes) was measured by placing the microelectrode in a series of seawater solutions with a reference Ag/AgCl electrode (pH range 7.5–8.3, $[CO_3^{2-}]$ range 20–130 µmol kg^{-1}, and $[Ca^{2+}]$ range 0.1–10 mmol kg^{-1}). Calibration curves were prepared for each new set of electrodes using seawater of varying pH (using HCl and NaOH) for pH electrodes, CO_2 bubbled seawater with $[CO_3^{2-}]$ ranging between 20–130 µmol kg^{-1} (calculated using pH and C_T) for $[CO_3^{2-}]$ microelectrodes and artificial seawater with $[Ca^{2+}]$ ranging between 0.1 and 10 mmol kg^{-1}. New electrodes were built for each fertilization. With this setup, we were able to resolve a minimum difference in pH of ~0.002, $[CO_3^{2-}]$ of ~1 µmol kg^{-1} and $[Ca^{2+}]$ of ~0.02 mmol kg^{-1}). A subsample of larvae from each treatment were sampled directly prior to microsensor measurements and fixed in 4% PFA buffered to pH 8.1 for determination of shell length at PD I. Thirty individuals for each treatment from $N = 5$ separate fertilizations were photographed using a stereomicroscope at ×100 magnification (Leica M165 FC) equipped with a Leica DFC 310 FX camera and shell length was measured using ImageJ.

Shell dissolution. Exp 4: A larval culture (one fertilization) was labeled with calcein from 21–24 hpf under control conditions (400 µatm). Subsequently, larvae were gently washed in FSW and distributed in culture vessels exposed to pCO_2 treatments of 400, 800, 1,250, 1,600, 2,000 and 2,500 µatm for 3 days. Samples were frozen at −20 °C for 2 weeks and analyzed using confocal microscopy as described above. No shell fluorescence loss occurred following the freezing procedure. To quantify loss of fluorescence from shell parts formed at 21–24 hpf in response to OA, 3D projections of one shell valve of 45–70 animals per pCO_2 level were generated and fluorescence intensity determined for a shell area of 100–150 $µm^2$.

Data analyses. Data were analysed using paired *t*-tests following tests for normality and homogeneity using Shapiro-Wilks test and Bartlett test respectively. If assumption for normality were not met, a non-parametric Wilcoxon signed-rank test was applied. To study the effect of OA on carbonate system speciation and $[Ca^{2+}]$ of the CS vs. SW, shell length and dissolution, regression analysis was conducted where linear model functions for each parameter were compared by applying an ANOVA (Supplementary Tables 2 and 3). Statistical analyses were conducted using R (Version 3.3.2, R Development Core Team, R: http://www.R.org/. 2011).

Data availability. Data can be accessed through PANGAEA database (https://doi.pangaea.de/10.1594/PANGAEA.881869).

Received: 14 March 2017 Accepted: 17 October 2017
Published online: 22 November 2017

References

1. Ekstrom, J. A. et al. Vulnerability and adaptation of US shellfisheries to ocean acidification. *Nat. Clim. Change* **5**, 207–214 (2015).
2. Ries, J. B., Cohen, A. L. & McCorkle, D. C. Marine calcifiers exhibit mixed responses to CO_2-induced ocean acidification. *Geology* **37**, 1131–1134 (2009).
3. Gazeau, F. et al. Impacts of ocean acidification on marine shelled molluscs. *Mar. Biol.* **160**, 2207–2245 (2013).
4. Wittmann, A. C. & Portner, H. O. Sensitivities of extant taxa to ocean acidification. *Nat. Clim. Change* **3**, 995–1001 (2013).
5. Gazeau, F. et al. Effect of ocean acidification on the early life stages of the blue mussel *Mytilus edulis*. *Biogeosciences* **7**, 2051–2060 (2010).
6. Ventura, A., Schulz, S. & Dupont, S. Maintained larval growth in mussel larvae exposed to acidified undersaturated seawater. *Sci. Rep.* **6**, 23728 (2016).
7. Frieder, C. A., Applebaum, S. L., Pan, T. C. F., Hedgecock, D. & Manahan, D. Metabolic cost of calcification in bivalve larvae under experimental ocean acidification. *ICES J. Mar. Sci.* fsw213 https://doi.org/10.1093/icesjms/fsw213 (2016).
8. Thomsen, J., Haynert, K., Wegner, K. M. & Melzner, F. Impact of seawater carbonate chemistry on the calcification of marine bivalves. *Biogeosciences* **12**, 1543 (2015).
9. Waldbusser, G. et al. Saturation-state sensitivity of marine bivalve larvae to ocean acidification. *Nat. Clim. Change* **5**, 273–280 (2014).
10. Melzner, F. et al. Future ocean acidification will be amplified by hypoxia in coastal habitats. *Mar. Biol.* **160**, 1875–1888 (2013).
11. Heuer, R. M. & Grosell, M. Physiological impacts of elevated carbon dioxide and ocean acidification on fish. *Am. J. Physiol. Regul. Integr. Comp. Physiol.* **307**, R1061–R1084 (2014).
12. Waldbusser, G. et al. A developmental and energetic basis linking larval oyster shell formation to acidification sensitivity. *Geophys. Res. Lett.* **40**, 2171–2176 (2013).
13. Mount, A. S., Wheeler, A. P., Paradkar, R. P. & Snider, D. Hemocyte-mediated shell mineralization in the Eastern oyster. *Science* **304**, 297–300 (2004).
14. Johnstone, M. B. et al. Cellular orchestrated biomineralization of crystalline composites on implant surfaces by the eastern oyster, *Crassostrea virginica* (Gmelin, 1791). *J. Exp. Mar. Biol. Ecol.* **463**, 8–16 (2015).
15. Vidavsky, N. et al. Initial stages of calcium uptake and mineral deposition in sea urchin embryos. *Proc. Nat. Acad. Sci. USA* **111**, 39–44 (2013).
16. Politi, Y., Arad, T., Klein, E., Weiner, S. & Addadi, L. Sea urchin spine calcite forms via a transient amorphous calcium carbonate phase. *Science* **306**, 1161–1164 (2004).
17. Weiss, I., Tuross, N., Addadi, L. & Weiner, S. Mollusc larval shell formation: amorphous calcium carbonate is a precursor phase for aragonite. *J. Exp. Zool.* **293**, 478–491 (2002).
18. Stumpp, M. et al. Acidified seawater impacts sea urchin larvae pH regulatory systems relevant for calcification. *Proc. Natl Acad. Sci. USA* **109**, 18192–18197 (2012).
19. Morse, J. W., Arvidson, R. S. & Lüttge, A. Calcium carbonate formation and dissolution. *Chem. Rev.* **107**, 342–381 (2007).
20. Ries, J. B., Ghazaleh, M. N., Connolly, B., Westfield, I. & Castillo, K. D. Impacts of seawater saturation state (Ω_A = 0.4–4.6) and temperature (10, 25 °C) on the dissolution kinetics of whole-shell biogenic carbonates. *Geochim. Cosmochim. Acta.* **192**, 318–337 (2016).
21. Medakovic, D. Carbonic anhydrase activity and biomineralization process in embryos, larvae and adult blue mussels *Mytilus edulis* L. *Helgoland Mar. Res.* **54**, 1–6 (2000).
22. Kudo, M. et al. Microtexture of larval shell of oyster, *Crassostrea nippona*: a FIB-TEM study. *J. Struct. Biol.* **169**, 1–5 (2010).
23. Yokoo, N. et al. Microstructures of the larval shell of a pearl oyster, *Pinctada fucata*, investigated by FIB-TEM technique. *Am. Mineral.* **96**, 1020–1027 (2011).
24. Carre, M. et al. Calcification rate influence on trace element concentrations in aragonitic bivalve shells: evidences and mechanisms. *Geochim. Cosmochim. Acta.* **70**, 4906–4920 (2006).
25. Tambutte, E. et al. Calcein labelling and electrophysiology: insights on coral tissue permeability and calcification. *Proc. R. Soc. B.* **279**, 19–27 (2012).
26. Gagnon, A. C., Adkins, J. F. & Erez, J. Seawater transport during coral biomineralization. *Earth. Planet. Sci. Lett.* **329–330**, 150–161 (2012).
27. Thomsen, J. et al. Calcifying invertebrates succeed in a naturally CO_2-rich coastal habitat but are threatened by high levels of future acidification. *Biogeosciences* **7**, 3879–3891 (2010).
28. Zhang, G. et al. The oyster genome reveals stress adaptation and complexity of shell formation. *Nature* **490**, 49–54 (2012).
29. Schönitzer, V. & Weiss, I. M. The structure of mollusc larval shells formed in the presence of the chitin synthase inhibitor Nikkomycin Z. *BMC Struct. Biol.* **7**, 71 (2007).
30. Wolf, S. E. et al. Nonclassical crystallization in vivo et in vitro (I): Process-structure property relationships of nanogranular biominerals. *J. Struct. Biol.* **196**, 244–259 (2016).
31. Gaylord, B. et al. Functional impacts of ocean acidification in an ecologically critical foundation species. *J. Exp. Biol.* **214**, 2586–2594 (2011).
32. Pan, T. C. F., Applebaum, S. L. & Manahan, D. Experimental ocean acidification alters the allocation of metabolic energy. *Proc. Natl Acad. Sci. USA* **112**, 4696–4701 (2015).
33. Palmer, A. R. Calcification in marine molluscs: How costly is it? *PNAS* **89**, 1379–1382 (1992).
34. Thomsen, J. et al. Naturally acidified habitat selects for ocean acidification–tolerant mussels. *Sci. Adv.* **3**, https://doi.org/10.1126/sciadv.1602411 (2017).
35. Lewis, E. & Wallace, D. *Program Developed for CO2 System Calculations*. (Oak Ridge NationalLaboratory, Oak Ridge, TN, 1998).
36. Dickson, A. G. Standard potential of the reaction—AgClS + 1/2 H2 = AgS + HClAq and the standard acidity constant of the ion HSO4—in synthetic sea-water from 273.15-K to 318.15-K. *J. Chem. Thermodyn.* **22**, 113–127 (1990).
37. Roy, R. N. et al. Determination of the ionization constants of carbonic acid in seawater. *Mar. Chem.* **44**, 249–259 (1993).
38. Dickson, A. G. & Millero, F. J. A comparison of the equilibrium-constants for the dissociation of carbonic-acid in seawater media. *Deep-Sea Res.* **34**, 1733–1743 (1987).
39. Mucci, A. The solubility of calcite and aragonite in seawater at various salinities, temperatures, and one atmosphere total pressure. *Am. J. Sci.* **283**, 780–799 (1983).
40. de Beer, D. et al. A microsensor for carbonate ions suitable for microprofiling in freshwater and saline environments. *Limnol. Oceanogr. Methods* **6**, 532–541 (2008).
41. Stumpp, M. et al. Digestion in sea urchin larvae impaired under ocean acidification. *Nat. Clim. Change* **3**, 1044–1049 (2013).

Acknowledgements

This study was funded by the European Union's Seventh Framework Programme [FP7] ITN project "CACHE" under REA grant agreement #[605051]13, the Kiel Excellence Cluster "Future Ocean" and the GEOMAR seed-funding grant "microsensors 70090/06". We are grateful to Claas Hiebenthal and Ulrike Panknin for Kiel Marine Organism Culture Centre (KIMOCC) support.

Author contributions

K.R. and F.M. designed the study. K.R., M.Y.H., J.T., M.B. and F.M. conducted experiments. K.R. and F.M. analysed the data and wrote the manuscript. All authors contributed to manuscript revisions.

Additional information

Supplementary Information accompanies this paper at doi:10.1038/s41467-017-01806-8.

Competing interests: The authors declare no competing financial interests.

Reprints and permission information is available online at http://npg.nature.com/reprintsandpermissions/

Publisher's note: Springer Nature remains neutral with regard to jurisdictional claims in published maps and institutional affiliations.

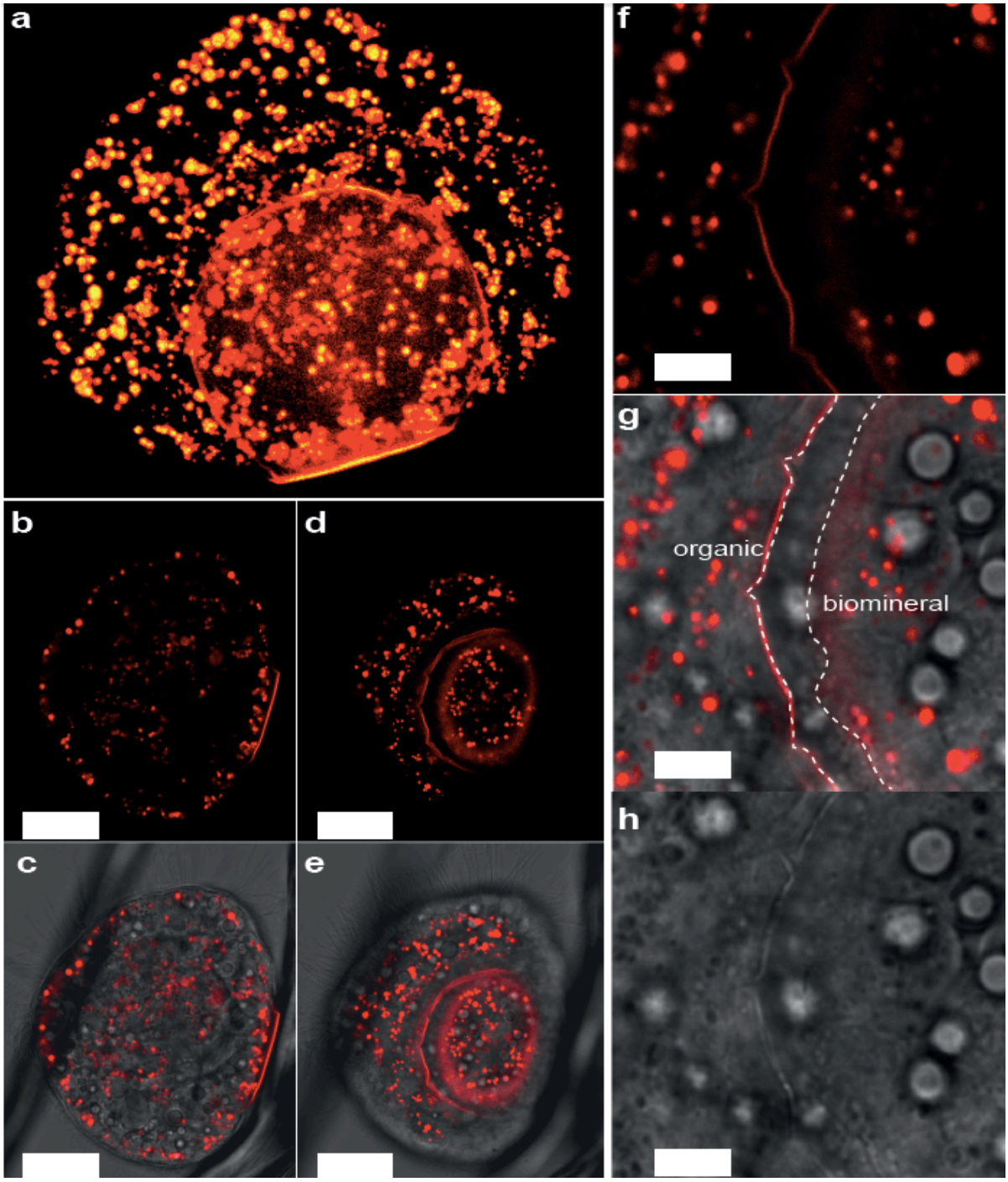

Supplementary Figure 1. Shell organic cover autofluorescence images. (**a**) Confocal projection of unstained 27hpf larva imaged at high laser intensity and using a long – pass filter (LP 505 nm) instead of the band – pass filter (BP 505-530 nm) used for calcein imaging. Autofluorescence of shell organic cover and of numerous vesicles is visible; (**b**) confocal section illustrating autofluorescence of organic portion of hinge. The hinge is not calcified at this point of time (see Fig. 1) (**c**) same larva, merged transmission and fluorescence images (**d**) same larva, different optical plane to illustrate organic shell cover; (**e**) same larva, merged transmission and fluorescence images (**f, g, h**) same larva, close – up of shell margin fluorescence (**f**), merged fluorescence and transmission images (**g**) and transmission light

image (**h**). Organic shell cover and organic shell matrix are fluorescent and illustrate the ca. 3-5 µm gap between growing edges of organic vs. biomineral phases. Scale bars: 20 µm (b,c,d,e), 5 µm (f,g,h).

Supplementary Table 1. Seawater carbonate chemistry parameters calculated from C_T and pH_{NBS} using CO2SYS. Carbonate chemistry measurements were obtained once for each fertilization / experimental run. The last three columns indicate, which measurements were conducted with the respective experimental runs (a: for Fig. 3 and 4 (microsensors), b: for Fig. 5 (shell length), c: for Fig. 5 (shell dissolution)).

Exp	Sal. (psu)	Temp. (°C)	Treatment	C_T (µmol/kg SW)	pH_{NBS}	pCO_2 (µatm)	A_T (µmol/kg SW)	CO_3^{2-} (µmol/kg SW)	Ω_{arag}	a	b	c
Exp 3_1	15.1	16.5	1	1915.83	8.19	445	2018.91	94.66	1.52	X		
	15.1	16.5	2	1955.05	8.07	607	2026.11	74.44	1.19	X		
	15.1	16.5	3	1994.27	7.86	1020	2013.69	46.71	0.75	X		
	15.1	16.5	4	2042.31	7.73	1398	2032.53	35.68	0.57	X		
	15.1	16.5	5	2045.25	7.64	1721	2014.06	28.89	0.46	X		
Exp 3_2	15.0	16.5	1	2008.59	8.14	534	2098.89	88.09	1.41	X	X	
	15.0	16.5	2	2033.09	8.04	687	2096.73	71.59	1.15	X	X	
	15.0	16.5	3	2055.64	7.86	1054	2074.63	47.85	0.77	X	X	
	15.0	16.5	4	2083.09	7.61	1879	2043.21	27.24	0.44	X	X	
	15.0	16.5	5	2088.97	7.40	3004	1990.86	16.56	0.27	X	X	
Exp 3_3	14.8	16.5	1	1903.7	8.12	528	1984.40	79.58	1.27	X	X	
	14.8	16.5	2	1938.99	8.01	693	1992.87	63.74	1.02	X	X	
	14.8	16.5	3	1986.04	7.77	1229	1985.66	37.96	0.61	X	X	
	14.8	16.5	4	2010.55	7.66	1602	1984.70	29.68	0.48	X	X	
	14.8	16.5	5	2018.39	7.60	1842	1978.15	25.88	0.41	X	X	
Exp 3_4	13.8	16.5	1	1917.55	8.16	474	2004.39	84.45	1.35	X	X	
	13.8	16.5	2	1956.65	8.09	572	2025.49	73.53	1.18	X	X	
	13.8	16.5	3	1982.23	7.81	1112	1986.16	39.46	0.63	X	X	
	13.8	16.5	4	2040.05	7.66	1616	2009.33	28.57	0.46	X	X	
	13.8	16.5	5	2038.88	7.59	1892	1991.36	24.22	0.39	X	X	
Exp 3_5	15.4	16.8	1	1903.70	8.14	500	1995.87	87.01	1.40		X	
	15.4	16.8	2	1938.99	8.00	701	1995.66	65.44	1.05		X	
	15.4	16.8	3	1986.05	7.76	1250	1986.99	38.77	0.62		X	
	15.4	16.8	4	2010.55	7.65	1634	1985.46	30.23	0.49		X	
	15.4	16.8	5	2018.39	7.55	2064	1968.32	23.87	0.38		X	
Exp 3_6	15.2	16.8	1	1899.53	8.16	476	1996.34	90.14	1.45		X	
	15.2	16.8	2	1953.97	8.03	666	2016.56	69.35	1.11		X	
	15.2	16.8	3	2001.23	7.78	1220	2004.86	40.15	0.64		X	
	15.2	16.8	4	2030.44	7.68	1555	2010.82	32.29	0.52		X	
	15.2	16.8	5	2056.19	7.58	1974	2011.90	25.86	0.42		X	
Exp 4_1	14.6	16.8	1	1909.79	8.14	507	1997.65	84.70	1.36			X
	14.6	16.8	2	1945.37	7.99	735	1994.95	61.61	0.99			X
	14.6	16.8	3	2009.76	7.77	1264	2008.99	38.46	0.62			X
	14.6	16.8	4	2030.36	7.69	1533	2011.12	32.26	0.52			X
	14.6	16.8	5	2059.10	7.57	2038	2010.33	24.68	0.40			X
	14.6	16.8	6	2084.12	7.47	2577	2007.78	19.69	0.32			X

Supplementary Table 2. Compiled information related to regressions reported in Fig. 4 with N=4 experimental fertilizations and 4-5 treatment levels per fertilization. Regressions were conducted on treatment mean values (all 4 replicate fertilizations). Test for heterogeneity of slopes were conducted using slopes of regressions for individual fertilizations. SW = sea water, CS = calcifying space, x = pCO_2 in µatm.

Parameter	Compartment	Regression Equation	ANOVA	P-value	R^2	Heterogeneity of Slopes	Intercepts
pH_{NBS}	SW CS	y = -0.0004x+8.3191 y = -0.0006x+8.5765	$F_{(1,17)}$=303.2 $F_{(1,17)}$=516.3	<0.001 <0.001	0.94 0.96	**P=0.01, t=5.2, df=3**	**P=0.001, t=15.8, df=3**
ΔpH_{NBS}	CS-SW	y = -0.0001x+0.2574	$F_{(1,17)}$=139.1	<0.001	0.89		
$\Delta[H^+]$ nmol kg^{-1}	CS-SW	y = 0.84+4/(1+exp(-(x-1612)/-16.6))	$F_{(3,15)}$=10.7	<0.001	0.68		
$[CO_3^{2-}]$ µmol kg^{-1}	SW CS	y = -43.51ln(x)+350.01 y = -48.51ln(x)+395.23	$F_{(1,17)}$=22.54 $F_{(1,17)}$=27.37	<0.001 <0.001	0.89 0.86	P>0.05, t=0.3, df=3	P>0.05, t=2.1, df=3
$\Delta[CO_3^{2-}]$ µmol kg^{-1}			$F_{(1,17)}$=2.546	>0.05	0.13		
Log $\Omega_{aragonite}$	SW CS	y = -0.001x+0.7236 y = -0.0013x+1.2994	$F_{(1,16)}$=263.2 $F_{(1,16)}$=468.3	<0.001 <0.001	0.94 0.96	**P<0.05, t=3.7, df=3**	**P=0.004, t=8.0, df=3**
Δlog $\Omega_{aragonite}$	CS-SW	y = -0.0004x+0.6595	$F_{(1,16)}$=155.5	<0.001	0.90		
$[Ca^{2+}]$ mmol kg^{-1}	SW CS		$F_{(1,17)}$=0.82 $F_{(1,17)}$=0.58	>0.05 >0.05	0.04 0.03		
$\Delta[Ca^{2+}]$ mmol kg^{-1}	CS-SW		$F_{(1,17)}$=0.20	>0.05	0.01		

Biogeosciences Discuss., https://doi.org/10.5194/bg-2017-342
Manuscript under review for journal Biogeosciences
Discussion started: 6 September 2017

Calcification in a marginal sea – influence of seawater [Ca^{2+}] and carbonate chemistry on bivalve shell formation

Jörn Thomsen[1], Kirti Ramesh[1,2], Trystan Sanders[1], Markus Bleich[2], Frank Melzner[1]
[1]Marine Ecology, GEOMAR Helmholtz Centre for Ocean Research, Kiel, Germany
[2]Institute of Physiology, Christian-Albrechts-University Kiel, 24098 Kiel, Germany

Running headline: Abiotic effects on mussel calcification

Abstract

In estuarine coastal systems such as the Baltic Sea, mussels suffer from low salinity which limits their distribution. Anthropogenic climate change is expected to cause further desalination which will lead to local extinctions of mussels in the low saline areas. It is commonly accepted that mussel distribution is limited by osmotic stress. However, along the salinity gradient environmental conditions for biomineralization are successively becoming more adverse as a result of reduced [Ca^{2+}] and dissolved inorganic carbon (C_T) availability. In larvae, calcification is an essential process starting during early development with formation of the prodissoconch I (PD I) shell which is completed under optimal conditions within 2 days.

Experimental manipulations of seawater [Ca^{2+}] start to impair PD I formation in *Mytilus* larvae at concentrations below 3 mM, which corresponds to conditions present in the Baltic at salinities below 8 g kg^{-1}. In addition, lowering dissolved inorganic carbon to critical concentrations (<1 mM) similarly affected PD I size which was well correlated with calculated $\Omega_{Aragonite}$ and $[Ca^{2+}][HCO_3^-]/[H^+]$ in all treatments. Comparing results for larvae from the western Baltic with a population from the central Baltic revealed significantly higher tolerance of PD I formation to lowered [Ca^{2+}] and $[Ca^{2+}][HCO_3^-]/[H^+]$ in the low saline adapted population. This may result from genetic adaptation to the more adverse environmental conditions prevailing in the low saline areas of the Baltic.

The combined effects of lowered [Ca^{2+}] and adverse carbonate chemistry represent major limiting factors for bivalve calcification and can thereby contribute to distribution limits of mussels in the Baltic Sea.

Key-words

Baltic Sea, bivalves, calcium, calcification, carbonate chemistry, climate change

1. Introduction

Salinity is one of the most important environmental parameters limiting the distribution of aquatic species. Many marine organisms exhibit little tolerance to reduced salinity and are thus not able to thrive in brackish water environments influenced by riverine inputs (Whitfield et al. 2012). On the other hand, some animals, such as bivalves and crustaceans tolerate the dilution of the ambient seawater and are able to inhabit estuarine, brackish water habitats (Westerbom et al. 2002). However, within these habitats, organisms need to tolerate a number of environmental stressors which are changing concomitantly.

Generally, lowered ambient ion concentrations affect an organism's ability to maintain cellular homeostasis. In response, some organisms such as crustaceans actively regulate the ionic composition of their extracellular fluids. However, mytilid mussels do not control haemolymph osmolarity and ionic composition mostly corresponds to that of ambient seawater (Thomsen et al. 2010). Thus tissues are subjected to a diluted medium in brackish water but the inorganic composition of the intracellular space needs to be regulated in order to maintain enzymatic functions. At moderately lowered salinity, intracellular [K^+] and [Na^+] are kept relatively stable at about 200 and 100 mM, respectively, but [K^+] drops rapidly under strong hypoosmotic stress to avoid cell swelling (Willmer 1978, Wright et al. 1989; Silva and Wright 1994). In order to stay iso-osmotic with their environment following long-term acclimation to lowered salinity, intracellular [K^+] and [Na^+] are maintained at lower concentrations (Willmer 1978, Natochin et al. 1979). In addition, bivalves reduce the

Biogeosciences Discuss., https://doi.org/10.5194/bg-2017-342
Manuscript under review for journal Biogeosciences
Discussion started: 6 September 2017

concentration of intracellular compatible organic osmolytes (Hochachka and Somero 2002) such as certain amino acids, taurine and betaine during the acclimation phase (Silva and Wright 1994, Kube et al. 2006). However, at a certain critical salinity threshold (S_{crit}), the intracellular organic osmolyte pools are depleted which has been suggested to eventually limit species fitness (Kube et al. 2006; Podbielski et al. 2016).

At the same time, bivalves produce an external shell composed of $CaCO_3$ and an organic matrix (Falini et al. 1996). The shell enables adult bivalves to live in intertidal habitats and is an effective protection against predation but shell formation has been shown to be sensitive to lowered salinity (Malone and Dodd 1967). Under favourable environmental conditions, calcification begins already in early development and the first larval shell (prodissoconch I, PD I) is completed within the first 48 hours after fertilization. PD I formation is an important prerequisite for the successful development of bivalve larvae as larvae seem to commence feeding only after completion of the shell which provides structural support (e.g. muscle attachment site) for the functional velum (Lucas and Rangel 1983; Cragg 1985). However, PD I formation is highly sensitive to chemical and environmental stressors (Williams and Hall 1999) and initiation of feeding is delayed under adverse carbonate chemistry (Waldbusser et al. 2015).

Recently, a number of studies investigated how changes of seawater carbonate chemistry affect marine calcifiers. Those studies were mostly motivated by the ongoing input of anthropogenic CO_2 into the oceans which results in a drop of pH and lowered $[CO_3^{2-}]$, a process called ocean acidification. Bivalve shell formation is highly sensitive to modifications of carbonate chemistry and therefore negatively affected by ocean acidification (Gazeau et al. 2013; Waldbusser et al. 2014; Thomsen et al. 2015). The exact reason for the sensitivity of calcification to adverse carbonate chemistry is still under debate (Cyronak et al. 2015). Lowered saturation of seawater with respect to calcium carbonate (Ω, $[Ca^{2+}][CO_3^{2-}]$/ K*sp) (with K*sp=stoichiometric solubility product (Mucci 1983)) could affect the kinetic of shell formation (according to $r = k(\Omega\text{-}1)^n$ with r=mineral precipitation rate, k=rate constant and n=reaction order, Waldbusser et al. 2014) and undersaturation leads to dissolution of existing calcium carbonate structures (Thomsen et al. 2010; Melzner et al. 2011, Haynert et al. 2014). Alternatively, the substrate inhibitor ratio (SIR) defined as the availability of the substrate for calcification in the form of dissolved inorganic carbon (C_T) or HCO_3^- and the inhibitory effect of lowered seawater pH (increased $[H^+]$) could restrict calcification rate (Bach 2015; Thomsen et al. 2015; Fassbender, et al. 2016).

Independent of the exact mode of action, larval bivalve calcification is driven by uptake of seawater Ca^{2+} and inorganic carbon (C_T) whereas metabolic carbon is only of minor importance and contributes by less than 10 % in larvae and adults (McConnaughey and Gillikin 2008, Waldbusser et al. 2015). Oceanic $[Ca^{2+}]$ is about 10 mM, but necessarily linearly related with seawater salinity and thus reduced in estuaries. Freshwater $[Ca^{2+}]$ are in general much lower (<1-2 mM $[Ca^{2+}]$, Ohlson and Anderson 1990; Juhna and Klavins 2000). Oceanic C_T is about 2 mM whereby HCO_3^- and CO_3^{2-} contribute about 90 and 8 % to the C_T pool, respectively. C_T of seawater equilibrated with the atmosphere is directly proportional to salinity as it is depending on seawater total alkalinity (A_T). Therefore, calcifiers are facing abiotic conditions in brackish water habitats which most likely affect their ability to form a shell.

The Baltic Sea is an example of a brackish water habitat which is substantially influenced by precipitation and riverine input (Gustafsson et al. 2014) which results in a salinity gradient from 25 g kg^{-1} in the Kattegat transition zone to basically freshwater in the Gulfs of Riga, Finland and Bothnia. As a consequence, $[Ca^{2+}]$, A_T and C_T decline linearly along the salinity gradient (Kremling and Wilhelm 1997; Beldowski et al. 2010). However, varying composition of riverine freshwater results in differing A_T -salinity correlations and in the Gulf of Riga, A_T and thus C_T even increases with lowered salinity (Beldowski et al. 2010).

The Baltic Sea is among the coastal ecosystems which are most heavily influenced by anthropogenic activity. Eutrophication enhanced hypoxia or even anoxia events in the benthic ecosystem. As respiratory oxygen consumption is coupled to CO_2 production, hypoxia is always accompanied by a pronounced increase of pCO_2 and thus affects the

Biogeosciences Discuss., https://doi.org/10.5194/bg-2017-342
Manuscript under review for journal Biogeosciences
Discussion started: 6 September 2017

carbonate system simultaneously (Melzner et al. 2013). Furthermore, climate change is expected to increase precipitation in the Baltic catchment area which may cause increased riverine runoff leading to reduced salinity (0 - 45 % reduction) in particular in the north-eastern and central Baltic Sea (Meier et al. 2006; Gräwe et al. 2013). This shift in salinity will most likely induce a substantial retreat of the marine fauna and flora and expansion of limnic species into the formerly brackish water habitats (Johannesson et al. 2011).
Mytilid mussels (*Mytilus* spp.) are among the most abundant organisms of the Baltic Sea (10^{13} individuals) contributing up to 90% to local hard bottom biomass, and thus are important habitat builders (Enderlein and Wahl 2004, Johannesson et al. 2011). Their distribution along the Finish, Swedish and Estonian coast is limited by salinities of about 4.5 g kg^{-1} when abundance, biomass and growth drastically decline (Westerbom et al. 2002; Martin et al. 2013; Riisgard et al. 2014). As growth combines both somatic growth and shell formation, it is unclear which physiological mechanism exactly limits performance and therefore the distribution of mussels (Riisgard et al. 2014).
Currently, distribution limits of marine bivalves in estuaries are commonly related to the inability of intracellular osmoregulatory adjustment at lowered salinity (Maar et al. 2015). However, as [Ca^{2+}] and C_T availability decline along the Baltic Sea salinity gradient it is likely that the calcification process is negatively affected as well. This process has not been previously considered as a factor contributing to distribution limits of mussels. In this study, we investigated the effects of seawater [Ca^{2+}] independently of salinity in combination with lowered C_T availability on the calcification performance of larval *Mytilus* spp. and correlated the experimental data with environmental conditions present in the Baltic Sea.

2. Material and Methods

2.1 Animal collection and spawning

Adult mussels were collected from subtidal depths at the pier of GEOMAR in Kiel Fjord (shell length: 4-6 cm, 54°19.8'N; 010°09.0'E) and at the wooden groynes close to Koserow on the island of Usedom (shell length: 2-3 cm, 54°03.4'N; 014°00.4'E) between May and June 2016 (Fig. 1). Median salinity for Kiel Fjord and Usedom, located ~350 km east of Kiel, are ~ 17 and 7 g kg^{-1}, respectively (Table 1).
Mussels in the Baltic Sea represent hybrids of *Mytilus edulis* x *trossulus* with increasing *trossulus* allele frequency towards the less saline, eastern Baltic (Stuckas et al. 2009). Thus mussels collected in Kiel represent the Baltic *M. edulis*-like and animals from Usedom belong to the *M. trossulus*-like genotype (Stuckas et al. 2017).
Specimens were either used for spawning immediately after collection or kept in cold storage (9°C) in order to delay gonad maturation for up to 3 months. Stored mussels (ca. 500 g mussel wet biomass per 20 L tank, 12 tanks) were fed 6 times a week with 500 mL of *Rhodomonas* solution (ca. 2 x 10^6 cells mL^{-1}) supplemented with a commercial bivalve diet (Acuinuga, Spain) and water was exchanged twice a week (Thomsen et al. 2010). *Rhodomonas* spp. were cultured in PES medium as described previously with the exception of using 40 L cylinders (Thomsen et al. 2010).
All experiments were performed at 17°C. Spawning was induced by exposing the animals to rapidly elevated water temperature between 18-25°C using heaters. Spawning specimens were separated from the remaining animals and eggs and sperms were collected individually in beakers filled with 0.2 µm filtered seawater (FSW). Subsequently, eggs were pooled and fertilized with a pooled sperm solution. For the Kiel population, 5 individual experimental runs were performed with varying number of dams and sires used for crossings in each run. In total 16 dams and 18 sires were used. For the Usedom population one run with 4 replicates was performed for which gonads from 5 dams and 4 sires were pooled. Fertilization success was determined by verifying the presence of a polar body and first and second cell division of zygotes and was above 90% in all runs. Embryos (4-8 cell stage) and non-calcified trochophora (in one experimental run of the Kiel population) from all parents were transferred in equal numbers into the experimental units (volume: 25 or 50 mL in round plastic beakers) at a density of 10 embryos/larvae mL^{-1}.

Biogeosciences Discuss., https://doi.org/10.5194/bg-2017-342
Manuscript under review for journal Biogeosciences
Discussion started: 6 September 2017

Three days post fertilization animals were removed from the experimental units by filtering the full water volume through a filter with a mesh size of 20 µm or by collecting larvae individually using a pipette in treatments with low survival. Subsequently, larvae were fixed using 40 % paraformaldehyde (PFA, pH 8.0) resulting in a final PFA concentration of 4%. Pictures of larvae were taken using a stereomicroscope (Leica M165 FC) equipped with a Leica DFC 310 FX camera and LAS V4.2 software. Calcification was assessed by measuring the larval shell length. PD I shell length was assessed using Image J 1.50i by measuring the maximal shell length in parallel to the hinge or the maximal shell diameter for larvae that had not developed a complete PD I shell.

2.2 Experimental manipulation of seawater [Ca^{2+}] and carbonate chemistry

Artificial seawater (ASW) was prepared according to Kester (1967) for salinities of 14 and 7 g kg^{-1} for experiments with *M. edulis*-like and *trossulus*-like, respectively, by adding NaCl, $NaSO_4$, KCl, $NaHCO_3$, KBr, H_3BO_3, $MgCl_2$, $CaCl_2$, and $SrCl_2$ to deionised water. Ca^{2+} free artificial seawater (CFSW) was prepared by omitting $CaCl_2$ and adjusting osmolarity similar to ASW by increasing NaCl concentrations. pH_{NBS} was adjusted to 8.0 using NaOH. All experimental treatments comprised 5 % of 0.2 µm filtered seawater (FSW) from Kiel Fjord which was adjusted to salinity 7 g kg^{-1} for the Usedom population experiment to ensure that trace elements were present. The comparison of shell sizes of larvae kept in control ASW + 5% FSW or 100 % FSW yielded no significant differences ($p>0.05$). Varying seawater [Ca^{2+}] treatments were prepared by mixing ASW and CFSW (lowered [Ca^{2+}]) or by addition of $CaCl_2$ from a 500 mM stock solution to ASW (elevated [Ca^{2+}]). Following mixing, water samples were taken and seawater [Ca^{2+}] was measured using a flame photometer (EFOX 5053, Eppendorf, Germany) calibrated with urine standards (Biorapid GmbH, Germany).
Seawater carbonate chemistry was manipulated by increasing alkalinity by addition of [$NaHCO_3$] to ASW or by lowering alkalinity by adding 1M HCl to the experimental units. Excess CO_2 was removed by aeration of the experimental units for 30 min and embryos were only added after pH had increased again to stable values (~7.8). Seawater pH was determined on the NBS scale using a WTW 3310 pH meter equipped with a Sentix 81 electrode. Seawater C_T was determined using an AIRICA CO_2 analyzer and verified by measuring certified reference material (Dickson et al. 2003). Seawater carbonate system parameters (HCO_3^-, CO_3^{2-}, $\Omega_{aragonite}$) were calculated using the CO2SYS program with KHSO4, K1 and K2 dissociation constants after Dickson et al. (1990) and Roy et al. (1993), respectively. pH_{NBS} was converted to total scale pH. $\Omega_{aragonite}$ and [Ca^{2+}][HCO_3^-]/[H^+] were linearly adjusted according to measured seawater [Ca^{2+}] (Table 2).

2.3 Microelectrode measurements of [Ca^{2+}] in the calcifying space of D-stage veliger

Using ion-selective electrodes, Ca^{2+} gradients were measured in seawater and in the calcification space (CS) below the surface of the shell in veliger larvae three days after fertilization. The experimental set up and hardware was identical to that of Stumpp et al. (2012), except for the addition of a metal plate connected to a water cooling system for temperature control.
Borosilicate glass capillary tubes (inner diameter 1.2 mm, outer diameter, 1.5 mm) with filament were pulled on a DMZ-Universal puller (Zeitz Instruments, Germany) to micropipettes with tip diameters of 1-3 µm. Micropipettes were silanized with dimethyl chlorosilane (Sigma-Aldrich, USA) in an oven at 200°C for 1h. Calcium sensitive liquid ion exchangers (LIX) and LIX-PVC membranes were prepared according to de Beer et al. (2000) with Ca^{2+} ionophore II (Sigma Aldrich). The microelectrodes were back filled with a KCl based electrolyte (200 mM KCl, 2 mM $CaCl_2.2H_2O$) and thereafter front loaded with LIX and finally LIX-PVC at a length of 150 µm and 50 µm, respectively. To measure calcium in the CS, larvae were placed into the temperature controlled perfusion chamber mounted on an inverted microscope (Axiovert 135, Zeiss, Germany) at a density of 100 mL^{-1} and were held in position using a holding pipette. The ion-selective probe was mounted on a remote-controlled micro-manipulator and was introduced beneath the shell from the side of the

Biogeosciences Discuss., https://doi.org/10.5194/bg-2017-342
Manuscript under review for journal Biogeosciences
Discussion started: 6 September 2017

growing edge, where stable measurements were obtained within 5-10 seconds. Microelectrode calibration was verified by measuring [Ca^{2+}] of seawater standards as described above and analogue outputs were channelled through an amplifier (WPI Instruments, USA) to a chart recorder (Gould Instruments, USA).

2.4 Seawater [Ca^{2+}] and carbonate chemistry of the Baltic Sea

Seawater [Ca^{2+}] (mM kg^{-1}) was calculated for salinities between 3 and 20 g kg^{-1} using the correlation for chlorinities <4.5 and >4.5 g kg^{-1} provided by Kremling and Wilhelm (1997) and a salinity-chlorinity conversion after Millero (1984). [Ca^{2+}] was calculated for salinity values measured in Kiel Fjord (N=4250, weekly measurements 2005-2009, 0-18 m, 54°19.8' N, 10°9.0' E, Clemmesen et al., unpublished, Casties et al. 2015) and at the Oder Bank (N=260,000, hourly measurements, 2000-2015, 3+12 m water depths, 54°4.6' N, 14°9.6' E, ~8 km off the *M. trossulus*-like collection site at Usedom (BSH 2000-2015, Table. 1). As distribution of mytilid bivalves is limited by salinities below 4.5 g kg^{-1} the calculation covers the full [Ca^{2+}] range relevant for mussels in this estuary (Westerbom et al. 2002). Carbonate chemistry calculations are based on the salinity-alkalinity correlation published by Beldowski et al. (2010) for salinities between 3 and 20 g kg^{-1} and a seawater surface pCO_2 of 400 µatm assuming equilibrium with current atmospheric CO_2 concentrations of ~400 ppm. Calculations were performed for seawater temperatures of 15°C which corresponds to average conditions experienced by larvae during the natural reproductive period from April to June. The Baltic Sea has four sub areas which are differentially impacted by the inflow of riverine freshwater and their respective chemical properties: the Central Baltic Sea with the Kattegat transition area, the Gulf of Riga, the Gulf of Finland and the Bothnian Sea with Gulf of Bothnia. Depending on the chemical properties of the riverine input, seawater carbonate chemistry can differ substantially for similar salinity values between the four regions. The same calculations were performed for predicting future conditions using atmospheric CO_2 concentration of 800 ppm.

2.5 Statistical analysis

All statistical analyses (t-test, Kruskal-Wallis test followed by Dunn's test, regression analysis, linear and nonlinear model parameter fitting) were performed using R and the mosaic package. Population comparisons were performed by fitting linear models for log transformed data. Each experimental unit was considered as a replicate. Values in text and figures are replicate means ± standard error.

3. Results

3.1 PD I shell formation and CS [Ca^{2+}] under varying seawater [Ca^{2+}]

Larval development until PD I formation was investigated for *M. edulis*-like collected in Kiel Fjord. The lowest seawater [Ca^{2+}] tested in the experiment was 0.51 mM which did not allow successful development of larvae to the trochophore stage in the Kiel population and was thus not considered in subsequent experiments. At all other [Ca^{2+}] treatments, early development was not adversely affected and larvae started to calcify prodissoconch I. However, at [Ca^{2+}] of <2 mM larvae were not able to produce a complete PD I shell. Even after 7 days, shell size did not increase above a mean diameter of 63.7 ± 6.0 µm although larvae stayed viable and continued to actively swim. In all other treatments, shells were fully developed within 72 h post fertilization, but shell length declined linearly at [Ca^{2+}] below 3 mM ranging between 104.5 ± 2.1 µm at 2.8 mM and 82.1 ± 1.5 µm at 1.6 mM, with significant reductions below 2.5 mM [Ca^{2+}] (H: 50.3, $p<0.001$, Dunn's test). Specimens kept at control [Ca^{2+}] of 4-5 mM had mean lengths of 108.2 ± 2.5 µm. Modifications of seawater [Ca^{2+}] in the range 4-10 mM had only minor impacts on lengths and elevated [Ca^{2+}] did not cause a further increase of shell lengths above control size (Fig. 2a, Table 3a).

Microelectrode measurements of [Ca^{2+}] in the CS of *M. edulis*-like revealed that CS [Ca^{2+}] drops with seawater [Ca^{2+}], (H: 21.2, $p<0.01$, Fig. 3a). However, larvae kept at 3.5 mM [Ca^{2+}] (above the critical [Ca^{2+}] threshold) are characterized by CS [Ca^{2+}] of 0.1 ± 0.01 mM above seawater concentrations (paired t-test: $t= 16.9$, $p<0.01$, Fig. 3b). In larvae raised at 2.6 and

Biogeosciences Discuss., https://doi.org/10.5194/bg-2017-342
Manuscript under review for journal Biogeosciences
Discussion started: 6 September 2017

2.3 mM [Ca^{2+}], the difference between seawater and CS [Ca^{2+}] declined to 0.06 ± 0.03 and 0.03 ± 0.02 mM which was not significantly enriched compared to the ambient seawater. In contrast, the gradient between CS and seawater increased to 0.28 ± 0.02 mM in larvae grown at 1.5 mM.

Results for shell formation rates of *M. edulis*-like larvae were compared with the *M. trossulus*-like population from Usedom. Larvae were exposed to [Ca^{2+}] between 0.4-5.8 mM (Fig. 1b,c). Overall, the response curve for *M. trossulus*-like was similar to *M. edulis*-like (Table 3b). Maximal shell sizes observed at 3.7 mM were 120 ± 1.5 µm and shell lengths started to decline at lower [Ca^{2+}]. Nevertheless, at comparable [Ca^{2+}] shell sizes were larger compared to *M. edulis*-like and larvae were able to calcify a full PD I even at 1.1 mM [Ca^{2+}] with an average size of 81.9 ± 3.2 µm. In contrast, PD I formation was not completed at 0.4 mM, yet larvae started to calcify. A linear model of the calcification response revealed a significant effect of [Ca^{2+}] and population on shell size but no interaction (Table 4a, Fig. 2c).

3.2 Combined effects of seawater [Ca^{2+}] and carbonate chemistry on larval calcification

M. edulis-like larvae were exposed to a range of seawater [Ca^{2+}] between 1 and 10 mM and C_T concentrations between 880-3520 µM. PD I size was not modulated by increased seawater C_T of 2900-3520 µM compared to control conditions (C_T: 1773 µM) and shell length was only negatively affected by seawater [Ca^{2+}] below 3 mM (Fig. 4a). In contrast, lowered seawater C_T (975 µM) significantly affected shell formation and PD I length declined to 72.5 ± 2.7 µm at control [Ca^{2+}]. Within these treatments shell length was marginally positively correlated with seawater [Ca^{2+}] but shell length remained reduced in all [Ca^{2+}] treatments (linear regression: 63 (± 2.2) µm + 2.9 (± 0.7) x [Ca^{2+}], F:18.6, $p<0.01$, R^2= 0.47, Fig. 4a).

Whereas, the correlation of shell length against [Ca^{2+}] under reduced C_T differed significantly from the three higher C_T treatments. Plotting PD I sizes against seawater $\Omega_{Aragonite}$ and [Ca^{2+}][HCO_3^-]/[H^+] revealed a similar correlation of calcification in all treatments (Fig. 4b, c). Calcification of larvae started to decline at $\Omega_{Aragonite}$ below 1 with significant reductions in the treatments with $\Omega_{Aragonite}$ below 0.5 (H: 44.5, $p<0.001$, Dunn's test). Similarly, PD I size declined at [Ca^{2+}][HCO_3^-]/[H^+] values below 0.7 and shells were significantly smaller below 0.3 (H:42.5, $p<0.01$, Dunn' test). In addition, the shell formation responses of *M. edulis*-like and *M. trossulus*-like to combined manipulations of [Ca^{2+}] and carbonate chemistry were more similar compared to the effects of lowered seawater [Ca^{2+}] alone (Fig. 2c, 4b,c, Table 3b,c). Nevertheless, whereas the response to $\Omega_{Aragonite}$ was similar for both hybrid populations they differed significantly in their response to [Ca^{2+}][HCO_3^-]/[H^+] (Table 4c,d).

3.3 Calculation of seawater [Ca^{2+}], Ω and [Ca^{2+}][HCO_3^-]/[H^+] for the Baltic Sea

Calculations of seawater [Ca^{2+}] were performed for the salinity range observed at the collections sites of *M. edulis*-like and *trossulus*-like in Kiel Fjord and Usedom, respectively. In Kiel Fjord, salinity fluctuated substantially between 10.5-24.7 g kg^{-1} in the period 2005 – 2009 which resulted in simultaneous strong variations of seawater [Ca^{2+}] between 3.6 – 7.7 mM with a mean of 5.6 mM (Table 1, Fig. 1d). In contrast, salinity in Usedom was lower with mean salinity of 7.1 g kg^{-1} and, in absolute numbers, more stable (3.4-9.1 g kg^{-1}, Table 1). Thus, seawater [Ca^{2+}] in Usedom was ranging between 1.5 and 3.2 mM with an average of 2.7 mM (Table 1, Fig. 2d).

Calculation of [Ca^{2+}] along the Baltic salinity gradient revealed that the critical concentrations of 3 and 2.5 mM at which calcification is negatively affected are reached at a salinity of about 7-8 g kg^{-1}, respectively, in all four sub regions (Fig. 5a). In contrast, calculated values for [HCO_3^-]/[H^+] are above 0.13 in almost all regions within the distribution range of mussels as long as the seawater is in equilibrium with current atmospheric CO_2 concentrations (Fig. 5b) Only in the Gulf of Bothnia, critical values lower than 0.1 are observed for salinities of 4.5 g kg^{-1} and below. For $\Omega_{Aragonite}$, undersaturation is observed at a salinity of 9 g kg^{-1} for the central Baltic. The Gulfs of Bothnia and Finland are always undersaturated for $\Omega_{Aragonite}$, but the Gulf of Riga seawater is supersaturated (Fig. 5c) and strong negative effects on larval calcification can be expected for salinities of about 5 g kg^{-1}. Similarly, critical values for

Biogeosciences Discuss., https://doi.org/10.5194/bg-2017-342
Manuscript under review for journal Biogeosciences
Discussion started: 6 September 2017

Biogeosciences Discussions Open Access EGU

$[Ca^{2+}][HCO_3^-]/[H^+]$ of 0.3 at which PD I formation is significantly affected are reached at a salinity of 5 g kg^{-1} in most regions of the Baltic excluding the Gulf of Riga (Fig. 5d). Conditions for calcification will become more adverse in future as atmospheric CO_2 concentrations are going to reach 800 ppm. In this scenario, critical values for $[HCO_3^-]/[H^+]$ will be observed in most areas of Baltic at salinities below 10 g kg^{-1} (Fig. 6b). In particular, $[Ca^{2+}][HCO_3^-]/[H^+]$ and $\Omega_{Aragonite}$ will be below the critical threshold in all areas of the Baltic Sea (Fig. 6c,d).

4. Discussion

This study investigated the impact of modifications of seawater $[Ca^{2+}]$ and carbonate chemistry on shell formation of bivalve larvae. The experimental results were compared to the environmental conditions prevailing in the Baltic Sea.

The laboratory experiments revealed that seawater $[Ca^{2+}]$ is a critical factor for shell formation in marine bivalves. Similarly, Ca^{2+} deposition into the shells of *Crassostrea gigas* larvae following PD I formation was similar at seawater $[Ca^{2+}]$ of 10 and 16.8 mM but reduced by 40% at 6.1 mM (Maeda-Martinez 1987). Thus, where high oceanic $[Ca^{2+}]$ of ~ 10 mM is not limiting bivalve calcification the low concentrations present in estuaries such as the Baltic, significantly affect biomineralization.

In both tested populations, *M. edulis*-like and *M. trossulus*-like the overall response curve was similar and both populations become calcium limited at $[Ca^{2+}]$ below 3 mM. *M. trossulus*-like appeared to be slightly more tolerant to lowered $[Ca^{2+}]$ as larvae maintained larger PD I lengths at similar $[Ca^{2+}]$ and PD I formation was successfully accomplished at 1.1 mM. The response matches seawater $[Ca^{2+}]$ observed in the respective habitats of the tested populations and may result from either phenotypic plasticity or genetic adaptation. It is also possible that *M. edulis*-like living in the western brackish Baltic may have already adapted to lower $[Ca^{2+}]$ compared to populations and species living in habitats characterized by higher $[Ca^{2+}]$ (Maeda-Martinez 1987). As PD I formation is a crucial but sensitive stage during larval life, impaired calcification by low $[Ca^{2+}]$ can have significant effects on larval performance and fitness. As the distribution of bivalves is depending on successful larval dispersal, low $[Ca^{2+}]$ can be an important factor which determines the distribution limits of mussels and represents a strong selective force. Additionally, the strong $[Ca^{2+}]$ gradient observed between the western Baltic-Kattegat transition zone and the central Baltic Sea can be one explanation for the simultaneously observed allele frequency shift from *M. edulis*-like to *trossulus*-like (Larsson et al. 2016, Stuckas et al. 2017).

Nevertheless, larval shell formation of Baltic mytilids starts to become $[Ca^{2+}]$ limited at concentrations of about 3 mM and was significantly affected at 2.5 mM. Consequently, in areas of the Baltic with salinities below 7-8 g kg^{-1} and corresponding $[Ca^{2+}] < 3$ mM, reduced shell formation starts to compromise overall larval performance. At the critical salinity of 4.5 g kg^{-1} which delineates the distribution boundary of mussels in the Baltic (Westerbom et al. 2002), $[Ca^{2+}]$ is as low as 1.8 mM whereby concentration below 2 mM substantially impaired PD I formation in our experiments. Importantly, even under these adverse conditions larvae were viable and continued active swimming for up to 7 days. Thus impaired calcification in low $[Ca^{2+}]$ seawater can result from two mechanisms acting independently or in combination: I) continuous dissolution of existing calcium carbonate crystals under highly corrosive conditions may prevent further net calcification or II) larvae only use a pre-determined fraction of the energy stored in the egg for calcification. If this amount is not sufficient to sustain full PD I formation under low $[Ca^{2+}]$ the budget does not seem to be adjusted to provide additional energy to complete calcification. Instead larvae do not continue calcification and may switch to an energy saving mode to stay alive. In our experiments, *M. trossulus*-like apparently developed a higher tolerance to low $[Ca^{2+}]$ compared to *M. edulis*-like but incipient impairment of calcification at about 3 mM was similar in both populations which suggests relatively conserved $[Ca^{2+}]$ transport mechanisms in both populations.

Impact of external $[Ca^{2+}]$ on calcification has previously been studied mostly in corals for which a significant correlation was observed in a number of studies (e.g. Chalker 1976; Ip and Krishnaveni 1991). Whereas cytosolic calcium concentration are tightly regulated and

Biogeosciences Discuss., https://doi.org/10.5194/bg-2017-342
Manuscript under review for journal Biogeosciences
Discussion started: 6 September 2017

Biogeosciences Discussions Open Access EGU

kept constantly low, calcifiers obviously developed a mechanism to accumulate high $[Ca^{2+}]$ in specialized compartments within or outside the cell for biomineralization. In corals, Ca^{2+} uptake and transport to the site of calcification is driven by a combination of diffusive and active transport and involves active transport by plasma membrane Ca^{2+}-ATPase (PMCA, Tambutte et al. 1996; Barott et al. 2015). In bivalves, calcification is performed by the outer mantle epithelium (OME) or the shell field in adults and larvae, respectively (Kniprath 1980), and a PMCA homolog has been localized in the OME of oysters and its inhibition negatively impacted shell growth in freshwater clams which might suggest a conserved function in bivalve calcification as well (Wang et al. 2008; Zhao et al. 2016).

Early studies suggested that the extrapallial fluid (EPF) of bivalves provides the microhabitat for calcification (Crenshaw 1972). However, $[Ca^{2+}]$ and acid-base status of bulk EPF of adult mussels corresponds to seawater and haemolymph conditions, respectively, which supports excretion of CO_2 via passive diffusion into the ambient seawater (Thomsen et al. 2010; Heinemann et al. 2012). In *M. edulis*-like larvae, kept above the critical threshold of 3 mM, CS $[Ca^{2+}]$ was marginally but significantly elevated compared to seawater $[Ca^{2+}]$. At lowered environmental $[Ca^{2+}]$ between 2-3 mM CS $[Ca^{2+}]$ was not significantly enriched compared to seawater concentration. At these seawater $[Ca^{2+}]$, calcification rates were significantly reduced but larvae were still able to produce a smaller but complete PD I. At even lower ambient $[Ca^{2+}]$ of 1.5 mM, CS $[Ca^{2+}]$ was again significantly elevated compared to seawater which was, however, accompanied by strongly reduced PD I formation. The incapacity of larvae to maintain transmembrane Ca^{2+} transport at lowered $[Ca^{2+}]$ potentially indicates a significant contribution of diffusion or involvement of a low affinity Ca^{2+} transporter (e.g. Na^+/Ca^{2+} Exchanger) in this process (Blaustein and Lederer 1999). Thus, larvae may actively enrich CS $[Ca^{2+}]$ to increase $\Omega_{Aragonite}$ and support the structural integrity of the shell under corrosive conditions. Alternatively, CS $[Ca^{2+}]$ only increased secondarily as a result of drastically reduced calcification rates.

In the present study, the effect of lowered $[Ca^{2+}]$ was most pronounced under conditions when seawater carbonate chemistry was not a limiting parameter for calcification. Lowering of seawater C_T, which has a similar effect on $\Omega_{Aragonite}$ and $[HCO_3^-]/[H^+]$ as acidification, significantly affects the rate of PD I formation. Under these C_T / HCO_3^- limiting conditions, seawater $[Ca^{2+}]$ had only a minor, yet slightly positive, linear effect on shell formation. Presumably the effect was smaller as Ca^{2+} uptake was not any longer the only rate limiting process but rather HCO_3^- uptake and / or H^+ extrusion (Bach 2015) or impaired kinetics of crystal formation (Waldbusser et al. 2014).

Importantly, the applied experimental seawater manipulations of calcium and carbonate chemistry can be integrated by calculation of $\Omega_{Aragonite}$ or extending the SIR term to $[Ca^{2+}][HCO_3^-]/[H^+]$ which also takes lowered availability of $[Ca^{2+}]$ into account (Bach 2015; Fassbender et al. 2016). Plotting shell length against these two parameters revealed a similar response for all manipulations independent whether they were manipulated by lowered $[Ca^{2+}]$ or C_T. The correlation of calcification with these parameters corresponded to previously observed shell formation performance of mussels and oysters resulting from modifications of seawater carbonate chemistry only (Waldbusser et al. 2014; Waldbusser et al. 2015; Thomsen et al. 2015). As salinity and temperature were not changed in the experiments performed with *M. edulis*-like $\Omega_{Aragonite}$ and $[Ca^{2+}][HCO_3^-]/[H^+]$ are linearly correlated and it is not possible to distinguish whether shell formation is modified by the changed kinetics of crystal formation (Waldbusser et al. 2015), higher dissolution due to undersaturation of the EPF with respect to calcium carbonate (Miller et al. 2009; Thomsen et al. 2010; Melzner et al. 2011, Frieder et al. 2017) or by lowered substrate availability and impaired H^+ removal from the calcifying fluids (Thomsen et al. 2015; Bach 2015; Fassbender et al. 2016). However, the calcification response of *M. trossulus*-like was similar to *M. edulis*-like when plotted against $\Omega_{Aragonite}$ but differed significantly for $[Ca^{2+}][HCO_3^-]/[H^+]$ in accordance with the higher tolerance to lowered $[Ca^{2+}]$. This could indicate local adaptation of *M. trossulus*-like to the adverse environment in the low saline areas of the Baltic. In contrast, the response to $\Omega_{Aragonite}$ was similar in animals from both populations which may

Biogeosciences Discuss., https://doi.org/10.5194/bg-2017-342
Manuscript under review for journal Biogeosciences
Discussion started: 6 September 2017

Biogeosciences Discussions Open Access EGU

indicate that shell dissolution under corrosive conditions impacts net shell formation to the same extent.

Our experimental data revealed that larval calcification is substantially compromised by environmental conditions encountered in the Baltic Sea. Calculation of Baltic seawater [Ca^{2+}] suggests [Ca^{2+}] limitation of calcification at salinities of about 8 g kg^{-1}. Thus, with exception of the western Baltic Sea with its higher salinity values, mussels inhabiting most areas of the Baltic suffer from low Ca^{2+} availability. Interestingly, studies measuring Baltic Sea [Ca^{2+}] revealed increasing concentrations over the last decades which may have a beneficial effect on calcification for a given salinity (Kremling and Wilhelm 1997). Nevertheless, the expected overall reduction of salinity will most likely exceed the minor positive effect of [Ca^{2+}] enrichment and negatively affect overall fitness by osmotic stress and secondarily calcification (Gräwe et al. 2013).

In contrast to [Ca^{2+}], estimating current carbonate chemistry for the four Baltic sub regions suggests that the influence is of less importance for limitation of calcification. The calculated [HCO_3^-]/[H^+] and $\Omega_{Aragonite}$ for seawater in equilibrium with current atmospheric CO_2 concentrations remain above the critical thresholds of 0.1-0.13 and 1, respectively (Thomsen et al. 2015, this study). However, this conclusion does not consider the substantial variability of carbonate chemistry in the surface water of the Baltic which is modified by biogeochemical processes such as riverine composition, photosynthesis and upwelling on a seasonal and spatial scale. Seawater carbonate chemistry can be substantially modified by phytoplankton blooms in spring and early summer causing a draw down of seawater pCO_2 to 150 µatm thereby causing elevated pH, [CO_3^{2-}] and [HCO_3^-]/[H^+] for several weeks (Schneider and Kuss 2004). Consequently, larvae can be exposed to environmental conditions which are beneficial for calcification. In contrast, local upwelling phenomena have the opposite effect leading to lowered pH and [CO_3^{2-}], [HCO_3^-]/[H^+] and elevated pCO_2 (Thomsen et al. 2010; Saderne et al. 2013). Upwelling events are common in the Baltic Sea in particular along the western coastlines (Myrberg and Andrejev 2003). However, research mostly focused on the effect of upwelling on temperature and nutrient supply but neglected the local impacts on carbonate chemistry (e.g. Haapala 1994). As upwelling causes rapid elevation of pCO_2 within a short period of hours but can last for several days to few weeks, thus for a significant part of a larval life time, its impact on calcification and performance of larvae can be substantial (Barton et al. 2012; Thomsen et al. 2015, 2017).

In addition to the present carbonate system variability, the successive increase of atmospheric CO_2 concentrations and coupled pH decline in the Baltic will result in progressively adverse conditions for calcification. This process is particularly critical for mussel populations inhabiting the low saline areas of the Baltic where conditions for calcification are less favourable already today and will become more adverse in the future. Nevertheless, it has recently been shown that increasing A_T (from an unaccounted source) may partly and even completely compensate the negative effects of CO_2 uptake (Müller et al. 2016). Consequently, bivalve calcification may benefit from higher A_T and thus favourable carbonate chemistry in future, but lowered salinity might still affect performance.

Both substrates relevant for calcification, Ca^{2+} and inorganic carbon are integrated in the terms Ω and the SIR extended to [Ca^{2+}][HCO_3^-]/[H^+]. In fact the calcification response of bivalve larvae in our experiments was accurately described by both terms for a given salinity and temperature. Nevertheless, calculations of the environmental conditions in the four Baltic sub regions revealed important differences. $\Omega_{Aragonite}$ remains favourable for calcification (>1) in most parts of the central Baltic and in the Gulf of Riga caused by high alkaline riverine runoff and therefore prohibits dissolution of shell crystals (Juhna and Klavins 2000). In contrast, calculated values for [Ca^{2+}][HCO_3^-]/[H^+] are below the critical threshold of 0.7 in all sub regions at a salinity of 11 g kg^{-1} caused by low [Ca^{2+}]. Thus, it is of high ecological relevance whether bivalve calcification is sensitive to the reduced kinetic of shell formation and dissolution depending on Ω or lowered substrate availability and inhibition by [H^+]. According to our experimental data most likely a combination of both parameters is determining sensitivity. However, compared to *M. edulis*-like, *M. trossulus*-like seems to have evolved a slightly higher tolerance to low [Ca^{2+}][HCO_3^-]/[H^+], but not to low $\Omega_{Aragonite}$. A similar

Biogeosciences Discuss., https://doi.org/10.5194/bg-2017-342
Manuscript under review for journal Biogeosciences
Discussion started: 6 September 2017

response has been observed in a comparison between Baltic and North Sea mussels under simulated ocean acidification (Thomsen et al. 2017).

In conclusion, this study reveals strong impacts of lowered [Ca^{2+}] and carbonate chemistry, which are naturally changing along the Baltic salinity gradient, on the early calcification of mussel larvae. Strong delays and impairment of complete shell formation most likely affect the energy budget and overall physiology of mussels in the low saline areas. Consequently, low [Ca^{2+}] and adverse carbonate chemistry impact mussel fitness substantially and therefore likely seem to contribute significantly in determining the distribution of marine mussels in estuaries such as the Baltic Sea.

Author Contributions:

JT conceived the study and led the writing of the manuscript; JT, KR, TS and FM collected data; JT, KR, MB, and FM analysed the data. All authors contributed to the various manuscript drafts.

Acknowledgements:

The authors thank Thomas Stegmann for performing Ca^{2+} measurements, Marian Hu for supporting Ca^{2+}-microelectrode measurements and Ulrike Panknin for maintaining *Rhodomonas* cultures. Furthermore, Detlev Machoczek and Rainer Kiko are acknowledged for providing and supporting processing of Oder Bank salinity data, respectively. This study was funded by the BMBF program BIOACID subproject 2.3 and CACHE, a Marie Curie Initial Training Network (ITN) funded by the People Programme (Marie Curie Actions) of the European Union's Seventh Framework Programme FP7/2007-2013/ under REA grant agreement n°[605051]13. The authors declare no conflict of interest.

Data availability:

All data are available under: Thomsen, Jörn; Ramesh, Kirti; Sanders, Trystan; Bleich, Markus; Melzner, Frank (2017): Effects of seawater calcium on calcification in mussel larvae. *PANGAEA*, Unpublished dataset #871804.

References:

Bach, L.T.: The role of carbonate ion concentration for the production of calcium carbonate by marine organisms, Biogeosciences, 12, 4939-4951, 2015.

Barott, K.L., Perez, S.O., Linsmayer, L.B., and Tresguerres, M.: Differential localization of ion transporters suggests distinct cellular mechanisms for calcification and photosynthesis between two coral species. Am. J. Physiol. Reg. I., 309, R235-R246, 2015.

Barton, A., Hales, B., Waldbusser, G.G., Langdon, C., and Felly, R.A.: The Pacific oyster *Crassostrea gigas*, shows negative correlation to naturally elevated carbon dioxide levels: Implications for near-term ocean acidification effects. Lim. Oceanog., 57, 698-710, 2012.

Beldowski, J., Löffler, A., and Joensuu, L.: Distribution and biogeochemical control of total CO_2 and total alkalinity in the Baltic Sea. J. Mar. Syst., 81, 252–259, 2010.

Blaustein, M.P., and Lederer W.J., Sodium/Calcium Exchange: Its physiological implications. Physiological Reviews, 79, 763-854, 1999.

BSH: Hourly meteorological observations at Station Oder Bank 2000-2015, Bundesamt für Seeschiffahrt und Hydrographie, Hamburg

Casties, I., Clemmensen, C., Melzner, F., and Thomsen, J.: Salinity dependence of recruitment success of the sea star *Asterias rubens* in the brackish western Baltic Sea. Helgoland Mar. Res., 69, 169-175, 2015.

Biogeosciences Discuss., https://doi.org/10.5194/bg-2017-342
Manuscript under review for journal Biogeosciences
Discussion started: 6 September 2017

548 Chalker, B.E.: Calcium transport during skeletogenesis in hermatypiccorals, Comp. Biochem.
549 Physiol. A, 54, 455-459,1976.
550
551 Cragg, S.M.: The adductor and retractor muscles of the veliger of *Pecten maximus* (L.)
552 (Bivalvia), J. Mollus. Stud., 51, 276-283, 1985.
553
554 Crenshaw, M.A.: The inorganic composition of molluscan extrapallial fluid, Biol. Bull., 143,
555 506-512, 1972.
556
557 Cyronak, T., Schulz, K.G., and Jokiel, P.L.: The Omega myth: what really drives lower
558 calcification rates in an acidifying ocean, ICES J. Mar. Sci., 73, 558-562, 2015.
559
560 De Beer, D., Kühl, M., Stambler, N., and Vaki, L.: A mirosensor study of light enhanced Ca^{2+}
561 uptake and photosynthesis in the reef-building hematypic coral *Favia* sp., Mar. Ecol. Prog.
562 Ser., 194, 75-85, 2000.
563
564 Dickson, A.G.: Standard potential of the reaction – AgClS+1/2 H2 = AgS+HClAq and the
565 standard acidity constant of the ion HSO4 – in synthetic sea-water from 273.15-K to 318.15-
566 K, J. Chem. Thermodyn., 22, 113–127, 1990.
567
568 Dickson, A.G., Afghan, J.D., and Anderson, G.G.: Reference materials for oceanic CO2
569 analysis: A method for the certification of total alkalinity. Mar. Chem., 80, 185-197, 2003.
570
571 Enderlein, P., and Wahl, M.: Dominance of blue mussels versus consumer-mediated
572 enhancement of benthic diversity, J. Sea Res., 51, 145-155, 2004.
573
574 Falini, G, Albeck, S, Weiner, S, and Addadi, L.: Control of aragonite or calcite polymorphism
575 by mollusk shell macromolecules, Science, 271, 67-69, 1996.
576
577 Fassbender, A.J., Sabine, C.L., and Feifel, K.M.: Consideration of coastal carbonate
578 chemistry in understanding biological calcification. Geophys. Res. Lett., 43, 4467-4476, 2016.
579
580 Frieder, C.A., Applebaum, S.L., Pan, T.C.F., Hedgecock, D., and Manahan, D.: Metabolic
581 cost of calcification in bivalve larvae under experimental ocean acidification. *ICES J. Mar.*
582 *Sci.*, 74, 941-954, 2017.
583
584 Gazeau, F., Parker, L.M., Comeau, S., Gattuso, J.P., O`Connor, W.A., Martin, S., Pörtner, H.
585 O., and Ross, P.M.: Impacts of ocean acidification on marine shelled molluscs. Mar. Biol.,
586 160, 2207-2245, 2013.
587
588 Gräwe, U., Freidland, R., and Burchard, H.: The future of the western Baltic Sea: two
589 possible scenarios, Ocean Dynam., 63, 901-921, 2013.
590
591 Gustafsson, E., Wällstedt, T., Humborg, C., Mörth, C.M., and Gustafsson, B.G.: External total
592 alkalinity loads versus internal generation: The influence of nonriverine alkalinity sources in
593 the Baltic Sea, Global Biochem. Cy., 28, 1358-1370, 2014.
594
595 Haapala, J.: Upwelling and its influence on nutrient concentration in the coastal area of the
596 Hanko Peninsula, Entrance of the Gulf of Finland, Estuar. Coast. Shelf S., 38, 507-521, 1994.
597
598 Haynert, K., Schönfeld, J., Schiebel, R., Wilson, B., and Thomsen, J.: Response of benthic
599 foraminifera to ocean acidification in their natural sediment environment: a long-term
600 culturing experiment, Biogeosciences, 11, 1581–1597, 2014.
601

Biogeosciences Discuss., https://doi.org/10.5194/bg-2017-342
Manuscript under review for journal Biogeosciences
Discussion started: 6 September 2017

Heinemann, A., Fietzke, J., Melzner, F., Böhm, F., Thomsen, J., Garbe-Schönberg, D. and Eisenhauer, A.: Conditions of *Mytilus edulis* extracellular body fluids and shell composition in a pH-treatment experiment: Acid-base status, trace elements and $\delta^{11}B$, Geochem. Geophy. Geosy., 13, Q01005, 2013.

Ip, Y.K., and Krishnaveni, P.: Incorporation of Strontium ($^{90}Sr^{2+}$) into the skeleton of the hermatypic coral *Galaxea fascicularis*, J. Exp. Zool., 258, 273-276, 1991.

Johannesson, K., Smolarz, K., Grahn, M., and Andre, C.: The Future of Baltic Sea Populations: Local Extinction or Evolutionary Rescue? AMBIO, 40, 179-190, 2011.

Juhna, T., and Klavins, M.: Water-quality changes in Latvian and Riga 1980-2000: Possibilities and Problems, AMBIO, 30, 306-314, 2001.

Kester, D.R., Duedall, I.W., Connors, D.N., and Pytkowicz, R.M.: Preparation of artificial seawater, Limnol. Oceanogr., 12, 176-179, 1967.

Kniprath, E.: Larval development of the shell and the shell gland in *Mytilus* (Bivalvia). *Roux's Arch. Dev. Biol.*, 188, 201-204, 1980.

Kremling, K., and Wilhelm, G.: Recent increase of the calcium concentrations in Baltic Sea waters. Mar. Pollut. Bull., 34, 763-767, 1997.

Kube, S., Gerber, A., Jansen, J.M. and Schiedek, D.: Patterns of organic osmolytes in two marine bivalves, *Macoma baltica*, and *Mytilus* spp., along their European distribution, Mar. Biol., 149, 1387-1396, 2006.

Lucas, A., and Rangel, C.: Detection of the first larval feeding in *Crassostrea gigas* using the epifluorescence microscope, Aquaculture, 30, 369-374, 1983.

Maar, M., Saurel, C., Landes, A., Dolmer, P., and Petersen, J.K.: Growth potential of blue mussels (*M. edulis*) exposed to different salinities evaluated by a Dynamic Energy Budget model, J. Mar. Sys., 148, 48-55, 2015.

Maeda-Martinez, A.N.: The rates of calcium deposition in shells of molluscan larvae, Comp. Biochem. Physiol. A, 86, 21-28, 1987.

Malone, P.G., and Dodd, J.R.: Temperature and salinity effects on calcification rate in *Mytilus edulis* and its paleoecological implications, Limnol. Oceanogr., 12, 432-436, 1965.

Martin, G., Kotta, J., Möller, T., and Herkül, K.: Spatial distribution of marine benthic habitats in the Estonian coastal sea, northeastern Baltic Sea. Est. J. Ecol., 62, 165-191, 2013.

McConnaughey T.A., and Gillikin, D.P.: Carbon isotopes in mollusk shell carbonates, Geo-Mar. Lett., 28, 287–299, 2008.

Meier, H.E.M., Kjellström, E., and Graham, L.P.: Estimating uncertainties of projected Baltic Sea salinity in the late 21st century, Geophys. Res. Lett., 33, L15705, 2006.

Melzner, F., Stange, P., Trübenbach, K., Thomsen, J., Casties, I., Panknin, U., Gorb, S., and Gutowska, M.A.: Food supply and seawater pCO_2 impact calcification and internal shell dissolution in the Blue Mussel *Mytilus edulis*, PLOS ONE, 6, e24223, 2011.

Biogeosciences Discuss., https://doi.org/10.5194/bg-2017-342
Manuscript under review for journal Biogeosciences
Discussion started: 6 September 2017

655 Melzner, F., Thomsen, J., Koeve, W., Oschlies, A., Gutowska, M.A., Bange, H. W., Hansen,
656 H.P., and Körtzinger, A.: Future ocean acidification will be amplified by hypoxia in coastal
657 habitats, Mar. Biol., 160, 1875-1888, 2013.
658
659 Miller, A.W., Reynolds, A.C., Sobrino, C., and Riedel, G.F.: Shellfish face uncertain future in
660 high CO_2 world: Influence of acidification on oyster larvae calcification and growth in
661 estuaries, PLOS ONE, 4, e5661, 2009.
662
663 Millero, F.: The conductivity-density-salinity-chlorinity relationships for estuarine water,
664 Limnol. Oceanogr., 29, 1317-1321, 1984.
665
666 Mucci, A.: The solubility of calcite and aragonite in seawater at various salinities,
667 temperatures, and one atmosphere total pressure. *Am. J. Sci.*, 28, 780-799, 1983.
668
669 Müller, J., Schneider, B., and Rehder, G.: Long-term alkalinity trends in the Baltic Sea and
670 implications for Co2-induced acidification, Limnol. Oceanogr., 61, 1984-2002, 2016.
671
672 Myrberg, K., and Andrejev, O.: Main upwelling regions in the Baltic Sea - a statistical analysis
673 based on three-dimensional modelling, Boreal Environ. Res., 8, 97-112, 2003.
674
675 Natochin, Y.V., Berger, V.Y., Khlebovich, V.V., Lavrova, E.A., and Michailova, O.Y.: The
676 participation of electrolytes in adaptation mechanisms of intertidal molluscs' cells to altered
677 salinity. Comp. Biochem. Physiol A, 63, 115-119, 1979.
678
679 Ohlson, M., and Anderson, L.: Recent investigation of total carbonate in the Baltic Sea:
680 changes from the past as a result of acid rain? Mar. Chem., 30, 259-267, 1990.
681
682 Podbielski, I., Bock, C., Lenz, M., and Melzner, F.: Using the critical salinity (S_{crit}) concept to
683 predict invasion potential of the anemone *Diadumene lineata* in the Baltic Sea, Mar. Biol.,
684 163, 227, 2016.
685
686 Riisgard, H.U., Larsen, P. S., Turja, R., and Lundgreen, K.: Dwarfism of blue mussels in the
687 lower saline Baltic Sea – growth to the lower salinity limit, Mar. Ecol. Prog. Ser., 517, 181-
688 192, 2014.
689
690 Roy, R.N., Roy, L.N., Vogel, K.M., Porter-Moore, C., Pearson, T., Good, C.E., Millero, F. J.,
691 and Campbell, D.: The dissociation constants of carbonic acid in seawater at salinities 5 to
692 45 and temperatures 0 to 45°C. Mar. Chem., 44, 249-267, 1993.
693
694 Saderne, V., Fietzek, P., and Herman, P.M.J.: Extreme variations of pCO_2 and pH in a
695 macrophyte meadow of the Baltic Sea in summer: Evidence of the effect of photosynthesis
696 and local upwelling, PLOS ONE, 8, e62689, 2013.
697
698 Schneider, B., and Kuss, J.: Past and present productivity of the Baltic Sea inferred from
699 pCO_2 data. Cont. Shelf Res., 24, 1611-1622, 2004.
700
701 Silva, A.L. and Wright, S.H.: Short-term cell volume regulation in *Mytilus californianus* gill, J.
702 Exp. Biol., 194, 47-68, 1994.
703
704 Stuckas, H., Knobel, L., Schade, H., Breusing, C., Hinrichsen, H.-H., Bartel, M., Langguth, K.
705 and Melzner, F.: Combining hydrodynamic modelling with genetics: Can passive larval
706 drift shape the genetic structure of Baltic *Mytilus* populations? Mol. Ecol., 26, 2765-2782,
707 2017.
708

Biogeosciences Discuss., https://doi.org/10.5194/bg-2017-342
Manuscript under review for journal Biogeosciences
Discussion started: 6 September 2017

709 Stumpp, M., Hu., M., Casties, I., Saborowski, R., Bleich, M., Melzner, F., and Dupont, S.:
710 Digestion in sea urchin larvae impaired under ocean acidification, Nature Clim. Change, 3,
711 1044-1049, 2013.
712
713 Tambutte, E., Allemand, D., Mueller, E. & Jaubert, J.: A compartimental approach to the
714 mechanism of calcification in hermatypic corals. J. Exp. Biol., 199, 102-1041 1996.
715
716 Thomsen, J., Gutowska, M.A., Saphörster, J., Heinemann, A., Trübenbach, K., Fietzke, J.,
717 Hiebenthal, C., Eisenhauer, A., Körtzinger, A., Wahl, M., and Melzner, F.: Calcifying
718 invertebrates succeed in a naturally CO_2-rich coastal habitat but are threatened by high
719 levels of future acidification, Biogeosciences, 7, 3879–3891, 2010.
720
721 Thomsen, J., Haynert, K., Wegner, K. M., and Melzner, F.: Impact of seawater carbonate
722 chemistry on the calcification of marine bivalves, Biogeosciences, 12, 4209-4220, 2015.
723
724 Thomsen, J., Stapp, L.S., Haynert, K., Schade, H., Danelli, M., Lannig, G., Wegner, K.M.,
725 and Melzner, F.: Naturally acidified habitat selects for ocean acidification–tolerant mussels,
726 Sci. Adv., 3, e1602411, 2017.
727
728 Waldbusser, G.G., Brunner, E.L., Haley, B.A., Hales,B. Langdon, C.J., and Prahl, F. G.: A
729 developmental and energetic basis linking larval oyster shell formation to acidification
730 sensitivity, Geophys. Res. Lett., 40, 1–6, 2013.
731
732 Waldbusser, G.G., Hales, B., Langdon, C.J., Haley, B.A., Schrader, P., Brunner, E.L., Gray.
733 M.W., Miller, C.A., and Gimenez, I.: Saturation-state sensitivity of marine bivalve larvae to
734 ocean acidification, Nature Clim. Change, 5, 273-280, 2014.
735
736 Waldbusser, G.G., Hales, B., Langdon, C.J., Haley, B.A., Schrader, P., Brunner, E.L., Gray.
737 M.W., Miller, C.A., Gimenez, I., and Hutchinson, G.: Ocean acidification has multiple modes
738 of action in bivalve larvae, PLOS ONE, 10, e0128376, 2015.
739
740 Wang, X., Fan, W., Xie, L., and Zhang, R.: Molecular cloning and distribution of a plasma
741 membane calcium ATPase homolog from the pearl oyster *Pinctada fucata*, Tsinghua Sci.
742 Technol., 13, 439-446, 2008.
743
744 Westerbom, M., Kilpi, M., and Mustonen, O.: Blue mussels, *Mytilus edulis*, at the edge of the
745 range: population structure, growth and biomass along a salinity gradient in the north-eastern
746 Baltic Sea, Mar. Biol., 140, 991-999, 2002.
747
748 Whitfield, A.K., Elliott, M., Basset, A., Blaber, S.J.M., and West, R.J.: Paradigms in estuarine
749 ecology – A review of the Remane diagram with a suggested revised model for estuaries,
750 Estuar. Coast. Shelf S., 97, 78-90, 2012.
751
752 Williams, E.K., and Hall, J.A.: Seasonal and geographic variability in toxicant sensitivity of
753 *Mytilus galloprovinicialis*, Australas. J. Ecotox., 5, 1-10, 1999.
754
755 Willmer, P.G.: Sodium fluxes and exchange pumps: Further correlates of osmotic conformity
756 in the nerves of an estuarine bivalve (*Mytilus edulis*). J. Exp. Biol., 77, 207-223, 1978).
757
758 Wright, S.H., Moon, D.A., and Silva, A.L.: Intracellular Na^+ and the control of amino acid
759 fluxes in the integumental epithelium of a marine bivalve, J. Exp. Biol., 142. 293-310, 1989.
760
761 Zhao, L., Schöne, B.R., and Mertz-Kruas, R.: Delineating the role of calcium in shell
762 formation and elemental composition of *Corbicula fluminea* (Bivalvia), Hydrobiologica, 790,
763 259-270, 2016.

Biogeosciences Discuss., https://doi.org/10.5194/bg-2017-342
Manuscript under review for journal Biogeosciences
Discussion started: 6 September 2017

764 Fig. 1 Bathymetric map of the Baltic Sea and its sub regions which are characterized by
765 specific carbonate chemistry. Sampling spots for mussel populations used in the experiments
766 are indicated by light blue dots.

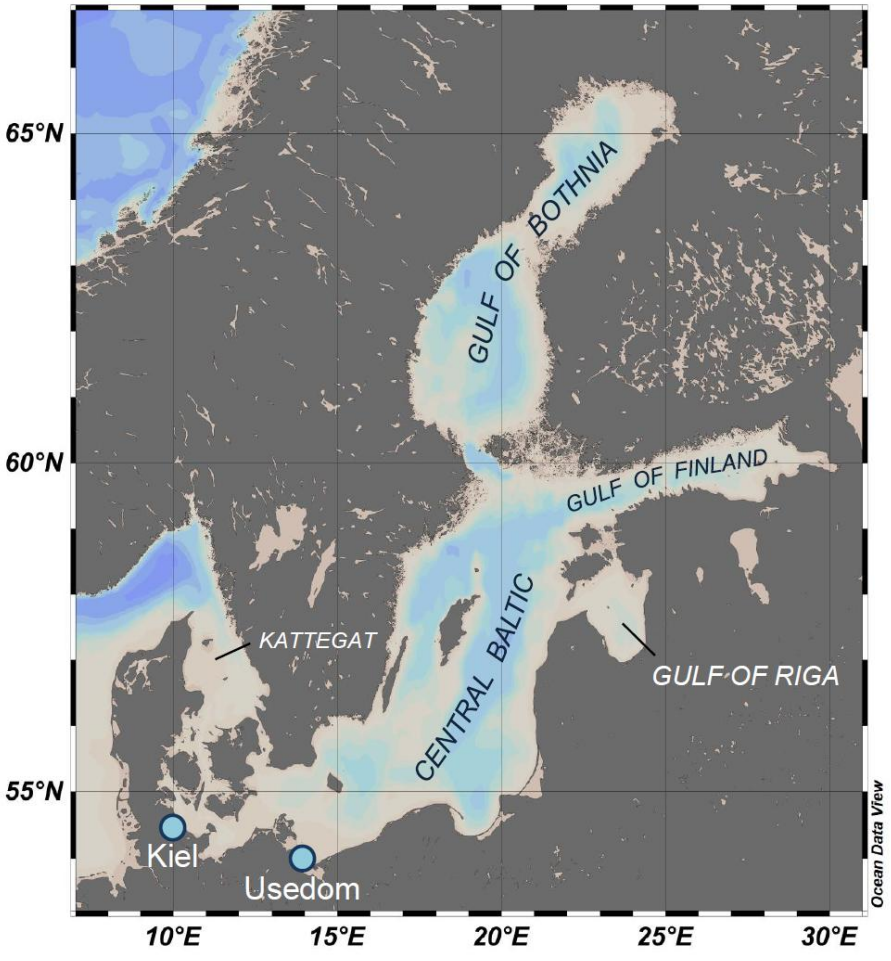

767
768
769
770
771
772
773
774
775
776
777
778
779
780
781
782

Biogeosciences Discuss., https://doi.org/10.5194/bg-2017-342
Manuscript under review for journal Biogeosciences
Discussion started: 6 September 2017

783 Fig. 2 Prodissoconch I length of mussel larvae as a function of seawater [Ca^{2+}]. A) *M. edulis*-
784 like, different symbols represent different experimental runs (1-5) B) *M. trossulus*-like, C)
785 Comparison of *M. edulis*-like and *trossulus*-like, D) Boxplots of seawater [Ca^{2+}] at the
786 collection site in Kiel Fjord and at Usedom depicting median, 25 and 75% quartiles and
787 outliers.

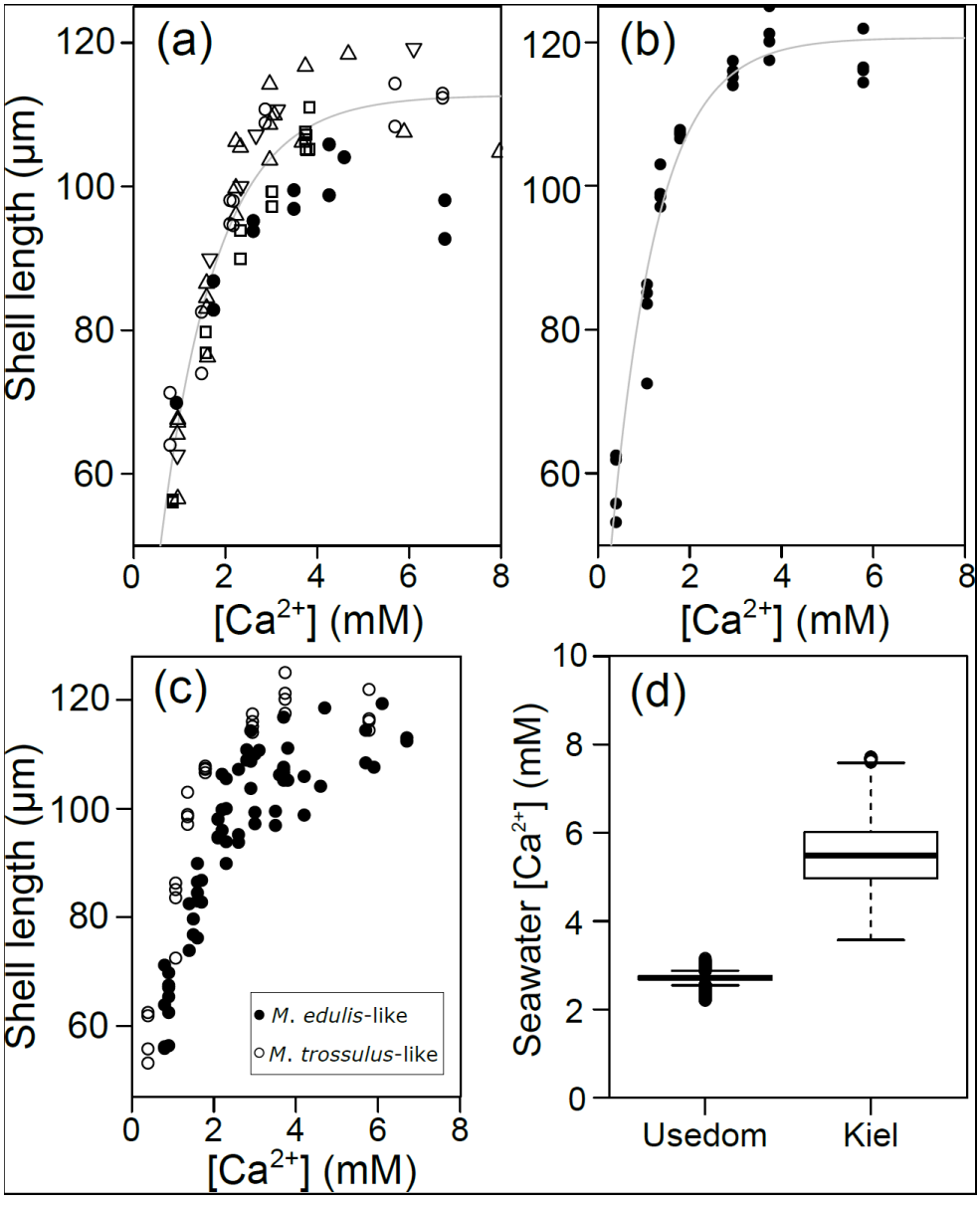

788
789
790
791
792
793
794

Biogeosciences Discuss., https://doi.org/10.5194/bg-2017-342
Manuscript under review for journal Biogeosciences
Discussion started: 6 September 2017

Fig. 3 $[Ca^{2+}]$ in the calcifying space (CS) of *M. edulis*-like larvae. A) CS $[Ca^{2+}]$ as a function of seawater $[Ca^{2+}]$, the line indicates the isoline B) Difference between CS $[Ca^{2+}]$ and seawater $[Ca^{2+}]$ at four $[Ca^{2+}]$ treatments expressed as $[Ca^{2+}]_{CS}$-$[Ca^{2+}]_{SW}$. Bar chart depicts mean ± standard error of the mean (N=6).

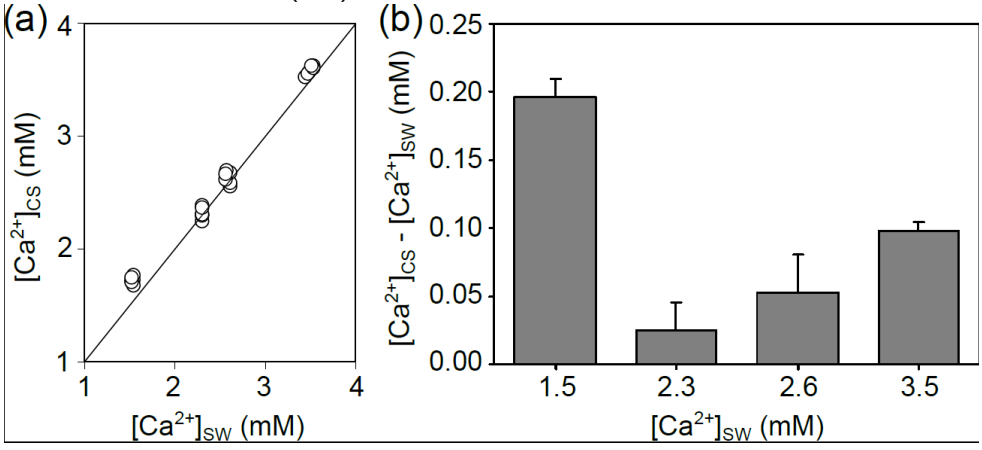

Biogeosciences Discuss., https://doi.org/10.5194/bg-2017-342
Manuscript under review for journal Biogeosciences
Discussion started: 6 September 2017

Fig. 4 Prodissoconch I length of mussel larvae exposed to varying C_T and $[Ca^{2+}]$ plotted against A) $[Ca^{2+}]$, B) $\Omega_{Aragonite}$, C) $[Ca^{2+}][HCO_3^-]/[H^+]$.

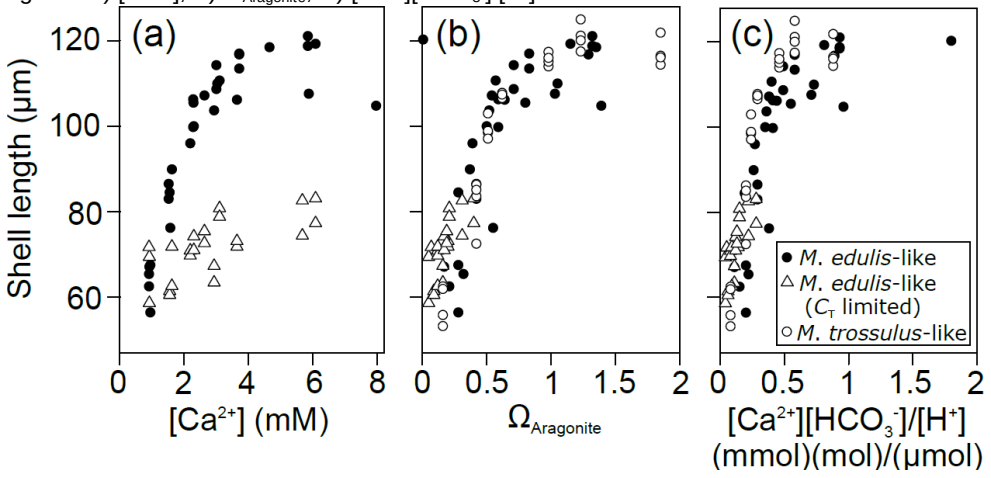

Biogeosciences Discuss., https://doi.org/10.5194/bg-2017-342
Manuscript under review for journal Biogeosciences
Discussion started: 6 September 2017

Fig. 5 Environmental parameters relevant for calcification in the Baltic Sea calculated for current salinity-A_T correlations and atmospheric CO_2 concentration (400 ppm). A) $[Ca^{2+}]$, B) $[HCO_3^-]/[H^+]$, C) $\Omega_{Aragonite}$ and D) $[Ca^{2+}][HCO_3^-]/[H^+]$ plotted against salinity for the four sub regions of the Baltic Sea. Dashed lines and grey areas indicate conditions of incipient and significant reduction of larval calcification rates, respectively.

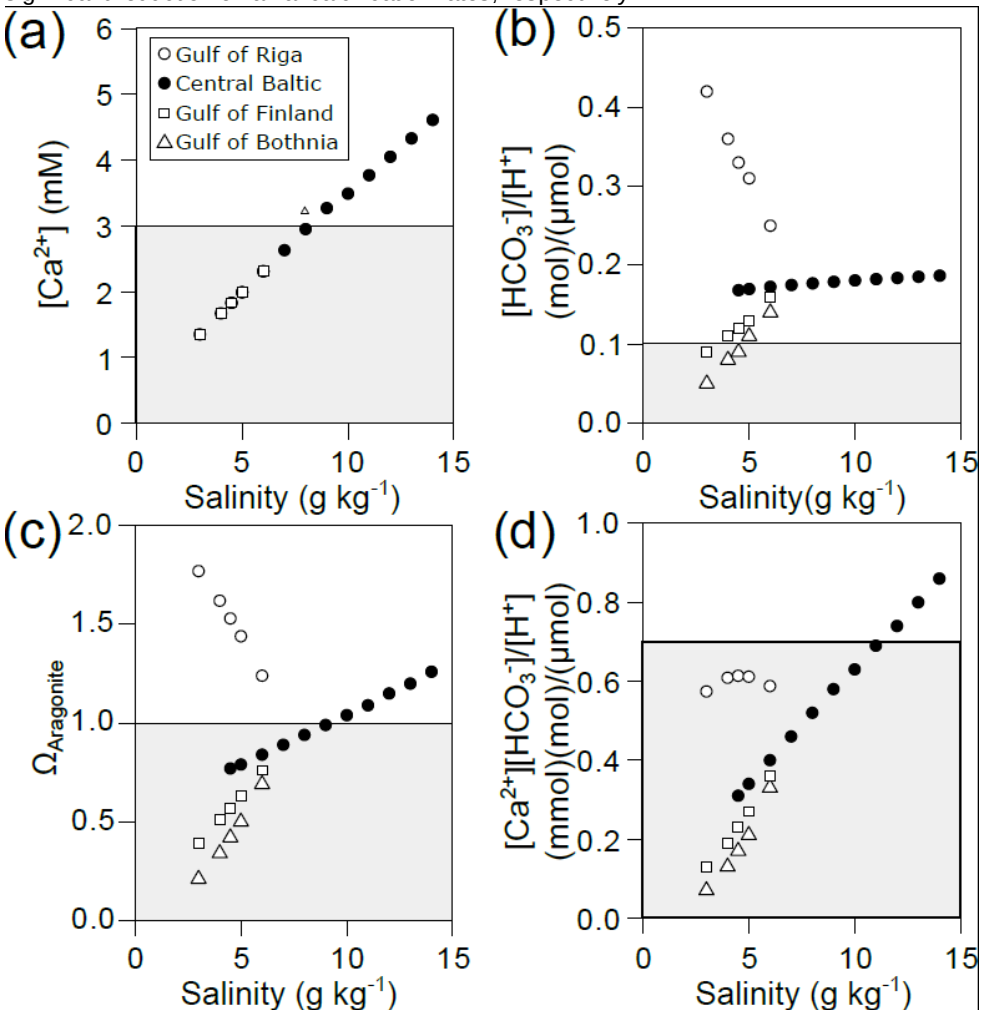

Biogeosciences Discuss., https://doi.org/10.5194/bg-2017-342
Manuscript under review for journal Biogeosciences
Discussion started: 6 September 2017

Fig. 6 Predicted environmental parameters relevant for calcification in the Baltic Sea calculated for current salinity-A_T correlations and future atmospheric CO_2 concentration (800 ppm). A) $[Ca^{2+}]$, B) $[HCO_3^-]/[H^+]$, C) $\Omega_{Aragonite}$ and D) $[Ca^{2+}][HCO_3^-]/[H^+]$ plotted against salinity for the four sub regions of the Baltic Sea. Dashed lines and grey areas indicate conditions of incipient and significant reduction of larval calcification rates, respectively.

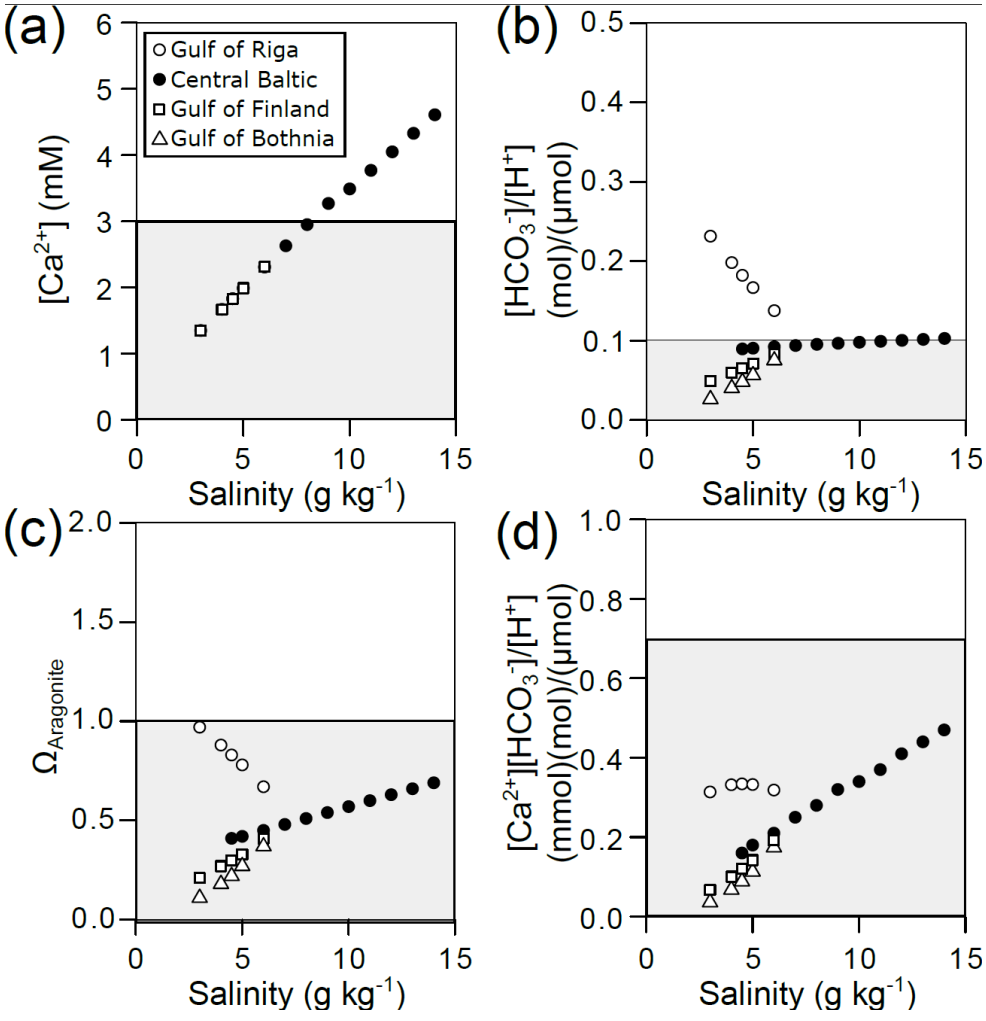

Biogeosciences Discuss., https://doi.org/10.5194/bg-2017-342
Manuscript under review for journal Biogeosciences
Discussion started: 6 September 2017

Table 1. Natural variability of salinity and $[Ca^{2+}]$ in Kiel Fjord and Usedom.

Salinity (g kg^{-1})	Usedom	Kiel
Min.	3.44	10.50
1st Qu.	6.81	15.30
Median	7.19	17.10
Mean	7.14	17.15
3rd Qu.	7.74	18.90
Max.	9.33	24.70

$[Ca^{2+}]$ (mM)	Usedom	Kiel
Min.	2.22	3.57
1st Qu.	2.67	4.97
Median	2.71	5.49
Mean	2.70	5.51
3rd Qu.	2.75	6.01
Max.	3.14	7.70

Biogeosciences Discuss., https://doi.org/10.5194/bg-2017-342
Manuscript under review for journal Biogeosciences
Discussion started: 6 September 2017

952 Table 2: Experimental conditions during larval experiments, N:1-10 determinations, $\Omega_{Aragonite}$
953 and $[Ca^{2+}][HCO_3^-]/[H^+]$ are calculated from measured $[Ca^{2+}]$, C_T and pH_{NBS}.

A) $[Ca^{2+}]$ manipulation experiments with *M. edulis*-like

$[Ca^{2+}]$ treatment	$[Ca^{2+}]$ (mmol/L)
<1 mM	0.86 ± 0.02
1.5 - 2 mM	1.56 ± 0.03
2.0 - 2.5 mM	2.19 ± 0.03
2.5 - 3 mM	2.82 ± 0.05
3.0 - 4.0 mM	3.62 ± 0.06
4.0 - 5.0 mM	4.42 ± 0.11
5.0 - 6.0 mM	5.74 ± 0.07
6.0 - 8.0 mM	6.83 ± 0.25
>8.0 mM	9.22 ± 0.10

B) $[Ca^{2+}]$ manipulation experiments with *M. trossulus*-like

$[Ca^{2+}]$ treatment	$[Ca^{2+}]$ (mmol/L)	$\Omega_{Aragonite}$	$[Ca^{2+}][HCO_3^-]/[H^+]$ [mmol][mol]/[µmol]
<1 mM	0.40 ± 0.02	0.16 ± 0.02	0.08 ± 0.01
1 mM	1.07 ± 0.04	0.43 ± 0.00	0.20 ± 0.01
1-1.5 mM	1.36 ± 0.00	0.51 ± 0.03	0.24 ± 0.01
1.5 - 2 mM	1.79 ± 0.03	0.62 ± 0.04	0.29 ± 0.02
2.5 - 3 mM	2.94 ± 0.03	0.98 ± 0.07	0.46 ± 0.03
3.0 - 4.0 mM	3.74 ± 0.04	1.23 ± 0.06	0.58 ± 0.03
>5.0 mM	5.78 ± 0.01	1.86 ± 0.11	0.88 ± 0.04

C) $[Ca^{2+}]$ and carbonate systems manipulation experiments with *M. edulis*-like

treatment	$[Ca^{2+}]$ (mmol/L)	$\Omega_{Aragonite}$	$[Ca^{2+}][HCO_3^-]/[H^+]$ [mmol][mol]/[µmol]
control + high C_T	0.93 ± 0.02	0.26 ± 0.07	0.18 ± 0.05
	1.55 ± 0.03	0.45 ± 0.09	0.31 ± 0.06
	2.25 ± 0.06	0.64 ± 0.15	0.44 ± 0.10
	2.99 ± 0.05	0.80 ± 0.22	0.55 ± 0.15
	3.69 ± 0.04	1.05 ± 0.23	0.73 ± 0.16
	5.45 ± 0.70	1.36 ± 0.04	0.94 ± 0.02
	8.69 ± 1.03	2.63	1.8
low C_T	0.92 ± 0.01	0.06 ± 0.01	0.04 ± 0.01
	1.59 ± 0.05	0.10 ± 0.03	0.07 ± 0.02
	2.25 ± 0.08	0.14 ± 0.03	0.10 ± 0.02
	2.78 ± 0.21	0.17 ± 0.02	0.12 ± 0.01
	3.37 ± 0.38	0.20 ± 0.01	0.14 ± 0.01
	5.88 ± 0.29	0. 36 ± 0.06	0.25 ± 0.05

954
955
956
957
958

Biogeosciences Discuss., https://doi.org/10.5194/bg-2017-342
Manuscript under review for journal Biogeosciences
Discussion started: 6 September 2017

Table 3: Model parameters (a, b, c) describing PD I size as a function of experimental seawater conditions for *Mytilus edulis*-like and *trossulus*-like: Shell length (µm) = a+ b * e^(c*[parameter]).

A) Seawater $[Ca^{2+}]$

M. edulis-like	Estimate	std Error	t-value	p
a	112.7	1.8	63.4	<0.001
b	-100.7	7.6	-13.3	<0.001
c	-0.8	0.1	-9.3	<0.001
M. trossulus-like	Estimate	std Error	t-value	p
a	120.6	1.8	66	<0.001
b	-94.5	5.2	-18.1	<0.001
c	-1	0.1	-10.3	<0.001

B) Seawater $\Omega_{Aragonite}$

M. edulis-like	Estimate	std Error	t-value	p
a	118.9	3.8	31.1	<0.001
b	-106.1	16.1	-6.6	<0.001
c	-3.1	0.6	-4.7	<0.001
M. trossulus-like	Estimate	std Error	t-value	p
a	121.6	2.3	53.5	<0.001
b	-100.8	6.4	-15.7	<0.001
c	-2.8	0.3	-9.0	<0.001

C) Seawater $[Ca^{2+}][HCO_3^-]/[H^+]$

M. edulis-like	Estimate	std Error	t-value	p
a	125.9	5.0	25.3	<0.001
b	-73.5	4.3	-17.2	<0.001
c	-1.8	0.3	-5.9	<0.001
M. trossulus-like	Estimate	std Error	t-value	p
a	121.4	2.2	54.0	<0.001
b	-104.8	7.1	-14.9	<0.001
c	-6.0	0.7	-9.0	<0.001

Biogeosciences Discuss., https://doi.org/10.5194/bg-2017-342
Manuscript under review for journal Biogeosciences
Discussion started: 6 September 2017

983 Table 4: Results for linear models fitted on log transformed data of shell length and seawater
984 parameters, significant results in bold.

A) Response to $[Ca^{2+}]$

	Estimate	std Error	t-value	p
Intercept	**4.17**	**0.07**	**59.2**	**<0.001**
Ca^{2+}	**0.31**	**0.06**	**4.9**	**<0.001**
population	**0.12**	**0.04**	**2.8**	**<0.01**
Ca^{2+}:population	-0.01	0.04	-0.3	>0.05
F: 82.1	p: <0.001	R2: 0.77		

B) Response to $\Omega_{Aragonite}$

	Estimate	std Error	t-value	p
Intercept	**4.64**	**0.05**	**90.4**	**<0.001**
$\Omega_{Aragonite}$	**0.13**	**0.04**	**3.08**	**<0.01**
population	0.04	0.03	1.23	>0.05
$\Omega_{Aragonite}$: population	**0.1**	**0.03**	**2.86**	**<0.01**
F: 116.4	p:<0.001	R2: 0.82		

C) Response to $[Ca^{2+}][HCO_3^-]/[H^+]$ (CHH)

	Estimate	std Error	t-value	p
Intercept	**4.69**	**0.08**	**60.1**	**<0.001**
CHH	**0.27**	**0.07**	**3.8**	**<0.001**
population	**0.13**	**0.05**	**2.5**	**<0.05**
CHH: population	0.02	0.04	0.5	>0.05
F: 67.4	p: <0.001	R2: 0.78		

985

Identification of ion transporters during calcification in the larval mussel, *Mytilus edulis*

Kirti Ramesh[1*], Tejaswi Yarra[2, 3*], Melody S. Clark[2], Uwe John[4] and Frank Melzner[1]

[1]GEOMAR Helmholtz Centre for Ocean Research, Kiel 24105, Germany

[2]British Antarctic Survey, Natural Environment Research Council, High Cross, Madingley Road, CB3 0ET Cambridge, UK

[3]University of Edinburgh, Institute of Evolutionary Biology, Ashworth Laboratories, Charlotte Auerbach Road, Edinburgh, EH9 3FL, UK

[4]Integrative Ecophysiology Section, Alfred-Wegener-Institut Helmholtz-Zentrum für Polar-und Meeresforschung, Bremerhaven, Germany

*Contributed equally to this work

Abstract

The physiological processes driving the rapid rates of calcification in larval bivalves are poorly understood. Here, we use a calcification - substrate limited approach (low dissolved inorganic carbon, C_T) and transcriptome sequencing to explore the cellular ion transport mechanisms underlying larval calcium and bicarbonate acquisition in the Baltic blue mussel, *Mytilus edulis*. We reared four families of *M. edulis* under ambient (ca. 1865 µmol kg^{-1}) and low C_T (ca. 941 µmol kg^{-1}) conditions and then compared expression patterns at six larval developmental time points. Although larvae reared under low C_T exhibited a developmental delay, only a small subset of genes was differentially regulated between ambient and low C_T conditions. Of these genes, we identified one anion transporter (SLC26) to be upregulated under low C_T conditions and the role of this protein in bicarbonate uptake during larval calcification is discussed. By analyzing gene expression profiles over the course of larval development, we are able to isolate genes encoding ion transport and shell matrix proteins to identify the cellular pathways underlying larval calcification. In particular, we observe the overexpression of sodium bicarbonate cotransporters, anion exchangers, calcium transporting ATPases and sodium/calcium exchangers. With a range of promising candidates, this work provides a foundation for further studies to functionally characterize the ion transport processes enabling bivalve larval calcification.

Introduction

During bivalve ontogeny, major developmental steps occur rapidly within the first days of life to produce the larval shell, prodissoconch I (PD I). Successful deposition of the PD I shell is essential for subsequent development as the calcified shell provides structural support for swimming and feeding

(Galtsoff 1964). Calcification begins as the precipitation of a calcium carbonate shell onto an organic template during the trochophore larval stage which is characterized by a free-swimming, ciliated larva (Bayne 1976). The supply of calcification substrates (Ca^{2+} and HCO_3^-) to the site of calcification by means of trans-epithelial transport is crucial. In addition, organic matrix components such as shell matrix proteins and carbohydrates (ca. 5% of shell mass, Simkiss & Wilbur 2012) are synthesized and incorporated into the growing shell. Although comprising a small proportion of the shell content, shell matrix proteins are a diverse assemblage of proteins that are important for polymorph control, crystal nucleation, deposition kinetics and structure (Marin et al 2008, Miyamoto et al 2013). Within two days of development, bivalve larvae precipitate an inorganic aragonitic shell that is almost equivalent to their somatic mass and covers the entire larval body (Waldbusser et al 2013). Accompanying this transition into the PD I larval stage is a 250-fold increase in larval calcium content within a few hours (Ramesh et al 2017). In bivalve larvae, the substrates for calcification (Ca^{2+} and HCO_3^-) are not accumulated prior to calcification but are continually supplied during larval shell formation, most likely by means of trans-epithelial transport (Ramesh et al 2017).

The transport of calcium and bicarbonate ions to and removal of protons from the calcification space, is regulated by the expression and activity of membrane bound ion transport proteins. The close relationship between calcification and acid-base related ion transport processes makes it difficult to distinguish between these processes - intracellular pH regulation is also achieved via movement of protons and bicarbonate across the cell membrane. Primary active ion transporters such as V-type H^+ ATPases and H^+/K^+-ATPases utilize energy (ATP) for proton translocation. Secondarily active proton transport is driven by the electrochemical gradient provided by other membrane bound transport proteins, often the ubiquitous Na^+/K^+ ATPase (NKA). Secondarily active proteins that are important for pHi regulation are involved in the translocation of protons and bicarbonate via Na^+-coupled pathways (Na^+/H^+ exchangers SLC9, Na^+ HCO_3^- cotransporters, SLC4), anion exchangers ($Cl^-/HCO3^-$ exchangers SLC4) or voltage gated proton channels. The cellular pathways elicited to regulate intracellular pH are fundamentally conserved in eukaryotes and presence of all relevant transporters in bivalves has been confirmed by genome and transcriptome sequencing projects in the last decade (Zhang et al 2012, Takeuchi et al 2012, Murgarella et al 2016, Li et al 2016a). Several of these membrane bound proteins have been functionally characterized to be involved in mollusc intracellular pH regulation as well (Boron and DeWeer 1976, Thomas 1977, Boron and Russell 1983, Zange et al 1990, Ellington 1993, Louzao et al 1993). For example, using pharmacological inhibitors, it has been shown that stilbene-sensitive anion exchangers and amiloride sentive Na^+/H^+ exchangers are critical to pH regulation in the mussel, *Mytilus edulis* (Zange et al 1990, Kaloyianni et al 2005). A consequent interest is the involvement of these cellular pathways in substrate translocation during calcification. In

the context of larval calcification in molluscs, the role and regulation of the ion transport proteins that facilitate substrate uptake and proton extrusion is not characterized. While there are a number of transcriptome sequencing studies available that challenged adult and larval mollusk calcification processes using future ocean acidification scenarios, there are no published accounts of direct functional characterization of putative calcification relevant ion transporters using knock down / knock out techniques (e.g. Hüning et al 2013, Kelly et al 2016, De Wit et al 2017, Goncalves et al 2016, 2017). On the other hand, much more is known about adult mollusk shell matrix proteins, as they can be readily extracted from the shell using proteomic methods (Arivalagan et al 2016, Feng et al 2017). In addition, a number of studies have successfully used RNAi to demonstrate functional roles of specific shell matrix proteins (Suzuki et al 2009, Fang et al 2011, Funabara et al 2014). Previous studies on mollusc larval development have only revealed a few shell matrix proteins and genes important for forming viable shells (Liu et al 2015, Li et al 2016b). For example, microarray analysis of gene expression in the pearl oyster, *Pinctada fucata*, revealed only five known shell organic matrix proteins to be upregulated during the D-veliger stage, relative to earlier ontogenetic development (Liu et al 2015). This may indicate that larval stages utilize different shell matrix proteins than adults.

The absence of information on the fundamental mechanisms of bivalve calcification physiology limits our ability to predict how these organisms can respond and adapt to environmental changes. One way to address hypotheses regarding the role of various ion transporters related to mineral formation and organic deposition in the larval calcification pathway is by challenging calcification in a substrate-limited environment. In this study, we used RNAseq techniques to identify ion transport and shell matrix proteins involved in the different developmental stages of calcifying larvae of the blue mussel, *Mytilus edulis*. We hypothesized that the genes involved in calcification in *M. edulis* would exhibit severe changes in expression related to the rapid rates of PD I calcification in these organisms. Based on previous empirical data on larval mussels that demonstrated that limiting conditions of dissolved inorganic carbon (C_T) elicited strong reductions in larval calcification (Thomsen et al 2015), we used a substrate limited approach (low C_T) to gain insight into the role of these genes, primarily those involved in inorganic carbon acquisition, in calcification.

Materials and Methods

Adult mussels (*Mytilus edulis*) were collected in Kiel Fjord (54°19.8'N; 10°9.0'E) from subtidal depths in June 2016. Kiel mytilids are *Mytilus edulis* x *trossulus* hybrids with high *edulis*-like allele frequencies (Stuckas et al 2009). We will refer to them as Baltic *Mytilus edulis*-like according to Stuckas et al (2017). Spawning was induced by exposing the adults to rapidly elevated water temperature between 18-25 °C. Spawning individuals were separated and gametes were collected in

individual beakers filled with 0.2 µm filtered seawater (FSW). Eggs were fertilized with sperm and fertilization success was estimated by the presence of polar bodies/cell cleavage. Cleaving embryos were reared in 10 L Duran glass bottles at a density of 10 embryos mL^{-1} bubbled with pressurized air through plastic tubing. All experiments were performed at 17 °C. A total of 4 separate fertilizations were obtained to conduct replicate experiments (n = 4).

Experimental treatments and sample collection

Seawater carbonate chemistry was manipulated by the addition of 1M HCl to FSW, thereby lowering the availability of calcification substrates (HCO_3^-). Excess carbon dioxide was removed by aeration with pressurized air for one hour. Seawater pH was determined on the NBS scale using a WTW 3310 pH meter equipped with a Sentix 81 electrode. Water for carbonate chemistry samples were collected from the culture bottles just before adding embryos to the bottles. Samples were collected in 52 mL Duran Schott glass bottles with glass stoppers and preserved by the addition of 10µl of saturated $HgCl_2$ solution. Seawater C_T was measured using an AIRICA C_T analyzer (Marianda, Germany) and verified with certified reference material (batch 142; Scripps Institution of Oceanography, University of California, San Diego, CA, USA). Seawater carbonate chemistry parameters were calculated using the CO2SYS program with $KHSO_4$, K1 and K2 dissociation constants after Dickson et al. (1990) and Roy et al. (1993), respectively. Cleaving embryos were added to treated water once pH had increased to stable values (ca. 8.14). Temperature, salinity, and carbonate chemistry parameters of experimental conditions are shown in Supplementary Table S1.

For each experiment, embryos from single fertilizations were added to both control (FSW) and treatment (low C_T) bottles and sampled at six developmental time points as determined by hours post fertilization (hpf). Samples were collected at 20, 22, 24, 27, 30 and 35 hpf from control bottles, based on timepoints that were previously identified to be critical for calcification (Ramesh et al 2017). To correct for developmental delay in treatment bottles, samples were collected at similar developmental stages to those in control bottles, as determined by ocular observation of percentage shell cover of the larval body (Figure 1). Samples were quickly concentrated on a mesh (55 µm), transferred to 1.5 ml Eppendorf tubes and centrifuged at 10,000 g to form a larval pellet (~6000 larvae). Seawater was removed using a pipette, samples were shock frozen in liquid nitrogen and stored at -80 °C.

For each sample time point, ca. 100 larvae for photographs were fixed in 4% paraformaldehyde prepared in FSW, buffered to pH 8.2 using 5 mM NaOH. Samples were photographed using a Zeiss Axio Scope A1 microscope equipped with a ProgRes CF Jenoptik camera and ProgRes Capture Pro software (v. 2.9.0.1).

RNA extractions and Sequencing

We extracted total RNA from samples using an RNeasy Mini Kit according to manufacturer's instructions (Catalog no. 74104, Qiagen). RNA yield and purity were initially assessed by measuring A260/A230 and A260/A280 ratio, with a NanoDrop spectrophotometer (NanoDrop2000, Thermo Scientific), followed by analysis on a bioanalyzer (Experion, Bio-Rad). The libraries were prepared from 1 µg RNA per sample with the TruSeq stranded mRNA HT sample preparation kit (Illumina, San Diego, CA, USA). The quality and concentration of the resulting libraries was checked with a bioanalyzer (Agilent 2100) using an Agilent DNA 7500 Kit (Agilent Technologies, Waldbronn, Germany). Library preparation and bioanalyzer validation was performed according to manufacturer protocols. DNA fragment length and concentration data were then used to calculate the molarity of individual libraries, which were subsequently pooled equimolarly (10 nM) and sequenced on an Illumina NextSeq500 sequencer to generate 75 bp single end reads. Illumina BCL files were converted to fastq files and de-multiplexed using bcl2fastq (v2.17, Illumina, San Diego, CA, USA) using default settings.

Bioinformatics analysis

All bioinformatics analyses were carried out using default parameters, unless otherwise specified. Illumina adapter trimming of the reads was performed using Trimmomatic v.0.33 (Bolger & Usedal 2014), and the reads were further trimmed based on quality and length using Fastq-mcf v.1.04.636 (Aronesty 2011) setting the Phred quality score to 30 and minimum read length to 60bp. The cleaned reads were aligned to the Baltic *M. edulis*-like mantle transcriptome (Yarra et al 2017, in prep) using Bowtie v.1.1.1 (Langmead et al 2009) and the digital measure of transcript abundance was calculated using RSEM (RNA-Seq by Expectation-Maximization) v.1.2.20 (Li & Dewey 2011). All contigs with digital expression levels less than 2 Counts Per Million (CPM) at the Trinity 'gene' level, in at least half the libraries, were filtered out before analysis for differential expression. Differentially expressed contigs between developmental stages and treatments were identified using edgeR 3.20 (Robinson et al 2010). Differential gene expression between the different libraries was assessed using the paired experimental model (Family + Treatment and Stage) and only results with FDR values of at least 0.001 were considered.

EBSeqHMM (Leng et al 2015) was used to assess the expression profile of genes over the developmental stages and to cluster genes by expression paths. The expression profile of both control and treatment libraries through the development stages were analyzed and compared. Only results with a FDR value of at least 0.001 were considered. For further GO enrichment analysis, only expression profiles with at least a 50% posterior probability (Max PP) were used. Enrichment of GO terms for genes clustered into the same expression profile using EBSeqHMM, was performed using downstream

Trinity pipeline for Trinotate and GOSeq (Grabherr et al 2011) and only results with at least FDR value of 0.05 were considered. For the purpose of further characterizing contigs of interest, translated proteins sequences were globally aligned to sequences from the public databases using Mafft (Katoh et al 2017), with the BLOSUM62 (Henikoff & Henikoff 1992) scoring matrix, and neighbor joining trees were constructed using the WAG matrix (Whelan & Goldman 2001) with a bootstrap value of 100, on only the conserved residues between all sequences. The expression profile for contigs of interest with the highest posterior probability was displayed, along with the normalized count values of all four larval families in the control libraries (with a trend line represented using lowess smoothing).

Results

Larval Development

Manipulation of seawater carbonate chemistry by the addition of 1M HCl resulted in a reduction of C_T from 1865.5 $\pm$ 26.2 µmol kg^{-1} seawater under control conditions to 941.7 $\pm$ 51.3 µmol kg^{-1} seawater. In addition, a reduction in bicarbonate availability from 1840.8 $\pm$ 23.2 to 888.3 $\pm$ 47.5 and carbonate availability from 108 $\pm$ 3.7 to 43.7 $\pm$ 5 was observed (Supplementary Table S1). Further, seawater C_T reductions were associated with a decrease in pCO_2 from 423.4 + 7.2 µatm under control conditions to 244.6 + 23.7 µatm and $\Omega_{aragonite}$ from 1.7 + 0.03 to 0.6 + 0.08. Development at reduced C_T resulted in a developmental delay starting at 22 hpf, corresponding to the onset of calcification (Ramesh et al 2017, Figure 1, Table 1). Morphologically distinct developmental stages were ascribed to stages 1-6 for further analyses. We did not observe any differences in shell abnormality between control and treatment groups.

QC of sequencing reads

Sequencing of 48 larval libraries yielded a total of 590 million reads, with 541 million reads remaining after filtering based on quality and length. Cleaned reads were aligned to the Baltic *M. edulis*-like mantle transcriptome (Yarra et al 2017, in prep), and mapping rates of approximately 80% were observed for all larval libraries. Filtering based on CPM values yielded 29,177 Trinity genes for further analysis.

Gene Expression Analysis

Very few contigs were found to be differentially expressed between control and treated libraries using a matched pair analysis by each developmental stage (Supplementary Table S2), with mean fold change 2.74 $\pm$ 2. A large number of contigs was differentially expressed between stage 1 and each subsequent developmental stage and multiple contigs were also found to be differentially expressed between each consecutive developmental stage (Supplementary Table S3). Although the overall pattern

on differential expression between the control and treated libraries was similar, the absolute number of differentially expressed contigs was different. This can be attributed to the overall variability of libraries between different biological replicates.

A time series based differential gene expression analysis revealed two expression paths to be the most prevalent during the PD I development in the Baltic *M. edulis*-like trochophore stage (Table 3). Most of the contigs with strong sequence similarity to known shell matrix proteins follow the most prevalent expression path with constantly increasing expression after the onset of calcification. Enrichment of GO terms in the most prevalent expression profile "Down-Up-Up-Up-Up" revealed multiple functions associated with biomineralization, whereas very few GO terms were enriched in the second most prevalent expression profile "Up-Down-Down-Down-Down" (Table 4). Although the absolute number of differentially expressed contigs within the control and treatment libraries were different between developmental stages, the term enrichment of the most prevalent expression profiles in both control and treatment libraries showed similar functionalities.

Identification of Transport Pathways Involved in Calcification

The primary objective of this paper was to identify candidates of ion transport proteins potentially involved in providing substrates (Ca^{2+}, HCO_3^-) to enable larval calcification. Substrate (C_T) limitation induced a small set of genes to be differentially regulated (Table 2, Supplementary Table S2) with fold change values between 0.26 and 16.11 (Figure 2). Only one contig was classified as an ion transporter of interest, belonging to solute carrier family (SLC) 26, a group of ion transport proteins that transport a diverse set of anions, including HCO_3^- (Cordat & Casey 2009). During the course of *M. edulis* larval development, the expression of this SLC26A11 contig is upregulated, where the expression profile displayed a continual increase between stages 4-6 (Figure 3). The expression of this contig is observed to be 2.3 and 2.9 fold higher under substrate limitation at Stage 4 and 5, respectively (Supplementary Table S2).

In contrast to the small number of genes exhibiting differential expression in response to substrate limitation, several contigs encoding ion transport proteins belonging to solute carrier families (SLC) 4, 9 and 26 were differentially expressed during the course of larval development and shell deposition. Amongst these SLC families, several genes exhibited progressive increases in expression during the course of development (Supplementary Table S3) and encoded sarco/endoplasmic reticulum Ca^{2+}-ATPase, sodium/calcium exchangers (NCX), sodium/potassium ATPases. 245 genes were differentially expressed following the onset of larval shell deposition in comparison to the pre-calcifying ontogenetic stage (at 20 hpf, Supplementary Table S4). The putative ion transport pathways involved in larval calcification based on expression patterns for contigs of interest (Figures 4, 5 and 6)

is presented in Figures 7 and is complemented by a recent study by Yarra et al (2017, in prep) that characterizes the differential expression of several identical pathways in adult *M. edulis* during induced shell repair.

Putative homology of bicarbonate ion transporters

There are multiple families of bicarbonate transporters present in eukaryotes. To further characterize the putative function of the differentially expressed contigs with bicarbonate transporting domains, a phylogenetic tree from the multiple sequence alignment of translated protein sequences was assessed (Figure 8). The bicarbonate transport phylogenetic tree was constructed based on 95 conserved sites of 43 sequences, including 10 Baltic *M. edulis*-like contigs, and a cystic fibrosis transmembrane conductance regulator from zebrafish as an outlier. All sequences are provided in Supplementary Table S5.

Shell Matrix Proteins

Multiple shell matrix proteins, previously identified in the shell matrices of adult *Mytilus* spp., and expressed by the adult mantle tissue, were found to be differentially expressed during larval shell development (Figure 9). Most of the shell proteins displayed an increasing expression profile throughout the trochophore stage, with a few shell matrix proteins appearing to reduce expression just before the completion of the PD I. Four of the shell matrix protein domains, α-carbonic anhydrase, β-lactamase, concanavalin A and cyclophilin PPIase, displayed decreasing expression levels as the initial shell was completed.

Discussion

We used a calcification substrate limited approach (low dissolved inorganic carbon, C_T) to challenge the acid-base regulatory systems necessary for larval calcification. In comparison to controls, substrate limitation treatments (mean C_T = 941.7 μmol kg^{-1} seawater) were characterized by a ca. 51% and ca. 59% decrease in bicarbonate and carbonate availability, respectively. Such modifications in seawater carbonate chemistry were accompanied by a developmental delay in shell accretion that is consistent with previous empirical data (Thomsen et al 2015). These observations in developmental delay demonstrate that low C_T conditions are strongly correlated to decreases in larval calcification rates in *Mytilus edulis* (Thomsen et al 2015). Developmental delays in response to changes in seawater carbonate chemistry have been reported for several bivalve species (Ross et al 2011, Timmins-Schiffman et al 2012). However, previous transcriptomic studies have not accounted for such developmental delays (Kelly et al 2016). Our results demonstrate the importance of correcting sample collection for developmental delays since we observe that differences in shell morphology (percentage

shell cover) are related to specific gene expression profiles, as has been demonstrated for larval echinoderms as well (Stumpp et al 2011a, b). We identified only 53 genes to be differentially expressed between control and low C_T conditions. However, median fold change of contigs significantly up – (down) regulated in low C_T libraries with respect to control libraries was 2.47- fold (Supplementary Fig. S2), indicating that more subtle changes in gene expression were not detected with the present experimental design. These comparatively high thresholds are in line with high coefficients of variation (CV, % SD of mean) of 190% in all libraries. While somewhat surprising (each of the four replicate samples per treatment was generated using 6,000 larvae), this high variability in gene expression between Baltic Sea mytilid families or individuals has been observed before (Hüning et al. 2013, Yarra et al. in prep.).

Of particular interest is the 2.32 and 2.96 fold upregulation of one gene (contigTRINITY_DN175059_c1_g4) at stages 4 and 5 encoding an anion transporter with strong similarity to the solute carrier family 26 (SLC26) members. SLC26 members transport a broad group of anions, including HCO_3^-, the putative substrate for larval calcification. Stages 4 and 5 are particularly interesting, as they are characterized by exponential increases in shell deposition (Ramesh et al 2017), corresponding to a shell cover increase from ca. 10% to ca. 76% of larval body.

Phylogenetic tree analyses revealed a close relationship between the *M. edulis* SLC26 contig, the human SLC26A11 sulfate/anion transporter and the SLC26 γ isoform anion transporter in the coral *Stylophora pistillata* (Figure 8). Recently, the function of SLC26A11 transporters as sodium independent-sulfate transporters has been critically reviewed based on observations of its function as a chloride channel in mice neurons using electrophysiological techniques (Rahmati et al 2013). Further, transfection of the SLC26A11 transporter in mouse neuronal cells hints towards the activation of V-type H^+-ATPases by SLC26A11 transporters inducing proton translocation (Rahmati et al 2013). Alternativly, the up-regulation of this transporter during larval development may be related to the uptake of sulfate for synthesis of sulfated macromolecules such as proteoglycans that are present in the organic matrix of mollusc shells (LeRoy & Marie 2012). Sulfated constituents of the organic matrix in calcified structures have been proposed to play a role in crystal nucleation (Cuif et al 2003, Cuif & Dauphin 2005).

In addition to the SLC26 candidate, the substrate limitation approach also yielded several contigs encoding proteins with speculative roles in *M. edulis* larval calcification. At least eight differentially regulated contigs have been previously demonstrated to be involved in bone mineralisation and resorption or have been shown to form components of organic matrices in mammals. For example, mice deficient of transcription factor Sox 8 (upregulated under low C_T at stages 5 and 6) exhibit

reduced bone mass and impaired osteoblast differentiation (Schmidt et al 2005). Interestingly the function of transcription factor Sox 8 is strongly linked to the expression of runt-related transcription factor 2 (Runx2) (Schmidt et al 2005), where Runx2 (upregulated under low C_T at stages 3 and 5) is an important regulator of mammalian bone formation (Franceschi &Xiao 2002, Fowlkes et al 2008, Takarada et al 2013) and arterial calcification (Ruffenach et al 2016). Two other proteins, tumor necrosis factor α inducing proteins and interleukin1 receptor-associated kinase 4 (IRAK4) that were observed to be differentially upregulated under low C_T conditions in *M. edulis* larvae have also been associated with osteoblast differentiation and bone resorption (Tintut et al 2000, Katsuyama et al 2014). Tumor necrosis factor α is involved in the activation of nuclear factor-kappa B (NF- κB, upregulated under low C_T at Stage 5), a protein whose activation is linked to arterial calcification in humans (Zhao et al 2012). Substrate limitation also induced upregulation of a contig encoding a zinc transporter during Stage 5 of *M .edulis* larval development. In mammals, the knockout of zinc transporters has been demonstrated to result in skeletal disorders (Fukada et al 2008) and the role is zinc is established in bone mineralisation (Yamaguchi 1998) and mollusc shell deposition (Tan & Mai 2001). Finally, the expression of a contig encoding putative C-type lectins was also upregulated under low C_T in *M. edulis* larvae. C-type lectins form important components of the shell organic matrix in molluscs (Mann et al 2012). For example, the shell matrix protein perlucin that is expressed in *M. edulis* larvae during PD I formation (Figure 3) contains a C-type lectin domain. Therefore, our substrate (C_T) limitation technique elicited an expression change in several contigs that can be related to *M. edulis* larval calcification and further characterization of these individual genes, e.g. by using RNAi screens (knockdown techniques), is required to understand their putative role in PD I formation.

The low number of differentially expressed genes with respect to substrate limitation is certainly linked to the high variability in gene expression (see above), but is also line with previous studies on calcifying larvae that observe no significant changes in gene expression in response to simulated ocean acidification (Evans et al 2013, Kelly et al 2016) and may point towards a limited molecular programme during ontogenetic development. In contrast, adult bivalves have been observed to exhibit differential regulation of genes related to ion and acid-base regulation in response to elevated seawater pCO_2 (Li et al 2016c). Differences in larval and adult transcriptomic responses to CO_2 in other studies may reflect differences in simulated CO_2 intensities, experimental design and individual variability. Alternatively, acid-base regulation may be ensued via post – translational mechanisms, e.g. the translocation of membrane bound transport proteins to compensate for increased transport of calcification substrates (Tresguerres et al 2007, Roa et al 2014) and phosphorylation of ion transport proteins (Levitan 1994, Flemmer et al 2010) that can induce their rapid activation (Ramnanan & Storey 2006, Rapport & Murad 1983).

In a second step, we analysed gene expression profiles over the developmental time course of *M. edulis* larvae and observed the dynamic expression of several genes encoding ion transport and shell matrix proteins. The putative roles of these candidate genes in acid-base homeostasis and larval calcification are discussed below.

HCO_3^- transport

In eukaryotes, the transport of HCO_3^- may occur via two possible families of membrane-bound transport proteins, the SLC4 and SLC26 transporters. Within the group of SLC4 transporters, proteins are characterized into three major groups, based on mechanism of action: Cl^-/HCO_3^- exchangers (also known as anion exchangers (AE), $Na^+ - HCO_3^-$ cotransporters (NBCs) and Na^+-driven Cl^-/HCO_3^- exchangers (NDCBE) (Romero et al 2013). The Cl^-/HCO_3^- exchangers are electroneutral and exchange Cl^- and HCO_3^- at 1:1 stoichometry, while the NBCs may function at a Na^+:HCO_3^- stoichiometry of 1:3/1:2 (electrogenic) or 1:1 (electroneutral) (Romero et al 2013). The SLC26 family of transport proteins transports a variety of anions including HCO_3^-, sulfate (SO_4^{2-}), oxalate, and others and may similarly also be functionally characterized into various groups depending on stoichiometry (Soleimani 2013). Therefore, depending on which HCO_3^- transporting protein is utilized, Cl^- or Na^+ is required to provide the electrochemical gradient required for HCO_3^- transport. The provision of such gradients using Na^+ through Na^+/K^+-ATPases, Na^+ channels or Na^+/Ca^{2+} exchangers is discussed in the following sections. However, if Cl^- was the coupled ion for HCO_3^- acquisition during larval calcification, Cl^- gradients may be maintained via proton exchange, cation coupled Cl^- exchange (Na^+-K^+-$2Cl^-$ cotransporters, SLC12) and Cl^- channels.

Among all the genes encoding ion transport and shell matrix proteins investigated in this study, sequences encoding NBC's exhibited high transcript abundance during the larval development of *M. edulis* with a peak in expression during early calcification (Figure 4). The peak in expression of NBC genes is accompanied by the onset of accumulation of calcium by mussel larvae (Ramesh et al 2017), following which expression levels rapidly decrease. Within the contigs encoding HCO_3^- transport in the transcriptome, two contigs clustering with SLC4 (DN167998_c0_g2) and SLC26 (DN173725_c0_g1) families have been observed to be upregulated during induced shell repair in adult *Mytilus edulis*, further supporting the role of these genes in substrate acquisition for calcification (Yarra et al 2017, in prep). Finally, the potential transport of HCO_3^- via the SLC26 candidate is discussed above (Figure 2C).

Ca^{2+} transport

Prior to the onset of calcification at the trochophore larval stage, Ca^{2+} is not accumulated and stored by mussel larvae (Ramesh et al 2017). Rapid calcification of the PD I shell in mussels is accompanied by

a tremendous uptake of calcium by larvae within a few hours (Ramesh et al 2017). In contrast to larval sea urchins (Vidavsky et al 2015, 2016), the acquisition of the calcification substrates Ca^{2+} and HCO_3^- from seawater via endocytotic transport is not a major pathway for calcium acquisition in larval mussels (Ramesh et al 2017), suggesting that uptake of Ca^{2+} must occur via a transepithelial pathway. Our study indicates that in *M. edulis*, four proteins (sarco/endoplasmic reticulum Ca^{2+}-ATPase (SERCA), Ca^{2+} channels, sodium/calcium exchangers (NCX) and mitochondrial Ca^{2+} uniporter protein, MCU) are mainly involved in Ca^{2+} transport during larval development (Figure 5). Expression of genes encoding these four Ca^{2+} transport proteins was up-regulated as ontogenetic development progressed, with largest increases in expression for genes encoding SERCA and NCX, suggesting a pivotal role of these transporters. In mammalian cells, SERCA is crucial for maintaining low intracellular Ca^{2+} concentrations by sequestering Ca^{2+} within the sarco/endoplasmic reticulum (Arruda and Hotamisligil 2015). In adult bivalves, SERCA has been suggested to play a role in biomineralization due to its high expression (Truebano et al 2010) and localized expression of one SERCA isoform (Fan et al 2007) in mantle tissue. Aside from SERCA, organisms may also employ calcium binding proteins to reduce free Ca^{2+} concentrations intracellularly. Expression of genes for one such calcium binding protein, calbindin was observed to increase during the course of *M. edulis* larval development with a peak in expression at PD I stage. NCX (SLC8) is a group of membrane-bound transport proteins that facilitate the reversible exchange of three sodium ions (Na^+) for one calcium ion and has an established role in mammalian osteoblast (bone) calcification and avian eggshell mineralisation (Cheidde et al 2003, Sosnoski & Gay 2007). The simultaneous elevated expression profiles of NKA and NCX during *M. edulis* ontogenetic development support the role of NCX in larval Ca^{2+} transport. Increased transcript abundances for genes encoding several Ca^{2+} channels (Ca^{2+} load activated Ca^{2+} channel, voltage dependent Ca^{2+} channels, Ca^{2+} channel subunit α) was observed during *M. edulis* larval development. In calcifying sea urchin larvae, Ca^{2+} channels play only a partial role in Ca^{2+} acquisition during skeletogenesis (Fujino et al 1985, Yasumasu et al 1985, Vidavsky et al 2016).

Na^+ transport

The Na^+/K^+ ATPase (NKA) is an active membrane-bound pump present on the basolateral membrane and is critical for maintenance of cell membrane potential and generates the electrochemical gradient necessary to facilitate the subsequent transport of ions by secondary transport proteins (Boron & Boulpaep 2009). The exchange of sodium and hydrogen ions via the sodium/hydrogen exchanger (NHE) belonging to SLC9 is one such secondary pathway driven by the NKA. The elevated co-expression patterns of a mitochondrial NHE and NKA, where genes encoding these proteins exhibit peaks in expression during early shell formation suggest that the NHE is critical for proton (H^+)

removal, (Figure 6). In accordance with the up-regulation of contigs encoding NKA during early shell formation, activity of this enzyme has also been recorded to peak during early shell formation in oyster larvae (Frieder et al 2017). Similar transport processes are present in the primary mesenchymal cells in sea urchin larvae which are responsible to calcification and skeletogenesis where amiloride-sensitive ion transport proteins such as the NHE have been demonstrated to be significant for cellular pH regulation (Stumpp et al 2012). In addition to elevated expression of genes encoding NHEs at the onset of larval calcification, we also observed a peak in expression of gene encoding Na^+/H^+ exchange regulatory factor (NHERF). NHERF proteins are involved in regulating function of NHE and have a pivotal role in bone formation, where their regulation of NHEs is crucial for osteoblast differentiation and strength (Liu et al 2012).

H^+ Transport

Aside from the overexpression of Ca^{2+}, HCO_3^- and Na^+ transporting proteins, several genes encoding H^+ transporters exhibit high transcript abundances. Among these genes, the expression profiles of genes encoding VHAs exhibited a peak in expression during the PD I stage of larval development. In addition to the active transport of H^+, secondary H^+ transport pathways such as voltage gated hydrogen channels also exhibit dynamic expression profiles during the development of *M. edulis*. The elevated expression of H^+ transport pathways during larval calcification is consistent with the requirement to extrude protons that are generated by the mineralisation of calcium carbonate from HCO_3^- and the observed increases in pH at the site of calcification in larval mussels (Ramesh et al 2017).

Transport of Other Ions

Parallel to the acquisition of substrates for calcification (Ca^{2+} and HCO_3^-) and removal of protons by-products of calcification, there are ion transport proteins that are essential for maintenance of cellular electrogenic gradients, cell volume, etc. During the ontogenetic development of *M. edulis*, expression of several genes encoding transport proteins of chloride (Cl^-) and potassium (K^+) is observed. In particular, elevated expression for various chloride channels (Ca^{2+} activated chloride channel, intracellular chloride channel, chloride channel) during PD I larval stage is detected (Figure 6). Efflux of Cl^- from the basolateral membrane due to acquisition of HCO_3^- in the calcification space via anion exchangers may be coupled to the elevated activity of Cl^- channels. Alternatively, Cl^- efflux may occur via cation coupled pathways (SLC12) or H^+/Cl^- exchange. However, genes encoding such Cl^- transport proteins did not exhibit high transcript abundances during larval development or shell formation in *M. edulis*. In adult mytilids, the activity of H^+/Cl^- antiporters has been suggested to be unimportant for maintenance of cell membrane potential based on patch-clamp techniques in hemocytes (Bregante et al 2016).

Expression of several K^+ channels is observed in the larval transcriptome. However, significant changes in the expression of only one K^+ channel was observed during the course of development, the inward rectifier K^+ channel (K_{ir}, Figure 4). Interestingly, this group of membrane bound transport proteins was also found to be upregulated during shell repair in adult *M. edulis* (Yarra et al 2017, in prep). K_{ir} channels are important sustaining electrochemical gradients and cell resting potential by recycling K^+ ions (Weber et al 2001). In addition, their absence in mammalian osteoblasts has been observed to inhibit osteoblastgenesis due to a decreased efficiency in production of an extracellular matrix (Sacco et al 2015).

Shell matrix proteins

Several shell matrix proteins (SMPs), ca. 65% of the SMPs expressed in the adult Baltic *M. edulis*-like mantle transcriptome (Yarra et al 2017, in prep) and ca. 65% of the SMPs extracted from adult shells (Appendix 1 from Yarra et al 2017, in prep) were expressed during larval development (Figure 9). Three of the SMPs expressed in *M. edulis* larvae (nacrein, EGF-like and tyrosinase) were also found to be expressed in other bivalve larvae (Fang et al 2011, Liu et al 2015, Li et al 2016b). Multiple contigs with sequence similarity to other adult shell SMPs, but not yet identified in larval shells, were found to be differentially expressed throughout PD I development. Most of the contigs containing domains involved in structuring the shell or tissue, such as β-hexosaminidase, glycoside hydrolase, chitin synthase, chitin binding, von Willebrand factor A, and Fibronectin type III, were found to have an increasing expression profile as the shell field is expanding over the surface of the larvae. Contigs containing copper binding domains such as amine oxidase, dopamine-β-hydroxylase and tyrosinase were also shown to increase in expression as the PD I shell is formed. Of particular interest are the contigs containing periostracum forming tyrosinase domains (Zhang et al 2006), which show a decrease in expression right before the end of PD I formation. The periostracum acts as a template for shell mineralisation and the drop in expression of contigs containing tyrosinase domains reflects the completion of periostracum formation in PD I.

Other SMPs that are linked to mineral deposition and crystallographic control include proteases and protease inhibitors that behave antagonistically, where the former are known to be important for crystal nucleation (Tiaden et al 2012, Hershey et al 2016). During the formation of the Baltic *M. edulis*-like PD I shell, contigs containing protease inhibitor domains such as BPTI/Kunitz and Kazal were increasing in expression throughout shell formation. BPTI/Kunitz exhibited a peak in expression prior to the completion of the PD I, supporting its involvement in terminating crystal growth. Conversely, the contig with the protease inhibitor domain β-lactamase (Gigasin 6) was highly expressed before larval calcification, suggesting its putative involvement in initial crystal deposition. The contig

containing the protease domain, peptidase C1A, was observed to increase in expression throughout shell formation, thus not following the pattern of other protease and protease inhibitors. One possible explanation could be that peptidase C1A domains are involved in immune functions, as opposed to shell calcification.

Although bivalve larval shells are composed of only one calcium carbonate polymorph, aragonite (Kudo et al 2010, Yokoo et al 2011), several SMPs that were previously identified in the calcitic fibrous prism structures of adult mytilid shells (Gao et al 2015, Liao et al 2015) were expressed in the Baltic *M. edulis*-like transcriptome. These SMPs include tyrosinase, gigasin-like and alveoline-like proteins, whilst the other SMPs expressed in the Baltic *M. edulis*-like transcriptome are proteins that are associated with the aragonite layers (nacre and myostracum) in adult mytilid shells.

Conclusions

By rearing mussel larvae under conditions of substrate limitation for calcification and analyzing differential gene expression patterns, we were able to identify a membrane-bound transport protein potentially involved in HCO_3^- acquisition, belonging to the SLC26 family of anion transporters. Interestingly, the present study identifies only a small subset of genes to be differentially expressed under substrate limitation. Although this may be improved by a stronger C_T treatment (> 50% decrease relative to control), higher sequencing depth and replication, bivalve larvae may possess a fixed capacity to modify their transcriptomic developmental program. This is consistent with previous studies on bivalve larvae that observe no significant changes in their transcriptomic repertoire in response to induced acid-base stress (Kelly et al 2016). Our data demonstrate an increased expression of contigs encoding for Ca^{2+} and HCO_3^- -transporting proteins once larval shell formation starts, indicating the transport of these ions to the calcification space that would consequently elevate the saturation state of aragonite and favour shell deposition. In particular, the dynamic expression patterns of SERCA, NCX and NBC contigs hint towards the role of these ion transport pathways in bivalve larval calcification. Finally, the analyses of SMP expression patterns during larval development reveal the conserved function of these proteins between adult and larval stages in Baltic *M. edulis*. In addition, several proteins with hypothesized roles in shell structure, crystallographic control and periostracum deposition were observed to be upregulated during larval development. Further in-depth analysis of the PD II could reveal more detail about these SMPs. Till date, functional analyses using RNA interference techniques have been limited to SMPs (Suzuki et al 2009, Fang et al 2011, Funabara et al 2014). However, knock out/ know down techniques are required to establish the role of candidate ion transporters in larval calcification. The identification of candidate in biomineralisation paves the way for future studies utilizing recombinant DNA techniques in heterologous expression, in

conjunction with electrophysiology techniques to characterize the substrate specificity and stoichiometry of these ion transport genes.

Acknowledgements

This study was funded by the European Union's Seventh Framework Programme [FP7] ITN project 'CACHE' under REA grant agreement #[605051]13. We thank Ulrike Panknin and Nancy Kühne for help with the library preparation and sequencing.

Author contributions

K.R. and F.M. designed the study. K.R. conducted the larval experiments, RNA extractions and sequencing library preparations. T.Y conducted the bioinformatics analysis. K.R. and T.Y. analyzed the data and wrote the manuscript. All authors contributed to paper revisions.

Ethics approval and consent to participate

Not applicable.

Consent for publication

Not applicable.

Competing interests

The authors declare that they have no competing interests.

References

Arivalagan, J., Yarra, T., Marie, B., Sleight, V.A., Duvernois-Berthet, E., Clark, M.S., Marie, A., Berland, S. (2016) Insights from the Shell Proteome: Biomineralization to Adaptation. Molecular Biology and Evolution 34: 66–77.

Aronesty, E. (2011) Command-line tools for processing biological sequencing data. In: ea-utils. url: http://code.google.com/p/ea-utils.

Arruda, A.P., Hotamisligil, G.S. (2015) Calcium homeostasis and organelle function in the pathogenesis of obesity and diabetes. Cell Metabolism 22: 381–397.

Bayne, B.L. (1976) The biology of mussel larvae. In: Marine mussels: their ecology and physiology, pp 8t-120. Edited by B.L. Bayne. Cambridge University Press.

Bolger, A.M., Lohse, M., Usadel, B. (2014) Trimmomatic: a flexible trimmer for Illu- mina sequence data. Bioinformatics 30: 2114–2120.

Boron, W. Boulpaep, E.L. (2009) Medical Physiology: a cellular and molecular approach (2nd edition). Saunders Elsevier, Canada.

Boron, W.F., Deweer, P. (1976) Intracellular Ph Transients in Squid Giant-Axons Caused by Co2, Nh3, and Metabolic-Inhibitors. Journal of General Physiology 67: 91-112.

Boron, W.F., Russell, J.M. (1983) Stoichiometry and ion dependencies of the intracellular pH regulating mechanisms in giant squid axons. Journal of General Physiology 81: 373-399.

Bregante, M., Carpaneto, A., Piazza, V., Sbrana, F., Vassalli, M., Faimali, M., Gambale, F. (2016) Osmoregulated Chloride Currents in Hemocytes from *Mytilus galloprovincialis*. PlosOne 11(12): e0167972.

Cheidde, L., Viera, T.C., Lima, P.R.M., Saad, S.T.O., Heilberg, I.P. (2003) A Novel Mutation in the Anion Exchanger 1 Gene Is Associated With Familial Distal Renal Tubular Acidosis and Nephrocalcinosis. Pediatrics 112 : 1361-1367.

Cordat, E., Casey, J.R. (2009) Bicarbonate transport in cell physiology and disease. Biochemical Journal 417: 423–439.

Cuif, J.P., Dauphin, Y. (2005) The two-step mode of growth in the Scleractinian coral skeletons from the micrometre to the overall scale. Journal of Structural Biology 150: 319–331.

Cuif, J.P., Dauphin, Y., Doucet, J., Salome, M., Susini, J. (2003) XANES mapping of organic sulfate in three scleractinian coral skeletons. Geochim. Cosmochim. Acta 67: 75–83.

DeWit, P., Durland, E., Ventura, A., Langdon, C. (in review) Gene expression correlated with delay in shell formation in larval Pacific oysters (*Crassostrea gigas*) exposed to experimental ocean acidification provides insights into shell formation mechanisms. Molecular Ecology.

Dickson, A.G. (1990) Standard potential of the reaction – AgClS+1/2 H2 = AgS+HClAq and the standard acidity constant of the ion HSO_4^- in synthetic sea-water from 273.15-K to 318.15-K. Journal of Chemical Thermodynamics 22: 113-127.

Ellington, W.R. (1993) Studies of Intracellular pH Regulation in Cardiac Myocytes from the Marine Bivalve Mollusk, *Mercenaria-Campechiensis*. Biological Bulletin 184: 209-215.

Evans, T.G., Chan, F., Menge, B.A., Hofmann, G.E. (2013) Transcriptomic responses to ocean acidification in larval sea urchins from a naturally variable pH environment. Molecular Ecology 22: 1609–1625.

Fan, W., Li, C., Li, S., Feng, Q., Xie, L., Zhang, R. (2007) Cloning, Characterization, and Expression Patterns of Three Sarco/Endoplasmic Reticulum Ca^{2+}-ATPase Isoforms from Pearl Oyster (*Pinctada fucata*). Acta Biochimica et Biophysica Sinica 39: 722–730.

Fang, D., Xu, G., Hu, Y., Pan, C., Xie, L., Zhang, R. (2011) Identification of Genes Directly Involved in Shell Formation and Their Functions in Pearl Oyster, *Pinctada fucata*. PLoS One 6: e21860.

Feng, D., Li, Q., Yu, H., Kong, L., Du, S. (2017) Identification of conserved proteins from diverse shell matrix proteome in *Crassostrea gigas*: characterization of genetic bases regulating shell formation. Scientific Reports 7: 45754.

Flemmer, A.W., Monette, M.Y., Djurisic, M., Dowd, B., Darman, R., Gimenez, I., Forbush, B. (2010) Phosphorylation state of the $Na^+/K^+/Cl^-$cotransporter (NKCC1) in the gills of Atlantic killifish (*Fundulus heteroclitus*) during acclimation to water of varying salinity. Journal of Experimental Biology 213: 1558-1566.

Fowlkes, J.L., Bunn, R.C., Liu, L., Wahl, E.C., Coleman, H.N., Cockrell, G.E., Perrien, D.S., Lumpkin, C.K., Thrailkill, K.M. (2008) Runt-Related Transcription Factor 2 (RUNX2) and RUNX2-Related Osteogenic Genes Are Down-Regulated throughout Osteogenesis in Type 1 Diabetes Mellitus Endocrinology 149: 1697–1700.

Franceschi, R.T., Xiao, G. (2002) Regulation of the osteoblast-specific transcription factor, Runx2: Responsiveness to multiple signal transduction pathways. Journal of Cellular Biochemistry 88: 446–454.

Frieder, C.A., Applebaum, S.L., Pan, T.C.F, Hedgecock, D., Manahan, D. (2017) Metabolic cost of calcification in bivalve larvae under experimental ocean acidification. ICES Journal of Marine Science fsw213 doi: https://doi.org/10.1093/icesjms/fsw213.

Fujino Y, Mitsunaga K, Fujiwara A, Yasumasu I. (1985) Inhibition of $^{45}Ca^{2+}$ uptake in the eggs and embryos of the sea urchin, *Anthocidaris crassispina*, by several calcium antagonists, anion transport inhibitor, and chloride transport inhibitors. Journal of Experimental Zoology 235: 281-288.

Fukada T, Civic N, Furuichi T, Shimoda S, Mishima K, et al. (2008) Correction: The Zinc Transporter SLC39A13/ZIP13 Is Required for Connective Tissue Development; Its Involvement in BMP/TGF-β Signaling Pathways. PLOS ONE 3. doi: 10.1371/journal.pone.0003642.

Funabara, D., Ohmori, F., Kinoshita, S., Koyama, H., Mizutani, S., Ota, A., Osakabe, Y., Nagai, K., Maeyama, K., Okamoto, K., Kanoh, S., Asakawa, S., Watabe, S. (2014) Novel genes participating in

the formation of prismatic and nacreous layers in the pearl oyster as revealed by their tissue distribution and RNA interference knockdown. PLoS One 9: e84706.

Galtsoff, P.S. (1964) The American oyster, *Crassostrea virginica* Gmelin. Chapter 16: Larval development and metamorphosis. Fishery Bulletin, North East Fishery Science Centre.

Gao, P., Liao, Z., Wang, X.X., Bao, L.F., Fan, M.H., Li, X.M., Wu, C.W. Xia, S.W. (2015) Layer-by-Layer Proteomic Analysis of *Mytilus galloprovincialis* Shell. PLosOne 10. doi: 10.1371/journal.pone.0133913.

Goncalves, P., Anderson, K., Thompson, E.L., Melwani, A., Parker, L.M., Ross, P.M., Raftos, D. (2016) Rapid transcriptional acclimation following transgenerational exposure of oysters to ocean acidification. Molecular Ecology. doi: 10.1111/mec.13808.

Goncalves, P., Jones, D.B., Thompson, E.L., Parker, L.M., Ross, P.M., Raftos, D. (2017) Transcriptomic profiling of adaptive responses to ocean acidification. Molecular Ecology. doi: 10.1111/mec.14333.

Grabherr, M.G., Haas, B.J., Yassour, M., Levin, J.Z., Thompson, D.A., Amit, I., Adiconis, X., Fan, L., Raychowdhury, R., Zeng, Q., Chen, Z., Mauceli, E., Hacohen, N., Gnirke, A., Rhind, N., di Palma, F., Birren, B.W., Nusbaum, C., Lindblad-Toh, K., Friedman, N., Regev, A. (2011) Full-length transcriptome assembly from RNA-Seq data without a reference genome. Nature Biotechnology 29:644-652.

Henikoff, S., Henikoff, J.G. (1992) Amino acid substitution matrices from protein blocks". Proceedings of the National Academy of Sciences of the United States of America 89: 10915-10919.

Hershey, D.M., Ren, X., Melnyk. R.A., Browne, P.J., Ozyamak, E., Jones, S.R., Chang, M.C., Hurley, J.H., Komeili, A. (2016) MamO Is a Repurposed Serine Protease that Promotes Magnetite Biomineralization through Direct Transition Metal Binding in Magnetotactic Bacteria". PLoS Biology 14: e1002402.

Hüning, A.K., Melzner, F., Thomsen J., Gutowska, M.A., Krämer, L., Frickenhaus, S., Rosenstiel, P., Pörtner, H.O., Philipp, E.V.E.R., Lucassen, M. (2013) Impacts of seawater acidification on mantle gene expression patterns of the Baltic Sea blue mussel: implications for shell formation and energy metabolism. Marine Biology 160:1845–1861.

Kaloyianni, M., Stamatiou, R., Dailianis, S. (2005) Zinc and 17 β-estradiol induce modifications in Na^+/H^+ exchanger and pyruvate kinase, activity, through protein kinase C in isolated mantle/gonad

cells of *Mytilus galloprovincialis*. Comparative Biochemistry and Physiology C-Toxicology & Pharmacology 141: 257-266.

Katoh, K., Rozewicki, J., Yamada, K.D. (2017) MAFFT online service: multiple sequence alignment, interactive sequence choice and visualization. Brief. Bioinformatics. doi: 10.1093/bib/bbx108.

Katsuyama. E., Miyamoto, H., Kobayashi, T., Sato, Y., Hao, W., Kanagawa, H., Fujie, A., Tando, T., Watanabe, R., Morita, M., Miyamoto, K., Niki, Y., Morioka, H., Matsumoto, M., Toyama, Y., Miyamoto, T. (2014) Interleukin-1 Receptor-associated Kinase-4 (IRAK4) Promotes Inflammatory Osteolysis by Activating Osteoclasts and Inhibiting Formation of Foreign Body Giant Cells. The Journal of Biological Chemistry 290: 716-726.

Kelly, M.W., Padilla-Gamino, J.L., Hofmann, G.E. (2016) High pCO_2 affects body size, but not gene expression in larvae of the California mussel (*Mytilus californianus*). Ices Journal of Marine Science 73: 962-969.

Kenkel, C.D., Meyer, E., Matz, M.V. (2013) Gene expression under chronic heat stress in populations of the mustard hill coral (*Porites astreoides*) from different thermal environments. Molecular Ecology 22: 4322-4334.

Langmead, B., Trapnell, C., Pop, M., Salzberg, S.L. (2009) Ultrafast and memory-efficient alignment of short DNA sequences to the human genome. Genome Biology 10: R25.

Leng, N., Li, Y., McIntosh, B.E., Nguyen, B.K., Duffin, B., Tian, S., Thomson, J.A., Dewey, C.N., (2015) Stewart, R., Kendziorski, C. (2015) EBSeq-HMM: a Bayesian approach for identifying gene-expression changes in ordered RNA-seq experiments. Bioinformatics 31: 2614-2622.

LeRoy, N., Marie, B. (2012) The formation and mineralization of mollusk shell. Frontiers in Bioscience S4, 1099-1125.

Levitan, I.B. (1994) Modulation of ion channels by protein phosphorylation and dephosphorylation. Annual Review of Physiology 56: 193-212.

Li, B., Dewey, C.N., (2011) RSEM: accurate transcript quantification from RNA- Seq data with or without a reference genome. BMC Bioinformatics 12: 323.

Li, H., Zhang, B., Huang, G., Liu, B., Fan, S., Zhang, D., Yu, D. (2016b) Differential Gene Expression during Larval Metamorphic Development in the Pearl Oyster, *Pinctada fucata*, Based on Transcriptome Analysis. International Journal of Genomics: 2895303.

Li, S., Huang, J., Liu, C., Liu, Y., Zheng, G., Xie, L., Zhang, R. (2016c) Interactive effects of seawater acidification and elevated temperature on the Transcriptome and Biomineralization in the pearl oyster *Pinctada fucata*. Environmental Science & Technology 50: 1157-1165.

Li, Y., Sun, X., Hu, X., Xun, X., Zhang, J., Guo, X., Jiao, W., Zhang, L., Liu, W., Wang, J., Li, J., Sun, Y., Miao, Y., Zhang, X., Cheng, T., Xu, G., Fu, X., Wang, Y., Yu, X., Huang, X., Lu,W., Lv, J., Mu, C., Wang, D., Li, X., Xia, Y., Li, Y., Yang, Z., Wang, F., Zhang, Lu., Xing, Q., Dou, Q., Ning, X., Dou, J., Li, Y., Kong, D., Liu, Y., Jiang, Z., Li, R., Wang, S., Bao, Z. (2016a) Scallop genome reveals molecular adaptations to semi-sessile life and neurotoxins. Nature Communications 8: 1721.

Liao, Z., Bao, L.F., Fan, M.H., Gao, P., Wang, X.X., Qin, C.L., Li, X.M., (2015) In-depth proteomic analysis of nacre, prism, and myostracum of *Mytilus* shell. Journal of Proteomics 122: 26-40.

Liu, J., Yang, D., Liu, S., Li, S., Xu, G., Zheng, G., Xie, L., Zhang, R. (2015) Microarray: a global analysis of biomineralization-related gene expres- sion profiles during larval development in the pearl oyster, *Pinctada fucata*. BMC Genomics 16 : 325.

Liu, L., Alonso, V., Guo, L., Tourkova, I., Hendererson, S.E., Almarza, A.J., Friedman, P.A., Blair, H.C. (2012) Na^+/H^+ Exchanger Regulatory Factor 1 (NHERF1) Directly Regulates Osteogenesis. The Journal of Biological Chemistry 287: 43312-43321.

Louzao, M.C., Vieytes, M.R., Alfonso, A., Botana, L. M. (1993) Characterization of the Na^+/H^+ Antiporter in Cells of the Mussel *Mytilus galloprovincialis*. Comparative Biochemistry and Physiology a-Physiology 104: 101-104.

Mann, K., Edsinger-Gonzales, E., Mann, M. (2012) In-depth proteomic analysis of a mollusc shell: acid-soluble and acid-insoluble matrix of the limpet *Lottia gigantea*. Proteome Science 10: 28.

Marin, F., Luquet, G., Marie, B., Medakovic, D. (2008) Molluscan shell proteins: Primary structure, origin, and evolution. Current Topics in Developmental Biology 80: 209-276.

Miyamoto, H., Endo, H., Hashimoto, N., Limura, K., Isowa, Y., Kinoshita, S., Kotaki, T., Masaoka, T., Miki, T., Nakayama, S., Nogawa, C., Notazawa, A., Ohmori, F., Sarashina, I., Suzuki, M., Takagi, R., Takahashi, J., Takeuchi, T., Yokoo, N., Satoh, N., Toyohara, H., Miyashita, T., Wada, H., Samata, T., Endo, K., Nagasawa, H., Asakawa, S., Watabe, S. (2013) The diversity of shell matrix proteins: genome-wide investigation of the pearl oyster, *Pinctada fucata*. Zoological Science 30:801-816.

Murgarella, M., Puiu, D., Novoa, B., Figueras, A., Posada, D., Canchaya, C. (2016) A First Insight into the Genome of the Filter-Feeder Mussel *Mytilus galloprovincialis*. PLOS ONE 11: e0160081.

Rahmati, N., Kunzelmann, K., Xu, J., Barone S., Sirianant, L., De Zeeuw, C.I., Soleimani, M. (2013) Slc26a11 is prominently expressed in the brain and functions as a chloride channel: expression in Purkinje cells and stimulation of V H+-ATPase. European Journal of Physiology 465: 1583–1597.

Ramesh, K., Hu, M.Y., Thomsen, J., Bleich, M., Melzner, F. (2017) Mussel larvae modify calcifying fluid carbonate chemistry to promote calcification. Nature Communications. doi : 10.1038/s41467-017-01806-8.

Ramnanan, C.J., Storey, K.B (2006) Suppression of Na^+/K^+-ATPase activity during estivation in the land snail *Otala lactea*. Journal of Experimental Biology 209: 677-688.

Rapoport, R.M., Murad, F. (1983) Effect of ouabain and alterations in potassium concentration on relaxation induced by sodium nitroprusside. Blood Vessels 20: 255.

Roa, J.N., Munévar, C.L., Tresguerres, M. (2014) Feeding induces translocation of vacuolar proton ATPase and pendrin to the membrane of leopard shark (Triakis semifasciata) mitochondrion-rich gill cells. Comparative Biochemistry and Physiology, Part A 174: 29–37.

Robinson, M.D., McCarthy, D.J., Smyth, G.K. (2010) edgeR: a Bioconductor package for differential expression analysis of digital gene expression data". Bioinformat ics 26: 139–140.

Romero, M.F., Chen, A.P., Parker, M.D., Boron, W.F. (2013) The SLC4 family of bicarbonate (HCO_3^-) transporters. Molecular Aspects of Medicine 34: 159-182.

Ross, P.M., Parker, L., O'Connor, W.A., Bailey, E.A. (2011) The Impact of Ocean Acidification on Reproduction, Early Development and Settlement of Marine Organisms. Water 3: 1005-1030.

Roy, R.N. Roy, L.N., Vogel, K.M., Porter-Moore, C., Pearson, T., Good, C.E., Millero, F.J., Campbell, D.M. (1993) Determination of the ionization constants of carbonic acid in seawater. Marine Chemistry 44: 249-259.

Ruffenach, G., Chabot, S., Tanguay, V.F., Courboulin, A., Boucherat, O., Potus, F., Meloche, J., Pflieger, A., Breuils-Bonnet, S., Nadeau, V., Paradis, R., Tremblay, E., Girerd, B., Hautefort, A., Montani, D., Fadel, E., Dorfmuller, P., Humbert, M., Perros, F., Paulin, R., Provencher, S., Bonnet, S. (2016) Role for Runt-related Transcription Factor 2 in Proliferative and Calcified Vascular Lesions in Pulmonary Arterial Hypertension. American Journal of Respiratory and Critical Care Medicine 194:1273-1285.

Sacco, S., Giuliano, S., Sacconi, S., Desnuelle, C., Barhanin, J., Amri, E., Bendahhou, S. (2015) The inward rectifier potassium channel Kir2.1 is required for osteoblastogenesis. Human Molecular Genetics 24: 471–479.

Schmidt, K., Schinke, T., Haberland, M., Prieme, M., Schilling, A.F., Mueldner, C., Rueger, J.M., Sock, E., Wegner, M., Amling, M. (2005) The high mobility group transcription factor Sox8 is a negative regulator of osteoblast differentiation. The Journal of Cell Biology 168: 899–910.

Simkiss, K., Wilbur, K., (2012) Biomineralization. 1st Edition. Elsevier Acadamic Press.

Soleimani, M. (2013) SLC26 Cl^-/HCO_3^- exchangers in the kidney: roles in health and disease. Kidney International 84: 657-666.

Sosnoski, D.M., Gay, C.V. (2007) NCX3 is a major functional isoform of the sodium–calcium exchanger in osteoblasts. Journal of Cellular Biochemistry 103: 1101–1110.

Stuckas, H., Knobel, L., Schade, H., Breusing, C., Hinrichsen, H.-H., Bartel, M., Langguth, K. and Melzner, F.: Combining hydrodynamic modelling with genetics: Can passive larval drift shape the genetic structure of Baltic *Mytilus* populations? Molecular Ecology 26: 2765-2782, 2017.

Stuckas, H., Stoof, K., Quesada, H., Tiedemann, R. (2009) Evolutionary implications of discordant clines across the Baltic *Mytilus* hybrid zone (*Mytilus edulis* and *Mytilus trossulus*). Heredity (Edinb) 103: 146-156.

Stumpp, M., Dupont, S., Thorndyke, M.C., Melzner, F. (2011b) CO_2 induced seawater acidification impacts sea urchin larval development II: gene expression patterns in pluteus larvae. Comparative Biochemistry and Physiology Part A: Molecular & Integrative Physiology 160: 320-330.

Stumpp, M., Hu, M.Y., Melzner, F., Gutowska, M.A., Dorey, N., Himmerkus, N., Holtmann, W.C., Dupont, S.T., Thorndyke, M.C., Bleich, M. (2012) Acidified seawater impacts sea urchin larvae pH regulatory systems relevant for calcification. Proceedings of the National Academy of Sciences of the United States of America 109: 18192-18197.

Stumpp, M., Wren, J., Melzner, F., Thorndyke, M.C., Dupont, S. (2011a) CO_2 induced seawater acidification impacts sea urchin larval development I: elevated metabolic rates decrease scope for growth and induce developmental delay. Comparative Biochemistry and Physiology Part A: Molecular & Integrative Physiology 160: 331-340.

Suzuki, M., Saruwatari, K., Kogure, T., Yamamoto, Y., Nishimura, T., Kato, T., Nagasawa, H. (2009) An acidic matrix protein, Pif, is a key macromolecule for nacre formation. Science 325: 1388–90.

Takarada, T., Hinoi, E., Nakazato, R., Ochi, H., Xu, C., Tsuchikane, A., Takeda, S., Karsenty, G., Abe, T., Kiyonari, H., Yoneda, Y. (2013) An analysis of skeletal development in osteoblast-specific and chondrocyte-specific runt-related transcription factor-2 (Runx2) knockout mice. Journal of Bone and Mineral Research 28: 2060-2063.

Takeuchi, T., Kawashima, T., Koyanagi, R., Gyoja, F., Tanaka, M., Ikuta, T., Shoguchi, E., Fujiwara, M., Shinzato, C., Hisata, K., Fujie, M., Usami, T., Nagai, K., Maeyama, K., Okamoto, K., Aoki, H., Ishikawa, T., Masaoka, T., Fujiwara, A., Endo, K., Endo, H., Nagasawa, H., Kinoshita, S., Asakawa, S., Watabe, S., Satoh, N. (2012) Draft Genome of the Pearl Oyster *Pinctada fucata*: A Platform for Understanding Bivalve Biology. DNA Research 19: 117–130.

Tan, B., Mai, K. (2001) Zinc methionine and zinc sulfate as sources of dietary zinc for juvenile abalone, *Haliotis discus hannai* Ino. Aquaculture 192: 67-84.

Thomas, R.C. (1977) The role of bicarbonate, chloride and sodium ions in the regulation of intracellular pH in snail neurons. Journal of Physiology-London 273: 317-338.

Thomsen, J., Haynert, K., Wegner, K.M., Melzner, F. (2015) Impact of seawater carbonate chemistry on the calcification of marine bivalves. Biogeosciences 12: 4209-4220.

Tiaden, A.N., Breiden, M., Mirsaidi, A., Weber, F.A., Bahrenberg, G., Glanz. S., Cinelli, P., Ehrmann, M., Richards, P.J. (2012) Human serine protease HTRA1 positively regulates osteogenesis of human bone marrow-derived mesenchymal stem cells and mineralization of differentiating bone-forming cells through the modulation of extracellular matrix protein. Stem Cells 30: 2271–2282.

Timmins-Schiffman, E., O'Donnell, M., Friedman, C., Roberts, S. (2012) Elevated pCO_2 causes developmental delay in early larval Pacific oysters, *Crassostrea gigas*. Marine Biology 160: 1973–1982.

Tintut, Y., Patel, J., Parhami, F., Demer, L.L. (2000) Tumor necrosis factor-alpha promotes in vitro calcification of vascular cells via the cAMP pathway. Circulation 102: 2636-2642.

Tresguerres, M., Parks, S.C., Wood, C.N., Goss, G.G. (2007) V-H^+-ATPase translocation during blood alkalosis in dogfish gills: interaction with carbonic anhydrase and involvement in the postfeeding alkaline tide. American Journal of Physiology - Regulatory, Integrative and Comparative Physiology Published 292: R2012-R2019.

Truebano, M., Burns, G., Thorne, M.A.S., Hillyard, G., Peck, L.S., Skibinski, D.O.F., Clark, M.S. (2010) Transcriptional response to heat stress in the Antarctic bivalve *Laternula elliptica*. Journal of Experimental Marine Biology and Ecology 391: 65–72.

Vidavsky, N., Addadi, S., Schertel, A., Ben-Ezra, D., Shpigel, M., Addadi, L., Weiner, S. (2016) Calcium transport into the cells of the sea urchin larvae in relation to spicule formation. Proceedings of the National Academy of Sciences of the United States of America 113: 12637–12642.

Vidavsky, N., Masic, A., Schertel, A., Weiner, S., Addadi, L. (2015) Mineral-bearing vesicle transport in sea urchin embryos. Journal of Structural Biology 192: 358-365.

Waldbusser, G.G, Brunner, E.L., haley, B.A., hales, B., Langdon, C.J., Prahl, F.G. (2013) A developmental and energetic basis linking larval oyster shell formation to acidification sensitivity. Geophysical Research Letters 40: 2171-2176.

Weber, P.C. (2001) Potassium Recycling Pathways in the Human Cochlea. Laryngoscope 111:1156-65.

Whelan, S., Goldman, N. (2001) A general empirical model of protein evolution derived from multiple protein families using a maximum-likelihood approach. Molecular Biology and Evolution18: 691–699.

Yamaguchi M (1998) Role of zinc in bone formation and bone resorption. Journal of Trace Elements in Experimental Medicine 11: 119–135.

Yarra, T., Hüning, A., Schilhabel, M., Blaxter, M., Gharbi, K., Clark, M.S., Melzner, F. (2017, in prep) Insights into shell formation in the blue mussel, *Mytilus edulis*, through shell damage-repair and RNASeq.

Yasumasu, I., Mitsunaga, K., Fujino, Y. (1985) Mechanism for electrosilent Ca^{2+} transport to cause calcification of spicules in sea urchin embryos. Experimental Cell Research159: 80-90.

Zange, J., Grieshaber, M.K., Hans, A.W.H. (1990) The regulation of intracellular pH estimated by ^{31}P-NMR spectroscopy in the anterior byssus retractor muscle of *Mytilus edulis*. Journal of Experimental Biology 150: 95-109.

Zhang, C., Xie. L-, Huang, J., Chen, L., Zhang, R.A. (2006) A novel putative tyrosinase involved in periostracum formation from the pearl oyster (*Pinctada fucata*)". Biochemical and Biophysical Research Communications 342: 632–639.

Zhang, G., Fang, X., Guo, X., Li, L., Luo, R., Xu, F., Yang, P., Zhang, L., Wang, X., Qi, H., Xiong, Z., Que, H., Xie, Y., Holland, P.W.H., Paps, J., Zhu, Y., Wu, F., Chen, Y., Wang, J., Peng, C., Meng, J., Yang, L., Liu, J., Wen, B., Zhang, N., Huang, Z., Zhu, Q., Feng, Y., Mount, A., Hedgecock, D., Xu, Z., Liu, Y., Domazet-Lošo, T., Du, Y., Sun, X., Zhang, S., Liu, L., Cheng, P., Jiang, X., Li, J., Fan, D., Wang, W., Fu, W., Wang, T., Wang, B., Zhang, J., Peng, Z., Li, Y., Li, N., Wang, J., Chen, M, He, Y., Tan, F., Song, X., Zheng, Q., Huang, R., Yang, H., Du, X., Chen, L., Yang, M., Gaffney, P.M., Wang, S., Luo, L., She, Z., Ming, Y., Huang, W., Zhang, S., Huang, B., Zhang, Y., Qu, T., Ni, P., Miao, G., Wang, J., Wang, Q., Steinberg, C.E.W., Wang, H., Li, N., Qian, L., Zhang, G., Li, Y., Yang, H., Liu,

X., Wang, J., Yin, Y., Wang, J. (2012) The oyster genome reveals stress adaptation and complexity of shell formation. Nature 490: 49–54.

Zhao, G., Xu, M.J., Zhao, M.M., Dai, X.Y., Kong, W., Wilson, G.M., Guan, Y., Wang, C.Y., Wang, X. (2012) Activation of nuclear factor-kappa B accelerates vascular calcification by inhibiting ankylosis protein homolog expression. Kidney International 82: 34-44.

Figure 1 | The morphologically distinct larval developmental stages sampled during the experiments. (a-b) Pre-calcification (c-d) Larvae exhibit dorsal flattening at the region of the shell field, (e-f) First trace of mineralization is observed by the presence of a small (ca. 20 µm) shell and birefringence at the hinge area, (g-h) 49% of the larval shell is covered by a mineralized shell, (i-j) 76% of the larval shell is covered by a mineralized shell, (k-l) Larvae have secreted the PD I shell and exhibits a distinctive 'D' shape. Scale bars are 20 µm.

Figure 2 | Mean expression fold change of the 53 genes differentially expressed between control and low C_T libraries.

Figure 3 | Developmental expression profile from control libraries of the SLC26 candidate gene for HCO_3^- transport identified by the substrate limitation experiment.

Figure 4 | Genes encoding putative HCO_3^- transport proteins differentially expressed during the course of larval development in *M. edulis* reared under ambient conditions. Expression values (normalized read counts) by EBSeqHMM for (a) Anion transport proteins (b) A candidate Na^+ HCO_3^- cotransporter and (c) Bicarbonate transporting proteins. EE refers to equally expressed. Contigs differentially expressed during adult shell repair are marked with a star.

Figure 5 | Genes encoding Ca^{2+} transport proteins differentially expressed during the course of larval development in *M. edulis* reared under ambient conditions. Expression values (normalized read counts) by EBSeqHMM for (a) Primary active Ca^{2+} transport proteins: Ca^{2+} transporting ATPase (green), Plasma membrane Ca^{2+} transporting ATPase (orange), SERCA contigs (purple and pink) (b) Primary Ca^{2+} transport proteins: Na^+/Ca^{2+} exchanger contigs (orange, purple, pink).

Figure 6 | Genes encoding Na^+ , K^+ and Cl^- transport proteins differentially expressed during the course of larval development in *M. edulis* reared under ambient conditions. Expression values (normalized read counts) by EBSeqHMM for (a) Primary active NKA: α subunit (green), β subunit (orange) (b) NHE: Mitochondrial NHE's (green and orange), NHE regulatory cofactor (purple) (c) Secondary K^+ transport proteins: Inward rectifier K^+ channels (green and orange) (d) Cl^- transporting proteins: Ca^{2+} activated Cl^- channel (green), Cl^- channel (orange), intracellular Cl^- channel (purple).

Figure 7 | An ion transport model depicting the cellular transport processes of membrane bound ion transport proteins exhibiting elevated expression during *M. edulis* larval development. The Na^+/K^+ ATPase provides the electrochemical gradient for secondary ion transport via proteins such as the Na^+/H^+ exchanger, sodium bicarbonate cotransporters and Na^+/Ca^{2+} exchangers. The putative precipitation of calcium carbonate in an extracellular calcification space is described in grey.

Figure 8 | Phylogenetic tree depicting relationships between bicarbonate transporter families in *Homo sapiens* (human), *Stylophora pistillata* (Spi), *Crassostrea gigas* (Cgi), *Strongylocentrotus purpuratus* (Spu) and larval mussels (TRINITY). All sequences, along with accession IDs are provided in Supplementary file.

Figure 9 | Shell matrix proteins and domains identified in the shell proteomes, expressed in the mantle transcriptomes, differentially expressed between edge and central mantle sections, differentially expressed in the central mantle during shell repair, and differentially expressed during larval PD I formation. Adapted from Yarra et al (2017, in prep).

Figure 1

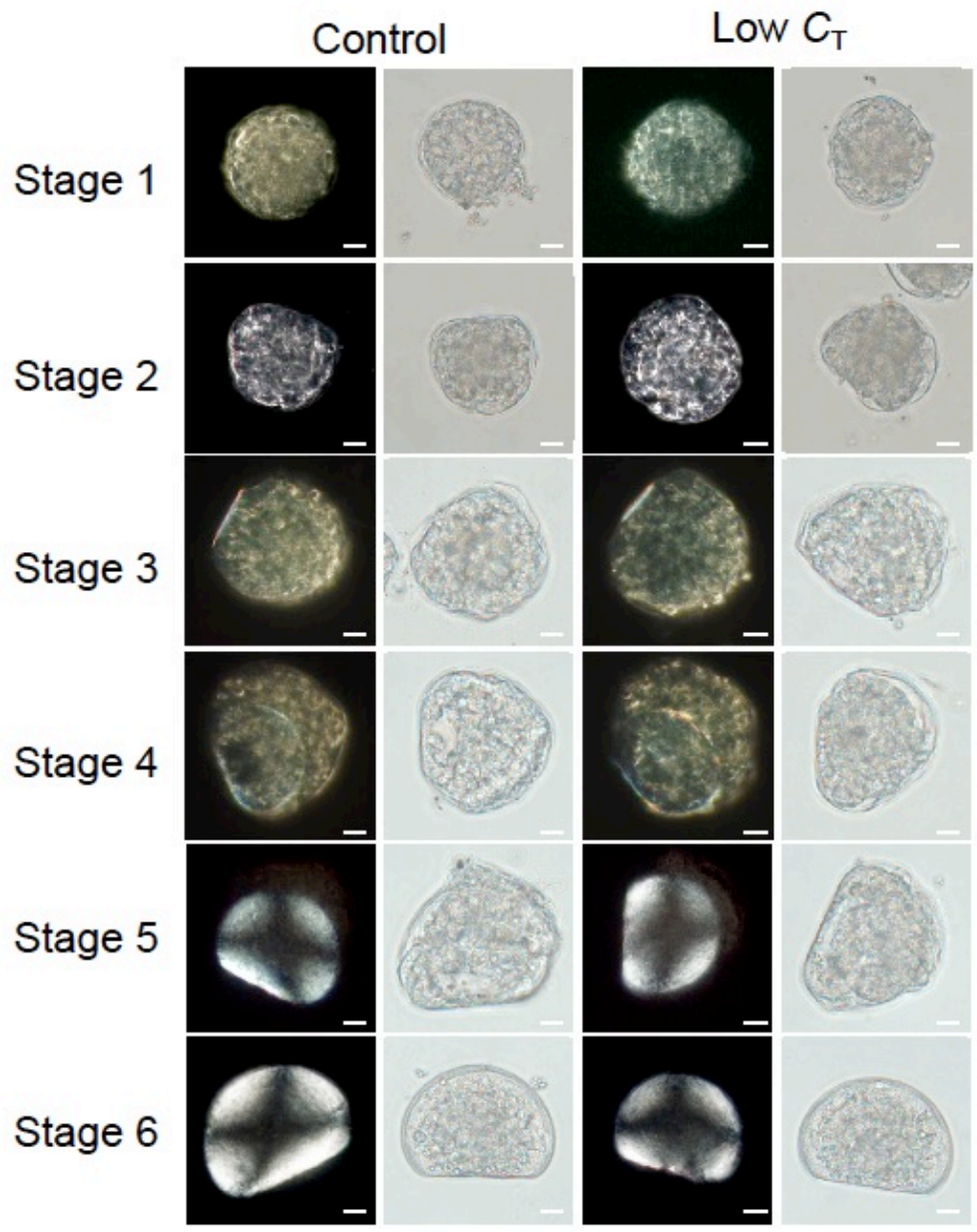

Figure 2

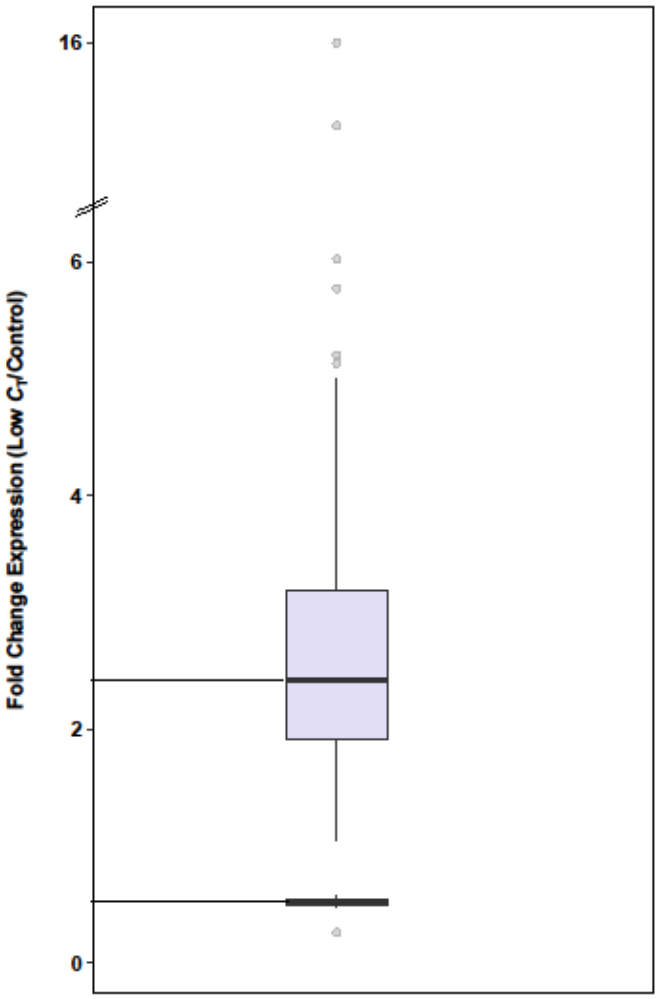

Figure 3

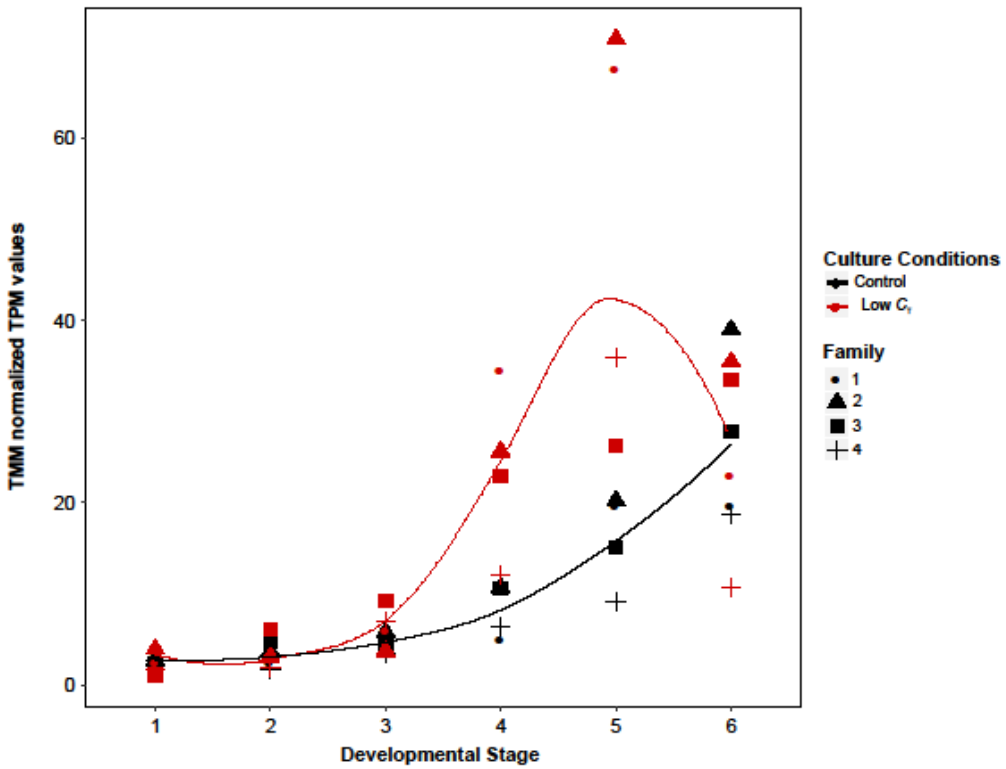
TMM normalized TPM values
0
20
40
60
1
2
3
4
5
6
Developmental Stage
Culture Conditions
Control
Low C_i
Family
1
2
3
4

Figure 4

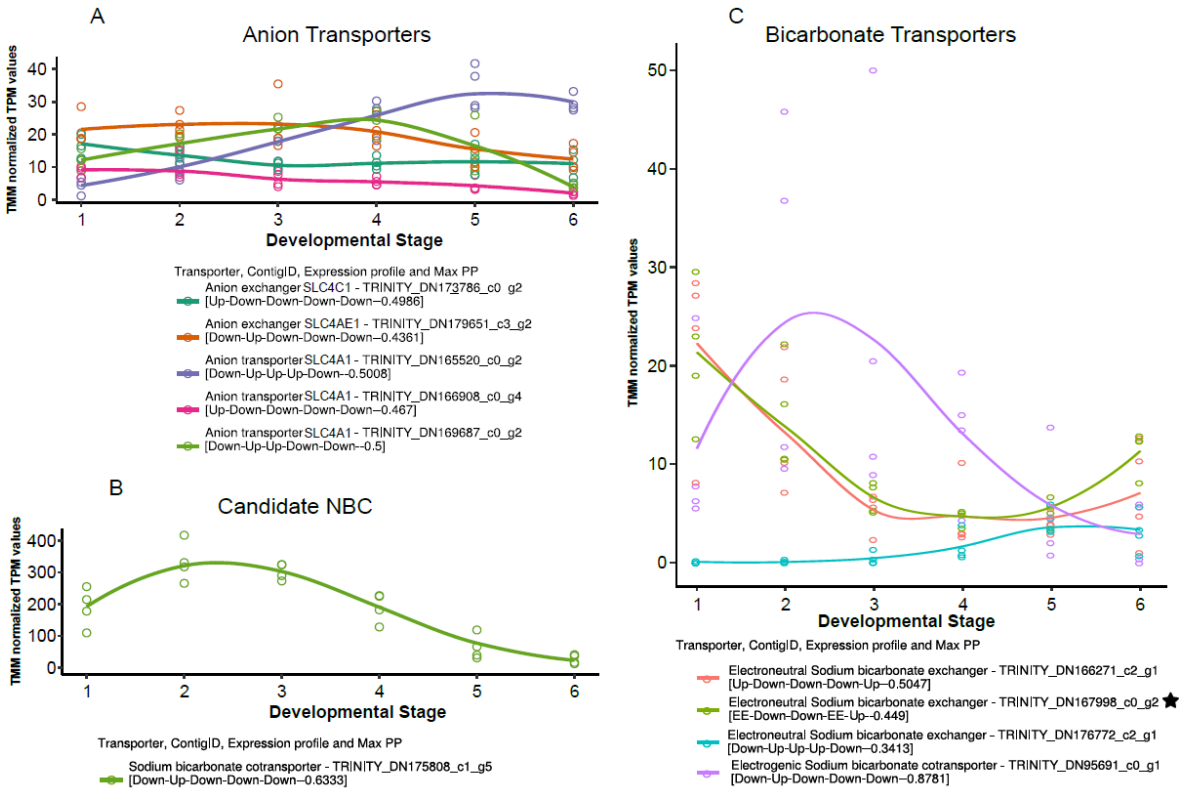
A
Anion Transporters
TMM normalized TPM values
Developmental Stage
Transporter, ContigID, Expression profile and Max PP
Anion exchanger SLC4C1 - TRINITY_DN173786_c0_g2 [Up-Down-Down-Down-Down--0.4986]
Anion exchanger SLC4AE1 - TRINITY_DN179651_c3_g2 [Down-Up-Down-Down-Down--0.4361]
Anion transporter SLC4A1 - TRINITY_DN165520_c0_g2 [Down-Up-Up-Up-Down--0.5008]
Anion transporter SLC4A1 - TRINITY_DN166908_c0_g4 [Up-Down-Down-Down-Down--0.467]
Anion transporter SLC4A1 - TRINITY_DN169687_c0_g2 [Down-Up-Up-Down-Down--0.5]
B
Candidate NBC
TMM normalized TPM values
Developmental Stage
Transporter, ContigID, Expression profile and Max PP
Sodium bicarbonate cotransporter - TRINITY_DN175808_c1_g5 [Down-Up-Down-Down-Down--0.6333]
C
Bicarbonate Transporters
TMM normalized TPM values
Developmental Stage
Transporter, ContigID, Expression profile and Max PP
Electroneutral Sodium bicarbonate exchanger - TRINITY_DN166271_c2_g1 [Up-Down-Down-Down-Up--0.5047]
Electroneutral Sodium bicarbonate exchanger - TRINITY_DN167998_c0_g2 [EE-Down-Down-EE-Up--0.449]
Electroneutral Sodium bicarbonate exchanger - TRINITY_DN176772_c2_g1 [Down-Up-Up-Up-Down--0.3413]
Electrogenic Sodium bicarbonate cotransporter - TRINITY_DN95691_c0_g1 [Down-Up-Down-Down-Down--0.8781]

Figure 5

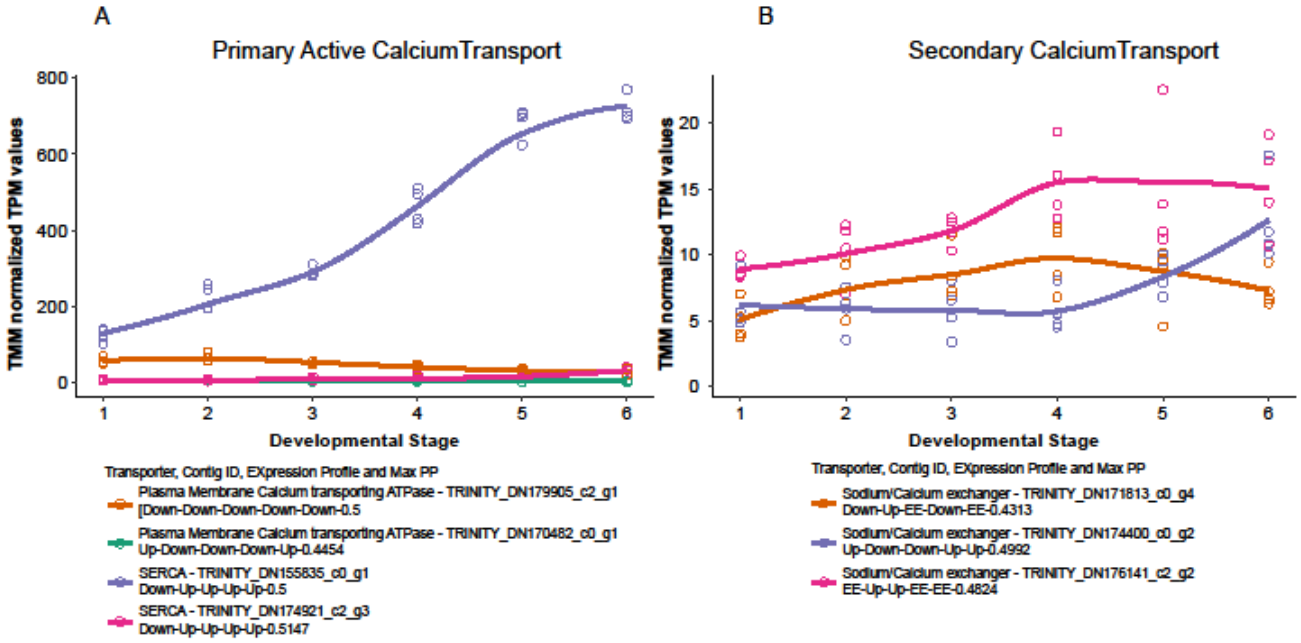
A
Primary Active CalciumTransport
TMM normalized TPM values
800
600
400
200
0
1
2
3
4
5
6
Developmental Stage
Transporter, Contig ID, EXpression Profile and Max PP
Plasma Membrane Calcium transporting ATPase - TRINITY_DN179905_c2_g1
[Down-Down-Down-Down-Down-0.5
Plasma Membrane Calcium transporting ATPase - TRINITY_DN170482_c0_g1
Up-Down-Down-Down-Up-0.4454
SERCA - TRINITY_DN155835_c0_g1
Down-Up-Up-Up-Up-0.5
SERCA - TRINITY_DN174921_c2_g3
Down-Up-Up-Up-Up-0.5147
B
Secondary CalciumTransport
TMM normalized TPM values
20
15
10
5
0
1
2
3
4
5
6
Developmental Stage
Transporter, Contig ID, EXpression Profile and Max PP
Sodium/Calcium exchanger - TRINITY_DN171813_c0_g4
Down-Up-EE-Down-EE-0.4313
Sodium/Calcium exchanger - TRINITY_DN174400_c0_g2
Up-Down-Down-Up-Up-0.4992
Sodium/Calcium exchanger - TRINITY_DN176141_c2_g2
EE-Up-Up-EE-EE-0.4824

Figure 6

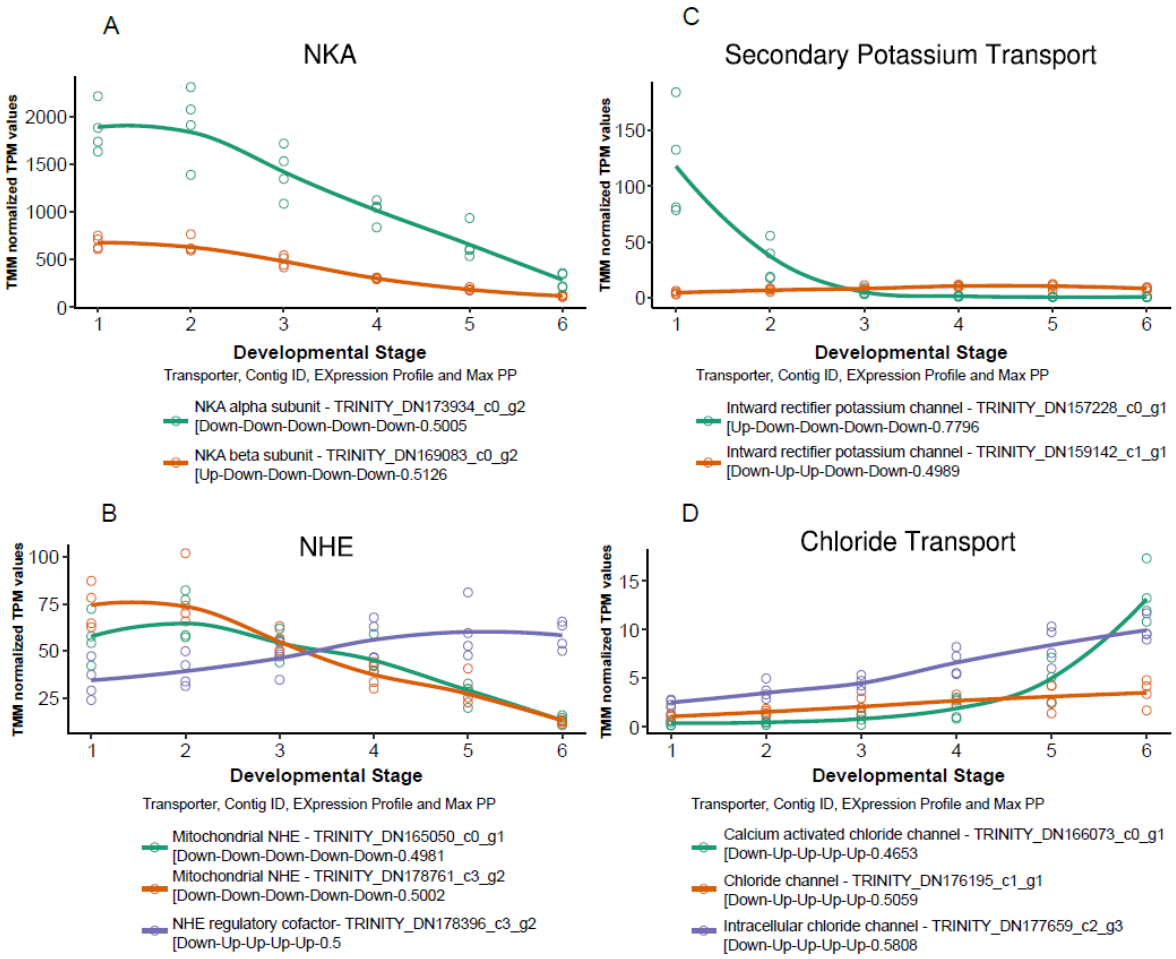
A
NKA
TMM normalized TPM values
Developmental Stage
Transporter, Contig ID, EXpression Profile and Max PP
NKA alpha subunit - TRINITY_DN173934_c0_g2 [Down-Down-Down-Down-Down-0.5005
NKA beta subunit - TRINITY_DN169083_c0_g2 [Up-Down-Down-Down-Down-0.5126
C
Secondary Potassium Transport
TMM normalized TPM values
Developmental Stage
Transporter, Contig ID, EXpression Profile and Max PP
Intward rectifier potassium channel - TRINITY_DN157228_c0_g1 [Up-Down-Down-Down-Down-0.7796
Intward rectifier potassium channel - TRINITY_DN159142_c1_g1 [Down-Up-Up-Down-Down-0.4989
B
NHE
TMM normalized TPM values
Developmental Stage
Transporter, Contig ID, EXpression Profile and Max PP
Mitochondrial NHE - TRINITY_DN165050_c0_g1 [Down-Down-Down-Down-Down-0.4981
Mitochondrial NHE - TRINITY_DN178761_c3_g2 [Down-Down-Down-Down-Down-0.5002
NHE regulatory cofactor- TRINITY_DN178396_c3_g2 [Down-Up-Up-Up-Up-0.5
D
Chloride Transport
TMM normalized TPM values
Developmental Stage
Transporter, Contig ID, EXpression Profile and Max PP
Calcium activated chloride channel - TRINITY_DN166073_c0_g1 [Down-Up-Up-Up-Up-0.4653
Chloride channel - TRINITY_DN176195_c1_g1 [Down-Up-Up-Up-Up-0.5059
Intracellular chloride channel - TRINITY_DN177659_c2_g3 [Down-Up-Up-Up-Up-0.5808

Figure 7

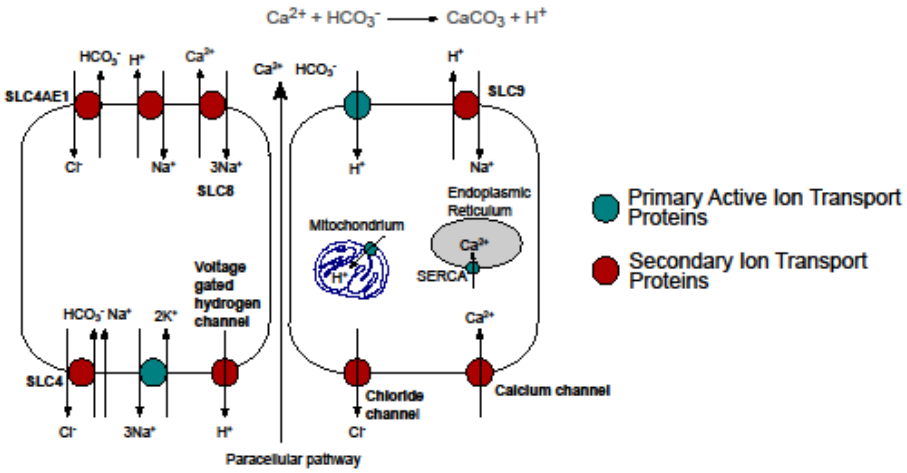
$Ca^{2+} + HCO_3^- \longrightarrow CaCO_3 + H^+$
SLC4AE1
SLC8
SLC9
SLC4
Voltage gated hydrogen channel
Mitochondrium
Endoplasmic Reticulum
SERCA
Chloride channel
Calcium channel
Paracellular pathway
Primary Active Ion Transport Proteins
Secondary Ion Transport Proteins

Figure 8

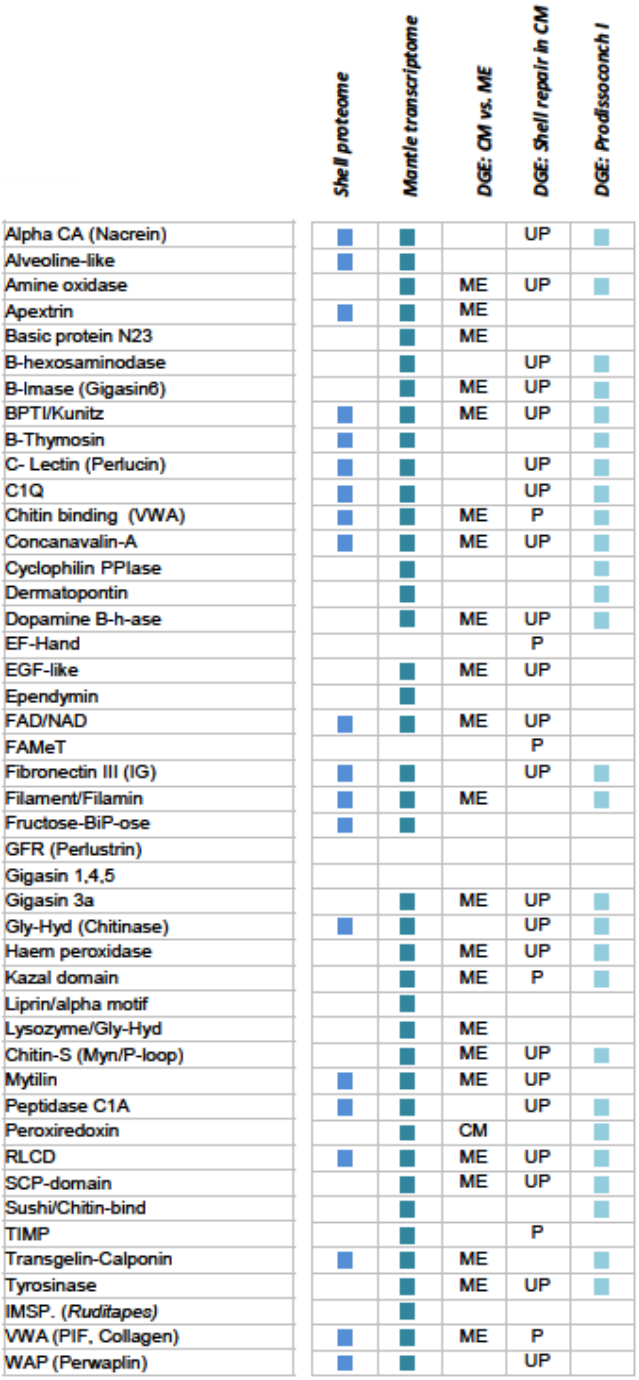

	Shell proteome	Mantle transcriptome	DGE: CM vs. ME	DGE: Shell repair in CM	DGE: Prodissoconch I
Alpha CA (Nacrein)	■	■		UP	■
Alveoline-like	■	■			
Amine oxidase		■	ME	UP	■
Apextrin	■	■	ME		
Basic protein N23		■	ME		
B-hexosaminodase		■		UP	■
B-Imase (Gigasin6)		■	ME	UP	■
BPTI/Kunitz	■	■	ME	UP	■
B-Thymosin	■	■			■
C- Lectin (Perlucin)	■	■		UP	■
C1Q	■	■		UP	■
Chitin binding (VWA)	■	■	ME	P	■
Concanavalin-A	■	■	ME	UP	■
Cyclophilin PPIase		■			■
Dermatopontin		■			■
Dopamine B-h-ase		■	ME	UP	■
EF-Hand				P	
EGF-like		■	ME	UP	
Ependymin		■			
FAD/NAD	■	■	ME	UP	
FAMeT				P	
Fibronectin III (IG)	■	■		UP	■
Filament/Filamin	■	■	ME		■
Fructose-BiP-ose	■	■			
GFR (Perlustrin)					
Gigasin 1,4,5					
Gigasin 3a		■	ME	UP	■
Gly-Hyd (Chitinase)	■	■		UP	■
Haem peroxidase		■	ME	UP	■
Kazal domain		■	ME	P	■
Liprin/alpha motif		■			
Lysozyme/Gly-Hyd		■	ME		
Chitin-S (Myn/P-loop)		■	ME	UP	■
Mytilin	■	■	ME	UP	
Peptidase C1A	■	■		UP	■
Peroxiredoxin		■	CM		■
RLCD	■	■	ME	UP	■
SCP-domain		■	ME	UP	■
Sushi/Chitin-bind		■			■
TIMP		■		P	
Transgelin-Calponin	■	■	ME		■
Tyrosinase		■	ME	UP	■
IMSP. (*Ruditapes*)		■			
VWA (PIF, Collagen)	■	■	ME	P	
WAP (Perwaplin)	■	■		UP	

Figure 9

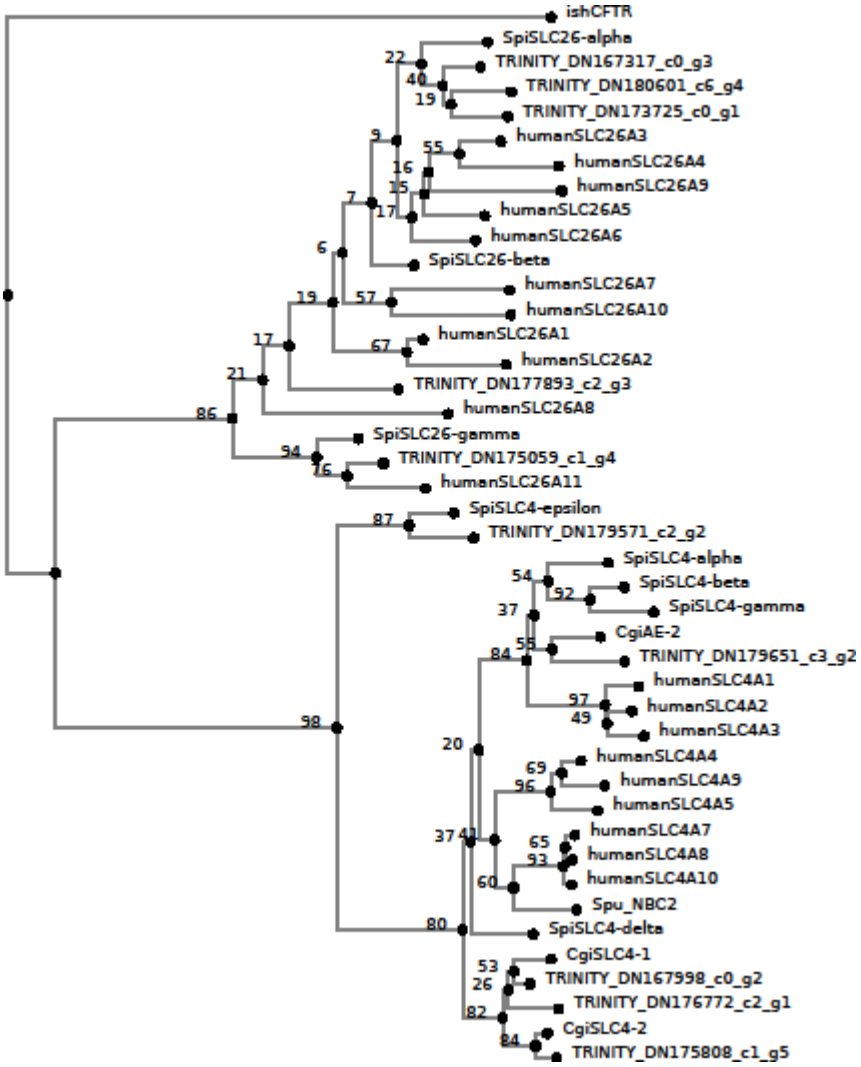
ishCFTR
SpiSLC26-alpha
TRINITY_DN167317_c0_g3
TRINITY_DN180601_c6_g4
TRINITY_DN173725_c0_g1
humanSLC26A3
humanSLC26A4
humanSLC26A9
humanSLC26A5
humanSLC26A6
SpiSLC26-beta
humanSLC26A7
humanSLC26A10
humanSLC26A1
humanSLC26A2
TRINITY_DN177893_c2_g3
humanSLC26A8
SpiSLC26-gamma
TRINITY_DN175059_c1_g4
humanSLC26A11
SpiSLC4-epsilon
TRINITY_DN179571_c2_g2
SpiSLC4-alpha
SpiSLC4-beta
SpiSLC4-gamma
CgiAE-2
TRINITY_DN179651_c3_g2
humanSLC4A1
humanSLC4A2
humanSLC4A3
humanSLC4A4
humanSLC4A9
humanSLC4A5
humanSLC4A7
humanSLC4A8
humanSLC4A10
Spu_NBC2
SpiSLC4-delta
CgiSLC4-1
TRINITY_DN167998_c0_g2
TRINITY_DN176772_c2_g1
CgiSLC4-2
TRINITY_DN175808_c1_g5

Table 1. Morphological stages at which Baltic *M. edulis*-like larvae were sampled during the experiment. Changes in shell cover are quantified from N = 20 larvae and are reported as mean ± SD.

Stage	Description	Hours post Fertilisation				
			Reared under low C_T conditions			
		Control Families	F001	F002	F003	F004
Early trochophore	Pre-calcification	20	20	20	20	20
Trochophore	Larvae exhibit dorsal flattening at the region of the shell field.	22	22	22	22	22
Trochophore	First trace of mineralization is observed by the presence of a small (ca. 20 μm) shell and birefringence at the hinge area	24	25	25	24	25
Trochophore	49 ± 7.7% of the larval shell is covered by a mineralized shell.	27	29	29	28	28
Late trochophore	76.9 ± 7.9% of the larval shell is covered by a mineralized shell.	30	33	32	31	31
D-veliger	Larvae have secreted the PD I shell and exhibits a distinctive 'D' shape.	35	41	35	36	36

Table 2. Number of differentially expressed contigs in treatment libraries compared to control libraries, at each stage.

Stage	Up-regulated	Sequence similarity to transmembrane transporters of interest	Down-regulated
1	0		0
2	0		0
3	16		0
4	13	Sodium-independent sulfate anion transporter	1
5	22	Sodium-independent sulfate anion transporter	1
6	21		5

Table 3. Top ten expression profiles and number of contigs within each expression profile. Only contig expression profiles with at least 0.001 FDR and posterior probability of at least 50% are summarized.

Control libraries			Treated libraries		
Expression profile	Num. Contigs	Num. SMP	**Expression profile**	Num. Contigs	Num. SMP
Down-Up-Up-Up-Up	1249	30	Down-Up-Up-Up-Up	1242	33
Up-Down-Down-Down-Down	837	4	Up-Down-Down-Down-Down	867	3
Up-Down-Down-Down-Up	492	0	Down-Down-Down-Down-Down	447	2
Down-Down-Down-Down-Down	470	3	Down-Up-Down-Down-Down	393	1
Down-Up-Down-Down-Down	357	1	Down-Up-Down-Down-Up	354	0
Down-Up-Up-Up-Down	333	5	Down-Up-Down-Up-Up	294	1
Down-Up-Up-Down-Down	137	2	Down-Up-Up-Up-Down	291	7
Up-Down-Down-Up-Up	105	0	Up-Down-Down-Down-Up	205	1
Down-Up-Down-Down-Up	99	0	Up-Down-Up-Down-Down	191	0
Up-Down-Up-Up-Up	92	0	Up-Down-Up-Up-Down	173	1

Table 4. Enrichment of GO terms in the top two expression profiles. Top ten Molecular Function (MF) terms with at least 0.05 FDR. Only contig expression profiles with at least 0.001 FDR and posterior probability of at least 50% were used for GOSeq analysis.

Control libraries	Treated libraries
Profile 1: "Down-Up-Up-Up-Up"	
calcium ion binding	calcium ion binding
transporter activity	hydrolase activity (O-glycosyl compounds)
chitin binding	transporter activity
catalytic activity	oxidoreductase activity
oxidoreductase activity	chitin binding
hydrolase activity (O-glycosyl compounds)	carbohydrate binding
heme binding	catalytic activity
ion channel activity	heme binding
polysaccharide binding	beta-N-acetylhexosaminidase activity
transmembrane transporter activity	polysaccharide binding
Profile 2: "Up-Down-Down-Down-Down"	
None	nucleic acid binding
	microtubule binding
	ATP binding

Supplementary Table S1. Seawater carbonate chemistry parameters of the experiments. Parameters of CO_2, HCO_3^- and CO_3^{2-} are calculated from measured C_T and pH_{NBS} using CO2SYS.

Experiment	Treatment	Salinity	Temperature (°C)	pH_{NBS}	C_T (µmol kg^{-1} seawater)	CO_2 (µmol/kg^{-1} seawater)	[HCO_3^-] (µmol kg^{-1} seawater)	[CO_3^{2-}] (µmol kg^{-1} seawater)	pCO_2 (uatm)	$\Omega_{aragonite}$
1	Control	15.3	17	8.211	1959.08	17.01	1837.62	104.44	433.81	1.67
1	C_T limited	15.3	17	8.12	879.83	9.49	831.98	38.34	242.19	0.61
2	Control	15.1	17	8.225	1942.27	16.37	1819.92	105.977	417.11	1.70
2	C_T limited	15.1	17	8.161	919.13	9.03	866.55	43.54	230.14	0.69
3	Control	16.1	17	8.217	1957.62	16.47	1832.14	108.99	422.09	1.74
3	C_T limited	16.1	17	8.104	987.03	10.88	933.33	42.80	278.92	0.68
4	Control	15.6	17	8.231	2003.24	16.47	1873.89	112.87	420.78	1.811
4	C_T limited	15.6	17	8.19	980.86	8.90	921.45	50.50	227.39	0.81

Supplementary Table S2. Annotations of differentially expressed contigs in treatment libraries compared to control libraries.

Contig ID	Annotation	Accession ID	Developmental Stage	Expression Profile	Fold Change
TRINITY_DN162334_c0_g3			3, 4, 5	Up, Up, Up	5.77, 4.95, 3.16
TRINITY_DN164559_c3_g2	TNFAIP3 interacting protein 2 (*Homo sapiens*)	TNIP2_HUMAN	3, 4, 5, 6	Up, Up, Up, Up	2.62, 2.53, 2.41, 2.02
TRINITY_DN161315_c0_g1	Cdc42 homolog (*Drosophila melanogaster*)	CDC42_DROME	3, 4	Up, Up	3.18, 2.42
TRINITY_DN175794_c1_g2	Interleukin 1 receptor associated kinase 4 (*Homo sapiens*)	IRAK4_HUMAN	3, 5	Up, Up	2.09, 1.75
TRINITY_DN157412_c0_g1	NF kappa B inhibitor α (*Gallus gallus*)	IKBA_CHICK	3, 4, 5, 6	Up, Up, Up, Up	1.91, 1.82, 1.86, 1,74
TRINITY_DN176188_c0_g5	Nuclear transcription factor Y subunit γ (*Pongo abelii*)	NFYC_PONAB	3, 4, 5	Up, Up, Up	2.15, 2.21, 2.18
TRINITY_DN164091_c3_g1	Excitatory amino acid transporter 3 (*Mus musculus*)	EAA3_MOUSE	3, 4	Up, Up	2.47, 2.65
TRINITY_DN154143_c0_g2	Putative uncharacterized transposon derived protein F54H12.3 (*Caenorhabditis elegans*)	YMD3_CAEEL	3	Up	2.98
TRINITY_DN164725_c0_g5			3, 4, 5, 6	Up, Up, Up, Up	2.32, 2.26, 2.47, 2.11

TRINITY_DN154643_c1_g1	Uncharacterized protein (*Crassostrea gigas*)	K1RHH1_CRAGI	3	Up	3.55
TRINITY_DN156025_c1_g3	Runt related transcription factor 1 (*Homo sapiens*)	RUNX1_HUMAN	3, 5	Up, Up	2.02, 1.91
TRINITY_DN175161_c0_g6			3, 5	Up, Up	5.13, 4
TRINITY_DN138179_c1_g3			3	Up	4.46
TRINITY_DN152071_c1_g3	Uncharacterized_protein (*Tetranychus urticae*)	A0A158P512_TETUR	3	Up	2.8
TRINITY_DN25158_c0_g1			3	Up	2.08
TRINITY_DN149718_c0_g9			3	Up	6.02
TRINITY_DN160667_c0_g2	Failed axon connections homolog (*Homo sapiens*)	FAXC_HUMAN	4	Down	0.52
TRINITY_DN175059_c1_g4	Sodium-independent sulfate anion transporter (*Mus musculus*)	S2611_MOUSE	4, 5	Up, Up	2.32, 2.96
TRINITY_DN169005_c1_g4	ETS related transcription factor Elf 3 (*Crassostrea gigas*)	K1QAA0_CRAGI	4, 5, 6	Up, Up, Up	1.82, 2.14, 2.05
TRINITY_DN170535_c0_g2			4, 5	Up, Up	3.16, 2.94
TRINITY_DN168878_c0_g1	α-glucosidase yihQ (*Crassostrea gigas*)	K1QZH8_CRAGI	4	Up	1.9
TRINITY_DN153040_c0_g1	Uncharacterized_prote	V3Z9W2_LOTGI	4	Up	1.55

	in (*Lottia gigantea*)				
TRINITY_DN143945_c0_g1			4	Up	2.46
TRINITY_DN158062_c0_g1	Transcription factor Sox 8 (*Xenopus laevis*)	SOX8_XENLA	5, 6	Up, Up	2.78, 3.41
TRINITY_DN165794_c0_g8	Adipocyte plasma membrane associated protein (*Bos taurus*)	APMAP_BOVIN	5, 6	Down, Down	0.5, 0.48
TRINITY_DN85247_c0_g1			5, 6	Up, Up	3.24, 3.41
TRINITY_DN177115_c1_g1	Tumor necrosis factor alpha induced protein 3 (*Mus musculus*)	TNAP3_MOUSE	5	Up	1.9
TRINITY_DN178440_c1_g3	Nuclear factor NF kappa B p105 subunit (*Rattus norvegicus*)	NFKB1_RAT	5	Up	1.54
TRINITY_DN164963_c0_g1			5	Up	1.6
TRINITY_DN153976_c2_g1	Nose resistant t fluoxetine protein 6 (*Caenorhabditis elegans*)	NRF6_CAEE	5	Up	1.59
TRINITY_DN176455_c1_g2			5	Up	2.23
TRINITY_DN158676_c0_g1	Ras related C3 botulinum toxin substrate 1 (*Rattus norvegicus*)	RAC1_RAT	5	Up	2.36
TRINITY_DN	Endoglucan	GUN4_T	5	Up	1.61

162758_c0_g2	ase E 4 (*Thermobifida fusca*)	HEFU			
TRINITY_DN160914_c0_g1	Putative Ankyrin repeat protein MM 0045 (*Methanosarcina mazei*)	Y045_METMA	5, 6	Up, Up	2.77, 3.31
TRINITY_DN178074_c2_g4	Zinc transporter ZIP13 (*Danio rerio*)	S39AD_DANRE	5	Up	2.41
TRINITY_DN166023_c2_g1	Uncharacterized protein (*Arion vulgaris*)	A0A0B6ZCF8_9EUPU	6	Up	3.7
TRINITY_DN160914_c0_g2			6	Up	3.2
TRINITY_DN160789_c2_g2			6	Up	1.74
TRINITY_DN144435_c0_g1	Putative C-type lectin (*Haliotis discus hannai*)	A0A0D3MJB9_HALDH	6	Up	16.11
TRINITY_DN159064_c3_g3			6	Up	7.16
TRINITY_DN180876_c0_g1	Retrovirus related Pol polyprotein from transposon 297 (*Drosophila melanogaster*)	POL2_DROME	6	Down	0.57
TRINITY_DN168079_c0_g2	Serine protease inhibitor dipetalogastin (*Crassostrea gigas*)	K1PRF2_CRAG	6	Down	0.26
TRINITY_DN83729_c0_g1	Mammalian	EPDR1_HUMAN	6	Up	2.6

	ependymin related protein 1 (*Homo sapiens*)				
TRINITY_DN169769_c2_g1	Heme-binding protein 2 (*Homo sapiens*)	HEBP2_HUMAN	6	Up	2.62
TRINITY_DN147142_c0_g1	DBH like monooxygenase protein 1 homolog (*Danio rerio*)	MOXD1_DANRE	6	Up	5.2
TRINITY_DN173237_c0_g2	Retinal dehydrogenase 2 (RALDH)(*Mus musculus*)	AL1A2_MOUSE	6	Up	1.69
TRINITY_DN137986_c0_g1	Expansin yoaJ (*Crassostrea gigas*)	K1QR45_CRAGI	6	Up	4.59
TRINITY_DN183378_c0_g1	Uncharacterized protein (*Lottia gigantea*)	V4BE89_LOTGI	6	Up	1.82
TRINITY_DN148276_c0_g1			6	Up	3.7
TRINITY_DN176745_c2_g2	DEP domain containing protein 1A (*Danio rerio*)	DEP1A_DANRE	6	Down	0.52
TRINITY_DN157627_c0_g2			6	Up	3.63
TRINITY_DN180865_c8_g1	Uncharacterized protein (*Crassostrea gigas*)	K1PTU7_CRAGI	6	Down	0.57
TRINITY_DN176739_c2_g1	Malate dehydrogenase (*Pyrococcu*	MDH_PYRAB	6	Up	1.84

s abyssi)

Supplementary Table S3. Number of differentially expressed contigs between developmental stages in both control and treated libraries.

	Control Group		**Treatment Group**	
	Number of contigs	Number of SMP contigs	Number of contigs	Number of SMP contigs
Stage 1 as baseline:				
Stage 2 vs. Stage 1	228 -17	228 -17	369 -70	228 -17
Stage 3 vs. Stage 1	1,104 -590	1,104 -590	1,763 -1,047	1,104 -590
Stage 4 vs. Stage 1	2,588 -1,830	2,588 -1,830	2,775 -2,282	2,588 -1,830
Stage 5 vs. Stage 1	3,677 -3,269	3,677 -3,269	3,723 -3,535	3,677 -3,269
Stage 6 vs. Stage 1	4,838 -4,423	4,838 -4,423	5,868 -5,544	4,838 -4,423
Consecutive stages				
Stage 2 vs. Stage 1	228 -17	228 -17	369 -70	19 -1
Stage 3 vs. Stage 2	87 -60	87 -60	283 -135	9 -2
Stage 4 vs. Stage 3	246 -85	246 -85	168 -173	4 -3
Stage 5 vs. Stage 4	174 -120	174 -120	50 -43	1 -1
Stage 6 vs. Stage 5	395 -589	395 -589	1,417 -1,278	25 -19

Supplementary Table S4. Annotations of differentially expressed contigs in larvae at Stage 2 (onset of calcification) compared to Stage 1 (pre-calcification).

Contig ID	Annotation	Accession ID
TRINITY_DN119635_c0_g1		
TRINITY_DN156475_c0_g1	Forkhead box protein L2 (*Crassostrea gigas*)	K1RVN0_CRAGI
TRINITY_DN135592_c0_g1		
TRINITY_DN135592_c0_g2		
TRINITY_DN30478_c0_g1		
TRINITY_DN162074_c1_g3	GTP-binding protein GEM (*Homo sapiens*)	GEM_HUMAN
TRINITY_DN146390_c1_g2		
TRINITY_DN93876_c0_g2		
TRINITY_DN48980_c0_g1	Uncharacterized protein (*Crassostrea gigas*)	K1QY92_CRAGI
TRINITY_DN157509_c0_g5	Zinc transporter ZIP1 (*Bos taurus*)	S39A1_BOVIN
TRINITY_DN160567_c0_g2		
TRINITY_DN146390_c0_g1		
TRINITY_DN99979_c0_g1		
TRINITY_DN17787_c0_g1		
TRINITY_DN143936_c0_g1		
TRINITY_DN160539_c4_g9		
TRINITY_DN161972_c1_g1		
TRINITY_DN153405_c3_g4		
TRINITY_DN117209_c0_g1		
TRINITY_DN167796_c1_g1		
TRINITY_DN51677_c0_g1		
TRINITY_DN218341_c0_g1		
TRINITY_DN57015_c0_g1		
TRINITY_DN106379_c0_g1	Uncharacterized protein (*Crassostrea gigas*)	K1S2E8_CRAG
TRINITY_DN128743_c0_g1		
TRINITY_DN149108_c0_g1		
TRINITY_DN163813_c0_g1	Parathyroid hormone/Parathyroid hormone related peptide receptor (*Didelphis virginiana*)	PTH1R_DIDVI
TRINITY_DN185973_c0_g1		
TRINITY_DN169595_c0_g2	Protein unc 93 homolog A (*Xenopus laevis*)	UN93A_XENLA
TRINITY_DN160411_c0_g2	Lactase phlorizin hydrolase (*Homo sapiens*)	LPH_HUMAN
TRINITY_DN64699_c0_g2		
TRINITY_DN169461_c0_g2	Major egg antigen (*Schistosoma mansoni*)	P40_SCHMA
TRINITY_DN17787_c0_g2		
TRINITY_DN43222_c0_g1	Ferric chelate reductase 1 (*Bathymodiolus platifrons*)	A0A100XKJ2_9BIVA
TRINITY_DN133286_c0_g1		
TRINITY_DN161508_c0_g1	EF hand domain containing protein D1 (*Crassostrea gigas*)	K1QRD1_CRAGI
TRINITY_DN144535_c0_g1		
TRINITY_DN172433_c0_g1	KS-rich protein (*Mytilus coruscus*)	A0A0K0YB04_MYTCO
TRINITY_DN157573_c0_g1		
TRINITY_DN134345_c0_g1		
TRINITY_DN145763_c0_g1	Meprin A subunit α (*Homo sapiens*)	MEP1A_HUMAN
TRINITY_DN170726_c0_g4		
TRINITY_DN145450_c0_g1	Metalloendopeptidase (*Crassostrea gigas*)	K1S6S4_CRAGI

TRINITY_DN168864_c0_g1	Uncharacterized protein (*Capitella teleta*)	R7UWJ8_CAPTE
TRINITY_DN162493_c0_g3	Uncharacterized protein (*Crassostrea_gigas*)	K1QCE7_CRAGI
TRINITY_DN170889_c0_g5		
TRINITY_DN53458_c0_g1	Phosphatidylethanolamine-binding protein homolog F40A3.3 (*Caenorhabditis elegans*)	PEBPH_CAEEL
TRINITY_DN132755_c0_g1	Uncharacterized protein (*Lottia gigantea*)	V4BE89_LOTGI
TRINITY_DN209435_c0_g1		
TRINITY_DN36379_c0_g1		
TRINITY_DN154992_c0_g1	Uncharacterized protein (*Lottia gigantea*)	V4BE89_LOTGI
TRINITY_DN177384_c6_g1	Delta-like protein 1 (*Rattus norvegicus*)	DLL1_RAT
TRINITY_DN165965_c0_g1		
TRINITY_DN162613_c0_g4		
TRINITY_DN171494_c0_g2		
TRINITY_DN153661_c0_g1	Uncharacterized protein (*Lottia gigantea*)	V4AXA0_LOTGI
TRINITY_DN181007_c7_g4		
TRINITY_DN181264_c6_g1	Uncharacterized protein (*Arion vulgaris*)	A0A0B7ARG1_9EUPU
TRINITY_DN174156_c1_g2	Carbonic anhydrase 12 (*Mus musculus*)	CAH12_MOUSE
TRINITY_DN126771_c0_g1	Uncharacterized protein (*Crassostrea gigas*)	K1QCL4_CRAGI
TRINITY_DN154918_c0_g1		
TRINITY_DN171240_c0_g1	Protein glutamine gamma glutamyltransferase K (TG) (*Canis lupus familiaris*)	TGM1_CANLF
TRINITY_DN161552_c1_g5	Follistatin A (*Danio rerio*)	FSTA_DANRE
TRINITY_DN181242_c1_g3		
TRINITY_DN164779_c2_g2	RS-rich protein 1(*Mytilus coruscus*)	A0A0K0YAY1_MYTCO
TRINITY_DN136857_c0_g1	Stress induced protein 1(*Caenorhabditis elegans*)	SIP1_CAEEL
TRINITY_DN165794_c0_g5		
TRINITY_DN147120_c0_g4		
TRINITY_DN136535_c0_g1	Uncharacterized protein (*Lottia gigantea*)	V4BE89_LOTGI
TRINITY_DN173208_c0_g1		
TRINITY_DN174212_c0_g2	Filamin A (*Crassostrea gigas*)	K1RZ99_CRAGI
TRINITY_DN172256_c0_g2		
TRINITY_DN168269_c1_g4		
TRINITY_DN39776_c1_g1	Tubulin β chain (*Lytechinus pictus*)	TBB_LYTPI
TRINITY_DN178147_c0_g1	Sushi von Willebrand factor type A EGF and pentraxin domain containing protein 1 (*Rattus norvegicus*)	SVEP1_RAT
TRINITY_DN163507_c2_g5	Cathepsin Z (*Crassostrea gigas*)	K1P5K4_CRAGI
TRINITY_DN55733_c0_g1		
TRINITY_DN180672_c0_g6		
TRINITY_DN160057_c0_g2	3-oxoacyl reductase FabG (*Thermotoga maritima*)	FABG_THEMA
TRINITY_DN130432_c0_g1		
TRINITY_DN172326_c0_g3	P3 protein (*Mus musculus*)	P3_MOUSE
TRINITY_DN168269_c1_g5		
TRINITY_DN119839_c0_g1	Transforming growth factor β induced protein ig-H3 (*Crassostrea gigas*)	K1PXW8_CRAGI
TRINITY_DN166617_c0_g1		
TRINITY_DN180979_c1_g2		
TRINITY_DN169712_c1_g3	Transgelin like protein 6 (*Mytilus galloprovincialis*)	A0A0K0YB42_MYTGA

TRINITY_DN178271_c1_g1	Calbindin 32 (*Drosophila melanogaster*)	CAB32_DROME
TRINITY_DN163693_c0_g3		
TRINITY_DN124911_c0_g1		
TRINITY_DN177904_c5_g1	Proline serine threonine phosphatase interacting protein 1 (*Mus musculus*)	PPIP1_MOUSE
TRINITY_DN156801_c0_g1	Protein Wnt-9a (*Gallus gallus*)	WNT9A_CHICK
TRINITY_DN151831_c0_g1	Uncharacterized protein (*Lottia gigantea*)	V4ADI7_LOTGI
TRINITY_DN165101_c2_g2	Excitatory amino acid transporter 2 (*Mus musculus*)	EAA2_MOUSE
TRINITY_DN170242_c0_g1	Uncharacterized protein (*Lottia gigantea*)	V4AFU8_LOTGI
TRINITY_DN111179_c0_g1	Insulin gene enhancer protein ISL-3 (*Oncorhynchus tshawytscha*)	ISL3_ONCTS
TRINITY_DN165794_c0_g8	Adipocyte plasma membrane-associated protein (*Bos taurus*)	APMAP_BOVIN
TRINITY_DN181243_c4_g2		
TRINITY_DN181242_c2_g3		
TRINITY_DN151365_c0_g1		
TRINITY_DN80739_c0_g1		
TRINITY_DN165520_c0_g2	Solute carrier organic anion transporter family member 4A1 (*Mus musculus*)	SO4A1_MOUSE
TRINITY_DN171085_c0_g2	Insulinoma associated protein 1a (*Danio rerio*)	INS1A_DANRE
TRINITY_DN180241_c1_g8	Myosin heavy chain striated muscle (*Argopecten irradians*)	MYS_ARGIR
TRINITY_DN168287_c2_g1		
TRINITY_DN172809_c0_g3	Uncharacterized protein (*Crassostrea gigas*)	K1RAV4_CRAGI
TRINITY_DN160389_c0_g2		
TRINITY_DN160241_c3_g4	Retinal-binding protein (*Todarodes pacificus*)	RALB_TODPA
TRINITY_DN169536_c0_g2	Asparagine synthetase (*Gallus gallus*)	ASNS_CHICK
TRINITY_DN164018_c0_g6	Telokin (*Meleagris gallopavo*)	MYLK_MELGA
TRINITY_DN167023_c0_g1	Uncharacterized protein (*Crassostrea gigas*)	K1QA71_CRAGI
TRINITY_DN157911_c0_g7		
TRINITY_DN163774_c0_g1	Uncharacterized protein (*Crassostrea gigas*)	K1RCI7_CRAGI
TRINITY_DN170121_c0_g1	Deleted in malignant brain tumors 1 protein (*Crassostrea gigas*)	K1QKF1_CRAGI
TRINITY_DN170676_c0_g4	α-mannosidase 2 (*Homo sapiens*)	MA2A1_HUMAN
TRINITY_DN147565_c0_g2		
TRINITY_DN181007_c6_g2		
TRINITY_DN113020_c0_g1		
TRINITY_DN175418_c0_g4	Atrial natriuretic peptide converting enzyme (*Homo sapiens*)	CORIN_HUMAN
TRINITY_DN168060_c0_g1	Uncharacterized protein (*Crassostrea gigas*)	K1REI1_CRAGI
TRINITY_DN155034_c0_g2	Cysteine and glycine-rich protein 2 (*Coturnix coturnix japonica*)	CSRP2_COTJA
TRINITY_DN180601_c6_g4	Prestin (*Homo sapiens*)	S26A5_HUMAN
TRINITY_DN177208_c0_g1	Protein FAM46C (*Danio rerio*)	FA46C_DANRE
TRINITY_DN169640_c1_g6		
TRINITY_DN181242_c2_g2	Twitchin (*Mytilus galloprovincialis*)	Q9GV22_MYTGA
TRINITY_DN172176_c0_g2	Neuronal calcium sensor 1 (*Aplysia californica*)	NCS1_APLCA
TRINITY_DN180542_c2_g2		
TRINITY_DN180672_c0_g3		
TRINITY_DN167040_c2_g1	Putative methyltransferase NSUN7 (*Homo sapiens*)	NSUN7_HUMAN

TRINITY_DN163304_c0_g1	Microtubule-associated protein (*Lottia gigantea*)	V4A5P5_LOTGI
TRINITY_DN162527_c0_g1		
TRINITY_DN178644_c0_g1	Adenylate cyclase type 1 (Ca/calmodulin-activated adenylyl cyclase (*Mus musculus*)	ADCY1_MOUSE
TRINITY_DN143151_c0_g1	Ceroid-lipofuscinosis neuronal protein 5 homolog (*Mus musculus*)	CLN5_MOUSE
TRINITY_DN178495_c2_g1		
TRINITY_DN181242_c3_g1	Twitchin (*Mytilus galloprovincialis*)	Q7YT99_MYTGA
TRINITY_DN181009_c3_g1	Inositol 1,4,5-trisphosphate receptor type 1 (*Mus musculus*)	ITPR1_MOUSE
TRINITY_DN160241_c2_g1	Retinal-binding protein (*Todarodes pacificus*)	RALB_TODPA
TRINITY_DN169132_c1_g3	Solute carrier family 15 member 4 (*Xenopus laevis*)	S15A4_XENLA
TRINITY_DN155034_c0_g3		
TRINITY_DN173511_c0_g5	Von Willebrand factor D and EGF domain-containing protein (*Crassostrea gigas*)	K1P6L3_CRAGI
TRINITY_DN165888_c0_g2	trembl- -Chitin_deacetylase-like_protein-1_(*Mytilus_coruscus_*)	A0A0K0YAZ8_MYTCO
TRINITY_DN164744_c0_g1	-sprot- -Paramyosin(*Mytilus_galloprovincialis*)	MYSP_MYTGA
TRINITY_DN145016_c0_g1		
TRINITY_DN159230_c0_g2	Uncharacterized protein (*Arion vulgaris*)	A0A0B6ZGK1_9EUPU
TRINITY_DN164980_c0_g1	Potassium voltage-gated channel protein Shaw (*Drosophila melanogaster*)	KCNAW_DROME
TRINITY_DN165814_c1_g3		
TRINITY_DN158951_c0_g1	Leucine-rich repeat-containing protein 74A (*Homo sapiens*)	LR74A_HUMAN
TRINITY_DN171746_c0_g5	Major egg antigen (*Crassostrea gigas*)	K1QBC3_CRAGI
TRINITY_DN165306_c0_g1	Kyphoscoliosis peptidase (*Crassostrea gigas*)	K1PQ64_CRAGI
TRINITY_DN173216_c0_g1	Voltage-gated hydrogen channel 1 (*Gallus gallus*)	HVCN1_CHICK
TRINITY_DN152699_c0_g1		
TRINITY_DN180224_c1_g1	Uncharacterized protein (*Crassostrea gigas*)	K1PYE4_CRAGI
TRINITY_DN169711_c0_g1	Neurotrypsin (*Crassostrea gigas*)	K1R3V1_CRAGI
TRINITY_DN168946_c1_g5	Transgelin-like protein-3(*Mytilus coruscus*)	A0A0K0YAZ6_MYTCO
TRINITY_DN169640_c1_g4		
TRINITY_DN176716_c1_g1	Whirlin (*Crassostrea gigas*)	K1QHV6_CRAGI
TRINITY_DN160107_c0_g2	Uncharacterized protein(*Crassostrea gigas*)	K1Q4Q0_CRAGI
TRINITY_DN171546_c0_g3	Matrix metalloproteinase-19 (*Homo sapiens*)	MMP19_HUMAN
TRINITY_DN156972_c0_g2	Aquaporin-4 (*Mus musculus*)	AQP4_MOUSE
TRINITY_DN108822_c0_g1	Uncharacterized protein (*Crassostrea gigas*)	K1Q679_CRAGI
TRINITY_DN165433_c1_g11		
TRINITY_DN141471_c0_g1	Forkhead box protein F1 (*Crassostrea gigas*)	K1QD97_CRAGI
TRINITY_DN158052_c0_g3	Uncharacterized protein (*Lottia gigantea*)	V4B5G7_LOTGI
TRINITY_DN169640_c1_g5		
TRINITY_DN153182_c0_g11	Four and a half LIM domains protein 2 (*Rattus norvegicus*)	FHL2_RAT
TRINITY_DN178500_c2_g1	Uncharacterized protein (*Lottia gigantea*)	V4B719_LOTGI
TRINITY_DN173065_c1_g8	Receptor-transporting protein 3 (*Crassostrea gigas*)	K1Q6J6_CRAGI
TRINITY_DN141305_c0_g1	CTL-9 (*Argopecten irradians*)	H9M3L7_ARGIR
TRINITY_DN159435_c1_g3	NACHT and WD repeat domain containing protein 1	K1PEH6_CRAGI

	(*Crassostrea gigas*)	
TRINITY_DN147647_c0_g1	Cysteine-rich protein 1 (*Homo sapiens*)	CRIP1_HUMAN
TRINITY_DN171746_c0_g8	Major egg antigen (*Schistosoma mansoni*)	P40_SCHMA
TRINITY_DN171622_c1_g5		
TRINITY_DN150421_c0_g3	Endoprotease bli-4 (*Caenorhabditis elegans*)	BLI4_CAEEL
TRINITY_DN169884_c0_g1		
TRINITY_DN180343_c1_g3		
TRINITY_DN178827_c2_g3	Uncharacterized protein (*Lottia gigantea*)	V4A8I7_LOTGI
TRINITY_DN165868_c1_g2	Lipopolysaccharide-induced tumor necrosis factor-α factor homolog (*Gallus gallus*)	LITAF_CHICK
TRINITY_DN151425_c0_g3		
TRINITY_DN180618_c0_g1	Filamin-A (*Homo sapiens*)	FLNA_HUMAN
TRINITY_DN158735_c0_g1	Xaa-Pro aminopeptidase 1 (*Homo sapiens*)	XPP1_HUMAN
TRINITY_DN149941_c0_g1	Uncharacterized protein (*Lottia gigantea*)	V3ZVL6_LOTGI
TRINITY_DN163285_c0_g1		
TRINITY_DN175808_c0_g1		
TRINITY_DN175789_c0_g1	Multidrug resistance-associated protein 1 (Leukotriene C transporter) (*Canis lupus familiaris*)	MRP1_CANLF
TRINITY_DN181321_c5_g1		
TRINITY_DN143314_c0_g2		
TRINITY_DN155835_c0_g1	Sarcoplasmic calcium-binding protein (*Mizuhopecten yessoensis*)	SCP_MIZYE
TRINITY_DN171569_c1_g1	Tripartite motif-containing protein 56 (*Crassostrea gigas*)	K1QSK1_CRAGI
TRINITY_DN70925_c0_g1	Uncharacterized protein (*Crassostrea gigas*)	K1PAP3_CRAGI
TRINITY_DN174264_c0_g1	Somatomedin-B and thrombospondin type-1 domain-containing protein (*Bos taurus*)	SBSPO_BOVIN
TRINITY_DN179350_c2_g4	PDZ and LIM domain protein 5(*Crassostrea gigas*)	K1PQ23_CRAGI
TRINITY_DN175603_c0_g1	Receptor-type tyrosine-protein phosphatase ε (*Homo sapiens*)	PTPRE_HUMAN
TRINITY_DN181141_c7_g1	Von Willebrand factor D and EG domain-containing protein(*Crassostrea gigas*)	K1RSH8_CRAGI
TRINITY_DN180790_c4_g3	Muscle M-line assembly protein unc-89 (*Crassostrea gigas*)	K1RUG0_CRAGI
TRINITY_DN158068_c0_g3	Actin-2 (*Lumbricus terrestris*)	ACT2_LUMTE
TRINITY_DN40608_c0_g2		
TRINITY_DN178763_c1_g1		
TRINITY_DN176510_c1_g2	Kyphoscoliosis peptidase (*Mus musculus*)	KY_MOUSE
TRINITY_DN137215_c0_g1	Uridine phosphorylase 1 (*Homo sapiens*)	UPP1_HUMAN
TRINITY_DN176604_c0_g2	Membrane metallo-endopeptidase-like 1 (NEP2) (*Homo sapiens*)	MMEL1_HUMAN
TRINITY_DN179325_c0_g2	Fibulin-2 (*Mus musculus*)	FBLN2_MOUSE
TRINITY_DN165677_c4_g1		
TRINITY_DN181271_c0_g2	Dystonin (*Mus musculus*)	DYST_MOUSE
TRINITY_DN157598_c0_g1	Junctophilin-1 (*Mus musculus*)	JPH1_MOUSE
TRINITY_DN171593_c0_g1	Protein fem-1 homolog C (*Danio rerio*)	FEM1C_DANRE
TRINITY_DN159603_c0_g2	Inhibitory POU protein (*Drosophila melanogaster*)	IPOU_DROME
TRINITY_DN157616_c1_g5	Myophilin (*Echinococcus granulosus*)	MYPH_ECHGR
TRINITY_DN180244_c4_g2	Uncharacterized protein (*Crassostrea gigas*)	K1Q3F5_CRAGI
TRINITY_DN167783_c1_g6	Actin adductor muscle (*Placopecten magellanicus*)	ACT_PLAMG
TRINITY_DN174226_c0_g5	Sodium and chloride-dependent glycine transporter 2	SC6A5_HUMAN

	(*Homo sapiens*)	
TRINITY_DN180737_c4_g1	Polypeptide N-acetylgalactosaminyltransferase 1 (*Homo sapiens*)	GALT1_HUMAN
TRINITY_DN174419_c2_g5	Aquaporin-4 (*Bos taurus*)	AQP4_BOVIN
TRINITY_DN172100_c0_g1	Synaptopodin-2 (*Crassostrea gigas*)	K1Q2X5_CRAGI
TRINITY_DN128736_c0_g1	Peroxidasin-like protein (*Crassostrea gigas*)	K1PG33_CRAGI
TRINITY_DN176703_c1_g2	Voltage-dependent L-type calcium channel subunit α (*Crassostrea gigas*)	K1QEL8_CRAGI
TRINITY_DN170085_c0_g1	Glutamate receptor ionotropic NMDA 2B (*Homo sapiens*)	NMDE2_HUMAN
TRINITY_DN173994_c1_g10	Troponin I (*Chlamys nipponensis akazara*)	TNNI_CHLNI
TRINITY_DN175773_c0_g2	Potassium voltage-gated channel protein Shal (*Drosophila melanogaste*r)	KCNAL_DROME
TRINITY_DN170789_c0_g1	Uncharacterized protein (*Crassostrea gigas*)	K1Q856_CRAGI
TRINITY_DN175685_c1_g2	Uncharacterized protein (*Arion vulgaris*)	A0A0B6YXZ9_9EUPU
TRINITY_DN164856_c3_g1	Calponin-1 (*Gallus gallus*)	CNN1_CHICK
TRINITY_DN169884_c0_g3		
TRINITY_DN151756_c0_g1	Integrin β-5 (*Bos taurus*)	ITB5_BOVIN
TRINITY_DN134224_c0_g1	Insulin gene enhancer protein ISL-1 (*Rattus norvegicus*)	ISL1_RAT
TRINITY_DN162423_c0_g3	Small conductance calcium-activated potassium channel protein 2 (*Homo sapiens*)	KCNN2_HUMAN
TRINITY_DN160540_c3_g2	Sodium-coupled monocarboxylate transporter 1 (*Homo sapiens*)	SC5A8_HUMAN
TRINITY_DN179779_c5_g2		
TRINITY_DN181260_c4_g1	LIM domain and actin-binding protein 1 (C*rassostrea gigas*)	K1QT91_CRAGI
TRINITY_DN179098_c3_g3	Uncharacterized protein (*Crassostrea gigas*)	K1RE15_CRAGI
TRINITY_DN137669_c0_g1		
TRINITY_DN180712_c8_g2		
TRINITY_DN170528_c0_g1	Inositol-3-phosphate synthase 1-B (*Xenopus laevis*)	INO1B_XENLA
TRINITY_DN147265_c0_g1	Heart and neural crest derivatives expressed protein 2 (*Danio rerio*)	HAND2_DANRE
TRINITY_DN63689_c0_g1		
TRINITY_DN179234_c0_g4	Trafficking protein particle complex subunit 4 (*Crassostrea gigas*)	K1QNE7_CRAGI
TRINITY_DN179091_c4_g1		
TRINITY_DN144067_c0_g2		
TRINITY_DN153348_c0_g1		
TRINITY_DN159919_c2_g3		
TRINITY_DN151657_c0_g1	Uncharacterized protein (*Crassostrea gigas*)	K1RQH6_CRAGI
TRINITY_DN169166_c0_g1	WEE1-like protein kinase 1-B (*Xenopus laevis*)	WEE1B_XENLA
TRINITY_DN179730_c7_g3		
TRINITY_DN109592_c0_g1	Collagen α-1 chain (*Crassostrea gigas*)	K1R0L2_CRAGI
TRINITY_DN179876_c1_g8		
TRINITY_DN151440_c0_g4		
TRINITY_DN167317_c0_g3	Prestin (*Mus musculus*)	S26A5_MOUSE

Supplementary Table S5. Protein ID's and sequences of anion transporting proteins used in Figure 8.

Protein ID	Sequence
SpiSLC4-alpha	MTSIENIPIDQSTCSPYEGFVELEELVSCDDELIWKESARWIKLEEDVDECADR WGKPHVPCLTYRSLREVETNLQNGVCLLDLNRDTLPSIWDAIIDEIKTLKKMED SECLVVKTLLMTRHEHHHQHKSGKRVQNFARRRSRIMPNGQRSRTNVSEDVH NLRERPQLSLEQNMLPSIDSKQDVSEFPANVAVSFSPDPVEGFVEQFDDHNKKS DLRGRLPENSQATTVLVGAHNGLSCTVSAFIRLAKGCELSNLAEVQIPIRFIFILV GPNDDRIDYHEVGRSFATLMADKLFLESAYLAKRQQDLLDSLFSFMGDSLIIPP GDWDRNLLSQTIPILASQTKELALRRRSGGIQSKDKPNERFREGFQENEVCDDP LSRTGKFCGGLIRDVKRRFPFYLSDFKDALDVHCLPTIIFVYFACLAPTIAFGGL LSEKTNAWMGVSEMIFATALSGVLFGLFAGQPLIIIGATGPLLIFEKSIFQLSERF EIEFLPWRAWVGIWVMVICFIIVAVEGCFLIKYFTRFTEEIFALVISIIFIYYAFNY VRHIFDLYPLNADVATTLLVPKNSTNPTKGKSVGNQSTANTALLTTVLMLGTF FVAYTLRKLHHSHFFGPKARRIVSDFGVFIAIVSMVTVGWLTEGVYTQKLSVP DGFSVSSPNRNSWLINPMGEQQHMSAVAISGAFIPAVLVSILIFMEIEFTGIILDK KEHKLKKGVGYNLDLFVLGLLVGLCSVLGLPWMCATPVHTLSHFHALTVLST NHAPGEHPRLVQVREQRLTNIVIHLLIGFTVLLSPVMRLIPIAVLFGVFLFLGVSS LSHIQLVKRIKLLFIPASHHPVEKFVTNVKTRKMHLFTIVQVCCVCALVALKLT VVAPAFPFLIICMIPLRKLLERFFTSLELEALDTEVEDVYDSDLDEYDSIHFPF
SpiSLC4-beta	MEWKETARWIKFEENVEDSNRWGKPHVASLTFHSLLELRKGLEKGTVLLDLE KFDLPSIAEAVVENMVITDQISQTDSNKVLAALLLRHRHQYQMSPPIARRPSSY NLLALARKDSKHPIEDSENKVLEPEEGETLGDGAIRLKIDESDSDFPGQEISPLSL SGDEKQDQKAEVSFAPEPAVVEGGSGKQESDVKSRIPEGAEATTVLVGTLDEL QYPVVAFVRLAKGCPLNITEVSIPVRFMFVLLGPSSEEESYYEIGRSVATLMSDQ AFHDIAYRADSREDLLSAINCFLDDTVVLPPGEWDRNVLLPILIAQSRARARRR KMAKAALAAVAEEQEIDPLERTGSFCGGLVEDIKRRAKVYLSDFKDGLNLQCL LTSIFLYFSVFAPNVAFGSLLDKKTEGWLGVSEVILATCMCGILFGLLAGQPLIII GATGPVLVFEQTIYEFCNVYNVEFLPWRCWIGFWVMMILFGVVALEGCFLVR YFTRFTEEIFACLISAIFVYEAIHFLEVVFKKNPLQKTYTESPKSPEYEVKGQPNT ALLSTIMVLGTFFVAFYLRKFRTSYFFGKKARRLVSDFGIVIAMACMLLVDVFL YDKVVTQKITIGDPTKRGFLPTRYTERGWFINPGGMKRPMEPGWIFAAIIPALF VGILLFMETELTGVLLNKKENKLLKGAGFNLDLIVMGCLSFVCSMMGLPWMC AATVRSVSHLNALSIWSTSQAPGVKPHLVEVKEQRVTNIAIHVLTGVSILLAPA LHRIPVAVMFGVLFYLGVCSLSGIQLVDRIIMMFMPPKYHPDVQYVRKVKTRK IHSYTIIQVVCLILLIVVKLNVIAPSFPFFIICLIPLRKVLTKFFEQNELEELDNEELP DDDSDLDEYDSVYMPV
SpiSLC4-gamma	MVKGEGDTTDNKRKGALPKIQEGTSESNYEGDHSHDDSRFMPSVEECRYLND QGQHIDSDKVPHYHHYRTISEREEFQSRIRNGAVSMKDIEVLQERLERDNDNNI LAGMSDSIQMAGLRKSQRKLSGMQTLYSSTDISASLDKFPVLYDRNPHEAFVE LEELSKHGEEMEWKETARWIKFEENVEDGDRWGKPHVASLTFHSLLELRKG LEKGTVLLDLEKFDLPNIAKAVVENMVLSDQLKQKDSNKVLTALLLRHRHQH QRRPSSKRRKKLAVAADNLGFNSLAETGNGVIRMNMNESNGDVPITQDKVDIE TAGLDEDEEKQESDVKDKIPQGAEATNVLVGTLDELQDPVMAFVRLAKGVHL EEMSEVSIPVRFLFIMLGPSSHGEIYHQIGRSVATLMSDQAFHDVAYRADSREE LLQSINEFLEDTLVLPPGNWDRSVLLPILIAQSRAIALRRKLAKAASSSHSEGDP ALARTGTFFGGLIQDVKRRGKVYLSDFRDGFNLHTLLASLFLYFALFATNIAFG GLFEDKTEGWLGLTEVIFAACACSILFGLFGGQPIMIIGATGPMLVFEQSIYEFC KAYDVEFLTWRCWIGFWVMIILFGVVALEGCFLIKYFTRFTEDIFELLISAIFIYE PLALLIKLFKKNPLNRVGSGKYSSVDEVKGEPNTALLSTILVLGTFFIAFYMRKL RTSHFFGKRARRLVSDSGIVIAMFIMAMIDFALGDKVITQHISINDPVTEGFKPT

QHDKRGWFINPGGMNKEMSMPWIFAAIIPAVFVGILLFMETEMTGVLLSKKEH
KLAKGPGYNMDMCVVGMLAFGCSLLGLPWMCADTVRSASHVNALSIWSTSH
APGEKPHLIEVKEQRISNIIVHVLTGLSILLAPGLNVIPIPIFFGVLLYLGIVSMYG
LQMVDRFIMMFMPRKHHPDVGYVRKVRTGKIHCYTVIQVLALAFLVGIKLSPL
APSFPFFIICLIPLRKLLTRFYKEEELEELDNSESEEEDSDFEL

SpiSLC4-delta MEIRQPSYDSIPGPVDAGISSRNGYFGELDYQNHRQVYVGVHIPLRQRKHHHH
QRHHHRRRHRSLLESKDELSSDAGTPSLPTDKVRFILGGEEADQEQHKMFSELL
EYHCDKDGNEEWREMARWLKFEEDVEEGGNRWSKPHVGTLSLYSLFELRSAL
LRGTVLLDMNATNLSQIADLVLDDLVNKNQLDQDNRQQVRDAILKKKRHQG
NKTQKKKSSNPMSSFGSFAKKSSTAGFTDMFKRSDSSQKTTAPKNLEVVNEVD
TNDGEFPHLPSAADLVGKGKESGVNGNAGLDQTDSETCLEAFDANFMKKIPQ
GAKASNVLVGEMDIIKKPVTAFVRLENASLLGDLTEVPVPSKFIFLMLGPSGTP
GRYMEVGRAIGTLMSDEVFHEVAYKAQCREDLLAGIDEFLMQVTVLPPGEWD
PSIRIEPPDAVPAQGNRLEVVKSGGGGEMEEHDPAGDREEQLQKTGRLCGGLI
ADIRRRAPWYWSDFKDALNPQCIASIIFIYFACLTPIITFGGLMGTKTGKNMAA
MEQILAGGIGGVLFSLFGGQPLIILGATGPMLVFEEILYTFCDKFGLDYMPFRLW
IGIWTMLYCFVLVVTDASALVRYFTRFTEESFATLIALIFIVEGFKKLFHVLDDS
PVSKGYITSHSCLCYPGEEDSSGHHMADSSSFVNKTPLDYPIGDCVRYGGQLV
GEACHSNVFFLSVILSLGTFFLAVTLKEFRSSSYFPTKVRSVISDFAILISIMVMV
GVDLAFGVNTPKLDIPLKFEPTNSKERGWIIPPLGKNPVWTIPAAAIPALLATIL
VFMDQQITALIVNRREHKLKKGAGYHLDLLLVALIIGICSLLGLPWVVAATVLS
VGHVQSLFVESQCTAPGEKAQFLGVREQRITGTFIFILIGLTVFIAPILKFVPMPV
LFGLFFYMGFSALRGLQFFERLKIMFMPVKHQPDLMFLRQVPLKRIHIFTLIQLL
CLGILWLIKSTDAALIFPVMVLMLVAVRKVMEKIFNLHELEVLDDLMPESIKKQ
QADEAAKKKDDDYDSDDDLDDEDGCNHYDETDGKKALSDGKELNGTANVV
APMNISEEMCRSSLWKQFVKDGTTAKNRKNKPSDKSKHKHKHHHKNRHHRH
KRDREGSADEEGLWMLEKKKEDGEDAGPDVEMGRKLSTINEDKQDIVIDMEE
IQKSLLELNEIGNTVTDEGADKQTPRDSENPV

SpiSLC4-epsilon MQRPFNQPKGVGKEDENGSTTGRSVDGFDIANIDERNLNNSQGDVTPAMEML
KFTDCDDDESEIETVEIINLNSCGQGFDNETVDESYLVEEDGVPGTSLMLSSHQ
KLPSKNFCAEIRAAKDVETFLERPILLLGLQETSLQGIIDAMLKKLITVIGGEDID
FEEARLAFFTHDSVHCLSKIIQGTEISEGGGWEETQNWLIALGELPSVQQSHVAF
AQLRHPVNLGRTLEETHLVVLVLAPSKAKSTKNSLETGRTFATLLSDIEIRQLLI
EAETEEEFKKVLSDRKGMLSSQLLPKRKSTIRQFGSQPKSSFIHQRDDENEKRSE
LFSFGRGVIRDFRRRWPHYLSDFKDGIRGHRTIPKVISTTLFLYFACILPSIAFGV
LNSRNTSGKIDVLKVIISQSVGGILFALFGGQPLIVLLTTAPLALYIKVIYNIAADF
DLDFFALYSCTGLWNSFFLFIYSTFGLSQIMKWSTRSTEEIFALFISLAFTVDAISS
IIKEYSSPHCTSLSSCWNSSSCVVGQGIANNFTHDQVPDVSVCSREGGLSYAVT
SLGTVWIGVALYNFRKSPFLDAGKREALADYALVVAVLVMSFIASFFVRDIDN
YKFESSSTFSFTVAPLHKLTWGAVFAGLGLGFSLSLLFFMDQNISSAMVNNPGN
RLKKGSAYHWDLLVVAVVNGFLSIFGLPWVHAALPHSPFHVRALADVEERVD
RGHVFEIIVKVRETRLTGFLSSTLIALSLLMLPIPLTLIPTPVLDGLFLFMAMTSL
YGNQMFERALLLVTEQAAYPPNHYIRHVPQRKMHLYTALQFLQLGILCGFGFA
PLPYLKMVFPVLLMFILPIRHLLVPKLISSKYLEALDAHL

humanSLC4A1 MEELQDDYEDMMEENLEQEEYEDPDIPESQMEEPAAHDTEATATDYHTTSHP
GTHKVYVELQELVMDEKNQELRWMEAARWVQLEENLGENGAWGRPHLSHL
TFWSLLELRRVFTKGTVLLDLQETSLAGVANQLLDRFIFEDQIRPQDREELLRA
LLLKHSHAGELEALGGVKPAVLTRSGDPSQPLLPQHSSLETQLFCEQGDGGTE
GHSPSGILEKIPPDSEATLVLVGRADFLEQPVLGFVRLQEAAELEAVELPVPIRF
LFVLLGPEAPHIDYTQLGRAAATLMSERVFRIDAYMAQSRGELLHSLEGFLDCS
LVLPPTDAPSEQALLSLVPVQRELLRRRYQSSPAKPDSSFYKGLDLNGGPDDPL

QQTGQLFGGLVRDIRRRYPYYLSDITDAFSPQVLAAVIFIYFAALSPAITFGGLL
GEKTRNQMGVSELLISTAVQGILFALLGAQPLLVVGFSGPLLVFEEAFFSFCETN
GLEYIVGRVWIGFWLILLVVLVVAFEGSFLVRFISRYTQEIFSFLISLIFIYETFSK
LIKIFQDHPLQKTYNYNVLMVPKPQGPLPNTALLSLVLMAGTFFFAMMLRKFK
NSSYFPGKLRRVIGDFGVPISILIMVLVDFFIQDTYTQKLSVPDGFKVSNSSARG
WVIHPLGLRSEFPIWMMFASALPALLVFILIFLESQITTLIVSKPERKMVKGSGFH
LDLLLVVGMGGVAALFGMPWLSATTVRSVTHANALTVMGKASTPGAAAQIQ
EVKEQRISGLLVAVLVGLSILMEPILSRIPLAVLFGIFLYMGVTSLSGIQLFDRILL
LFKPPKYHPDVPYVKRVKTWRMHLFTGIQIICLAVLWVVKSTPASLALPFVLIL
TVPLRRVLLPLIFRNVELQCLDADDAKATFDEEEGRDEYDEVAMPV

>humanSLC4A2 MSSAPRRPAKGADSFCTPEPESLGPGTPGFPEQEEDELHRTLGVERFEEILQEAG
SRGGEEPGRSYGEEDFEYHRQSSHHIHHPLSTHLPPDARRRKTPQGPGRKPRRR
PGASPTGETPTIEEGEEDEDEASEAEGARALTQPSPVSTPSSVQFFLQEDDSADR
KAERTSPSSPAPLPHQEATPRASKGAQAGTQVEEAEAEAVAVASGTAGGDDG
GASGRPLPKAQPGHRSYNLQERRRIGSMTGAEQALLPRVPTDEIEAQTLATADL
DLMKSHRFEDVPGVRRHLVRKNAKGSTQSGREGREPGPTPRARPRAPHKPHE
VFVELNELLLDKNQEPQWRETARWIKFEEDVEEETERWGKPHVASLSFRSLLE
LRRTLAHGAVLLDLDQQTLPGVAHQVVEQMVISDQIKAEDRANVLRALLLKH
SHPSDEKDFSFPRNISAGSLGSLLGHHHGQGAESDPHVTEPLMGGVPETRLEVE
RERELPPPAPPAGITRSKSKHELKLLEKIPENAEATVVLVGCVEFLSRPTMAFVR
LREAVELDAVLEVPVPVRFLFLLLGPSSANMDYHEIGRSISTLMSDKQFHEAAY
LADEREDLLTAINAFLDCSVVLPPSEVQGEELLRSVAHFQRQMLKKREEQGRL
LPTGAGLEPKSAQDKALLQMVEAAGAAEDDPLRRTGRPFGGLIRDVRRRYPH
YLSDFRDALDPQCLAAVIFIYFAALSPAITFGGLLGEKTQDLIGVSELIMSTALQ
GVVFCLLGAQPLLVIGFSGPLLVFEEAFFSFCSSNHLEYLVGRVWIGFWLVFLA
LLMVALEGSFLVRFVSRFTQEIFAFLISLIFIYETFYKLVKIFQEHPLHGCSASNSS
EVDGGENMTWAGARPTLGPGNRSLAGQSGQGKPRGQPNTALLSLVLMAGTFF
IAFFLRKFKNSRFFPGRIRRVIGDFGVPIAILIMVLVDYSIEDTYTQKLSVPSGFSV
TAPEKRGWVINPLGEKSPFPVWMMVASLLPAILVFILIFMETQITTLIISKKERM
LQKGSGFHLDLLLIVAMGGICALFGLPWLAAATVRSVTHANALTVMSKAVAP
GDKPKIQEVKEQRVTGLLVALLVGLSIVIGDLLRQIPLAVLFGIFLYMGVTSLNG
IQFYERLHLLLMPPKHHPDVTYVKKVRTLRMHLFTALQLLCLALLWAVMSTA
ASLAFPFILILTVPLRMVVLTRIFTDREMKCLDANEAEPVFDEREGVDEYNEMP
MPV

humanSLC4A3 MANGVIPPPGGASPLPQVRVPLEEPPLSPDVEEEDDDLGKTLAVSRFGDLISKPP
AWDPEKPSRSYSERDFEFHRHTSHHTHHPLSARLPPPHKLRRLPPTSARHTRRK
RKKEKTSAPPSEGTPPIQEEGGAGVDEEEEEEEEEEGESEAEPVEPPHSGTPQKA
KFSIGSDEDDSPGLPGRAAVTKPLPSVGPHTDKSPQHSSSSPSPRARASRLAGEK
SRPWSPSASYDLRERLCPGSALGNPGGPEQQVPTDEAEAQMLGSADLDDMKS
HRLEDNPGVRRHLVKKPSRTQGGRGSPSGLAPILRRKKKKKKLDRRPHEVFVE
LNELMLDRSQEPHWRETARWIKFEEDVEEETERWGKPHVASLSFRSLLELRRTI
AHGAALLDLEQTTLPGIAHLVVETMIVSDQIRPEDRASVLRTLLLKHSHPNDDK
DSGFFPRNPSSSSMNSVLGNHHPTPSHGPDGAVPTMADDLGEPAPLWPHDPDA
KEKPLHMPGGDGHRGKSLKLLEKIPEDAEATVVLVGCVPFLEQPAAAFVRLNE
AVLLESVLEVPVPVRFLFVMLGPSHTSTDYHELGRSIATLMSDKLFHEAAYQA
DDRQDLLSAISEFLDGSIVIPPSEVEGRDLLRSVAAFQRELLRKRREREQTKVEM
TTRGGYTAPGKELSLELGGSEATPEDDPLLRTGSVFGGLVRDVRRRYPHYPSD
LRDALHSQCVAAVLFIYFAALSPAITFGGLLGEKTEGLMGVSELIVSTAVLGVL
FSLLGAQPLLVVGFSGPLLVFEEAFFKFCRAQDLEYLTGRVWVGLWLVVFVLA
LVAAEGSFLVRYISPFTQEIFAFLISLIFIYETFYKLYKVFTEHPLLPFYPPEGALE
GSLDAGLEPNGSALPPTEGPPSPRNQPNTALLSLILMLGTFFIAFFLRKFRNSRFL

GGKARRIIGDFGIPISILVMVLVDYSITDTYTQKLTVPTGLSVTSPDKRSWFIPPL
GSARPFPPWMMVAAAVPALLVLILIFMETQITALIVSQKARRLLKGSGFHLDLL
LIGSLGGLCGLFGLPWLTAATVRSVTHVNALTVMRTAIAPGDKPQIQEVREQR
VTGVLIASLVGLSIVMGAVLRRIPLAVLFGIFLYMGVTSLSGIQLSQRLLLILMP
AKHHPEQPYVTKVKTWRMHLFTCIQLGCIALLWVVKSTAASLAFPFLLLLTVP
LRHCLLPRLFQDRELQALDSEDAEPNFDEDGQDEYNELHMPV

humanSLC4A4 MEDEAVLDRGASFLKHVCDEEEVEGHHTIYIGVHVPKSYRRRRRHKRKTGHK
EKKEKERISENYSDKSDIENADESSSSILKPLISPAAERIRFILGEEDDSPAPPQLFT
ELDELLAVDGQEMEWKETARWIKFEEKVEQGGERWSKPHVATLSLHSLFELR
TCMEKGSIMLDREASSLPQLVEMIVDHQIETGLLKPELKDKVTYTLLRKHRHQ
TKKSNLRSLADIGKTVSSASRMFTNPDNGSPAMTHRNLTSSSLNDISDKPEKDQ
LKNKFMKKLPRDAEASNVLVGEVDFLDTPFIAFVRLQQAVMLGALTEVPVPTR
FLFILLGPKGKAKSYHEIGRAIATLMSDEVFHDIAYKAKDRHDLIAGIDEFLDEV
IVLPPGEWDPAIRIEPPKSLPSSDKRKNMYSGGENVQMNGDTPHDGGHGGGGH
GDCEELQRTGRFCGGLIKDIKRKAPFFASDFYDALNIQALSAILFIYLATVTNAIT
FGGLLGDATDNMQGVLESFLGTAVSGAIFCLFAGQPLTILSSTGPVLVFERLLF
NFSKDNNFDYLEFRLWIGLWSAFLCLILVATDASFLVQYFTRFTEEGFSSLISFIF
IYDAFKKMIKLADYYPINSNFKVGYNTLFSCTCVPPDPANISISNDTTLAPEYLP
TMSSTDMYHNTTFDWAFLSKKECSKYGGNLVGNNCNFVPDITLMSFILFLGTY
TSSMALKKFKTSPYFPTTARKLISDFAIILSILIFCVIDALVGVDTPKLIVPSEFKPT
SPNRGWFVPPFGENPWWVCLAAAIPALLVTILIFMDQQITAVIVNRKEHKLKK
GAGYHLDLFWVAILMVICSLMALPWYVAATVISIAHIDSLKMETETSAPGEQP
KFLGVREQRVTGTLVFILTGLSVFMAPILKFIPMPVLYGVFLYMGVASLNGVQF
MDRLKLLLMPLKHQPDFIYLRHVPLRRVHLFTFLQVLCLALLWILKSTVAAIIFP
VMILALVAVRKGMDYLFSQHDLSFLDDVIPEKDKKKKEDEKKKKKKKGSLDS
DNDDSDCPYSEKVPSIKIPMDIMEQQPFLSDSKPSDRERSPTFLERHTSC

humanSLC4A5 MKVKEEKAGVGKLDHTNHRRRFPDQKECPPIHIGLPVPTYPQRKTDQKGHLSG
LQKVHWGLRPDQPQQELTGPGSGASSQDSSMDLISRTRSPAAEQLQDILGEEDE
APNPTLFTEMDTLQHDGDQMEWKESARWIKFEEKVEEGGERWSKPHVSTLSL
HSLFELRTCLQTGTVLLDLDSGSLPQIIDDVIEKQIEDGLLRPELRERVSYVLLRR
HRHQTKKPIHRSLADIGKSVSTTNRSPARSPGAGPSLHHSTEDLRMRQSANYGR
LCHAQSRSMNDISLTPNTDQRKNKFMKKIPKDSEASNVLVGEVDFLDQPFIAFV
RLIQSAMLGGVTEVPVPTRFLFILLGPSGRAKSYNEIGRAIATLMVDDLFSDVA
YKARNREDLIAGIDEFLDEVIVLPPGEWDPNIRIEPPKKVPSADKRKSVFSLAEL
GQMNGSVGGGGGAPGGGNGGGGGGSGGGAGSGGAGGTSSGDDGEMPAM
HEIGEELIWTGRFFGGLCLDIKRKLPWFPSDFYDGFHIQSISAILFIYLGCITNAIT
FGGLLGDATDNYQGVMESFLGTAMAGSLFCLFSGQPLIILSSTGPILIFEKLLFDF
SKGNGLDYMEFRLWIGLHSAVQCLILVATDASFIIKYITRFTEEGFSTLISFIFIYD
AIKKMIGAFKYYPINMDFKPNFITTYKCECVAPDTVNTTVFNASAPLAPDTNAS
LYNLLNLTALDWSLLSKKECLSYGGRLLGNSCKFIPDLALMSFILFFGTYSMTL
TLKKFKFSRYFPTKVRALVADFSIVFSILMFCGIDACFGLETPKLHVPSVIKPTRP
DRGWFVAPFGKNPWWVYPASILPALLVTILIFMDQQITAVIVNRKENKLKKAA
GYHLDLFWVGILMALCSFMGLPWYVAATVISIAHIDSLKMETETSAPGEQPQF
LGVREQRVTGIIVFILTGISVFLAPILKCIPLPVLYGVFLYMGVASLNGIQMGTG
GSEFKIQKKLTPFWERCKLFLMPAKHQPDHAFLRHVPLRRIHLFTLVQILCLAV
LWILKSTVAAIIFPVMILGLIIVRRLLDFIFSQHDLAWIDNILPEKEKKETDKKRK
RKKGAHEDCDEEPQFPPPSVIKIPMESVQSDPQNGIHCIARKRSSSWSYSL

humanSLC4A7 MERFRLEKKLPGPDEEAVVDLGKTSSTVNTKFEKEELESHRAVYIGVHVPFSKE
SRRRHRHRGHKHHHRRRKDKESDKEDGRESPSYDTPSQRVQFILGTEDDDEEH
IPHDLFTEMDELCYRDGEEYEWKETARWLKFEEDVEDGGDRWSKPYVATLSL
HSLFELRSCILNGTVMLDMRASTLDEIADMVLDNMIASGQLDESIRENVREALL

KRHHHQNEKRFTSRIPLVRSFADIGKKHSDPHLLERNGEGLSASRHSLRTGLSA
SNLSLRGESPLSLLLGHLLPSSRAGTPAGSRCTTPVPTPQNSPPSSPSISRLTSRSS
QESQRQAPELLVSPASDDIPTVVIHPPEEDLEAALKGEEQKNEENVDLTPGILAS
PQSAPGNLDNSKSGEIKGNGSGGSRENSTVDFSKVDMNFMRKIPTGAEASNVL
VGEVDFLERPIIAFVRLAPAVLLTGLTEVPVPTRFLFLLLGPAGKAPQYHEIGRSI
ATLMTDEIFHDVAYKAKDRNDLLSGIDEFLDQVTVLPPGEWDPSIRIEPPKSVPS
QEKRKIPVFHNGSTPTLGETPKEAAHHAGPELQRTGRLFGGLILDIKRKAPFFLS
DFKDALSLQCLASILFLYCACMSPVITFGGLLGEATEGRISAIESLFGASLTGIAY
SLFAGQPLTILGSTGPVLVFEKILYKFCRDYQLSYLSLRTSIGLWTSFLCIVLVAT
DASSLVCYITRFTEEAFAALICIIFIYEALEKLFDLGETYAFNMHNNLDKLTSYSC
VCTEPPNPSNETLAQWKKDNITAHNISWRNLTVSECKKLRGVFLGSACGHHGP
YIPDVLFWCVILFFTTFFLSSFLKQFKTKRYFPTKVRSTISDFAVFLTIVIMVTIDY
LVGVPSPKLHVPEKFEPTHPERGWIISPLGDNPWWTLLIAAIPALLCTILIFMDQ
QITAVIINRKEHKLKKGAGYHLDLLMVGVMLGVCSVMGLPWFVAATVLSISH
VNSLKVESECSAPGEQPKFLGIREQRVTGLMIFILMGLSVFMTSVLKFIPMPVLY
GVFLYMGVSSLKGIQLFDRIKLFGMPAKHQPDLIYLRYVPLWKVHIFTVIQLTC
LVLLWVIKVSAAAVVFPMMVLALVFVRKLMDLCFTKRELSWLDDLMPESKK
KKEDDKKKKEKEEAERMLQDDDDTVHLPFEGGSLLQIPVKALKYSPDKPVSV
KISFEDEPRKKYVDAETSL

humanSLC4A8 MPAAGSNEPDGVLSYQRPDEEAVVDQGGTSTILNIHYEKEELEGHRTLYVGVR
MPLGRQSHRHHRTHGQKHRRRGRGKGASQGEEGLEALAHDTPSQRVQFILGT
EEDEEHVPHELFTELDEICMKEGEDAEWKETARWLKFEEDVEDGGERWSKPY
VATLSLHSLFELRSCLINGTVLLDMHANSIEEISDLILDQQELSSDLNDSMRVKV
REALLKKHHHQNEKKRNNLIPIVRSFAEVGKKQSDPHLMDKHGQTVSPQSVPT
TNLEVKNGVNCEHSPVDLSKVDLHFMKKIPTGAEASNVLVGEVDILDRPIVAF
VRLSPAVLLSGLTEVPIPTRFLFILLGPVGKGQQYHEIGRSMATIMTDEIFHDVA
YKAKERDDLLAGIDEFLDQVTVLPPGEWDPSIRIEPPKNVPSQEKRKMPGVPNG
NVCHIEQEPHGGHSGPELQRTGRLFGGLVLDIKRKAPWYWSDYRDALSLQCL
ASFLFLYCACMSPVITFGGLLGEATEGRISAIESLFGASMTGIAYSLFAGQALTIL
GSTGPVLVFEKILFKFCKDYALSYLSLRACIGLWTAFLCIVLVATDASSLVCYIT
RFTEEAFASLICIIFIYEAIEKLIHLAETYPIHMHSQLDHLSLYYCRCTLPENPNNH
TLQYWKDHNIVTAEVHWANLTVSECQEMHGEFMGSACGHHGPYTPDVLFWS
CILFFTTFILSSTLKTFKTSRYFPTRVRSMVSDFAVFLTIFTMVIIDFLIGVPSPKLQ
VPSVFKPTRDDRGWIINPIGPNPWWTVIAAIIPALLCTILIFMDQQITAVIINRKEH
KLKKGCGYHLDLLMVAIMLGVCSIMGLPWFVAATVLSITHVNSLKLESECSAP
GEQPKFLGIREQRVTGLMIFVLMGCSVFMTAILKFIPMPVLYGVFLYMGVSSLQ
GIQFFDRLKLFGMPAKHQPDFIYLRHVPLRKVHLFTLIQLTCLVLLWVIKASPA
AIVFPMMVLALVFVRKVMDLCFSKRELSWLDDLMPESKKKKLDDAKKKAKE
EEEAEKMLEIGGDKFPLESRKLLSSPGKNISCRCDPSEINISDEMPKTTVWKALS
MNSGNAKEKSLFN

humanSLC4A9 MEMKLPGQEGFEASSAPRNIPSGELDSNPDPGTGPSPDGPSDTESKELGVPKDP
LLFIQLNELLGWPQALEWRETGSSSASLLLDMGEMPSITLSTHLHHRWVLFEEK
LEVAAGRWSAPHVPTLALPSLQKLRSLLAEGLVLLDCPAQSLLELVEQVTRVE
SLSPELRGQLQALLLQRPQHYNQTTGTRPCWGSTHPRKASDNEEAPLREQCQN
PLRQKLPPGAEAGTVLAGELGFLAQPLGAFVRLRNPVVLGSLTEVSLPSRFFCL
LLGPCMLGKGYHEMGRAAAVLLSDPQFQWSVRRASNLHDLLAALDAFLEEVT
VLPPGRWDPTARIPPPKCLPSQHKRLPSQQREIRGPAVPRLTSAEDRHRHGPHA
HSPELQRTGRLFGGLIQDVRRKVPWYPSDFLDALHLQCFSAVLYIYLATVTNAI
TFGGLLGDATDGAQGVLESFLGTAVAGAAFCLMAGQPLTILSSTGPVLVFERL
LFSFSRDYSLDYLPFRLWVGIWVATFCLVLVATEASVLVRYFTRFTEEGFCALI
SLIFIYDAVGKMLNLTHTYPIQKPGSSAYGCLCQYPGPGGNESQWIRTRPKDRD

DIVSMDLGLINASLLPPPECTRQGGHPRGPGCHTVPDIAFFSLLLFLTSFFFAMA
LKCVKTSRFFPSVVRKGLSDFSSVLAILLGCGLDAFLGLATPKLMVPREFKPTLP
GRGWLVSPFGANPWWWSVAAALPALLLSILIFMDQQITAVILNRMEYRLQKG
AGFHLDLFCVAVLMLLTSALGLPWYVSATVISLAHMDSLRRESRACAPGERPN
FLGIREQRLTGLVVFILTGASIFLAPVLKFIPMPVLYGIFLYMGVAALSSIQFTNR
VKLLLMPAKHQPDLLLLRHVPLTRVHLFTAIQLACLGLLWIIKSTPAAIIFPLML
LGLVGVRKALERVFSPQELLWLDELMPEEERSIPEKGLEPEHSFSGSDSEDSEL
MYQPKAPEINISVN

humanSLC4A10 MEIKDQGAQMEPLLPTRNDEEAVVDRGGTRSILKTHFEKEDLEGHRTLFIGVH
VPLGGRKSHRRHRHRGHKHRKRDRERDSGLEDGRESPSFDTPSQRVQFILGTE
DDDEEHIPHDLFTELDEICWREGEDAEWRETARWLKFEEDVEDGGERWSKPY
VATLSLHSLFELRSCILNGTVLLDMHANTLEEIADMVLDQQVSSGQLNEDVRH
RVHEALMKQHHHQNQKKLTNRIPIVRSFADIGKKQSEPNSMDKNAGQVVSPQ
SAPACVENKNDVSRENSTVDFSKGLGGQQKGHTSPCGMKQRHEKGPPHQQER
EVDLHFMKKIPPGAEASNILVGELEFLDRTVVAFVRLSPAVLLQGLAEVPIPTRF
LFILLGPLGKGQQYHEIGRSIATLMTDEVFHDVAYKAKDRNDLVSGIDEFLDQV
TVLPPGEWDPSIRIEPPKNVPSQEKRKIPAVPNGTAAHGEAEPHGGHSGPELQR
TGRIFGGLILDIKRKAPYFWSDFRDAFSLQCLASFLFLYCACMSPVITFGGLLGE
ATEGRISAIESLFGASMTGIAYSLFGGQPLTILGSTGPVLVFEKILFKFCKEYGLS
YLSLRASIGLWTATLCIILVATDASSLVCYITRFTEEAFASLICIIFIYEALEKLFEL
SEAYPINMHNDLELLTQYSCNCVEPHNPSNGTLKEWRESNISASDIIWENLTVS
ECKSLHGEYVGRACGHDHPYVPDVLFWSVILFFSTVTLSATLKQFKTSRYFPTK
VRSIVSDFAVFLTILCMVLIDYAIGIPSPKLQVPSVFKPTRDDRGWFVTPLGPNP
WWTVIAAIIPALLCTILIFMDQQITAVIINRKEHKLKKGCGYHLDLLMVAVMLG
VCSIMGLPWFVAATVLSITHVNSLKLESECSAPGEQPKFLGIREQRVTGLMIFIL
MGSSVFMTSILKFIPMPVLYGVFLYMGASSLKGIQFFDRIKLFWMPAKHQPDFI
YLRHVPLRKVHLFTIIQMSCLGLLWIIKVSRAAIVFPMMVLALVFVRKLMDLLF
TKRELSWLDDLMPESKKKKLEDAEKEEEQSMLAMEDEGTVQLPLEGHYRDDP
SVINISDEMSKTALWRNLLITADNSKDKESSFPSKSSPS

fishCFTR MQRSPVEDANCLSRYFFWWTNPIMRKGFKEKLRPSDVYQAPSQDAADILAER
LEKEWDREVASGKKKPSLLRAMARCYIKPFLLFGFLLYIGEATKTVQPQLLGRI
IASFDPAHEPERANGYFLAFGLGLLFTARFLLLQPAMFGLHHLGMQIRIALFSII
YKKTLKLSSRVLDKISTGQLVSLMSANLGKFDQSLGMAHFIWISPLQCILCTGLI
WELIDVNSFCALAAISLLGVLQAFLSHKMGPYKAQKVLLTNKRLALTSEIMEN
LHSVKAYGWEEIMETLIKNIRQDEVKLTRKIGSLRYFYSSAYFFSAIFVIVAAVV
PHALSRGINLRRIFTTLSYCMVLRMTVTRQLPGSIQMWYDTMRLIWKIEEFLSK
EEYKLMEYDLSITELELQDVTASWDEGPGELLERIKQENKANGHHNGDAGLFF
TNLYVAPVLKDISLKLKKGEMLAVTGSMGSGKSSLLMTILGELVPSSGKIRHSG
RISYSSQTAWIMPGTIRDNILFGLTYDEYRYKSVVKACQLEEDLAALPEKDKTP
MAEGGLNLSGGQKARVALARAVYRDADLYLLDAPFTHLDIATEKEIFDKCLC
KLMASKTRILVTNKIEHLKRADKILLLHNGESFFYGTFPELQSERPDFSSLLLGL
EAYDNISAERRCSILTETLHRVSVDESAGMQPERSAFRQVPPTKPMYIDERKAS
VIVNPLGVARKASFIQVPEEEVRRTLPDRKFSLVPENELVDESFMGSDVYHNHG
VHMAGQRRQSVLAFMTNAQGQGRREHLQSSFRRRLSVVPQSELASELDIYTRR
LSDSTYDMTGILEEENIEACLTDEIDEIEETFETTKWNTYVRYVSNNKSLLYVLI
FILFIAAIEIAGSVAGIFLITDELWREEHQRSEPNMTKHSNASSSGQTYAITVTPTS
SYYILYIYVATSESLLAMGFFRGLPFVHTTITISKKLHQKMLHAVLSAPMSVLN
TMKTGRIMNRFTKDMATIDDMLPLLMFDFVQLTVVVVGCILVVSIVRPYIFLA
ATPLAIIFIVMRKYFLRTGQQLKQLETEARSPIFSHLIMSLKGLWTIRAFERQAYF
EALFHKTLNTHTATWFLYLSTLRWFLFRADILFVFFFTLAAWIAVGTNQDKPG
EIGIIICLAMLILGTFQWCVATSIAVDGMMRSVDRVFKFIDLPSETPKPDKGKDS

DLIIENVDAQADSSWPHRGQIEVRNLTVKYTEAGHAVLKNLSFSAEGRQRVGI
LGRTGSGKSSLFNALLKLVYTDGEISIDGVNWNKMPLQKWRKAFGVVPQKVFI
FTGPLRMNLDPYGCHSDEELWRVAEEVGLKTVIEQFPDKLDFQLEYGGYVLSN
GHKQLICLARSILSGARILLLDEPSAHLDPVTIKVLKKTLRQSFSTCTILLSEHKV
EPLLECQSFLMMDKGQVKTYDSIQKLLNETSHLKQAISPAERLKLFPRRNSSMR
TPQSKLSSVTQTLQEEAEDNIQDTRL

CgiAE-2 MALHGRDNHEDLVSTVFSLPQTTAGHRSSSFPHIHHPLRPLRSKSQKNVRHAD
HHHKKKKKKKKRRMHVNKSFPSKMAVQSPPIPEDNEEEYTSDSDSDSSLSRRN
STASQDFADGPLVITEIGDIDRSSSVDLDKALGDVPLEPPSPSPSSPQLVVPVNGT
PKKKSSGRKVADFFIGENESSPPRDSSKGSMDSKQYKYISDETSQQSDFNMEDQ
FSLLDIGTTEQEPLLSVQAQHKPAGSARSLNEDGRSRVHFSVGGDESSANLLSIN
REGSDPSLSSGNKQNKASIGSLSSGKSSKSHRSKRHHHYDHYKTEDLLLRRQK
GSEVRLDIMMQSEPTEVDEAKMLHKVDLDEMASHRLDNLHGGRRHRLRKNH
SAMSSIVHVGKHKKAKHKIFQPRKKVDHRPHEVFVELDELYEGEGENYEWRE
KARWIKFEEDVEEGAERWGKPHVASLSFHSLLELRRGLENGTMVLDLVAEDL
PSIVTYVVDDLVIHDHIKSEHKGKVLKTLLMKHKHQKEKSLRRSLTSSASFRSS
TSLEKMLDSPTSENLAKKEKEAAQKAKDNEVKNLEFVKVDVDNNLHADGVHI
GITTNESRQKNIQDIMKRIPKDAEALTVLVGCVDYLEKPAMAFVRLAEGQVLD
NLTEVPLPVRFLFILLGPENAMDYHEVGRSISTLMANQHFHDIAYKAISRDELL
HAINEFLDESIVLPPALLKKEEKDKIPLDPIKRTGRLFGGLVNDVKRRYPQYLSD
FKDALHFQCVTSFIFIFFACLSPTIAFGGLLGEKTKEYMGVTETILSTSFSGVLFG
LFSAQPMMILGATGPVLVFEESLYQFCTSYDIEFLPMRFWIGFWVMIITFVVIGL
EGSFLVKNITRFTEEIFTIVISLIFIYEVVKKMKATFYDHPLQVSYTNCGGVGPAY
NVSFNDTKSLDNSTAYSTLSTPENLYHVQQDHAFHDEVPQPNTALLSLVLMLG
TFFIAYFLRIFRNSKFLGRSARRALGDFGVVIALFLMVLLDAITPTVYTQKLIISD
NFEPTDSSKRGWIVPPMGSKKRMNADMIIGASLPAFLLFILLFLETQITEMTLNK
KEFKMKKGSGYHLDQVLLGIITFIGGVFGLPWMCAATVRTLCHVSSLSVYSRY
HAPGEKPKLVKVREQRVTNIAVNLLLGLSLLWGPLLRLIPMAVLFGIFLYVGVS
ALSSLQLYRRMKLLFIPVKHHPSTGYVRRVRTIKMHLFTVIQVLLLALMFGLKL
SSAAIAFPLFVILLIPVRLRIMNYFFSEHELEELPSPRWVGLKCRSVIRQLPSNKS
KETQQGLKVKPNPADNSLPDNEVHSYASTVRQNEELTTNLYCLFESLPQAEVR
VPQAKVIVSQGSTEIPTGQDKGSTGEKVGLMFPQGKVLDPVCHQLFEFYRSKES
ELKTFSRELIPVVIWTYLSALSTSGKKSVRGLEAFLLGVYNLETTLPDGKPNVK
TFRIPTFSQPSIYHEKSFGFTIDIKDTSSTMVQHALGTQEIGPMVVHWSGERDLIV
KGSAASSILQAILSTVLQTFTTEIAELTTQSHHWFCKSCSRIATTGFLSLGDIQSQ
EETAFSLSDSPEPRRRHSQYGDLPPRLAVSPSLIIEMLSGLYYVTFNSQPHLGLK
AIYDLHYRASYELYADVLLVTSAMTNSLQTVVSSSRDSLRGMMAVTPSTSAHS
ISKSAITNASFRAKKLPDDISIVQDEDASKLATIDEDSIETTTSKAAAKSSKFNLA
KAILKGDKSKPKDTKRDSIDHKTSLTNGDAPDSVHVGVVKNNSRVVVDNIEM
QPYNRKNVDHDNNDDKAASSPLIPKPRSTGSISKEMKVKLQDHQRNPSGSSVN
SDNYSTNL

CgiSLC4-1 MPAEADDTGAVMIGVRLPRRQQRPGRSSSSRRHRDQNGHPRSSDASSPTSVSP
SEHIQQLLLENDDTHNVFCQMDTLYTALNEYQWRETARWVKYEEDVEDGGE
RWSKPHVASLSLHSLFELRSSLLMGAVMLDMDAYHITQVADLIIDQLINAKLLE
SNLRDNVRAAITANHAHQHQKRRRSMMPTQQESMADFRKRSMKRNFSNSSA
KLNRNPNSVPENIGDLLSDSASSAKLNQQFMKKIPDGSEAANILVGEMDCLKY
QITAFVRLTEARSIGDLTEVPLPTKFIFLLLGPPGSHNKNVEMGRSMSTMMVDE
VFREVAYRAKSRQDILSGIDEFLDQVTVLPPGEWDPKIRIEPPDKVPSQDPRRQQ
NAKVPEGPKVAAEQIEEEESHIDPTLVRTGRLFGGLVADIKRKIPWYASDFKDC
LHIQCVASTLYLYLATLTPNVTFGGLLGLATNQYMGTMECILTAAIVGILFALF
AGQPLNILGSTGPMLVLEMIVYSFCIDQGWDYMPFRAWTGIWTTVIIMLVVAF

DLSALVRYITRFTEESFACLIAIIFIYEAIKKVIGITKKYPVNLNPEHEYFFNCTCT
PPIDNSTYFNATNLTMAAGPTYAVQEMTTMSYANSSSIDFSTLTEDMCEMYNG
TMVGPDCGHHPYAADVFFLSVILFFGTYVIATSLKDFKTSGYFPSFVRQIFSDFA
VLLAIILMVGLDMAIGIPTPKLEVPENFAPTKPGRPWFINPISDKNPWWVILVSAI
PAFLSTILIFLDQQITAVIVNRKENKLKKGNGYHLDMFVVGICVLICSLLGLPWY
VAATVSALAHIMSLKKESECSAPGEKPVFLGCREQRVTALVVGILSGLSVFMT
KILKVIPMPVLYGVFLFMGVAALKGMQFVDRLALIFMPKKYQPDHMYLRHVPI
KRVHLFTLFQIVCLAILWVVKMIKSISILFPVMVLGTCIVRKLFDYIFEQRELKW
LDDLMPEDKKMAKEDQEMAGDGEKDQLLNEEESKFNYNRVNISEEVNKTGM
WLQVRRSSTREDSLHDKNRKNMKNEENSEKKGQKAAFYFGENA

CgiSLC4-2 MSYSVRGSLLILKKYLYFFKYIELVVTIIFKNSTIVDVYIYLIHSETSMDESDRNN
SANGQFVGVRMPNRRDRPRVVSNGGPKDDSEKYNPSEWVQNLINNVKSEGHK
AHGVFSELDVLKEYNGNIEWREAARWVKYEEVVEEGGKRWSKPHVASLSMQ
TMFNLRKTLKEAPIIIDYDCHTLSQVIDKFTDEWVDSNQLDPRFRPHIRDVALK
GHKHHHVKRAKNQRRGSTTLRPLADIMDESNTGSRANLPSSASMASINSDGLG
SSNSNNDLQEMGMVESPSQSSIATGWKPNTNFLRKIPKDSHVANIMVGEVEDL
PSRVVGFMRLKEPRVLQNDLSEVNIPTRFVFFCLGRRGEEEELIEFGRCMGTMM
VDDIFREVAYKARDRDDLLAGFDEFMEQVIVLPPGEWDPKIRLEPPGKVQSQE
HRRQSVVAGSSGLPGLPLKKPDDAEEESHCDPTLVMSKIPFKGLIDDIRRKVPF
YLSDFKDSLHVQCLGSFVYVFLGTLTPNVTFGGLLGQATDQYMGVMECIFAA
AVTGILFALFSGQPLNILGSTGPMLVLEAIIYNLCKDNDWDFMPMRFWVGMW
TVGFILIIVIFNLSALVKYITRFTEESFATLIAVIFIVEAFKKVIEIGQDSPVNFNPN
APLPSCACVPRDCNITEITTSAALTASTGISTVLPSTTPSIVNYTCADLANMTIDW
ASLSNDTCAMYGSYMEGAGCGVHYVADVFFFSILLFIGTFALALAFIDFKRTTL
FPTMIRQRISDFGVLLAILIMVGVDIAVGIDTPKLIVPEQFKPTRRAQWTVNPFSE
KNPWWLYLAAGIPALLSTILIFLDQQITAVIVNRKENKLKKGVGYHLDMFVVAI
CVGIHSFLGLPWYVAATVSALAHINSLKKESECTAPGEKPSFLGVREQRVTALG
IGILSGCAVLITSVLKYIPMPVLYGVFFYMGFSALRGMQLVDRLFLFVQPVKYQ
PDLPYVRHVPLWRIHIFTIIQVLCLAILWVVKTIKVISIGFPMMVLATGVVRKIIE
CFFQQRELRWLDDLLPGAGKKESEKSVVSKVPYKSFYSSSSNNGSSVDINDKE
DSIKPTFFVSDECDASIMHHRKSNGTGNTKL

SpiSLC26-alpha MKDLGESECPPLITRQRRRRYRINLSRHVYNEQEFTESFINQEEYTASSEFEPSSF
AKTLRRNFLPSRCTCKEILQSWFPIVEWLPAYNVRRDLAHDIAGGITVAIMHIPQ
GLAYALLASLPAVTGLYTAFVPILVYMAMGTSRHISLGTFAVVCLMVGHVVD
REVEHSLSPTPTAPATTNQPPGGSTGVVLQNSIYKHESDGSSLDEQDLLDEKKL
EVAVALSMLVGLLQLLMGLFKLGFVAVYLSDPIISGFTTGAAILVFTSQVKHIL
GLEVPRYSGAFAVVKTYLFMFKNITLSVPGSVITGVVCILILIALKYISEKLKHK
MKFPIPAELIVVVLGTVVSYFVGLNEKFQVSVLHDIPKGLRVPSAPSFMLMGNI
VTDAIVISIVIFATNISLAKTFAKRNNYVIDSNQELIACGSANVLGSFFSCFPVSGS
LSRSVIQESIARTQLCSIPVVVVIIMVLLFIAPLFYHLPKAILAAVVVVALKGLFR
QFSRLVQLWRMCKPDAVVWFAAWLGVVLLGIDIGLGVGVIMALLVVIWKSSR
PPASLLGQIPNTGIYRDIQRIPSAQPIPGIKIFRFESAMFYANSEYFRSTLIEMTGV
DPQNPNKRSRLGSSAVRYRHREEDTGGPAIEITRTVAVSINRAVENGDVEVSLN
DLGNQRSPSGYDPIPTHAIIIDASTFNFIDTQGVNTLLQLGVEYEKIGVKFYLAH
CRYHIREMLEKAGFTARIGTEHLFVSVHDAVTHAVGIHSEDASYSSPVMSDTES
ALGAGPSNQQVEE

SpiSLC26-beta MVKLSSEDLNKMESSPGERSIHRQSPEIDIARNVYDENFFTATKRDRFPLSTKD
DSAKKNYYWRVVHPKLFPCSCSWKGLISFLAGLMPIIRWLPKYNVKEDLFPDL
NGGVTVAVMHVPQGLAFAMLASLPPVTGLYTAIIPVLVYMIMGTSRHLSVGSF
AVICLMVAQVVEREVGSMPLAPTPTPGNDSMSSPSPTEGTALWTPEMSAKME
VALSLSLLVGIIQIIMGAVKMGFLATFLSEPLISGFTTGSAVLVVNSQLKHILGV

KVPQISGAFAAVKIFIHMLKNIPSANVGAIITGVLCLIVLIGLKQVNERYKQKMK
VPIPAELLVVVVGTLISYGAKISLNYGTQIIGDIPKGLPPLSVPSLSRISNIFSDAFV
IAVVIFATNISISKMFAKKRGYSVDPNQELIAYGAGNLAGSFFSCFPICNALART
AVQENLANTQLCSVVVVALVLMVLLFIAPLFFHLPKAILAAVVIANLIGLLKQF
SRLRALWGIYKPDAFVWFFSCFGVILLGVDKGLGVGVICALFAVVLTLSRSSYT
ILGRVTATELYRDVKQCPTAFEVPGVKVLRLESPLYFGNAERFRSALVSTTGLD
PSAEQKAGEEVKQKNDEENNDLLRNEDKGNSNRGNPGSKPKPQEKGGTSTTT
AVKVDEPKNRIHTVVIDCSSFTYIDSVGLHVLPSLLSEFKKAGIHIYLAGCSSLLI
EKFTSSSGEASTQAIPQQAMFPSIHDAVVSAIRSRDHAAWGEDVDKETCF

SpiSLC26-gamma
MSCSALQGKCREFCSPGPVKVFVKKRFPIASWLPEYNLRKLQCDMIAGLTVGL
MVVPQGLAYAQLAGLPQQYGLYSAFMGCFLYCILGTSKDITLGPTAIMSLVVS
AYGKPEIPHYVVALTLYTGIILLAMGFLRLGFVVNFISIPIVSGFTSAATIIIAFSQL
KDLFGLQKIPRKFAQNVYFTFKNIGQTNKWDLTLGLLCIIILITLRKVGRLEWV
KRKDSSDSRWLKAAKKTVWLISISRNALIILIAAVVSSSLYQHGHKDIFTLPSRI
KPGLPLMQVPALSFQVGNATRSTLEVFKDLGPGLAVVPLIGFLESIAIAKAFAR
KNRYTVDASQELIALGVANCLSSFVSSYPVTGSFSRTAVNAQSGVATPAGGIFT
GAIVLLALGLLTDSFKYIPKASLAALIMSSVITMIEYHIVPNIWKVRRIDLVPLAI
TFFGCFYDIEVGILAGIAVALCILLYNVVWPPITRIARGDYVLLKINGNLNYPGV
EHLTNEIQEVAAMEPSPPGIVIDFSLVTSIDFTVTQALLTILEDMENKRIPIFFSGV
QDNVRNMMMNSGIDSGIINQGTQSVIDSINSLEIVEQN

humanSLC26A1
MDESPEPLQQGRGPVPVRRQRPAPRGLREMLKARLWCSCSCSVLCVRALVQD
LLPATRWLRQYRPREYLAGDVMSGLVIGIILVPQAIAYSLLAGLQPIYSLYTSFF
ANLIYFLMGTSRHVSVGIFSLLCLMVGQVVDRELQLAGFDPSQDGLQPGANSS
TLNGSAAMLDCGRDCYAIRVATALTLMTGLYQVLMGVLRLGFVSAYLSQPLL
DGFAMGASVTILTSQLKHLLGVRIPRHQGPGMVVLTWLSLLRGAGQANVCDV
VTSTVCLAVLLAAKELSDRYRHRLRVPLPTELLVIVVATLVSHFGQLHKRFGSS
VAGDIPTGFMPPQVPEPRLMQRVALDAVALALVAAAFSISLAEMFARSHGYSV
RANQELLAVGCCNVLPAFLHCFATSAALAKSLVKTATGCRTQLSSVVSATVVL
LVLLALAPLFHDLQRSVLACVIVVSLRGALRKVWDLPRLWRMSPADALVWAG
TAATCMLVSTEAGLLAGVILSLLSLAGRTQRPRTALLARIGDTAFYEDATEFEG
LVPEPGVRVFRFGGPLYYANKDFFLQSLYSLTGLDAGCMAARRKEGGSETGV
GEGGPAQGEDLGPVSTRAALVPAAAGFHTVVIDCAPLLFLDAAGVSTLQDLRR
DYGALGISLLLACCSPPVRDILSRGGFLGEGPGDTAEEEQLFLSVHDAVQTARA
RHRELEATDAHL

humanSLC26A2
MSSESKEQHNVSPRDSAEGNDSYPSGIHLELQRESSTDFKQFETNDQCRPYHRI
LIERQEKSDTNFKEFVIKKLQKNCQCSPAKAKNMILGFLPVLQWLPKYDLKKNI
LGDVMSGLIVGILLVPQSIAYSLLAGQEPVYGLYTSFFASIIYFLLGTSRHISVGIF
GVLCLMIGETVDRELQKAGYDNAHSAPSLGMVSNGSTLLNHTSDRICDKSCYA
IMVGSTVTFIAGVYQVAMGFFQVGFVSVYLSDALLSGFVTGASFTILTSQAKYL
LGLNLPRTNGVGSLITTWIHVFRNIHKTNLCDLITSLLCLLVLLPTKELNEHFKS
KLKAPIPIELVVVVAATLASHFGKLHENYNSSIAGHIPTGFMPPKVPEWNLIPSV
AVDAIAISIIGFAITVSLSEMFAKKHGYTVKANQEMYAIGFCNIIPSFFHCFTTSA
ALAKTLVKESTGCHTQLSGVVTALVLLLVLLVIAPLFYSLQKSVLGVITIVNLR
GALRKFRDLPKMWSISRMDTVIWFVTMLSSALLSTEIGLLVGVCFSIFCVILRTQ
KPKSSLLGLVEESEVFESVSAYKNLQIKPGIKIFRFVAPLYYINKECFKSALYKQ
TVNPILIKVAWKKAAKRKIKEKVVTLGGIQDEMSVQLSHDPLELHTIVIDCSAI
QFLDTAGIHTLKEVRRDYEAIGIQVLLAQCNPTVRDSLTNGEYCKKEEENLLFY
SVYEAMAFAEVSKNQKGVCVPNGLSLSSD

humanSLC26A3
MIEPFGNQYIVARPVYSTNAFEENHKKTGRHHKTFLDHLKVCCSCSPQKAKRI
VLSLFPIASWLPAYRLKEWLLSDIVSGISTGIVAVLQGLAFALLVDIPPVYGLYA
SFFPAIIYLFFGTSRHISVGPFPILSMMVGLAVSGAVSKAVPDRNATTLGLPNNS

NNSSLLDDERVRVAAAASVTVLSGIIQLAFGILRIGFVVIYLSESLISGFTTAAAV
HVLVSQLKFIFQLTVPSHTDPVSIFKVLYSVFSQIEKTNIADLVTALIVLLVVSIV
KEINQRFKDKLPVPIPIEFIMTVIAAGVSYGCDFKNRFKVAVVGDMNPGFQPPIT
PDVETFQNTVGDCFGIAMVAFAVAFSVASVYSLKYDYPLDGNQELIALGLGNI
VCGVFRGFAGSTALSRSAVQESTGGKTQIAGLIGAIIVLIVVLAIGFLLAPLQKS
VLAALALGNLKGMLMQFAEIGRLWRKDKYDCLIWIMTFIFTIVLGLGLGLAAS
VAFQLLTIVFRTQFPKCSTLANIGRTNIYKNKKDYYDMYEPEGVKIFRCPSPIYF
ANIGFFRRKLIDAVGFSPLRILRKRNKALRKIRKLQKQGLLQVTPKGFICTVDTI
KDSDEELDNNQIEVLDQPINTTDLPFHIDWNDDLPLNIEVPKISLHSLILDFSAVS
FLDVSSVRGLKSILQEFIRIKVDVYIVGTDDDFIEKLNRYEFFDGEVKSSIFFLTIH
DAVLHILMKKDYSTSKFNPSQEKDGKIDFTINTNGGLRNRVYEVPVETKF

humanSLC26A4

MAAPGGRSEPPQLPEYSCSYMVSRPVYSELAFQQQHERRLQERKTLRESLAKC
CSCSRKRAFGVLKTLVPILEWLPKYRVKEWLLSDVISGVSTGLVATLQGMAYA
LLAAVPVGYGLYSAFFPILTYFIFGTSRHISVGPFPVVSLMVGSVVLSMAPDEHF
LVSSSNGTVLNTTMIDTAARDTARVLIASALTLLVGIIQLIFGGLQIGFIVRYLAD
PLVGGFTTAAAFQVLVSQLKIVLNVSTKNYNGVLSIIYTLVEIFQNIGDTNLADF
TAGLLTIVVCMAVKELNDRFRHKIPVPIPIEVIVTIIATAISYGANLEKNYNAGIV
KSIPRGFLPPELPPVSLFSEMLAASFSIAVVAYAIAVSVGKVYATKYDYTIDGNQ
EFIAFGISNIFSGFFSCFVATTALSRTAVQESTGGKTQVAGIISAAIVMIAILALGK
LLEPLQKSVLAAVVIANLKGMFMQLCDIPRLWRQNKIDAVIWVFTCIVSIILGL
DLGLLAGLIFGLLTVVLRVQFPSWNGLGSIPSTDIYKSTKNYKNIEEPQGVKILR
FSSPIFYGNVDGFKKCIKSTVGFDAIRVYNKRLKALRKIQKLIKSGQLRATKNGI
ISDAVSTNNAFEPDEDIEDLEELDIPTKEIEIQVDWNSELPVKVNVPKVPIHSLVL
DCGAISFLDVVGVRSLRVIVKEFQRIDVNVYFASLQDYVIEKLEQCGFFDDNIR
KDTFFLTVHDAILYLQNQVKSQEGQGSILETITLIQDCKDTLELIETELTEEELDV
QDEAMRTLAS

humanSLC26A5

MDHAEENEIPAETQKYLVERPIFSHPVLQERLHVKDKVTDSIGDKLKQAFTCTP
KKVRNIIYMFLPITKWLPAYKFKEYVLGDLVSGISTGVLQLPQGLAFAMLAAV
PPVFGLYSSFYPVIMYCFFGTSRHISIGPFAVISLMIGGVAVRLVPDDIVIPGGVN
ATNGTEARDALRVKVAMSVTLLSGIIQFCLGVCRFGFVAIYLTEPLVRGFTTAA
AVHVFTSMLKYLFGVKTKRYSGIFSVVYSTVAVLQNVKNLNVCSLGVGLMVF
GLLLGGKEFNERFKEKLPAPIPLEFFAVVMGTGISAGFNLHESYSVDVVGTLPL
GLLPPANPDTSLFHLVYVDAIAIAIVGFSVTISMAKTLANKHGYQVDGNQELIA
LGICNSIGSLFQTFSISCSLSRSLVQEGTGGKTQLAGCLASLMILLVILATGFLFES
LPQAVLSAIVIVNLKGMFMQFSDLPFFWRTSKIELTIWLTTFVSSLFLGLDYGLI
TAVIIALLTVIYRTQSPSYTVLGQLPDTDVYIDIDAYEEVKEIPGIKIFQINAPIYY
ANSDLYSSALKRKTGVNPAIIMGARRKAMRKYAKEVGNANIANATVVKVDAE
VDGENATKPEEEDDEVKFPPIVIKTTFPEELQRFLPQGENIHTVILDFTQVNFMD
SVGVKTLAGIVKEYGDVGIYVYLAGCSAQVVNDLTSNRFFENPALKELLFHSIH
DAVLGSQVREAMAEQETTVLPPQEDMEPNATPTTPEA

humanSLC26A6

MGLPDGSDQGTHQTQALLSAAQEMELQRRDYHVERPLLNQEQLEDLGHWGP
AAKTHQWRTWFRCSRARAHSLLLQHVPVLGWLPRYPVREWLLGDLLSGLSV
AIMQLPQGLAYALLAGLPPMFGLYSSFYPVFIYFLFGTSRHISVGTFAVMSVMV
GSVTESLTADKAFVQGLNATADDARVQVAYTLSFLVGLFQVGLGLVHFGFVV
TYLSEPLVRSYTTAASVQVLVSQLKYVFGIKLSSHSGPLSVIYTVLEVCAQLPET
VPGTVVTAIVAGVALVLVKLLNEKLHRRLPLPIPGELLTLIGATGISYGVKLND
RFKVDVVGNITTGLIPPVAPKTELFATLVGNAFAIAVVGFAIAISLGKIFALRHG
YRVDSNQELVALGLSNLIGGFFQCFPVSCSMSRSLVQESTGGNTQVAGAVSSLF
ILLIIVKLGELFRDLPKAVLAAVIIVNLKGMMKQFSDICSLWKANRVDLLIWLV
TFVATILLNLDIGLAVSIVFSLLLVVVRMQLPHYSVLGQVPDTDIYRDVAEYSG
AKEVPGVKVFRSSATLYFANAELYSDSLKEKCGVDVDRLITQKKKRIKKQEMK

LKRMKKAKKSQKQDASSKISSVSVNVNTNLEDVKSNDVEGSEAKVHQGEELQ
DVVSSNQEDAKAPTMTSLKSLGLPQPGFHSLILDLSTLSFVDTVCIKSLKNIFRD
FREIEVEVYIAACYSPVVAQLEAGHFFDESITKQHVFASVHDAVTFALSHRKSV
PKSPVLATKL

humanSLC26A7 MTGAKRKKKSMLWSKMHTPQCEDIIQWCRRRLPILDWAPHYNLKENLLPDTV
SGIMLAVQQVTQGLAFAVLSSVHPVFGLYGSLFPAIIYAIFGMGHHVATGTFAL
TSLISANAVERIVPQNMQNLTTQSNTSVLGLSDFEMQRIHVAAAVSFLGGVIQV
AMFVLQLGSATFVVTEPVISAMTTGAATHVVTSQVKYLLGMKMPYISGPLGFF
YIYAYVFENIKSVRLEALLLSLLSIVVLVLVKELNEQFKRKIKVVLPVDLVLIIA
ASFACYCTNMENTYGLEVVGHIPQGIPSPRAPPMNILSAVITEAFGVALVGYVA
SLALAQGSAKKFKYSIDDNQEFLAHGLSNIVSSFFFCIPSAAAMGRTAGLYSTG
AKTQVACLISCIFVLIVIYAIGPLLYWLPMCVLASIIVVGLKGMLIQFRDLKKYW
NVDKIDWGIWVSTYVFTICFAANVGLLFGVVCTIAIVIGRFPRAMTVSIKNMKE
MEFKVKTEMDSETLQQVKIISINNPLVFLNAKKFYTDLMNMIQKENACNQPLD
DISKCEQNTLLNSLSNGNCNEEASQSCPNEKCYLILDCSGFTFFDYSGVSMLVE
VYMDCKGRSVDVLLAHCTASLIKAMTYYGNLDSEKPIFFESVSAAISHIHSNKN
LSKLSDHSEV

humanSLC26A8 MAQLERSAISGFSSKSRRNSFAYDVKREVYNEETFQQEHKRKASSSGNMNINIT
TFRHHVQCRCSWHRFLRCVLTIFPFLEWMCMYRLKDWLLGDLLAGISVGLVQ
VPQGLTLSLLARQLIPPLNIAYAAFCSSVIYVIFGSCHQMSIGSFFLVSALLINVL
KVSPFNNGQLVMGSFVKNEFSAPSYLMGYNKSLSVVATTTFLTGIIQLIMGVLG
LGFIATYLPESAMSAYLAAVALHIMLSQLTFIFGIMISFHAGPISFFYDIINYCVA
LPKANSTSILVFLTVVVALRINKCIRISFNQYPIEFPMELFLIIGFTVIANKISMATE
TSQTLIDMIPYSFLLPVTPDFSLLPKIILQAFSLSLVSSFLLIFLGKKIASLHNYSVN
SNQDLIAIGLCNVVSSFFRSCVFTGAIARTIIQDKSGGRQQFASLVGAGVMLLL
MVKMGHFFYTLPNAVLAGIILSNVIPYLETISNLPSLWRQDQYDCALWMMTFS
SSIFLGLDIGLIISVVSAFFITTVRSHRAKILLLGQIPNTNIYRSINDYREIITIPGVKI
FQCCSSITFVNVYYLKHKLLKEVDMVKVPLKEEEIFSLFNSSDTNLQGGKICRC
FCNCDDLEPLPRILYTERFENKLDPEASSINLIHCSHFESMNTSQTASEDQVPYT
VSSVSQKNQGQQYEEVEEVWLPNNSSRNSSPGLPDVAESQGRRSLIPYSDASLL
PSVHTIILDFSMVHYVDSRGLVVLRQICNAFQNANILILIAGCHSSIVRAFERNDF
FDAGITKTQLFLSVHDAVLFALSRKVIGSSELSIDESETVIRETYSETDKNDNSR
YKMSSSFLGSQKNVSPGFIKIQQPVEEESELDLELESEQEAGLGLDLDLDRELEP
EMEPKAETETKTQTEMEPQPETEPEMEPNPKSRPRAHTFPQQRYWPMYHPSM
ASTQSQTQTRTWSVERRRHPMDSYSPEGNSNEDV

humanSLC26A9 MSQPRPRYVVDRAAYSLTLFDDEFEKKDRTYPVGEKLRNAFRCSSAKIKAVVF
GLLPVLSWLPKYKIKDYIIPDLLGGLSGGSIQVPQGMAFALLANLPAVNGLYSS
FFPLLTYFFLGGVHQMVPGTFAVISILVGNICLQLAPESKFQVFNNATNESYVDT
AAMEAERLHVSATLACLTAIIQMGLGFMQFGFVAIYLSESFIRGFMTAAGLQILI
SVLKYIFGLTIPSYTGPGSIVFTFIDICKNLPHTNIASLIFALISGAFLVLVKELNAR
YMHKIRFPIPTEMIVVVVATAISGGCKMPKKYHMQIVGEIQRGFPTPVSPVVSQ
WKDMIGTAFSLAIVSYVINLAMGRTLANKHGYDVDSNQEMIALGCSNFFGSFF
KIHVICCALSVTLAVDGAGGKSQVASLCVSLVVMITMLVLGIYLYPLPKSVLG
ALIAVNLKNSLKQLTDPYYLWRKSKLDCCIWVVSFLSSFFLSLPYGVAVGVAF
SVLVVVFQTQFRNGYALAQVMDTDIYVNPKTYNRAQDIQGIKIITYCSPLYFAN
SEIFRQKVIAKTGMDPQKVLLAKQKYLKKQEKRRMRPTQQRRSLFMKTKTVS
LQELQQDFENAPPTDPNNNQTPANGTSVSYITFSPDSSSPAQSEPPASAEAPGEP
SDMLASVPPFVTFHTLILDMSGVSFVDLMGIKALAKLSSTYGKIGVKVFLVNIH
AQVYNDISHGGVFEDGSLECKHVFPSIHDAVLFAQANARDVTPGHNFQGAPGD
AELSLYDSEEDIRSYWDLEQEMFGSMFHAETLTAL

humanSLC26A MRLDLASLMSAPKSLGSAFKSWRLDKAPSPQHTFPSTSIPGMAFALLASVPPVF

10	GLYTSFFPVLIYSLLGTGRHLSTGTFAILSLMTGSAVERLVPEPLVGNLSGIEKE QLDAQRVGVAAAVAFGSGALMLGMFVLQLGVLSTFLSEPVVKALTSGAALHV LLSQLPSLLGLSLPRQIGCFSLFKTLASLLTALPRSSPAELTISALSLALLVPVKEL NVRFRDRLPTPIPGEVVLVLLASVLCFTSSVDTRYQVQIVGLLPGGFPQPLLPNL AELPRILADSLPIALVSFAVSASLASIHADKYSYTIDSNQEFLAHGASNLISSLFS CFPNSATLATTNLLVDAGGKTQLAGLFSCTVVLSVLLWLGPFFYYLPKAVLAC INISSMRQVFCQMQELPQLWHISRVDFLLQVPGLCILSYPTPLYFGTRGQFRCNL EWHLGLGEGEKETSKPDGPMVAVAEPVRVVVLDFSGVTFADAAGAREVVQV RERLASRCRDARIRLLLAQCNALVQGTLTRVGLLDRVTPDQLFVSVQDAAAY ALGSLLRGSSTRSGSQEALGCGK
humanSLC26A 11	MPSSVTALGQARSSGPGMAPSACCCSPAALQRRLPILAWLPSYSLQWLKMDFV AGLSVGLTAIPQALAYAEVAGLPPQYGLYSAFMGCFVYFFLGTSRDVTLGPTAI MSLLVSFYTFHEPAYAVLLAFLSGCIQLAMGVLRLGFLLDFISYPVIKGFTSAAA VTIGFGQIKNLLGLQNIPRPFFLQVYHTFLRIAETRVGDAVLGLVCMLLLLVLK LMRDHVPPVHPEMPPGVRLSRGLVWAATTARNALVVSFAALVAYSFEVTGYQ PFILTGETAEGLPPVRIPPFSVTTANGTISFTEMVQDMGAGLAVVPLMGLLESIA VAKAFASQNNYRIDANQELLAIGLTNMLGSLVSSYPVTGSFGRTAVNAQSGVC TPAGGLVTGVLVLLSLDYLTSLFYYIPKSALAAVIIMAVAPLFDTKIFRTLWRV KRLDLLPLCVTFLLCFWEVQYGILAGALVSLLMLLHSAARPETKVSEGPVLVL QPASGLSFPAMEALREEILSRALEVSPPRCLVLECTHVCSIDYTVVLGLGELLQD FQKQGVALAFVGLQVPVLRVLLSADLKGFQYFSTLEEAEKHLRQEPGTQPYNI REDSILDQKVALLKA
TRINITY_DN1 67317_c0_g3	HHHVYGDFFHEVFPFVDIMRNYSPRKSLLKDFVAGITVGIIHIPQGMAYGFLSG LPPVYGLYTSFFPVIMYFFFGSSKHISMGTFAVTSLMVGAVVERGYDQYSSETT FTSDFSELNSTQVNQTNTTTMSPVADQNFDHIKLGMAMSVTFVAGVIQLLLGIF RLGYLASFLSDPLISGFTCGAAVHVFSSQVSHLFGVPVPNYHGAFKLIYYYRDF FKNLHLTNPVTSTASVTCTFVLILIKEGINNNPTCEPDLLVPVPVELIVVVASTVI SHYTKIHDEFKVEVVGHIPVGLPPMEVTHLGYVWDVIGDSFAIACISFAISYSM AKILAERNDYKINPNQELVASGVCNVFGSMCSSFCSAASLSRSLVQENAGGRS QIVGLFSSSLVLIVLLYLGPMFESLPTCILACVIIVTLKGIFKQFYDMIILWRLCKR DFTVWFVTFLATVILDVGLGLMVGIAFAFFFVLRNSLRPHMCVLGNVPGTSVY RDIATNRTVTEVPGIKIFRFESNLYFANADQFRDRLYDKTKINPRKLKSKKQKT LYKALLQRKRELELAEIEAKAEKKRTKKELEKQKSSIEEEVNKEIPVEWTEEHD QLLAKEKKELKRIFLRAWIPPIHTLIIDCSVVSYLDTVAVKVLTQIFADFKEIGIK VFLAGCREDVRDLLKRTEFYRSVDYNPIYYTVHEAVIIANELNTINLFQREPGR VDMHSIETETDIDQSLATTSGNTYSSANEPQGTESKIKQIQV
TRINITY_DN1 67998_c0_g2	QDILNGIDEFLDQVTVLPPGEWDPKIRIEPPTTVPSQQGRKENKPQPAGPKEAAL IIEEEESHVDPTLVRTGRLFGGLVADIKRKIPWYPSDFKDCLHIQCVASVVYLYL ATLTPNVTFGGLLGLATDNYMGTMECILTAALTGILFALFAGQPLNILGSTGPM LVLEMIIYKFCNDQGWEFLPLRAWVGLWSAFFLLIIVAFDLSALVKYITRFTEES FACLIAIIFIVEAFKKLFAITDKHPYNIHPEIPLDYTCGCYHKNFTMPDHNNATL MNTTSQIAYSVIDMNKGMSTAFNQNETDSNVTDYSKFLTKAKCEEEGGKMMG TGCDTIVYHDNVFFLSIILFLFTFGIAWVLKMSKTSRFFPTFVRQYLSDFAVLISI LCMVCLDLYLGVPTPKLEVPAKFAPSNPKRGWFINPFHPNNPWWTILVAAGPA IVAVILIFMDQQITAVIVNRKENKLRKGNGYHLDMMVVTVCIVICSLFGLPWY VAATVSALAHIMSLRKETESAAPGEKPTFLGVREQRVTALLVGILSGLSVFMTP ILTIIPMPVLYGVFLYMGVAALKGMQLTDRILILLMPTKYQPDHIFLRHVKTTR VHLFTLIQILCLAVLWAIKTTKSISIVFPVMVLGTCFVRKAIEKVFTHDELKWLD DIMPDDSKKKREDEEELKDDDDDDEETESLLGDEKRRLNEMKTIYGQGDKFG GTKTPFAQDRVNITEEVNKTGIWLQVRRDSMPVIRDPDQNNGGLHNRKNGSRE KKAAEKTSFFVGEDERTPLKEEHEEDDMV

TRINITY_DN173725_c0_g1 MSDSNGDIKTVQQTVQNGDVETGSIAETSISNGNEPPKLHQANTFRKEYRQPHS
EDSIKDSCCDHFNSMCNCSSEQLKKGFFKTVPSINIMKKYKIRTDLPNDIIAGFT
VGVMQLPQGMAYAMLADLPPIVGLYVAFFPVLLYYIFGTSKHISMGTVAVVSL
MTGSIVSQLDEKPGVVTLTVEPYNVTGGNYSTTTPGTPDLISALDVEKMALAA
SVCFLVGVIQTLFGVFRLGFVTTYMSDPLVSGFTTGAAVHVFTSQVKYIFGLKI
KRFPNLYQIFNTYKAIIENIGDTNPATIIMSAICIVILYIVKVQVNTRFKKHLKIPIP
VELVVVVIGTLASHYGHFHDTYGMKTVGKVPAGLPLPKIPSFRDATDNFSEAII
VAVVAFAQSVSLAALMAKKHHYRIDSNQEFIAYGVSNIFGSFFSCYPAAASVS
RSSVQESAGGKTQLTSVFSAALVLVVILVIGPLFEDLPNCVLSSIIVVALRSMFM
QLFQLRKLFHVSAYDFVIWIVTFVSVVVFYVDIGLWVGIGFSFVTVVVRTQVA
KARILKKIDPVNAFADESKYIKTRGFSGIRIVGFNAPLYFANGDLFLRQVYTLSD
TKPERVRKQIKRLGSISEFRRQSSLKSLESISSFRSARSDTSTRSSNPGSSLEENGF
LPTSNDLAPMGRPIDTSMADCGYVHHIILDCSAMCFIDTVGGKILKQLCDDYKS
IHVTVLLACICDQAWSVLEKTKFVEKYGDNTYMTVEDAVTAARLASPAEERK
LQIYLETIMEESEINTETQLISDNT

TRINITY_DN175059_c1_g4 MSFNSEESESTPLLRGHRVSVQTTRGQACRRKMVQVGKLARKHISNACCNSEV
WKTRFPITKWILKYRVNDLTSDFIAGLTVAMTVIPQGLAYSTLAGLPPQYGLYS
AFMGCFIYTFLGTSKDITLGPTAIMSLMTATFAMSPIKGDATYAIVLCLMTGVV
QLAMGLLNLGILVNFISHPVINAFTSAAAITIAFGQVEGILGLKNIPRDFLDMVY
ETFKHIPKTNVWDLTMGLSSLVLLILMKKLRVIQWKDDPGTTPSRCVKVARYI
LWLVGTSANAIVVISASGIVAILLSYDVDKLTITGHIKSGLPPVKVPAFSVSDGN
TTISTSEIFTGIGAGFIIVPLLGLVELIAIAKAFSRRNNYKIYPSQELIAIGIANIVSS
FFSSYPVTGSFSRTAVNSQSGVRTPASGIVTGAIILLALQVLTPLFKYIPKSALAA
VIISAVIQMVDYEIPRTLWRVKKLDLIPLVITFISSLAVGIEYGIIIGIGISLIMLLYP
MARPKIKIVPTDANNILVLKINHGLNFPAVDYILEEMEHLSEKDGRYQSVVLDC
SHISEIDFSSIQCIKEMIVEFARRDSKIVFACITEKVFQYIEYADINDLVVSATIKD
GCRILQDELKKELKNGELSHTLGEATVIVDISSHL

TRINITY_DN175808_c1_g5 SIFCELDVLRKHNDNYEWKESARWVKYEENLEEGGKRWSKPHVASLSMHSLF
ELRCAFVEGVVSLDHDAHSLSNVIDKLLEEWQDQNDMDTRLRPHLRDIMLAG
HKHSHIKRSKASKGSRTLSDISDERSEAEKGGNGFHLSSSASLASMDSSGLQSV
PSTQDLSNDPTSPSYKPNLNFMRKIPKDAEAANVMIGEVEDLEQRLVGFMRLK
EPRLLGDVTEVALPSRFVCFMLGPKGSMTQLMELGRCISTMMVDEIFRELAYK
CLDKEEFLAGVDEFMEQVTVLPPGEWDPKIRLEPPSKVPCQNFRKNSVNPLLG
KLLPAEEEGHSIDDPALSWSKIPFKGLIDDVKRKIPHYPSDFKDSLHIQCFASFV
YVFLGTLTPNVTFGGLLGQATDQYMGVMECIFAAAVSGVLFALCGGQPMNIL
GSTGPMLVLETIIYNLCKDNDWDFMPARFWVGMWTVLFILIIVIFNLSSCVKYI
TRFTEDSFATLIAVIFIVEAFKKLFEIEKDYPVNFHPDDPIPFNCSCSSTCNENVTT
ALGALAYGAFTNYTCTGTENFT

TRINITY_DN176772_c2_g1 MSVEGNPKTNGIPDIVIDKDESEVCHFVFCQMDALRPFHDESVWKEVRRWVKF
EEELEEDGKRWSKPHVSSLSMQYLTELHLIVTANPVLLDLEATSMHEIVDLLLE
HWSSDGTLQPLLLNHVRTVLLKKHKHKTLHKHLHNILPKSLPKIKSGIQLSENH
SQSEDEDRDTPNESKSHINQAYNDSSESTETLDSTENGTSDHRNEVALSDGERN
SKFKKKIPPGSEVMNIMVGEVEGLMGNLCAFVRLQTASDIGMITEVDLPTRFLF
ILLVPKGNLEPAEEAARCMGTLITDDIFREVAYKAESEIDLLTGIQEFTSQTTVLP
PGCWNPSTRIEPPHTLPTKETRKAGQSFKKKEPQTHIDATLQRTGRLFGGLVAD
VKRKLPWYKSDFTDGLHIQCFASFIYLFLATLAPNVTFGGLLGDEIDNFMGPME
CILAAAITGVVFALFSGQPMNILGSTGPMLVLEMILYSFCVDRDWDYMPFRCW
VGIWIAFIIFIIVALDLSALVRFITRFTEECFACLIALIFIFQAFENLIKIEDKFPIHFL
ASPTNSCVCENFTIPFNRSTYFNVSEYTTNISNNSAYERDFNISVHDAGTINNSV
LPAYCSKYGGYLTGSGCSDKLYEPNVFFMSCLLFLGTFGIAIFLVNIKGGTFAT
ATIRRTISDFGVLLSIISMVVVDALVGVQTQKLSVPAEFKPSNAARGWFINPWS

DKNPWWLILVAAIPALLTTILIFMDQQITAVIVNRPAHKLRKGGGYHLDMLILG
ILIVVLSLFGLPWYVAATVSALAHIKSLTRESECAAPGEKPTFLGVREQRVTALL
VGILSGFAVLITSVLKFIPMPVLYGVFLYMGVASLKGMQLVQRIKIVFIPPKYQP
DYEYLRHVPLTKVHLFTFIQIICLGVLWAVKSIHEISIIFPVMVLATCFVRKGMD
YFFSEHELKWLDGSPPKKKEIEKEKHIDNTRRRESVSARRERCKSLPASTNMGF
RPHLPSVDETAMNTNNLHAFDKRQRKISLMALPDERTYRKSSERSINSDFQLSV
SCLNRSLSQENTDGIRNQEIFDKRKTRRPSLLAIPSPTLHE

TRINITY_DN177893_c2_g3 MVSESPSMSRSMSVVDGMAVAPGGGVGPTKGRRFSAPSGAFGEESTIFVKRQP
FTQVAFDEIHLKDDIEEDPSLATTLKNNLFCSKKRLWKIISTYLPIIKVLRYYNIK
ESIVTDIMAGITIGILHIPQALAFGLLTSVKVENGLYTSVWPVLLYVIFGTSAHVS
MGTSAVICIVTASVVDRQAENFKATFEFNNATTNFTTWEDIPEFMDYKENISLC
VAMLSGLILLFMGFLRLGFITAYLSESFFNAFTSGAAVHIATSQLPALLGINVKR
FGGAFKIIYTYQEIFSNITSLSWQTPLVALVSIAILLFFKEFINEKFKHKLPIPIPVE
LLVVILATAISYGANLAEEVAVVGEIPGTIPPPVIPDLTGFQDYFVDCFVLAILIF
ANTIAMAKICAKKHNYEIDDSQELIAYGMCNFASSFLKCFPSAVAPPRSMIASN
MGTKSTLAGIFVTILMLLVIMAMSVLFEPLPKAALAAIIVVALKGLFIQMADCR
KFWRINKFDFVIWFFTIVSVVFLDIDFGLGIGVIVSLITVVFQTQFSRGFRVGRTM
KESAFVEHKRYKDSIESNGVKIFRFQSNLYFANAEIFRNNLYKATVNPRKLLKF
LKKQEKNQEREEKRMKKLGIEPPKKDLNALSEVSIIPITGDGRKMSKTSETGVA
TNGNVKKSNSQLALVTGDNPAFAMDEVNLQNNGVQKPYGGLKRPLSIASNLT
SICDDDDEVDPEDGEEFVTDDKIRRMRRTHHIIIDCSTVNYMDSSGANVLGHISS
EYEHVNIKLFLAGVAASVRDTMEHAGTYEKIPQHHIFLELHDAIAVARSKAVV
PLQPFLEDFTYDEAAEESYVTNM

TRINITY_DN179571_c2_g2 MVKITFDLPQEEARVMSDSENHQNGMFPEWEKGSEKSGNSADALHLIETGKPN
GKQHLDFTEHAVVNRYETSESDDEEISLMHGCFEKIPMKDFHAEIRAYKDVED
FLNSTLLLLNLQQSGLTEIIDAMLKKLHENSDDGSEFTLEEARHAIFTQDSVQTL
SRTIQGTTTSEDSGFDFDQSWICAMCELSNLTKRHVVIARLAHPANLGSTSQEV
QLVILVLTPTVEKSTKSALETARTFSTLFIDMDYRHKLLEVQTESEFKQLLQQRT
KLLSSHQGLPENRKSHLVLSDFEKDEAEESKCPLGRGMINDLKRRLPHYWSDY
KDGVFGKRTIHKVISTTFFLYFACVLPNIAFGMLNDSNTAGAIGVQKILFSQCLG
GLLFAVFGGQPLIVLLTTAPLALYTKIIYSISEDFDLDFNAMFACVGLWNAFFLII
YSVFNLSKLMKYSSRSTEEIFSLFIVFAFSADAIKDTVKDFNKNYYSSSCDSLSQ
GSLVNQTNISAVTTVMPSVNDTTTPAGNMIQDCLKENSILFLLLMLGTVWLGIT
LYNFTKTPFLNAGKREMLADYALPVAVLAMSFFGSFVFKDIKLKPFTYRANVE
FFVVAPIHTLPWGAVLGAAGLGFCLSLLFFMDQNISSALVNAPANKLKKGAAY
HWDLFTVAIINAFLSIFTFPWVHAALPHSPLHVKALADMEDRVDQGHVHQIVV
YVRETRLTGIISHIMIGLSLLLLPYPMSYIPRPVLDGLFLYIAITALFGNQMFDRI
MLFFTEQAAYPPNHYIRRVPQRKIHLFTVTQILQLFVLCIFGFSPIPYMKMVFPIL
IMLLMPIRHKLTPKFIEPKYLKALDGH

TRINITY_DN179651_c3_g2 RRQKGSEVHLDKKLQRVPTEADEANLLQTADLDEMASHRLENLQGIRRHKIN
RKKRNAMASIVHIGKADKGKKKFYKEPKKKFDHSPHEVFVELDELYVGESKEF
EWREKARWIKFEEDVEEGAERWGKPHVASLSFHSLLELRRGLENGTMLLDIEA
TDLPTIVNNIIDSMIIHDQIKPENKGNILRTLLLKHKHVGQRENFIRRNFSYMNLR
GLDRYRHQSTKHSLMKSLSTASFNSEASRNSLDHKDKNFSRQDSVREKLLDEN
HDNKGKLEFVKVDVDNNMPSDGVHIGIAPAQDPRQKNIQDIMRRIPKGAEATT
VLVGCVDYLTKPAVAFVRLAEGQYLDNLTEVPLPVRFLFLLLGPENSGMDYHE
VGRSISTLMSNQHFHDVAYKAESRSELLGAINEFLDESIVLPPGDWDQKTLLPI
MDMARKKARQKRKKQQKEEEKQALLEKEKKDKIPLDPLKRTKKIFGGLYYDI
KRRYPHYISDFKDGFNLKCLAAIVFIFFACFAPCIAFGGLLSEKTYDYLGVKETV
ISTSVCGIIFALLAGQPLMLVGATGPVLVFEQSLYMFCKNNNIEFLTMRVWIGF
WVMLISIVAVAAESSVLVRHISRFTEEIFAILISLIFIFEVIKKIDETFKDHPLLLDY

	CAKDNLTNLSSNSNVTLHSVLNVTSLPGYTFANDSFQEEAESDTHYNKYRHYK EVTNRPNTALMSTILTLGTFLIAYFLRIFRNSKFLGRRARRALGDFGIVISIILMV LLDLSIGESVYTEKLHVPPTLEPTLRRGWFVNPVGTKKRIEVYIIFASFIPAALIF MLLYLETQITEMILNKKEFKMKKGSGFHLDMVLVGVMTFMCSLFGLPWMCPA TVR
TRINITY_DN1	MGNSVMPVNKGFRRSNWDISADDKGRPASVQNGILLNISTLQDAPDVSKKLEN
80601_c6_g4	NDLEGKQRMKKEDSELGESLIDITENGHAKMVIDRPIFNQQKLDEGFEAGVRP QSSLKSSCRKACSKCACSKTCCKNFLFGIFPFLSILKGYNVKSDLPSDIISGLTVG IMHIPQGMAYGMLTGLDPVYGLYVSFFPVIVYFFLGTSRHVSMGTFAVACLMV GSAVDKGVAKFGGVFEGCNDTTVSIADVNGTNVTQIGSTGACQDEIKLQVAM AVTLMVGLIQLGMGVAQLGFITTYLSDPLVSGFTTGAACHVFTSQITHVFGIST ARYSGALKLVYTYRDFFTNIPHTNAVTLIASVICMVFLYTIKTYINQNPKIKPRL KMPVPVELIAVVLGTLISYGANLQRDFGVTQVGDIPVGMPIPKVPNFSMIPDVI ADAFAISIVVFAISVSMGKILAKKYDYEINSNQELIAYAACNIVSSFFSAFVSSAS LSRSLVQENVGGKTQVVGLVSSALLLMVLLLLGPYFKTLPKCILASIIIVALQG MFRQFFELQRLWKLSKIDFFIWLSTFLATVLLDVDLGLLVGVVIGLLTIVYRVQ RPYACVLGQIPNTDIYRDVKVYKEAQEFPRLKIFRFENAIFFVSVEHFRNTLYKC TINPRHLKTEISKAKMKAHKQREQQEVEYNIRNSSSNMDGGSMELAPAIDLPE VTVNIPAIPYDIVILDCSTWSFIDSMGVKALTNVIKEYRDVEIDIYLAFCKAGVR EMFEKTGFFDMLDRDKLFPTIHDAVLHTFQAQKKDEPKTETSEDGGPSKDESE TSPLATDGSSTDEGLANQASEDERL
Spu_NBC2	MPIFEKRSENSQDKDRGLLQESPVSSRIRRARGNMNGPVGDDTDVVVDTGAGR ASRHIDNKDISNHRSEEMYAGTDKDRKKGHQNGHASPVSNGPNSPQSPAAQM NFENEVGETPLQRVQFLLGGDGEGRQKDTPPVYSEMEELFYDKEGRLLEWKE TARWVKYEENVEHGAGRWSKPHVATLSLHSLFELRKFIRNGGVQLDMVADD LEQIIDLALDNLVATNVLEEDQRIIAREALLTRHRHHKQKKKKEPENKAYNKG RRKSSMFPGMDRAMSDIGRSQSTGNNTVSMEQEAQEKDGEMRKNSSANALSK MPDGARTESRGSVGRVGTSDSLDQKEKEVKNEKAKFLRKIPAGAEASNVLVG EVDFVEKPMVAFIRLNEGKVLSEITEVPIPTRFVFLLLGPPTTDKKKYREIGRCM ATLMTDDVFHEVAYKARDREDLLAGLDEFLEQVTVLPPGTWDPNIRIEPPKQT LSSEMRRQSQHFTHPIDIIKEEEEDKVELARTGRLFGGLINDIKKKAPFYWSEYY HALNIQCLASFVFMYIACITPIITFGGLLGDATEDYIAAFESLIGAAICGVVYHIFS GQPLTIIGSTGPILIFETIMYQLCGSFGIDYISFRVWIGFWTCVICIVLVATDASAL VRYFTRFTEEAFSSLISFIFIVEAFENLFEISHEYPIKTHVKLGEYFEEHSTNVTDM CMCEYENETIDPAMYNWTEKLTEEDCKTVNGTLVGDCETHHEAVPDVFLFSC ALFFGTFVLSYALKNFRNANFFPTKVRYIISDFGVFMAFLAMTGIDIWVGIPTPK LTVPDTFRPTRADRGWVIPLFNNPWWTYFAAIVPALLCSILIFMDQQITAVIVNR RENKLKKGFGYHLDLLVIAILLFVMSVLGMPWFVAATVLSINHVDSLRVMSDT TIPGEPPKVVGCREQRITGILVFAMIGISSLLTSVLKFIPMPVLFGVFLYMGISSLR GVQFVDRMMLYLIPAKHQPDYVYLRHVKLWRVHLFTLVQLTCLVLLWLIKTS KASIVFPLMVLAVVFVRKLLEFVFTQYELNVLDDVIPESQKRAKDDEEKHLED QREQVTRARTGTLTIALESGQTLTVPAEKVTYNPRDSEPNSDFETAKALSKLSG SPLPTVRNRRAASKTIKDPEANPGANTEEGIDLPSGTGTSSFGVQADMDDTRF

3. Discussion

Within this thesis, I investigated the physiology underlying the rapid rates of larval calcification in the blue mussel *Mytilus edulis*. Previously, it has been proposed that ACC is a transient precursor phase to aragonite, during bivalve larval calcification (Weiss et al 2002). However, more recently, lack of evidence for ACC in D-veliger larval shells has suggested that the composition of larval shell carbonates requires critical review (Kudo et al 2010, Yokoo et al 2011). Using confocal Raman microscopy (CRM), FTIR and polarised light microscopy, I demonstrate that there is no evidence for ACC during bivalve larval shell calcification (Manuscript 1 and discussion part 3.1).

I further examined the abiotic conditions at the mineral interface for the first time in molluscan larvae using calcifying *M. edulis* D-veliger stages (Manuscript 2). Using ion-selective microelectrodes, I demonstrate that *M. edulis* larvae can increase pH_{NBS} by ca. 0.2 pH units and $[CO_3^{2-}]$ by 14 µmol kg^{-1}, beneath the growing shell (Manuscript 2 and discussion 3.3). Using these data to calculate the Ω_{arag} in the calcification space (CS) of *M. edulis* larvae, I demonstrate that these conditions lead to a ~1.5-fold elevation in Ω_{arag} (discussion 3.3). In several bivalve species, larval calcification has been demonstrated to be particularly sensitive to elevated atmospheric pCO_2 (Gazeau et al 2013, Ventura et al 2016, Frieder et al 2017). Microelectrode measurements in the CS of *M. edulis* larvae exposed to elevated pCO_2 concentrations reveal a drop in pH, $[CO_3^{2-}]$ and Ω_{arag} in the CS, which correlates with decreased shell growth and eventually, shell dissolution (discussion 3.4).

Within the Baltic Sea, mussels of the genus *Mytilus* are hybrids of *Mytilus edulis* x *trossulus*, with increasing *edulis* allele frequencies towards the more saline, Western Baltic (Stuckas et al 2009, 2017). Utilizing the *Mytilus* population from Kiel that is characterized by a higher frequency of *edulis* alleles, I investigated the $[Ca^{2+}]$ in the larval CS along a $[Ca^{2+}]$ gradient (Manuscript 3). Impaired PD I shell formation was observed at concentrations <3mM $[Ca^{2+}]$. Larvae originating from an eastern Baltic population exhibited higher tolerance towards low $[Ca^{2+}]$ in their PD I shell calcification in comparison to the population from Kiel, indicating significant potential for local adaptation of shell formation capabilities (Manuscript 3 and discussion 3.5).

Finally, this thesis examines the expression of genes related to ion transport to identify the ionic pathways for substrate acquisition during larval calcification. Using a substrate-limited approach, an ion transport protein with homology to solute carrier (SLC) family 26 is identified and its putative role in calcification discussed (Manuscript 4 and discussion 3.6). In addition, expression of several HCO_3^- and Ca^{2+} transporting proteins is elevated during larval ontogeny and their role in larval shell deposition is discussed (Manuscript 4 and discussion 3.6).

3.1 Role of amorphous precursors in bivalve larval shell formation

3.1.1 No evidence for ACC during larval calcification in *M. edulis*

Amorphous calcium carbonate (ACC) is the least stable polymorph of calcium carbonate (Raz et al 2002). However, several calcifying organisms have been reported to utilize stable forms of ACC as a transient precursor during calcification (Beniash et al 1997, Politi et al 2008, Weiss et al 2002). Previously, ACC has not only been reported as a precursor but a major phase in biogenic carbonates (Addadi et al 2003). ACC has a solubility that is ca. 30 fold higher than the crystalline calcium carbonate polymorph, aragonite (Kurihara 2008) and as a major component of biogenic carbonates, it has been used to infer organismal vulnerability to environmental stress in calcifying organisms. In bivalve larvae, ACC has been reported as a precursor to aragonite for two bivalve species, *Mercenaria mercenaria* and *Crassostera gigas* using Raman and FTIR spectroscopy (Weiss et al 2002). However, more recently conflicting data has been presented in two oyster species, *Pinctada fucata* and *Crassostera nippona* based on FIB-TEM techniques (Kudo et al 2010, Yokoo et al 2011). With this in mind, I aimed to elucidate whether ACC constitutes a majority of larval shell carbonate in the Baltic blue mussel, *Mytilus edulis*.

In *M. edulis* larvae reared at 17ºC, the onset of calcification is observed at 21 hours post fertilization (hpf) based on shell birefringence (Manuscripts 1 and 2). At this ontogenetic stage, using confocal Raman microscopy (CRM), characteristic spectra for crystalline aragonite were recorded *in vivo*, with spectral peaks at 703.1-703.8 and 1086 rel. cm^{-1}. This represents the first *in vivo* phase measurements in a mollusc species and the first investigation of shell composition at the onset of calcification (trochophore stage, 21hpf). The studies conducted within the framework of this thesis do not point towards evidence for ACC as a major carbonate phase prior to or during the process of larval calcification in *M. edulis*. In agreement with the Raman data presented, the FTIR spectra collected on *M. edulis* D-veliger larval shells also exhibited characteristic bands of aragonite, with a v_4 peak at 713 cm^{-1}.

Apart from ACC precursors during larval calcification, ACC has also been detected in adult molluscs close to the periostracum using Raman spectroscopy and FIB-TEM, high resolution TEM and electron energy-loss spectroscopy methods (Jacob et al 2008, 2011). However, cross sections of juvenile *M. edulis* shells reveal a distinctive separation between aragonitic and calcitic areas and nanometer scale CRM scans exhibit no evidence for ACC close to the periostracum. To demonstrate that CRM techniques have a high sensitivity to detect nanometer sized particles of ACC, identical analyses as performed on larval samples were conducted on a synthetic ACC – aragonite mixture. These data illustrate that had ACC been present, CRM techniques would have detected ACC. Similarly, the presence of biogenic ACC has been

established using CRM in several taxa, including marine species, lending additional support to the CRM techniques applied in Manuscript 1 (Hild et al 2008, Raz et al 2002, Weiner et al 2003, Wehrmeister et al 2010).

3.1.2 Conflicting data with key study on mollusc larval shell composition

The key paper defining the composition of mollusc larval shells, and suggesting the presence of ACC as a precursor phase during larval calcification is presented by Weiss et al (2002). Inferences of ACC precursors were based on Raman and FTIR spectroscopy analyses on the veliger larval shells of *Mercenaria mercenaria* and *Crassostera gigas*. However, using the same techniques, no evidence for ACC in the veliger shells of *M. edulis* was detected (Manuscript 1). This apparent conflict in our data to those presented in Weiss et al (2002) can be attributed to several issues that will be discussed in the present section.

Weiss et al (2002) infer the presence of ACC in *M. mercenaria* larval shells based on the presence of the Raman peak at 1087 rel. cm^{-1} in Raman spectra (Fig. 3.1). However, a peak at 1087 cm^{-1} in Raman spectra is typically assigned to crystalline polymorphs such as calcite and aragonite, whereas the characteristic peak for ACC is ca. 8 cm^{-1} lower (1079 cm^{-1}) (Raz et al 2002, Rodriguez-Blanco et al 2008). This is illustrated in Fig. 3.1, where the v_1 peak for carbonates in biogenic ACC acquired from the spicules of the tunicate, *Pyura pachydermatina* shows a distinct shift to the left in comparison to the v_1 peak measured from *M. mercenaria* larval shells in Weiss et al (2002). Furthermore, weak peaks or the absence of peaks at 156 and 205 cm^{-1} (lattice modes) and subsequent analyses of peak height ratios (205 cm^{-1}/1085 cm^{-1}) were construed to be indicative of ACC in *M. mercenaria* larval shells (Weiss et al 2002). However, peak heights at these positions (the lattice modes of calcium carbonate) are influenced by the orientation of crystallites as described by Nehrke and Nouet (2011). Additionally, the peak heights at the lattice modes can be related to high background to signal ratios. To illustrate this, I performed CRM analyses using two different objectives, a 20x and a 60x water immersion objective with a high numerical aperture (reducing background) and demonstrated the effect of background to signal ratios on peak heights in spectra collected from the same *M. mercenaria* larval shell (Manuscript 1).

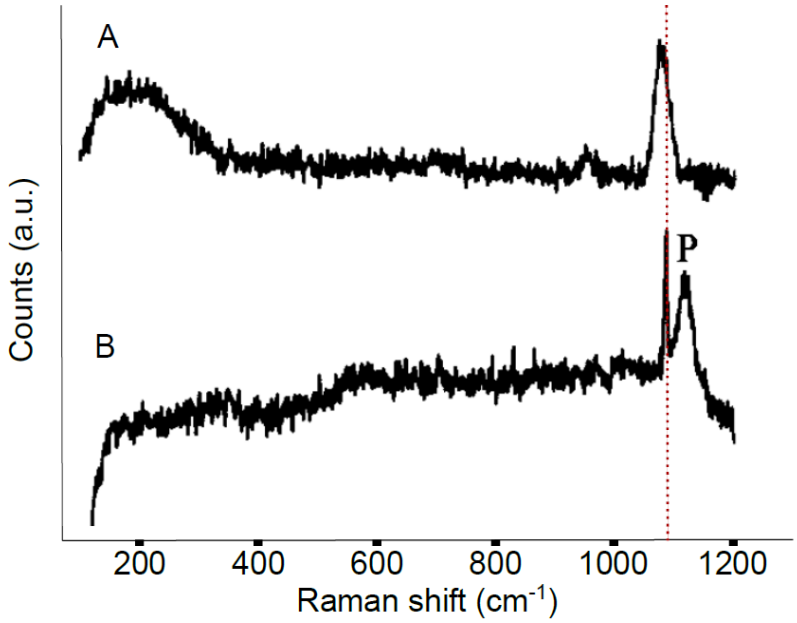

Figure 3.1. The Raman data presented in Weiss et al (2002) (A) Raman spectra of ACC in the spicules of *Pyura pachydermatina* which was used as reference spectra for ACC. (B) Raman spectra of a nine day old *Mercenaria mercenaria* larval shell. The red line has been plotted to indicate the difference in peak positions of the CO_3^{2-} peaks in the two spectra demonstrating that *M. mercenaria* shells are composed of a crystalline calcium carbonate polymorph.

Finally, repeated CRM analyses on the same *M. mercenaria* larval shell also highlights the importance of the focal plane that Raman spectra are collected from when investigating presence of ACC in wet samples. This is due to the spectral similarities between ACC and water between wavenumbers 100-300 cm^{-1}, where the key difference is that spectra for water are not accompanied by a v_1 peak for carbonate, as observed for ACC. In light of these differences in Raman spectral interpretation, Manuscript 1 re-analysed the shells of both species (*M. mercenaria* and *C. gigas*) studied by Weiss et al (2002) for presence of ACC. Inference of ACC in *C. gigas* by Weiss et al (2002) is based on FTIR spectroscopy due to high intrinsic fluorescence in their Raman setup for shells from this species. However, using a 488 nm laser, Raman spectra could be collected for *C. gigas* larval shells in this thesis. CRM analyses exhibited characteristic spectra for aragonite in larval shells of both species. Weiss et al (2002) infer the presence of ACC in *C. gigas* larval shells based on peak height ratios of FTIR peaks at 856 cm^{-1}/713 cm^{-1} in FTIR spectra. However, such ratios have been empirically demonstrated to be related to crystallite size (Kristova et al 2015). In other calcifying taxa, the characteristic FTIR peak at 713 cm^{-1} is typically attributed to presence of crystalline calcium carbonate polymorphs (Hodson et al 2015). In contrast, absence of a peak at 713 cm^{-1} is characteristic of ACC phases (Aizenberg et al 2002, Salter et al 2017), where its appearance can be empirically induced *in vitro* by the addition of water, from resulting crystallization (Khouzani et al 2015).

3.1.3 An alternative model of bivalve larval shell formation

Evidence from the present thesis suggests that the major mineral phase during biomineralization in *Mytilus* larvae and juveniles is crystalline calcium carbonate. Additionally, the three other bivalve species also investigated in this thesis secreted aragonitic shells, with no evidence for ACC. Based on a similar lack of evidence for ACC during bivalve larval calcification, it has been suggested that molluscan larvae may utilize seed crystals to initiate shell formation (Yokoo et al 2011). Direct precipitation of seed crystals onto an organic matrix template is suggested to induce the subsequent inorganic precipitation of carbonate mineral (Yokoo et al 2011). Based on this novel hypothesis and the observations in this thesis, the direct deposition of crystalline aragonite may be an alternative mechanism for initial shell formation in bivalve larvae. These results indicate that the observed sensitivity of larval bivalves to anthropogenic stressors such as ocean acidification (Gazeau et al 2013, Waldbusser et al 2013, 2015, Ventura et al 2016) is not related to the high solubility of ACC. Rather, the high sensitivity of larval bivalves and their empirically observed calcification responses to seawater acidification may be driven by the reduced ability of these organisms to modulate the carbonate chemistry of their calcification space (Manuscript 2), limited maternally derived energy reserves (Waldbusser et al 2013) and the very high rates of shell deposition during larval life stages (Waldbusser et al 2013, Galtsoff, 1964). Alternatively, the rapid transformation of ACC precursor phases to aragonite cannot be excluded. Rapid transformation of ACC to crystalline polymorphs in molluscs is suggested by DeVol et al (2015), where authors attribute the presence of ACC precursor phases limited to nanometer sized particles in the nacreous layer of the red abalone (*Haliotis rufescens*) shell to rapid crystallization of ACC.

3.2 No evidence for intracellular larval calcification

Experiments within this thesis investigated the pathways for substrate acquisition from seawater for larval calcification using the fluorescent dye, calcein and confocal microscopy. The accumulation of calcium during the course of development was measured using flame photometry (Fig. 1a, Manuscript 2). Prior to the onset of calcification, during the eighteen hours of development, a small increase in larval calcium content by ca. 3-fold is observed. Between 22-40 hpf, an exponential, 250-fold increase in larval calcium content is observed which is accompanied by the initial presence of calcein-positive particles on the organic cover of the larval shell. These data illustrate that mussel larvae do not accumulate a significant reservoir of calcium prior to calcification. Continuous deposition of a mineralized larval shell is observed by the extension of the calcein label. The appearance of a calcein label in the larval shell is supplemented by the presence of a calcein label in several intracellular vesicles all over the

surface of the larval body. In order to determine the role of these vesicles in larval calcification, larvae were reared in filtered seawater containing calcein at various stages of shell deposition during the first two days of development. Larvae exposed to calcein between 0-20 hpf (prior to calcification) and subsequently reared in calcein-free seawater until 48 hpf exhibited the calcein-positive vesicles and the absence of a calcein label in the PD I shell. Larvae reared in calcein in several time series experiment ranging between 15-180 minutes during the shell formation and then cultured in non-labeled FSW for several more hours were observed to comprise a calcein label in the shell and in intracellular vesicles. However, the intracellular vesicular calcein label was not transferred to the larval shell once calcein from the culture media was removed. These observations suggest that large intracellular vesicles do not play a role in larval calcification in the mussel, *Mytilus edulis*. This is in contrast to calcifying sea urchin larvae, where intracellular calcein labelled vesicles have been observed to transport mineral to the site of calcification (Vidavsky et al 2015).

3.3 Abiotic conditions of the bivalve larval calcification space

For a comprehensive understanding of the conditions enabling the rapid larval shell formation processes, the abiotic conditions characterizing the calcification space (CS) of mollusc larvae need to be identified. The ion-sensitive microelectrode measurements of pH, $[CO_3^{2-}]$ and $[Ca^{2+}]$ performed in this thesis provides the first direct evidence for actively modulated carbonate chemistry in molluscan larvae at the tissue-mineral interface (Manuscript 2). *M. edulis* larvae exhibited an elevation in pH, $[CO_3^{2-}]$ and $[Ca^{2+}]$ at the CS with respect to the surrounding seawater by 0.2 pH units, 14 $\mu mol\,kg^{-1}$ and by ca. 0.1 $mmol\,kg^{-1}$ respectively. According to equation 1, these abiotic conditions resulted in an increased Ω_{arag} at the CS to ca. 2.2) from seawater values of ca. 1.4 and may maintain structural integrity of the early shell by preventing dissolution. In addition, using equation 2, an elevation in Ω_{arag} will also elevate mineral precipitation rates by a factor of ca. 2.7 (Manuscript 1). Such elevations in pH and Ω_{arag} at the tissue-mineral interface in *M. edulis* larvae is comparatively different to adult mussels, where the pH and Ω_{arag} of the extrapallial fluid are lower than the respective seawater values (Thomsen et al 2010, Heinemann et al 2012). Similar increases in pH, $[CO_3^{2-}]$ and $[Ca^{2+}]$ have been recorded at the CS of coral polyps, in comparison to surrounding seawater (Al-Horani et al. 2003, Cai et al 2016). The acid-base regulatory mechanisms facilitating these abiotic conditions are largely unexplored in bivalve larvae. The synchronous increase of pH and Ca^{2+} in the CS of other organisms has been related to the active transport of Ca^{2+} in exchange for protons by means of an ATP driven calcium-proton exchanger (Kingsley and Watabe 1987, McConnaughey and Falk 1991, McConnaughey and Gillikin 2008, Waldeck-Weiermair et al 2011). However, the role of

active calcium-proton exchangers in mollusc biomineralisation is under debate, where functional characterization for this pathway is limited to mammalian cell types (Niggli et al 1982). In calcifying sea urchin larvae, proton extrusion via the H^+/K^+-ATPase (HKA) pathway has been demonstrated to be crucial for calcification processes, where pharmaceutical inhibition of the HKA specifically impedes cellular ion concentrations and voltage potentials of calcifying cells and inhibits spicule elongation and branching (Schatzberg et al 2015). The specific role of HKA in sea urchin larval calcification is further supported by data from Stumpp et al (2015) where the authors demonstrate that this cellular pathway does not play a key role in gastric alkalization, another key acid-base process in sea urchin larvae. Gene expression analyses during oyster ontogeny suggest that all typical pH regulatory proteins that are generally employed for acid-base regulation are expressed in bivalve larvae (Zhang et al 2012). The role of these various pathways in larval calcification and pH elevation of the calcification space are discussed in section 3.5.

3.4 Impact of elevated pCO_2 on carbonate chemistry of the calcification space in *Mytilus edulis*

Despite the extensive literature regarding the effects of anthropogenic seawater acidification on bivalve larvae, the underlying mechanisms driving the sensitivity of these organisms to acidification stress are still unknown. Larval calcification in particular has been demonstrated to be negatively impacted in several bivalve species, with decreases in calcification rates and increased shell dissolution and malformation (Gazeau et al 2013, Waldbusser et al 2013, 2015, Ventura et al 2016, Frieder et al 2017). Therefore, in order to determine how seawater carbonate chemistry affects the carbonate chemistry of the calcification space in bivalve larvae, we reared *M. edulis* larvae under simulated OA conditions and determined the abiotic conditions in their calcification space using ion-selective microelectrodes (Manuscript 2). Microelectrode measurements demonstrate that pH in the calcification space (pH_{CS}) and seawater (pH_{SW}) declined linearly with increasing pCO_2. In *M. edulis* larvae, elevated pH_{CS} relative to pH_{SW} could be maintained up to pCO_2 values of about 1500 µatm. At such pCO_2 conditions (1500 µatm), proton gradients between the calcification space and seawater could not be maintained by increased rates of proton removal. The sigmoidal collapse of proton gradients between the calcification space and seawater highlights the sensitivity of larval ion regulatory capabilities. Carbonate sensitive microelectrodes indicated a continuous decline in $[CO_3^{2-}]$ in the calcification space from ca. 100 to 39 µmol kg^{-1} with increasing pCO_2. However, calcium in the calcification space ($[Ca^{2+}]_{CS}$) remained constant over the entire range of pCO_2 levels tested. The progressive decline in $[CO_3^{2-}]_{CS}$ over the range of pCO_2 values investigated resulted in an exponential

decline in Ω_{arag} at the calcification space (by using equation 1). However, we observe that mussel larvae exhibit a significant offset for the point when Ω_{arag} reaches undersaturation in their calcification space (ca. 999.5 µatm) in comparison to external seawater (ca. 723.6 µatm). In conjunction with the continuous decrease in Ω_{arag} in the calcification space, rates of mineral precipitation also decreased linearly, as observed by a decrease in larval shell lengths (Manuscript 1). This is similar to results observed on other bivalves species (Talmage and Gobler 2010, Gobler and Talmage 2014, Waldbusser et al 2015) and also in accordance with equation 2, describing rates of mineral precipitation in relation to Ω_{arag}.

In the context of present conditions, recent records of pCO_2 in Kiel Fjord show regular elevations above 2000 µatm during summer and autumn (Fig. 3.2, Thomsen et al 2017a, Hiebenthal et al. 2016), levels for which we found an impaired ability to regulate pH and carbonate in the calcification space in *M. edulis*. Short term fluctuatios in pCO_2 were observed to occur during the natural spawning season of adult *M. edulis* and were followed by subsequent successful juvenile recruitment (Fig. 3.2, Thomsen et al 2017a). Therefore, despite hindered ability for extracellular pH regulation, *M. edulis* are able to cope with chronic exposure to low pH during larval development (average pCO_2 during larval development: >1000 µatm, Thomsen et al 2017a). Our results suggest that although shell growth is affected, there appears to be no shell dissolution for conditions up to 2000 µatm. Recent research demonstrates that although larval shell lengths (PD I) decrease under OA, there is potential for adaptation in *M. edulis*, where evolutionary responses to seawater acidification in larval survival are observed in populations that are periodically exposed to seawater acidification due to seasonal upwelling (Thomsen et al 2017a). Adaptive potential of bivalves to OA has also been demonstrated in oysters based on selective breeding techniques that have resulted in improved growth rates (Nell and Perkins 2005). Therefore, there may be an ability to control Ω_{arag} at crystal nucleation sites or modulate the composition and fraction of the organic layer to prevent shell dissolution during early life stages. This modulation of the organic matrix and regulation of Ω_{arag} at crystal nucleation sites may be accompanied by altered energy budgets of *M. edulis* larvae. Recently it has been reported that bivalve larvae are not energetically limited to secrete the first shell (PD I) by maternally derived energy reserves, under conditions of ambient pCO_2 (Frieder et al 2017). However, an increased metabolic cost of shell deposition can be expected due to costs associated with maintaining shells under conditions of high seawater pCO_2 (Frieder et al 2017). Previously, it has been demonstrated that the metabolic cost for producing the organic component of the shell in mussels is relatively high although it comprises a small fraction of the shell (Thomsen et al 2013). Further, secreting a thicker periostracum to offset shell dissolution, will elicit drastic increases in energy required for shell production (Palmer 1983, 1992).

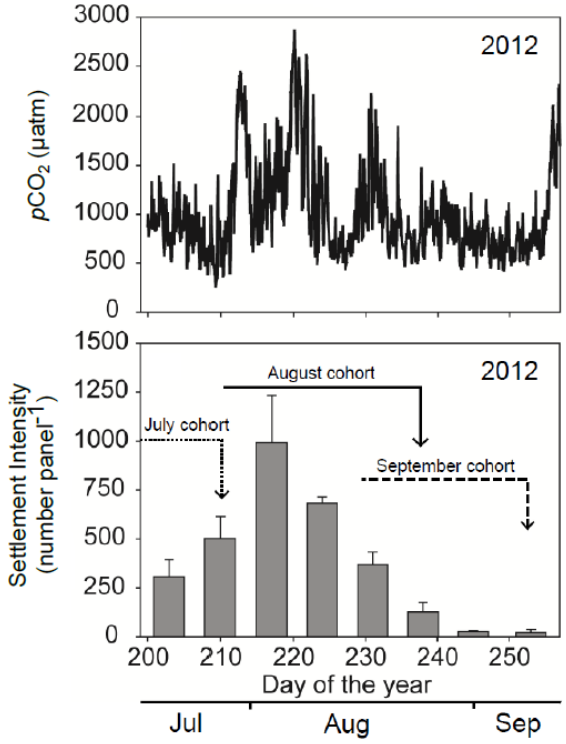

Figure 3.2 Variability of the carbonate system in Kiel Fjord and accompanying settlement of juvenile mussels, *M. edulis*. Top panel illustrates pCO_2 variability during the summer of 2012 in Kiel Fjord and the bottom panel reports the larval settlement intensity on panels between July and September. Arrows illustrate the corresponding planktonic phases of larvae settled in July, August and September that have experienced conditions of elevated seawater pCO_2. Adapted from Thomsen et al (2017a).

3.5 Seawater [Ca^{2+}] determines Baltic *Mytilus* larval success

Blue mussels in the Baltic Sea are *Mytilus edulis* x *trossulus* hybrids with increasing *edulis* allele frequency towards the western Baltic, which is characterized by a relatively higher salinity (Stuckas et al 2017). Manuscript 3 examined the influence of seawater chemistry on the [Ca^{2+}] dynamics of the larval calcification space and shell formation in the Baltic *Mytilus* sp. complex.

Experiments within Manuscript 3 reveal that Baltic *Mytilus* larval PD I shell formation is limited at seawater [Ca^{2+}] concentrations less than 3mM, which corresponds to a salinity of 8 g kg^{-1} according to (Kremling and Wilhelm 1997). Interestingly, larval shell formation in the low salinity-adapted eastern Baltic *Mytilus* population appeared to be more tolerant to reduced [Ca^{2+}] since larvae were observed to accrete larger PD I shells at comparable [Ca^{2+}] than larvae from the western Baltic population. In addition, PD I formation was successfully accomplished at seawater [Ca^{2+}] of 1.1 mM in the low salinity-adapted eastern population (Manuscript 3).

Calcium-sensitive microelectrode measurements of in the CS of the western Baltic *Mytilus* sp. population revealed that $[Ca^{2+}]_{CS}$ declined with seawater [Ca^{2+}]. Larvae reared under $[Ca^{2+}]_{SW}$ of 3.5 mM exhibit significant elevated $[Ca^{2+}]_{CS}$ by 0.1 ± 0.01 mM with respect to seawater. Further

decreases in $[Ca^{2+}]_{SW}$ between 2.3-2.6 mM were not related to elevated $[Ca^{2+}]_{CS}$. However, larvae reared under $[Ca^{2+}]_{SW}$ of 1.5 mM exhibited an enrichment of $[Ca^{2+}]_{CS}$ by 0.28 ± 0.02 mM. Therefore, enrichment of $[Ca^{2+}]_{CS}$ under conditions of low $[Ca^{2+}]_{SW}$ may enable increased Ω_{arag} at the mineral interface to maintain shell deposition when undersaturated conditions prevail in surrounding seawater, as observed in Manuscript 2.

Manuscript 3 demonstrates that $[Ca^{2+}]$ is a crucial factor driving larval shell formation and distribution of bivalves in low saline environments such as the Baltic Sea. The distribution of blue mussels in the Baltic Sea has previously been demonstrated to be limited below salinities of 4.5‰ (Westerbom et al 2002), which corresponds to $[Ca^{2+}]$ of 1.8 mM, where PD I shell formation was observed to be significantly compromised (Manuscript 3). The low salinity conditions prevailing in large parts of the Baltic Sea represent a significant limitation to the successful recruitment of bivalve larvae, whose calcification response is impaired under such low $[Ca^{2+}]$ conditions, hindering overall larval performance. In addition, projected reductions in the salinity of the Baltic Sea due to increased freshwater inflow (Meier et al 2006) will likely impair *Mytilus* larval calcification performance due to concomitant decreases in seawater $[Ca^{2+}]$. Finally, the interaction between the limiting low salinity conditions and projected increases in seawater pCO_2 will present a significant challenge to successful recruitment of Baltic *Mytilus* larvae, where independently, these factors have been associated with impaired larval performance (Thomsen et al 2010, Barton et al 2012, Waldbusser et al 2015). The limited data on the interactive effects of OA and salinity suggest significant reduction in larval growth rates and metamorphosis (Ko et al 2014).

3.6 Acid-base regulation during larval calcification

3.6.1 Identification of candidate genes involved in ion transport during larval calcification

The widespread observances of negative impacts of anthropogenic seawater acidification on calcifying organisms have stimulated an interest in the genetic mechanisms that define organismal sensitivity (Parker et al 2013, Kelly et al 2016). In bivalve larvae, previous studies have examined the molecular responses of larvae reared under elevated pCO_2 and observed no significant differences in expression of genes in comparison to larvae reared under present-day conditions of pCO_2 (Kelly et al 2016). However, these studies have observed reductions in larval size and shell length under OA stress.

In order to identify key ion transport proteins involved in larval calcification, gene expression patterns were examined with respect to substrate-limitation (low C_T) and developmental stage (20, 22, 24, 27, 30 and 35 hpf) in Baltic *Mytilus edulis*-like larvae. To appropriately compare gene expression patterns between larvae reared under ambient and low C_T, larval stages with

similar percentage shell cover during ontogenetic development (Table 1 and Fig. 1, Manuscript 4) were compared. Differential gene expression analyses revealed that substrate-limitation only induced differential expression in fifty three genes throughout ontogenetic development (Supplementary Table S2, Manuscript 4). Of these genes, only one contig was characterized to be an ion transporter of interest with an annotation to SLC26 family of anion transporting proteins (Fig. 6, Manuscript 4). This contig (TRINITY_DN175059_c1_g4) shared a close homology to the human SLC26A11 sulfate/anion transporter and the SLC26 γ isoform anion transporter in coral *Stylophora pistillata* (Fig. 6, Manuscript 4). The function of SLC26 anion transporting proteins in bicarbonate transport during calcification has been previously proposed by Kenkel et al (2013). The cellular function of the SLC26A11 family of transport proteins has recently been reviewed (Rahmati et al 2013). Electrophysiology techniques in mice neurons suggest a role of SLC26A11 proteins in chloride translocation and activation of V-type proton ATPases (Rahmati et al 2013). Alternatively, SLC26A11 transporters may also play a role in the acquisition of sulfate for the synthesis of sulfated macromolecules such as proteoglycans present in the organic matrix of mollusc shells (LeRoy and Marie 2012). The production of such sulfated macromolecules has been postulated to enable crystal nucleation (Cuif et al 2003, Cuif and Dauphin 2005).

The low number of differentially expressed genes under conditions of low seawater C_T (50% decrease compared to control conditions) is, in part, explained by the sensitivity thresholds of the experimental design (coefficients of variation 190%). The high variability in gene expression between Baltic Sea mytilid families or individuals is consistent with previous studies (Hüning et al. 2013, Yarra et al. in prep.) and suggests that more subtle changes in gene expression were not detected with the present experimental design. Lack of differential gene expression is consistent with previous studies on calcifying larvae that observe no significant changes in gene expression in response to conditions of unfavorable seawater carbonate chemistry (Evans et al 2013, Kelly et al 2016) and may indicate a fixed capacity to alter the transcriptomic programme during larval development. In contrast, adult bivalves have been observed to exhibit differential regulation of genes related to ion and acid-base regulation in response to elevated seawater pCO_2 (Li et al 2016). Alternatively, acid-base regulation may be ensued via the translocation of membrane bound transport proteins to compensate for increased transport of calcification substrates. Such changes in cellular acid-base machinery have been described in detail for elasmobranch species (Tresguerres et al 2007, Roa et al 2014). In addition, it has been demonstrated that absence of significant transcriptomic responses of ion regulatory proteins is not correlated to *in vivo* physiological activity of membrane bound ion transporters. This has been demonstrated in calcifying sea urchin larvae in response to seawater acidification, where

expression and *in vivo* activity of the Na^+/K^+-ATPase (NKA), a protein that is the drives the electrochemical gradient necessary for subsequent transport of ions by secondary transport proteins (Boron and Boulpaep 2009) are not correlated (Pan et al 2015).

3.6.2 Cellular pathways involved in substrate acquisition during ontogenetic development

During the course of larval development in *M. edulis*, highest transcript abundance was observed for genes encoding bicarbonate transport proteins, with a peak in expression of sodium bicarbonate cotransporters at stage 2 (onset of calcification). Following the onset of calcification at 22 hpf, 245 ion transport genes were differentially expressed in comparison to pre-calcifying larval stages (Supplementary Table S4, Manuscript 4). Elevated transcript abundances of seven contigs encoding ion transport proteins including voltage gated calcium channels, sarco/endoplasmic reticulum calcium ATPases (SERCA) and a SLC4 bicarbonate transporting protein were observed, suggesting putative roles in calcification. Further analyses of gene expression profiles throughout the process of larval shell calcification highlighted several cellular ion transport pathways of interest. Since the focus of this thesis is the mechanisms of substrate acquisition during larval calcification, the following section will discuss gene expression patterns of contigs encoding HCO_3^- and Ca^{2+} transport proteins in the larval *M. edulis* transcriptome. However, the expression profiles of other ion transport proteins (Na^+, H^+, Cl^-, K^+) and shell matrix proteins is discussed in detail in Manuscript 4.

HCO_3^- Acquisition

The transport of HCO_3^- via membrane bound transport proteins occurs through two key cellular pathways: the SLC4 and SLC26 transporters. These families of ion transporting proteins are further classified based on the mechanism of action and stoichometries where the group of SLC4 transporters is characterized into three major groups: Cl^-/HCO_3^- exchangers (also known as anion exchangers, $Na^+-HCO_3^-$ cotransporters and Na^+-driven Cl^-/HCO_3^- exchangers (Romero et al 2013). Within SLC4, transport of HCO_3^- may occur electroneutrally via the anion exchangers or electrogenically via the sodium bicarbonate cotransporters (Romero et al 2013).

In contrast, the SLC26 family of ion transport proteins is responsible for the transport of a broad variety of anion such as sulfate, oxalate, formate in addition to HCO_3^- (Soleimani 2013).

As discussed previously, among all contigs encoding ion transport proteins that exhibited differential gene expression profiles during the course of development, contigs annotated to sodium bicarbonate cotransporters exhibited the highest transcript abundance with a peak in expression during early calcification (Fig. 2, Manuscript 4). Phylogenetic analyses of the sodium bicarbonate cotransporters with enriched transcript abundances in the *M. edulis* larval

transcriptome clustered with SLC4 homologs in human (SLC4A10), the coral, *Stylophora pistillata* (δ isoform) and the sea urchin, *Strongylocentrotus purpuratus* (Fig. 6, Manuscript 4). Two contigs encoding sodium bicarbonate cotransporters that are expressed in the *M. edulis* larval transcriptome have also been observed to exhibit increased expression during induced shell repair in adults (Yarra et al, in prep). In addition, the peak in expression of NBC contigs is accompanied by the onset of accumulation of calcium by mussel larvae (Ramesh et al 2017). Together, these data support the role of sodium bicarbonate cotransporters during substrate acquisition for larval calcification.

Ca^{2+} Acquisition

The observations of calcium accumulation kinetics in *M. edulis* larvae during the formation of the PD I shell demonstrates that prior to the onset of calcification during the trochophore stage, calcium is not accumulated and stored in *M. edulis* larvae (Manuscript 2). In addition, the calcein labelling experiments performed on calcifying *M. edulis* larvae demonstrate that acquisition of calcification substrates Ca^{2+} and HCO_3^- from seawater does not occur via an endocytotic transport pathway (Manuscript 2), as has been previously described for sea urchin larvae (Vidavsky et al 2015, 2016). These observations suggest substrate acquisition for calcification must occur via the transcellular or paracellular pathway in larval *M. edulis*. In agreement, Manuscript 4 reports the elevated expression of four transmembrane proteins involved in calcium transport: SERCA, calcium channels, sodium/calcium exchangers (NCX) and calcium uniporter proteins. As larval development and PD I shell calcification progressed, the expression of these four calcium transporting proteins increased and contigs encoding SERCA and NCX exhibited the largest changes in expression. SERCA has been postulated to play a role in adult bivalve calcification, due to its high expression and localized presence of one isoform in adult bivalve mantle tissue (Truebano et al 2010, Fan et al 2007). This protein is crucial for maintaining low intracellular calcium concentrations by sequestering calcium within the sarco/endoplasmic reticulum. However, organisms may also utilize calcium binding proteins to reduce free calcium concentrations intracellularly and the expression of one calcium binding protein, calbindin exhibited continual increases in expression over the course of development with a peak in expression at the PD I shell stage (Manuscript 4). NCX proteins belong to the SLC8 family of membrane-bound transport proteins and are responsible for the reversible exchange of three sodium ions for one calcium ion. This group of ion transport proteins has been observed to partake in mammalian bone and avian eggshell calcification (Cheidde et al 2003, Sosnoski and Gay 2007). Further, the simultaneous increased expression of the NKA and NCX group of proteins is in agreement with previous descriptions of NCX functions, where NCX

proteins are driven by the electrochemical gradient provided by the NKA (Cheidde et al 2003). Finally, elevated gene expression of several types of calcium channels was observed in the *M. edulis* larval transcriptome: Ca^{2+} load activated Ca^{2+} channel, voltage dependent Ca^{2+} channels, Ca^{2+} channel subunit α (Manuscript 4). In contrast, calcium channels have been reported to only have a partial role in Ca^{2+} acquisition during skeletogenesis in sea urchin larvae (Fujino et al 1985, Yasumasu et al 1985, Vidavsky et al 2016).

4. Conclusions & outlook

The results within this thesis demonstrate that the rapid calcification of PD I shell in *M. edulis* larvae occurs via the deposition of crystalline aragonite and observed no evidence for ACC precursor phases in larval *M. edulis*. Direct precipitation of crystalline calcium carbonate phases has been proposed during PD I shell formation in other bivalve species (Kudo et al 2010, Yokoo et al 2011) and also for nacre formation in adult molluscs (Saruwatari et al 2009). The direct precipitation of a crystalline shell supports the physiological necessity of a rigidified external skeleton during larval development in bivalves, where rapid PD I shell formation enables muscle attachment and lateral compression of the larval body for swimming and feeding (Galtsoff 1964).

The results obtained within the framework of thesis demonstrate for the first time that bivalve larvae are capable of increasing Ω_{arag} at the site of calcification. In addition, experiments performed when rearing larvae under a range of pCO_2 conditions revealed that *M. edulis* larvae are capable of offsetting the impacts of OA at the site of calcification to some extent. However, drastic increases in pCO_2 exhibit the limited capacity of the ion regulatory system in *M. edulis* larvae and likely impacts the catalytic function of extracellular pH sensitive enzymes involved in shell matrix processing and carbonate precipitation/dissolution dynamics. Although the capacity to regulate Ω_{arag} at the site of calcification is impaired under extreme OA, *M. edulis* larvae are observed to secrete shells (Manuscript 2). These observations hint towards the possibility of modifying larval shell matrix proteins to enable mineral precipitation when Ω_{arag} is under saturated. Till date, no information is available on the composition of organic matrix in larval bivalves with few studies identifying single components of interest, such as chitin (Schönitzer and Weiss 2007).

Empirical manipulations of seawater chemistry reveal that salinity associated decreases in calcium are linked to impaired calcification performance in Baltic *Mytilus* sp. Larval calcification performance was observed to have a salinity threshold at ca. 8 g kg^{-1}. *In vivo* characterization of the calcium concentrations at the site of calcification in Baltic *Mytilus edulis*-like larvae demonstrate that larvae exhibit significant increases in calcium concentrations in the calcification space at seawater calcium concentrations lower than 3.5 mM. In addition, populations of *Mytilus* derived from the Eastern Baltic (characterized by low salinity and calcium conditions) are observed to lower calcium thresholds to maintain larval calcification performance. Therefore, low

seawater calcium concentrations may have a significant contribution in the observed genetic structure of the Baltic *Mytilus* population (Stuckas et al 2009, 2017).

By using a substrate limitation approach, this thesis was able to isolate one membrane-bound transport protein putatively involved in HCO_3^- acquisition, belonging to the SLC26 family of anion transporters. The single contig related to ion transport differentially expressed under substrate limitation was annotated as a sodium-independent sulfate anion transporter (SLC26). The small set of contigs to exhibit differential expression under substrate limitation in the larval *M. edulis* transcriptome is consistent with previous studies on bivalve larvae (Kelly et al 2016) and may imply that bivalve larvae possess a limited capacity to modify their transcriptomic developmental program. Alternatively, it may be of interest to challenge the larval acid-base regulatory machinery by reductions in seawater [Ca^{2+}] which have been demonstrated to impair calcification performance in larval mussels (Manuscript 3) or combined reductions in [Ca^{2+}] and C_T to elicit larger transcriptomic responses in comparison to the C_T reductions performed in this thesis. In addition to the SLC26 candidate transport protein in larval calcification identified by substrate limitation, developmental course analyses revealed the putative role of several proteins including sodium bicarbonate transporters, anion exchangers, sodium/calcium exchangers and sarco/endoplasmic reticulum calcium ATPase in *M. edulis* larval calcification. Further characterization of the involvement of the SLC26 and NBC candidate genes in larval calcification may be performed using molecular techniques such as *in situ* hybridization to investigate localized gene expression patterns or gene knock-down to ascertain the role of specific genes in substrate acquisition or mineral deposition. Finally, the cellular functions of biomineralisation candidate genes identified in Manuscript 4 may be assessed by heterologous expression conjunction with electrophysiology techniques (e.g. Piermarini et al. 2007). Such studies provide useful insight regarding ion transport protein specificity for substrates and/or stoichometries.

5. References

Addadi, L., Joester, D., Nudelman, F.,Weiner, S. (2006) Mollusk shell formation: a source of new concepts for understanding biomineralization process. Chemistry: A European Journal 12: 980–987.

Addadi, L., Raz, S., Weiner, S. (2003) Taking Advantage of Disorder: Amorphous Calcium Carbonate and its roles in Biomineralization. Advanced Materials 15: 959-970.

Aizenberg, J., Lambert, G., Weiner, S., Addadi, L. (2002) Factors involved in the formation of amorphous and crystalline calcium carbonate: A study of an ascidian skeleton. Journal of the American Chemical Society 124: 32-39.

Al-Horani, F.A., Al-Moghrabi, S.M., de Beer, D. (2003) The mechanism of calcification and its relation to photosynthesis and respiration in the scleractinian coral *Galaxea fascicularis*. Marine Biology 142: 419-426.

Almada-Villela, P.C. (1984) The Effects of Reduced Salinity on the Shell Growth of Small *Mytilus edulis*. Journal of the Marine Biological Association of the United Kingdom 64: 171-182.

Aranda-Burgos, J.A., Da Costa, F., Novoa, S., Ojea, J., Martinez-Patino, D. (2014) Embryonic and Larval Development of *Ruditapes Decussatus* (Bivalvia: Veneridae): A Study of the Shell Differentiation Process. Journal of Molluscan Studies 80: 8-16.

Arivalagan, J., Yarra, T., Marie, B., Sleight, V.A., Duvernois-Berthet, E., Clark, M.S., Marie, A., Berland, S. (2016) Insights from the Shell Proteome: Biomineralization to Adaptation. Molecular Biology and Evolution 34: 66–77.

Auzoux-Bordenave, S., Badou, A., Gaume, B., Berland, S., Helléouet, M.N., Milet, C., Huchette, S. (2010) Ultrastructure chemistry and mineralogy of the growing shell of the European abalone *Haliotis tuberculata*. Journal of Structural Biology 171: 277–290.

Balbi, T., Franzellitti, S., Fabbri, R., Montagna, M., Fabbri, E., Canesi, L. (2016) Impact of bisphenol A (BPA) on early embryo development in the marine mussel *Mytilus galloprovincialis*: Effects on gene transcription. Environmental Pollution 218: 996-1004.

Barron, M.E., Roa, J.N.B., Tresguerres, M. (2012) Pacific oyster mantle, gill and hemocytes express the bicarbonate-sensing enzyme soluble adenylyl cyclase. FASEB J. 26: 1070.2.

Barton, A., B. Hales, G. G. Waldbusser, C. Langdon, and R. A. Feely (2012), The Pacific oyster, *Crassostrea gigas*, shows negative correlation to naturally elevated carbon dioxide levels: Implications for near-term ocean acidification effects, Limnology and Oceanography 57: 698-710.

Bechmann, R.K., Taban, I.C., Westerlund, S., Godal, B.F., Arnberg, M., Vingen, S., Ingvarsdottir, A., Baussant, T., (2011) Effects of ocean acidification on early life stages of shrimp (*Pandalus borealis*) and mussel (*Mytilus edulis*). Journal of Toxicology and Environmental Health Part A 74: 424–438.

Beldowski, J., Loeffler, A., Schneider, B., Joensuu, L. (2010) Distribution and biogeochemical control of total CO_2 and total alkalinity in the Baltic Sea. Journal of Marine Systems 81: 252–259.

Beniash, E., Aizenberg, J., Addadi, L., Weiner, S. (1997) Amorphous calcium carbonate transforms into calcite during sea-urchin larval spicule growth. Proceedings of the Royal Society B: Biological Sciences 264:461–465.

Bentov, S., Abehsera, S., Sagi, A. (2016) The Mineralized Exoskeletons of Crustaceans. In: Extracellular Composite Matrices in Arthropods. Edited by Cohen, E., Moussian, B. Spinger. 137-145.

Bentov, S., Erez, J. (2006) Impact of biomineralization processes on the Mg content of foraminiferal shells: A biological perspective. Geochemistry Geophysics Geosystems 7: Q01P08, doi: 10.1029/2005GC001015.

Bleher, R., Machado, J. (2004) Paracellular pathway in the shell epithelium of *Anodonta cygnea*. Journal of Experimental Zoology Part a-Comparative Experimental Biology 301A: 419-427.

Boron, W., Boulpaep, E.L. (2009) Medical Physiology: a cellular and molecular approach (2nd edition). Saunders Elsevier, Canada.

Cai, W.J., Ma, Y.N., Hopkinson, B.M., Grottoli, A.G., Warner, M.E., Ding, Q., Hu, X.P., Yuan, X.C., Schoepf, V., Xu, H., Han, C.H., Melman, T.F., Hoadley, K.D., Pettay, D.T., Matsui, Y., Baumann, J.H., Levas, S., Ying, Y., Wang, Y.C. (2016) Microelectrode characterization of coral daytime interior pH and carbonate chemistry. Nature Communications 7. doi: 10.1038/Ncomms11144.

Carre, M., Bentaleb, I., Bruguier, O., Ordinola, E., Barrett, N.T., Fontugne, M. (2006) Calcification rate influence on trace element concentrations in aragonitic bivalve shells: Evidences and mechanisms. Geochimica et Cosmochimica Acta 70: 4906-4920.

Carriker, M.R., Palmer, R.E. (1979) Ultrastructural Morphogenesis of Prodissoconch and Early Dissoconch Valves of the Oyster '*Crassostrea virginica*'. Proceedings of the National Shellfisheries Association, 69: 103-128.

Castilho, F., Machado, J., Reis, M.L., Sá, C. (1989) Ultrastructural study of the embryonic and larval shell of *Anodonta cygnea*. Canadian Journal of Zoology 67: 1659-1664.

Cheidde, L., Viera, T.C., Lima, P.R.M., Saad, S.T.O., Heilberg, I.P. (2003) A Novel Mutation in the Anion Exchanger 1 Gene Is Associated With Familial Distal Renal Tubular Acidosis and Nephrocalcinosis. Pediatrics 112: 1361-1367.

Comeau, S., Tambutté, E., Carpenter, R.C., Edmunds, P.J., Evensen, N.R., Allemand, D., Ferrier-Pagès, C., Tambutté, S., Venn, A.A. (2017) Coral calcifying fluid pH is modulated by seawater carbonate chemistry not solely seawater pH. Proc Biol Sci. 284: 20161669. doi: 10.1098/rspb.2016.1669.

Cornwall, C.E., Comeau, S., McCulloch, M.T. (2017) Coralline algae elevate pH at the site of calcification under ocean acidification. Global Change Biology doi: 10.1111/gcb.13673

Cuif, J.P., Dauphin, Y. (2005) The two-step mode of growth in the Scleractinian coral skeletons from the micrometre to the overall scale. Journal of Structural Biology 150: 319–331.

Cuif, J.P., Dauphin, Y., Doucet, J., Salome, M., Susini, J. (2003) XANES mapping of organic sulfate in three scleractinian coral skeletons. Geochimica Cosmochimica Acta 67: 75–83.

de Nooijer, L.J., Toyofuku, T., Kitazato, H. (2009) Foraminifera promote calcification by elevating their intracellular pH. Proceedings of the National Academy of Sciences of the United States of America 106: 15374-15378.

DeVol, R.T., Sun, C.Y., Marcus, M.A., Coppersmith, S.N., Myneni, S.C.B., Gilbert, P.U.P.A. (2015) Nanoscale Transforming Mineral Phases in Fresh Nacre. Journal of the American Chemical Society 137: 13325-13333.

Ebanks, S., O'Donnell, M., Grosell, M. (2010a) Characterization of mechanisms for Ca^{2+} and HCO_3^-/CO_3^{2-} acquisition for shell formation in embryos of the freshwater common pond snail *Lymnaea stagnalis*. Journal of Experimental Biology 213: 4092-4098.

Ebanks, S., O'Donnell, M., Grosell, M. (2010b) Acquisition of Ca^{2+} and HCO_3^-/CO_3^{2-} for shell formation in embryos of the common pond snail *Lymnaea stagnalis*. Journal of Comparative Physiology B: 180: 953–965.

Ekstrom, J.A., Suatoni, L., Cooley, S.R., Pendleton, L.H., Waldbusser, G.G., Cinner, J.E., Ritter, J., Langdon, C., van Hooidonk, R., Gledhill, D., Wellman, K., Beck, M.W., Brander, L.M., Rittschof, D., Doherty, C., Edwards, P.E.T., Portela, R. (2015) Vulnerability and adaptation of US shellfisheries to ocean acidification. Nature Climate Change 5: 207-214.

Erez J., Braun, A. (2007) Calcification in hermatypic corals is based on direct seawater supply to the biomineralization site, 17th Annual V M Goldschmidt, Cologne, Germany. Geochimica Cosmochimica Acta 71: A260–A260.

Erez, J. (2003) The source of ions for biomineralisation in foraminifora and their implications for paleoceanographic proxies. Reviews in Mineralogy and Geochemistry 54: 115-149.

Erwin, D.H. (1994) Early introduction of major morphological innovations. Acta Palaeontologica Polonica 38: 281-294.

Evans, T.G., Chan, F., Menge, B.A., Hofmann, G.E. (2013) Transcriptomic responses to ocean acidification in larval sea urchins from a naturally variable pH environment. Molecular Ecology 22: 1609–1625.

Eyster, L.S. (1983) Ultrastructureof early embryonic shell formation in the opisthobranch gastropod *Aeolidia papillosa*. Biological Bulletein 165: 394-408.

Eyster, L.S. (1986) Shell inorganic composition and onset of shell mineralization during bivalve and gastropod embryogenesis. Biological Bulletin 170:, 211-231.

Fan, W., Li, C., Li, S., Feng, Q., Xie, L., Zhang, R. (2007) Cloning, Characterization, and Expression Patterns of Three Sarco/Endoplasmic Reticulum Ca^{2+}-ATPase Isoforms from Pearl Oyster (*Pinctada fucata*). Acta Biochimica et Biophysica Sinica 39: 722–730.

Feng, D., Li, Q., Yu, H., Kong, L., Du, S. (2017) Identification of conserved proteins from diverse shell matrix proteome in *Crassostrea gigas*: characterization of genetic bases regulating shell formation. Scientific Reports 7: 45754.

Fitzer, S.C., Chung, P., Maccherozzi, F., Dhesi, S.S., Kamenos, N.A., Phoenix, V.R., Cusack, M. (2016) Biomineral shell formation under ocean acidification: a shift from order to chaos. Scientific Reports 6: 21076. doi: 10.1038/srep21076.

Frieder, C.A., Applebaum, S.L., Pan, T.C.F., Hedgecock, D., Manahan, D.T. (2017) Metabolic cost of calcification in bivalve larvae under experimental ocean acidification. ICES Journal of Marine Science 74: 941–954.

Fujino, Y., Mitsunaga, K., Fujiwara, A., Yasumasu, I. (1985) Inhibition of $^{45}Ca^{2+}$ uptake in the eggs and embryos of the sea urchin, *Anthocidaris crassispina*, by several calcium antagonists, anion transport inhibitor, and chloride transport inhibitors. Journal of Experimental Zoology 235: 281–288.

Gagnon, A.C., Adkins, J.F., Erez, J. (2012) Seawater transport during coral biomineralization. Earth and Planetary Science Letters 329-330: 150–161.

Galtsoff, P.S. (1964) The American oyster, *Crassostrea virginica* Gmelin. Chapter 16: Larval development and metamorphosis. Fishery Bulletin, North East Fishery Science Centre.

Gaylord, B., Hill, T.M., Sanford, E., Lenz, E.A., Jacobs, L.A., Sato, K.N., Russell, A.D., Hettinger, A. (2011) Functional impacts of ocean acidification in an ecologically critical foundation species. The Journal of Experimental Biology, 214: 2586-2594.

Gazeau, F., Gattuso, J.P., Dawber, C., Pronker, A.E., Peene, F., Peene, J., Heip, C.H.R., Middelburg, J.J. (2010) Effect of ocean acidification on the early life stages of the blue mussel *Mytilus edulis*. Biogeosciences, 7: 2051-2060.

Gazeau, F., Parker, L.M., Comeau, S., Gattuso, J.P., O'Connor, W.A., Martin, S., Portner, H.O., Ross, P.M. (2013) Impacts of ocean acidification on marine shelled molluscs. Marine Biology 160: 2207-2245.

Gobler, C.J., Talmage, S.C. (2014) Physiological response and resilience of early life-stage Eastern oysters (*Crassostrea virginica*) to past, present and future ocean acidification. Conservation Physiology 2. doi: 10.1093/conphys/cou004.

Gräwe, U., Freidland, R., Burchard, H. (2013) The future of the western Baltic Sea: two possible scenarios. Ocean Dynamics 63: 901-921.

Gripenberg, S. (1937) The Calcium Content of Baltic Water. Thalassological Institute, Helsingfors.

Hasse, B., Ehrenberg, H., Marxen, J.C., Becker, W., Epple, M. (2000) Calcium carbonate modifications in the mineralized shell of the freshwater snail *Biomphalaria glabrata*. Chemistry: A European Journal 6, 3679-3685.

Haszprunar, G., Schander, C., Halanych, K.M. (2008) Relationships of Higher Molluscan Taxa. In: Phylogeny and Evolution of the Mollusca. Edited by Ponder, W.F., Lindberg, D.R. London: University of California Press, Ltd. 19-32.

Heinemann, A., Fietzke, J., Melzner, F., Bohm, F., Thomsen, J., Garbe-Schonberg, D., Eisenhauer, A. (2012) Conditions of *Mytilus edulis* extracellular body fluids and shell composition in a pH-treatment experiment: Acid-base status, trace elements and delta B-11. Geochemistry Geophysics Geosystems 13. doi: 10.1029/2011gc003790.

Hiebenthal, C., Fietzek, P., Thomsen, J., Saderne, V., Melzner, F. (2016) Kiel fjord pCO_2 datasets 2012, 2013, 2014.

Hild, S., Marti, O., Ziegler, A. (2008) Spatial distribution of calcite and amorphous calcium carbonate in the cuticle of the terrestrial crustaceans *Porcellio scaber* and *Armadillidium vulgare*. Journal of Structural Biology 163: 100-108.

Hodson, M.E., Benning, L.G., Demarchi, B., Penkman, K.E.H., Rodriguez-Blanco, J.D., Schofield, P.F., Versteegh, E.A.A. (2015) Biomineralisation by earthworms - an investigation into the stability and distribution of amorphous calcium carbonate. Geochemical Transactions 16: 4.

Hohagen, J. (2013) Molecular and cellular differentiation during the early shell field development in Lymnaea stagnalis. PhD Thesis, University of Göttingen.

Hohagen, J., Jackson, D.J. (2013) An ancient process in a modern mollusc: early development of the shell in *Lymnaea stagnalis*. BMC Developmental Biology 13: 27 doi:10.1186/1471-213X-13-27.

Hüning, A.K., Lange, S.M., Ramesh, K., Jacob, D.E., Jackson, D.J., Panknin, U., Gutowska, M.A., Philipp, E.E., Rosenstiel, P., Lucassen, M., Melzner, F. (2016) A shell regeneration assay to identify biomineralization candidate genes in mytilid mussels. Marine Genomics 27: 57-66.

Hüning, A.K., Melzner, F., Thomsen, J., Gutowska, M.A., Kramer, L., Frickenhaus, S., Rosenstiel, P., Pörtner, H.O., Philipp, E.E.R., Lucassen, M. (2013) Impacts of seawater acidification on mantle gene expression patterns of the Baltic Sea blue mussel: implications for shell formation and energy metabolism. Marine Biology 160: 1845-1861.

Innes, D.J., Haley, L.E. (1977) Genetic Aspects of Larval Growth under Reduced Salinity in *Mytilus edulis*. Biological Bulletin 153: 312-321.

Iwata, K. (1980) Mineralization and Architecture of the Larval Shell of *Haliotis discus* hannai Ino, (Archaeogastropoda). Journal of the Faculty of Science, Hokkaido University 19: 305-320.

Jackson, D.J., McDougall, C., Green, K.M., Simpson, F., Worheide, G., Degnan, B.M. (2006) A rapidly evolving secretome builds and patterns a sea shell. BMC Biology 4: 40

Jackson, D.J., McDougall, C., Woodcroft, B., Moase, P., Rose, R.A., Kube, M., Reinhardt, R., Rokshar, D.S., Montagnani, C., Joubert, C., Piquemal, D., Degnan, B.M. (2010) Parallel evolution of nacre building gene sets in molluscs. Mol Biol Evol 27: 591-608.

Jacob, D.E., Soldati, A.L., Wirth, R., Huth, J., Wehrmeister, U., Hofmeister, W. (2008) Nanostructure, composition and mechanisms of bivalve shell growth. Geochimica et Cosmochimica Acta 72: 5401–5415.

Jacob, D.E., Wirth, R., Soldati, A.L., Wehrmeister, U., Schreiber, A. (2011) Amorphous calcium carbonate in the shells of adult Unionoida. J. Struct. Biol. 173: 241-249.

Jansson, A.M., Kautsky, N. (1977) Quantitative survey of hard bottom communities in a Baltic archipelago. In: Keegan BF, Ceidigh PO, Boaden PJS (eds). Biology of benthic organisms. Pergamon, Oxford New York. Pages: 359-356.

Jardillier, E., Rousseau, M., Gendron-Badou, A., Frohlich, F., Smith, D.C., Martin, M., Helleouet, M.N., Huchette, S., Doumenc, D., Auzoux-Bordenave, S. (2008) A morphological and structural study of the larval shell from the abalone *Haliotis tuberculata*. Marine Biology 154: 735-744.

Johnstone, M.B., Gohad, N.V., Falwell, E.P., Hansen, D.C., Hansen, K.M., Mount, A.S. (2015) Cellular orchestrated biomineralization of crystalline composites on implant surfaces by the eastern oyster, *Crassostrea virginica* (Gmelin, 1791). Journal of Experimental Marine Biology and Ecology 463: 8-16.

Kaloyianni, M., Stamatiou, R., Dailianis, S. (2005) Zinc and 17 beta-estradiol induce modifications in Na^+/H^+ exchanger and pyruvate kinase, activity, through protein kinase C in isolated mantle/gonad cells of *Mytilus galloprovincialis*. Comparative Biochemistry and Physiology C-Toxicology & Pharmacology 141: 257-266.

Kautsky, H. (1982) Growth and Size Structure in a Baltic *Mytilus edulis* Population. Marine Biology 68: 117-133.

Kautsky, H., van der Maarel, E. (1990) Multivariate approaches to the variation in phytobenthic communities and environmental vectors in the Baltic Sea. Marine Ecology Progress Series 60: 169-184.

Kelly, M.W., Padilla-Gamino, J.L., Hofmann, G.E. (2016) High pCO_2 affects body size, but not gene expression in larvae of the California mussel (*Mytilus californianus*). Ices Journal of Marine Science 73: 962-969.

Kenkel, C.D., Meyer, E., Matz, M.V. (2013) Gene expression under chronic heat stress in populations of the mustard hill coral (*Porites astreoides*) from different thermal environments. Molecular Ecology 22: 4322-4334.

Khouzani, M.F., Chevrier, D.M., Guettlein, P., Hauser, K., Zhang, P., Hedin, N., Gebauer, D. (2015) Disordered amorphous calcium carbonate from direct precipitation. Cryst. Eng. Comm. 17: 4842-4849.

Kingsley, R.J., Watabe, N. (1987) Role of Carbonic Anhydrase in Calcification in the Gorgonian *Leptogorgia virguiata*. The Journal of Experimental Zoology 241: 171-180.

Kniprath, E. (1977) Ontogeny of Shell Field in Lymnaea-Stagnalis. Wilhelm Rouxs Archives of Developmental Biology 181: 11-30.

Kniprath, E. (1980) Larval development of the shell and the shell gland in *Mytilus* (Bivalvia). Wilhelm Roux's archives of developmental biology 188: 201-204.

Kniprath, E. (1981) Ontogeny of the Molluscan Shell Field: A Review. Zoologica Scripta 10: 61-79.

Ko, G.W.K., Dineshram, R., Campanati, C., Chan, V.B.S., Havenhand, J., Thiyagarajan, V. (2014) Interactive Effects of Ocean Acidification, Elevated Temperature, and Reduced Salinity on Early-Life Stages of the Pacific Oyster. Environmental Science and Technology 48: 10079−10088.

Kocot, K.M., Cannon, J.T., Todt, C., Citarella, M.R., Kohn, A.B., Meyer, A., Santos, S.R., Schander, C., Moroz, L.L., Lieb, B., Halanych, K.M. (2011) Phylogenomics reveals deep molluscan relationships. Nature 477: 452–456.

Kremling, K., Wilhelm, G. (1997) Recent increase of the calcium concentrations in Baltic Sea waters. Marine Pollution Bulletin 34: 763-767.

Kristova, P., Hopkinson, L.J., Rutt, K.J. (2015) The Effect of the Particle Size on the Fundamental Vibrations of the [CO32-] Anion in Calcite. Journal of Physical Chemistry A 119: 4891-4897.

Kudo, M., Kameda, J., Saruwatari, K., Ozaki, N., Okano, K., Nagasawa, H., Kogure, T. (2010) Microtexture of larval shell of oyster, *Crassostrea nippona*: A FIB-TEM study. Journal of Structural Biology 169: 1-5.

Kurihara, H. (2008) Effects of CO_2-driven ocean acidification on the early developmental stages of invertebrates. Marine Ecology Progress Series 373: 275–284.

LaBarbera, M. (1974) Calcification of the First Larval Shell of *Tridacna squamosa* (Tridacnidae: Bivalvia). Marine Biology 25: 233-239.

Lee, D.D. (1990) The Structure and Mechanism of Growth of Calcium-Carbonate Minerals in Early Stages of Shells of the Oyster *Crassostrea Virginica*. Journal of Crystal Growth 102: 262-268.

Lee, S.W., Hong, S.M., Choi, C.S. (2006) Characteristics of calcification processes in embryos and larvae of the Pacific oyster, *Crassostrea gigas*. Bulletin of Marine Science 78: 309-317.

LeRoy, N., Marie, B. (2012) The formation and mineralization of mollusk shell. Frontiers in Bioscience S4: 1099-1125.

Li, S., Huang, J., Liu, C., Liu, Y., Zheng, G., Xie, L., Zhang, R. (2016). Interactive effects of seawater acidification and elevated temperature on the Transcriptome and Biomineralization in the pearl oyster *Pinctada fucata*. Environmental Science and Technology 50: 1157-1165.

Li, S., Liu, C., Huang, J., liu, Y., Zhang, S., Zheng, G., Xie, L., Zhang, R. (2016) Transcriptome and biomineralization responses of the pearl oyster *Pinctada fucata* to elevated CO_2 and temperature. Scientific Reports 6, Article number: 18943. doi:10.1038/srep18943

Mahamid, J., Sharir, A., Addadi, L., Weiner, S. (2008) Amorphous calcium phosphate is a major component of the forming fin bones of zebrafish: Indications for an amorphous precursor phase. Proceedings of the National Academy of Sciences of the United States of America 105:12748–12753.

Mann, K., Jackson, D.J. (2014) Characterization of the pigmented shell-forming proteome of the common grove snail *Cepaea nemoralis*. BMC Genomics 15: 249.

Mao Che, L., Golubic, S., Le Campion-Alsumard, T., Payri, C. (2001) Developmental aspects of biomineralisation in the Polynesian pearl oyster *Pinctada margaritifera* var. *cumingii*. Oceanologica Acta 24: S37–S49.

Marali, S., Schone, B.R., Mertz-Kraus, R., Griffin, S.M., Wanamaker, A.D., Matras, U., Butler, P.G. (2017) Ba/Ca ratios in shells of *Arctica islandica* - Potential environmental proxy and crossdating tool. Palaeogeography Palaeoclimatology Palaeoecology 465: 347-361.

Marie, B., Joubert, C., Tayale, A., Zanella-Cleon, I., Belliard, C., Picquemal, D., Cochennec-Laureau, N., Marine, F., Gueguen, Y., Montagnani, C. (2012) Different secretory repertoires control the biomineralization processes of prism and nacre deposition of the pearl oyster shell. Proceedings of the National Academy of Sciences of the United States of America 109: 20986-20991.

Marie, B., Le Roy, N., Zanella-Cleon, I., Becchi, M., Marin, F. (2011) Molecular evolution of mollusc shell proteins: insights from proteomic analysis of the edible mussel *Mytilus*. J Mol Evol. 72:531-546.

Marin, F., Luquet, G. (2004) Molluscan shell proteins. Comptes Rendus Palevol 3: 469-492.

Marxen, J.C., Prymak, O., Beckmann, F., Neues, F., Epple, M. (2008) Embryonic shell formation in the snail *Biomphalaria glabrata*: A comparison between scanning electron microscopy (SEM) and synchrotron radiation micro-computer tomography (SR mu CT). Journal of Molluscan Studies 74: 19-26.

Marxen, J.C., Witten, P.E., Finke, D., Reelsen, O., Rezgaoui, M., Becker, W. (2003) A light and electron-microscopic study of enzymes in the embryonic shell-forming tissue of the freshwater snail, *Biomphalaria glabrata*. Invertebrate Biology 122: 313-325.

McConnaughey TA, Falk RH (1991) Calcium-proton exchange during algal calcification. The Biological Bulletin 180:185-195.

McConnaughey, T.A., Gillikin, D. (2008) Carbon isotopes in mollusk shell carbonates. Geo-Marine Letters 28: 287–299.

Medakovic, D. (1989) X-ray diffraction study of the first larval shell of *Ostrea edulis*. Marine Biology 101: 205-210.

Medakovic, D. (2000) Carbonic anhydrase activity and biomineralization process in embryos, larvae and adult blue mussels *Mytilus edulis* L. Helgoland Marine Research 54: 1-6.

Medakovic, D., Popovic, S., Grzeta, B., Plazonic, M., Hrs-Brenko, M. (1997) X-ray diffraction study of calcification processes in embryos and larvae of the brooding oyster *Ostrea edulis*. Marine Biology 129: 615–623.

Meier, H.E.M., Kjellström, E., Graham, L.P. (2006) Estimating uncertainties of projected Baltic Sea salinity in the late 21st century. Geophysical Research Letters 33 doi: 10.1029/2006GL026488.

Melzner, F., Thomsen, J., Koeve, W., Oschlies, A., Gutowska, M.A., Bange, H. W., Hansen, H.P., Körtzinger, A. (2013) Future ocean acidification will be amplified by hypoxia in coastal habitats, Marine Biology 160: 1875-1888.

Mette, M.J., Wanamaker, A.D., Carroll, M.L., Ambrose, W.G., Retelle, M.J. (2016) Linking large-scale climate variability with *Arctica islandica* shell growth and geochemistry in northern Norway. Limnology and Oceanography 61: 748-764.

Miller, A.W., Reynolds, A.C., Sobrino, C., Riedel, G.F. (2009) Shellfish face uncertain future in high CO_2 world: influence of acidification on oyster larvae calcification and growth in estuaries. PLoS ONE 4:e5661. doi:10.1371/journal.pone.0005661.

Misogianes, M.J., Chasteen, N.D. (1979) A chemical and spectral characterization of the extrapallial fluid of *Mytilus edulis*. Analytical Biochemistry 100, 324–334.

Miyazaki, Y., Nishida, T., Aoki, H., Samata, T. (2010) Expression of genes responsible for biomineralization of *Pinctada fucata* during development. Comparative Biochemistry and Physiology B-Biochemistry & Molecular Biology 155: 241-248.

Morse, J.W., Arvidson, R.S., Luttge, A. (2007) Calcium carbonate formation and dissolution. Chemical Reviews 107: 342-381.

Mount, A.S., Wheeler, A.P., Paradkar, R.P., Snider, D. (2004) Hemocyte-mediated shell mineralisation in the Eastern Oyster. Science 304: 297-300.

Nehrke, G., Nouet, J. (2011) Confocal Raman microscope mapping as a tool to describe different mineral and organic phases at high spatial resolution within marine biogenic carbonates: case study on *Nerita undata* (Gastropoda, Neritopsina). Biogeosciences 8: 3761-3769.

Nehrke, G., Poigner, H., Wilhlems-Dick, D., Brey, T., Abele, D. (2012) Coexistence of three calcium carbonate polymorphs in the shell of the Antarctic clam *Laternula elliptica*. Geochemistry, Geophysics and Geosystems 13. doi: 10.1029/2011GC003996

Nell, J.A., Perkins, B. (2005) Evaluation of progeny of fourth generation Sydney rock oyster *Saccostrea glomerata* (Gould, 1850) breeding lines. Aquaculture Research 36: 753–757.

Niggli, V., Sigel, E., Carafoli, E. (1982) The Purified Ca^{2+} Pump of Human Erythrocyte Membranes Catalyzes an Electroneutral Ca^{2+}-H^{+} Exchange in Reconstituted Liposomal Systems. Journal of Biological Chemistry 257: 2350-2356.

Norling, P., Kautsky, N. (2008) Patches of the mussel *Mytilus* sp. are islands of high biodiversity in subtidal sediment habitats in the Baltic Sea. Aquatic Biology 4: 75–87.

Ohlson, M., Anderson, L. (1990) Recent Investigation of Total Carbonate in the Baltic Sea - Changes from the Past as a Result of Acid-Rain. Marine Chemistry 30: 259-267.

Palmer, A.R. (1983) Relative cost of producing skeletal organic matrix versus calcification: evidence from marine gastropods. Marine Biology 75: 287-292.

Palmer, A.R. (1992) Calcification in marine mollusks – how costly is it, Proceedings of the National Academy of Sciences of the United States of America 89:1379–1382.

Pan, T.C.F., Applebaum, S.L., Manahan, D. (2015) Experimental ocean acidification alters the allocation of metabolic energy. Proceedings of the National Academy of Sciences of the United States of America 112: 4696–4701.

Parker, L.M., Ross, P.M., O'Connor, W.A., Pörtner, H.O., Scanes, E., Wright, J.M. (2013) Predicting the Response of Molluscs to the Impact of Ocean Acidification. Biology (Basel) 2: 651-692.

Piermarini, P.M., Choi, I., Boron, W.F. (2007) Cloning and characterization of an electrogenic Na^+/HCO_3^- cotransporter from the squid giant fiber lobe. American Journal of Physiology Cell Physiology 292: C2032–C2045.

Politi, Y., Metzler, R.A., Abrecht, M., Gilbert, B., Wilt, F.H., Sagi, I., Addadi, L., Weiner, S., Gilbert, P.U.P.A. (2008) Transformation mechanism of amorphous calcium carbonate into calcite in the sea urchin larval spicule. Proceedings of the National Academy of Sciences of the United States of America 105: 17362–17366.

Rahmati, N., Kunzelmann, K., Xu, J., Barone S., Sirianant, L., De Zeeuw, C.I., Soleimani, M. (2013) Slc26a11 is prominently expressed in the brain and functions as a chloride channel: expression in Purkinje cells and stimulation of V H^+-ATPase. European Journal of Physiology 465: 1583–1597.

Ramesh, K., Hu, M.Y., Thomsen, J., Bleich, M., Melzner, F. (2017) Mussel larvae modify calcifying fluid carbonate chemistry to promote calcification. Nature Communications. doi: 10.1038/s41467-017-01806-8.

Raz, S., Hamilton, P.C., Wilt, F.H., Weiner, S., Addadi, L. (2003) The transient phase of amorphous calcium carbonate in sea urchin larval spicules: The involvement of proteins and magnesium ions in its formation and stabilization. Advanced Functional Materials 13:480–486.

Raz, S., Testeniere, O., Hecker, A., Weiner, S., Luquet, G. (2002) Stable amorphous calcium carbonate is the main component of the calcium storage structures of the crustacean *Orchestia cavimana*. The Biological Bulletin 203: 269-274.

Roa, J.N., Munévar, C.L., Tresguerres, M. (2014) Feeding induces translocation of vacuolar proton ATPase and pendrin to the membrane of leopard shark (*Triakis semifasciata*) mitochondrion-rich gill cells. Comparative Biochemistry and Physiology, Part A 174: 29–37.

Rodriguez-Blanco, J.D., Shaw, S., Benning, L.G. (2008) How to make 'stable' ACC: protocol and preliminary structural characterization, Mineral Magazine 72: 283-286.

Romero, M.F., Chen, A.P., Parker, M.D., Boron, W.F. (2013) The SLC4 family of bicarbonate (HCO_3^-) transporters. Molecular Aspects of Medicine 34: 159-82.

Sabine, C.L., Feely, R.A., Wanninkhof, R., Takahashi, T., Khatiwali, S., Park, G.H. (2010) The global ocean carbon cycle. p. S100–S108. In State of the Climate in 2010, 3. Glob. Oceans. Bull. Am. Meteorol. Soc. 92: S100–S108, doi:10.1175/1520-0477-92.6.S1.

Saderne, V., Fietzek, P., Herman, P.M.J. (2013) Extreme variations of pCO_2 and pH in a macrophyte meadow of the Baltic Sea in summer: Evidence of the effect of photosynthesis and local upwelling, PLOS ONE, 8: e62689.

Salter, M.A., Harborne, A.R., Perry, C.T., Wilson, R.W. (2017) Phase heterogeneity in carbonate production by marine fish influences their roles in sediment generation and the inorganic carbon cycle. Scientific Reports 7. doi: 10.1038/s41598-017-00787-4.

Sanders, T., Schmittmann, L., Nascimento-Schulze, J., Melzner, F. (2018, in review) High cost of calcification limits growth in mussels from the low saline Baltic Sea. Proceedings of the Royal Society of the UK B: Biological Sciences.

Saranchova, O.L., Flyachinskaya, L.P. (2001) The influence of environmental salinity on early ontogenesis of the mussel *Mytilus edulis* and the starfish *Asterias rubens* from the White Sea. Biologiya Morya 27: 110-116.

Saruwatari, K., Matsui, T., Mukai, H., Nagasawa, H., Kogure, T. (2009) Nucleation and growth of aragonite crystals at the growth front of nacres in pearl oyster, *Pinctada fucata*. Biomaterials 30: 3028–3034.

Schatzberg, D., Lawton, M., Hadyniak, S.E., Ross, E.J., Carney, T., Beane, W.S., Levin, M., Bradham, C.A. (2015) H^+/K^+ ATPase activity is required for biomineralization in sea urchin embryos. Developmental Biology 406: 259-270.

Schönitzer, V., Weiss, I.M. (2007) The structure of mollusc larval shells formed in the presence of the chitin synthase inhibitor Nikkomycin Z. BMC Structural Biology 7. doi: 10.1186/1472-6807-7-71.

Soleimani, M. (2013) SLC26 Cl^-/HCO_3^- exchangers in the kidney: roles in health and disease. Kidney International 84: 657-666.

Sosnoski, D.M., Gay, C.V. (2007) NCX3 is a major functional isoform of the sodium–calcium exchanger in osteoblasts. Journal of Cellular Biochemistry 103: 1101–1110.

Stenzel, H.B. (1964) Oysters: Composition of the Larval Shell. Science 145: 155-156.

Stuckas, H., Knobel, L., Schade, H., Breusing, C., Hinrichsen, H.-H., Bartel, M., Langguth, K., Melzner, F. (2017) Combining hydrodynamic modelling with genetics: Can passive larval drift shape the genetic structure of Baltic *Mytilus* populations? Molecular Ecology 26: 2765-2782.

Stuckas, H., Stoof, K., Quesada, H., Tiedemann, R. (2009) Evolutionary implications of discordant clines across the Baltic *Mytilus* hybrid zone (*Mytilus edulis* and *Mytilus trossulus*). Heredity (Edinb) 103: 146-156.

Stumpp, M., Hu, M.Y., Tseng, Y.C., Guh, Y.J., Chen, Y.C., Yu, J.K., Su, Y.H., Hwang, P.P. (2015) Evolution of extreme stomach pH in bilateria inferred from gastric alkalization mechanisms in basal deuterostomes. Scientific Reports 5: 10421.

Talmage, S.C., Gobler, C.J. (2010) Effects of past, present, and future ocean carbon dioxide concentrations on the growth and survival of larval shellfish. Proceedings of the National Academy of Sciences of the United States of America 107: 17246-17251.

Tambutté, E., Tambutté, S., Segonds, N., Zoccola, D., Venn, A., Erez, J., Allemand, D. (2012) Calcein labelling and electrophysiology: insights on coral tissue permeability and calcification. Proceedings of the Royal Society B: Biological Sciences 279: 19–27.

Tambutté, S., Holcomb, M., Ferrier-Pagès, C., Reynaud, S., Tambutté, E., Zoccola, D., Allemand, D. (2011) Coral biomineralization: from the gene to the environment. Journal of Experimental Marine Biology and Ecology 408: 58–78.

Thompson, C.M., North, E.W., White, S.N., Gallager, S.M. (2014) An analysis of bivalve larval shell pigments using micro-Raman spectroscopy. Journal of Raman Spectroscopy 45: 349-358.

Thomsen, J., Casties, I., Pansch, C., Körtzinger, A., Melzner, F. (2013) Food availability outweighs ocean acidification effects in juvenile *Mytilus edulis*: laboratory and field experiments, Global Change Biology 19: 101–1027.

Thomsen, J., Gutowska, M.A., Saphörster, J., Heinemann, A., Trübenbach, K., Fietzke, J., Hiebenthal, C., Eisenhauer, A., Körtzinger, A., Wahl, M., and Melzner, F. (2010) Calcifying invertebrates succeed in a naturally CO_2-rich coastal habitat but are threatened by high levels of future acidification, Biogeosciences 7: 3879–3891.

Thomsen, J., Haynert, K., Wegner, K.M., Melzner, F. (2015) Impact of seawater carbonate chemistry on the calcification of marine bivalves. Biogeosciences 12: 4209-4220.

Thomsen, J., Ramesh, K., Sanders, T., Bleich, M., Melzner, F. (2017b) Calcification in a marginal sea – influence of seawater [Ca^{2+}] and carbonate chemistry on bivalve shell formation. Biogeoscienes (in review).

Thomsen, J., Stapp, L.S., Haynert, K., Schade, H., Danelli, M., Lannig, G., Wegner, K.M., Melzner, F. (2017a) Naturally acidified habitat selects for ocean acidification–tolerant mussels. Science Advances 3: e1602411. doi: 10.1126/sciadv.1602411.

Togo, Y., Suzuki, S., Iwata, K., Uozumi, S. (1991) Larval Shell Formation and Mineralogy in *Neptunea arthritica* (Bernardi) (Neogastropoda: Buccinidae). In: Mechanisms and Phylogeny of Mineralization in Biological Systems. Springer-Verlag Tokyo.

Tresguerres, M., Parks, S.C., Wood, C.N., Goss, G.G. (2007) V-H^+-ATPase translocation during blood alkalosis in dogfish gills: interaction with carbonic anhydrase and involvement in the postfeeding alkaline tide. American Journal of Physiology - Regulatory, Integrative and Comparative Physiology Published 292: R2012-R2019.

Truebano, M., Burns, G., Thorne, M.A.S., Hillyard, G., Peck, L.S., Skibinski, D.O.F., Clark, M.S. (2010) Transcriptional response to heat stress in the Antarctic bivalve Laternula elliptica. Journal of Experimental Marine Biology and Ecology 391: 65–72.

Ventura, A., Schulze, S., Dupont, S. (2016) Maintained larval growth in mussel larvae exposed to acidified undersaturated seawater. Scientific Reports 6: 23728.

Vidavsky, N., Addadi, S., Mahamid, J., Shimoni, E., Ben-Ezra, D., Shpigel, M., Weiner, S., Addadi, L. (2014) Initial stages of calcium uptake and mineral deposition in sea urchin embryos. Proceedings of the National Academy of Sciences of the United States of America 111: 39-44.

Vidavsky, N., Addadi, S., Schertel, A., Ben-Ezra, D., Shpigel, M., Addadi, L., Weiner, S. (2016) Calcium transport into the cells of the sea urchin larvae in relation to spicule formation. Proceedings of the National Academy of Sciences of the United States of America 113: 12637–12642.

Vidavsky, N., Masic, A., Schertel, A., Weiner, S., Addadi, L. (2015) Mineral-bearing vesicle transport in sea urchin embryos. Journal of Structural Biology 192: 358-365.

Von Euw, S., Zhang, Q., Manichev, V., Murali, N., Gross, J., Feldmann, L.C., Gustafsson, T., Flach, C., Mendelsohn, R., Falkowski, P.G. (2017) Biological control of aragonite formation in stony corals. Science 356: 933–938.

Waldbusser, G.G., Brunner, E.L., Haley, B.A., Hales, B., Langdon, C.J., Prahl, F.G. (2013) A developmental and energetic basis linking larval oyster shell formation to acidification sensitivity. Geophysical Research Letters 40: 2171-2176.

Waldbusser, G.G., Hales, B., Langdon, C.J., Haley, B.A., Schrader, P., Brunner, E.L., Gray, M.W., Miller, C.A., Gimenez, I. (2015) Saturation-state sensitivity of marine bivalve larvae to ocean acidification. Nature Climate Change 5: 273-280.

Waldeck-Weiermair, M., Jean-Quartier, C., Rost, R., Khan, M.J., Vishnu, N., Bondarenko, A.I., Imamura, H., Malli, R., Graier, W.F. (2011) Leucine zipper EF hand-containing transmembrane

protein 1 (Letm1) and uncoupling proteins 2 and 3 (UCP2/3) contribute to two distinct mitochondrial Ca^{2+} uptake pathways. Journal of Biological Chemistry 286: 28444-28455.

Waller, T.R. (1981) Functional Morphology and Development of Veliger Larvae of the European Oyster, *Ostrea edulis* Linne. Smithsonian Contributions to Zoology 328.

Wang, A., Wang, Y., Gu, Z., Li, S., Shi, Y., Guo, X. (2011) Development of expressed sequence tags from the pearl oyster, *Pinctada martensi* Dunker. Marine Biotechnology 13: 275-283.

Wang, X., Fan, W., Xie, L., Zhang, R. (2008) Molecular Cloning and Distribution of a Plasma Membrane Calcium ATPase Homolog from the Pearl Oyster *Pinctada fucata*. Tsinghua Science & Technology 13: 439-446.

Wanninger, A., Koop, D., Moshel-Lynch, S., Degnan, B.M. (2008) Molluscan Evolutionary Development. In: Phylogeny and Evolution of the Mollusca. Edited by Ponder, W.F. & Lindberg, D.R. London: University of California Press, Ltd. Pages 427-445.

Wehrmeister, U., Jacob, D.E., Soldati, A.L., Loges, N., Häger, T., Hofmeister, W. (2010) Amorphous, nanocrystalline and crystalline calcium carbonates in biological materials. Journal of Raman Spectroscopy 42: 926-935.

Weiner, S., Addadi, L. (2011) Crystallization Pathways in Biomineralization. Annual Review of Materials Research 41: 21-40.

Weiner, S., Levi-Kalisman, Y., Raz, S., Addadi, L. (2003) Biologically formed amorphous calcium carbonate. Connective Tissue Research 44: 214-218.

Weiss I.M., Schönitzer, V. (2006) The distribution of chitin in larval shells of the bivalve mollusk *Mytilus galloprovincialis*. Journal of Structural Biology 153: 264–277.

Weiss, I.M., Tuross, N., Addadi, L., Weiner, S. (2002) Mollusc larval shell formation: amorphous calcium carbonate is a precursor phase for aragonite. Journal of Experimental Zoology 293: 478–491.

Wolf, S.E., Bohm, C.F., Harris, J., Demmert, B., Jacob, D.E., Mondeshki, M., Ruiz-Agudo, E., Rodriguez-Navarro, C. (2016) Nonclassical crystallization *in vivo et in vitro* (I): Process-structure-property relationships of nanogranular biominerals. Journal of Structural Biology 196: 244-259.

Wolf, S.E., Lieberwirth, I., Natalio, F., Bardeau, J. F., Delorme, N., Emmerling, F., Barrea, R., Kappl, M., Marin, F. (2012) Merging models of biomineralisation with concepts of nonclassical crystallisation: is a liquid amorphous precursor involved in the formation of the prismatic layer of the Mediterranean Fan Mussel *Pinna nobilis*? Faraday Discussions 159: 433-448.

Yarra, T., Hüning, A., Schilhabel, M., Blaxter, M., Gharbi, K., Clark, M.S., Melzner, F. (in prep) Insights into shell formation in the blue mussel, *Mytilus edulis*, through shell damage-repair and RNASeq.

Yasumasu, I., Mitsunaga, K., Fujino, Y. (1985) Mechanism for electrosilent Ca^{2+} transport to cause calcification of spicules in sea urchin embryos. Experimental Cell Research159: 80–90.

Yokoo, N., Suzuki, M., Saruwatari, K., Aoki, H., Watanabe, K., Nagasawa, H., Kogure, T. (2011) Microstructures of the larval shell of a pearl oyster, Pinctada fucata, investigated by FIB-TEM technique. American Mineralogist 96: 1020-1027.

Zeebe, R.E., Wolf-Gladrow, D.A. (2001) CO_2 in Seawater: Equilibrium, Kinetics, Isotopes 65: 346. Amsterdam. Elsevier Oceanography Series. Halpern, David.

Zhang, G., Fang, X., Guo, X., Li, L., Luo, R., Xu, F., Yang, P., Zhang, L., Wang, X., Qi, H., Xiong, Z., Que, H., Xie, Y., Holland, P.W.H., Paps, J., Zhu, Y., Wu, F., Chen, Y., Wang, J., Peng, C., Meng, J., Yang, L., Liu, J., Wen, B., Zhang, N., Huang, Z., Zhu, Q., Feng, Y., Mount, A., Hedgecock, D., Xu, Z., Liu, Y., Domazet-Lošo, T., Du, Y., Sun, X., Zhang, S., Liu, L., Cheng, P., Jiang, X., Li, J., Fan, D., Wang, W., Fu, W., Wang, T., Wang, B., Zhang, J., Peng, Z., Li, Y., Li, N., Wang, J., Chen, M, He, Y., Tan, F., Song, X., Zheng, Q., Huang, R., Yang, H., Du, X., Chen, L., Yang, M., Gaffney, P.M., Wang, S., Luo, L., She, Z., Ming, Y., Huang, W., Zhang, S., Huang, B., Zhang, Y., Qu, T., Ni, P., Miao, G., Wang, J., Wang, Q., Steinberg, C.E.W., Wang, H., Li, N., Qian, L., Zhang, G., Li, Y., Yang, H., Liu, X., Wang, J., Yin, Y., Wang, J. (2012) The oyster genome reveals stress adaptation and complexity of shell formation. Nature 490: 49–54.

Eidesstattliche Erklärung

Hiermit versichere ich, dass ich die vorliegende Arbeit mit dem Titel:

The mechanisms of larval calcification in the mussel, *Mytilus edulis*

selbständig geschrieben und keine anderen als die angegebenen Quellen und Hilfsmittel verwendet habe. Die vorliegende Arbeit entspricht den von der Christian-Albrechts-Universität Kiel erklärten Regeln guter wissenschaftlicher Praxis und wurde nicht schon an anderer Stelle im Rahmen eines Prüfungsverfahrens vorgelegt. Veröffentlichte Manuskripte sind dementsprechend gekennzeichnet. Ich stimme zu, dass diese Arbeit der Bibliothek des GEOMAR Helmholtz-Zentrum für Ozeanforschung Kiel sowie der Universitätsbibliothek der Christian-Albrechts-Universität Kiel zugängig gemacht wird.

Kiel, Kirti Ramesh

Acknowledgments

After three and half years of reading, preparing, performing experiments and sometimes performing them several times over, my PhD is drawing to a close. The support of a cohort of people has allowed the last few years to materialize into a thesis and I have many people to thank.

At the very outset, I would like to thank my PhD advisor, PD. Dr. Frank Melzner for giving me the opportunity to become a part of your research group. I am very grateful for the countless ways you have progressed my development, as a scientist and a person. I would also like to thank my second supervisor, Prof. Dr. med. Markus Bleich for providing me with a suite of resources to carry out novel experiments and making time to give me valuable feedback.

I would like to express my gratitude to the many members of the Ecophysiology group at GEOMAR past and present. In particular, I would like to thank my colleagues Ulrike Panknin, Claas Heibenthal, Trystan Sanders, Lara Schmittmann, Jennifer Schulze, Etienne Lein for supporting my experiments, proofreading various pieces of work and importantly, for your company during the several nights and weekends in the basement of Dusternbrooker Weg 20.

I am also incredibly grateful to the informal supervisors I had, Dr. Marian Hu, Dr. Nina Himmerkus and Dr. Jörn Thomsen whose doors were always open for discussions and the many questions I had. I would also like to thank Dr. Meike Stumpp, who as I see a mentor for my career and is a wonderful friend.

I have greatly benefited from the financial support of European Union's Seventh Framework Programme ITN project 'CACHE' that I was privileged to be a part of. This project has enabled my fruitful collaboration with several scientists whom I also wish to thank: Dr. Gernot Nehrke, Dr. Uwe John, Prof. Kristina Sundell, Kirsikka Silanpää, Dr. Melody Clark, Tejaswi Yarra, Alexander Ventura, Prof. Dr. Deniz Tasdemir, Dr. Christpher Gobler, Andrew Griffith, Dr. Caroline Rouger and Dr. Mathieu Bennet.

My time in Kiel has given me many treasured experiences due to the many friends I have made. In particular I would like to thank: Isabel, Felix, Lara, Anna Chagas, Anna Schukat, Mica, Sue, Allen, Carsten, Rike and Sophie. I would like to especially thank my friends Giannina Hattich and Christian Pansch who opened their home for many hours of laughter and have become a family to me.

To my parents, Vinodhini and Raju Ramesh, thank you for the sacrifices you have made to allow my dreams to transpire. To Dave, you have always supported me unconditionally through this process and in life.